

Development of Energy Efficient Distillation Configurations for Separation of Binary Azeotropic systems

by

Pravin Devram Ghuge
20EE18J26015

A thesis submitted to the
Academy of Scientific & Innovative Research
for the award of the degree of
DOCTOR OF PHILOSOPHY
in
ENGINEERING

Under the supervision of
Dr. Nilesh A. Mali



CSIR- National Chemical Laboratory, Pune

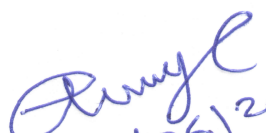


Academy of Scientific and Innovative Research
AcSIR Headquarters, CSIR-HRDC campus
Sector 19, Kamla Nehru Nagar,
Ghaziabad, U.P. – 201002, India

June 2023


Certificate

This is to certify that the work incorporated in this Ph.D. thesis entitled, "Development of Energy Efficient Distillation Configurations for Separation of Binary Azeotropic systems", submitted by Pravin Devram Ghuge to the Academy of Scientific and Innovative Research (AcSIR) in fulfillment of the requirements for the award of the Degree of Doctor of Philosophy in Engineering, embodies original research work carried-out by the student. We, further certify that this work has not been submitted to any other University or Institution in part or full for the award of any degree or diploma. Research materials obtained from other sources and used in this research work has been duly acknowledged in the thesis. Images, illustrations, figures, tables etc., used in the thesis from other sources, have also been duly cited and acknowledged.


27/06/2023

(Signature of Student)

Pravin Devram Ghuge
Name with date


27/06/2023

(Signature of Supervisor)

Dr. Nilesh A. Mali
Name with date

STATEMENTS OF ACADEMIC INTEGRITY

I Pravin Devram Ghuge, a Ph.D. student of the Academy of Scientific and Innovative Research (AcSIR) with Registration No. 20EE18J26015 hereby undertake that, the thesis entitled “Development of Energy Efficient Distillation Configurations for Separation of Binary Azeotropic systems” has been prepared by me and that the document reports original work carried out by me and is free of any plagiarism in compliance with the UGC Regulations on “Promotion of Academic Integrity and Prevention of Plagiarism in Higher Educational Institutions (2018)” and the CSIR Guidelines for “Ethics in Research and in Governance (2020)”.



Signature of the Student

Date : 27/06/2023

Place : CSIR-NCL, Pune

It is hereby certified that the work done by the student, under my supervision, is plagiarism-free in accordance with the UGC Regulations on “Promotion of Academic Integrity and Prevention of Plagiarism in Higher Educational Institutions (2018)” and the CSIR Guidelines for “Ethics in Research and in Governance (2020)”.



Signature of the Supervisor

Name : Dr. Nilesh A. Mali

Date : 27/06/2023

Place : CSIR-NCL, Pune

Acknowledgments

It gives me great pleasure to express my gratitude to everyone who supported me during my Ph.D. at CSIR-NCL, directly or indirectly. I want to express my deepest gratitude to my research supervisor, Dr. Nilesh A. Mali, for his continuous intellectual, technical, and spiritual support during my Ph.D. studies. I am thankful to him for his rigorous training in recognizing, thinking about, and dealing with scientific problems, designing experiments, critical analysis, scientific paper writing, and delivering a technical presentation, all of which have helped me improve my technical and intellectual skills.

I am also extremely grateful to Dr. Sunil Joshi for his valuable guidance and for giving me an opportunity to use the lab facility for my research work. I would like to thank Dr. D. S. Reddy (Chairperson), Dr. Ravindar Kontham (Chairperson), and Dr. Rahul Bhambure (member) of my doctorate advisory committee for constant review of my research work and timely advice during each DAC meeting.

I would like to express my gratitude to the Council of Scientific and Industrial Research (CSIR) for sponsoring a research scholarship. I would like to thank the HOD CEPD Division and the Director of the CSIR-National Chemical Laboratory, Pune for providing the facility for conducting research, as well as the Academy of Scientific and Innovative Research (AcSIR) for administrative assistance.

I would like to express my deepest gratitude to my wife, Yogita, for her unwavering love and patience. She has been my best companion, lover, listener, chef, personal adviser, and even proofreader as she has stood by me in any critical tasks to support my Ph.D. studies so that everything goes as smoothly as possible. Thank you for always being a dear buddy, VEER, who has given colorful life to our family since 2019. I am glad to have made friends and new families in the NCL colony, and to have made locations where I resided throughout my Ph.D. studies my second home far from my homeland. I am grateful for the support of my friends and lab mates. I would like to thank everyone at the CEPD office. At this point, I want to convey my heartfelt appreciation to my parents and all family members. I can't even begin to imagine how stressful I would be if they weren't there to support me constantly.

.....Pravin Devram Ghuge

List of Contents

Certificate	2
Statements of Academic Integrity.....	3
Acknowledgments.....	4
List of Contents.....	5
List of Figures.....	9
List of Tables	13
List of Symbols.....	16
Synopsis.....	17
Chapter 1 Introduction	25
1.1 Introduction	25
1.2 Azeotropy	25
1.3 Types of Azeotrope.....	26
1.3.1 Minimum Boiling Azeotrope.....	26
1.3.2 Maximum Boiling Azeotrope	29
1.3.3 Homogeneous Azeotrope.....	29
1.3.4 Heterogeneous Azeotrope.....	29
1.4 Different Methods for Separation of Azeotrope.....	31
1.4.1 Using Membrane	31
1.4.2 Azeotropic Distillation	31
1.4.3 Pressure Swing Distillation.....	32
1.4.3 Extractive Distillation.....	32
1.5 Statement of the Problem	33
1.6 Structure of Thesis	35
1.7 Reference.....	36

Chapter 2 Comparative Analysis of Extractive and Pressure Swing Distillation for Separation of THF-Water Separation	39
Abstract	39
2.1 Introduction	39
2.2 THF-Water Separation Using Extractive Distillation.....	41
2.2.1 Basis of Economical Analysis	43
2.2.2 Simulation Analysis of Extractive Distillation System	44
2.2.3 Heat Integration for Extractive Distillation	58
2.3 Pressure Swing Distillation (PSD)	59
2.3.1 Simulation Analysis of Pressure Swing Distillation System	60
2.3.2 Selection of Pressure and N_T for Columns	61
2.3.3 Heat Integration of Pressure Swing Distillation	65
2.4 Comparison of Extractive Distillation and PSD for THF-Water Separation.....	71
2.5 Conclusion.....	71
2.6 References	72
Chapter 3 Extractive Distillation Configuration for Nitric Acid Dehydration Using Sulphuric Acid as a Solvent	75
Abstract	75
3.1 Introduction	75
3.2 Thermodynamic Framework.....	76
3.2.1 Chemical Reactions.....	77
3.2.2 Vapour-Liquid Equilibrium (VLE)	77
3.2.3 eNRTL-RK Activity Coefficient Model.....	79
3.2.4 Data for Regression	82
3.3 Extractive Distillation Configuration.....	86
3.3.1 Basis for TAC Analysis	89
3.3.2 Simulation Analysis and Economic Optimization	90
3.4 Result and Discussion	94

3.4.1 Operating Pressure for Column.....	94
3.4.2 Selection of Number of Stages (N_T).....	94
3.4.3 Selection of Solvent to Feed (E/F) Ratio.....	100
3.4.4 Binary Mixture Feed Stage (N_{FF}) and Solvent Feed Stage (N_{EF}).....	102
3.4.5 Solvent Feed Temperature (T_{EF}).....	105
3.4.6 Complete Conceptual Design of Proposed of Nitric Acid Dehydration ED System Configuration.....	106
3.5 Conclusions.....	113
3.6 References.....	114
Chapter 4 Effect of $CaCl_2$, $ZnCl_2$ and $LiBr$ salts on Isobaric Vapour-liquid Equilibrium in Separation of the Azeotropic Mixture of Ethanol + Water	118
Abstract.....	118
4.1 Introduction.....	118
4.2 Experimental.....	120
4.2.1 Materials.....	120
4.2.2 Experimental Apparatus and Procedure.....	121
4.2.3 Analysis.....	123
4.3 Results and Discussion.....	127
4.3.1 Experimental Data.....	127
4.3.2 Correlation of the VLE Data.....	135
4.3.3 Thermodynamic Consistency Test.....	141
4.3.4 Effect of Salts on Vapour-Liquid Equilibrium.....	141
4.3.5 Extractive Distillation Configuration.....	146
4.4 Conclusions.....	148
4.5 References.....	149
Chapter 5 Isobaric Vapour-Liquid Equilibrium Measurements and Modeling of Binary Systems of Methylcyclohexane with Toluene, Anisole, and NEP at 92 kPa	154
Abstract.....	154
5.1 Introduction.....	154

5.2 Experimental	156
5.2.1 Materials/Chemicals	156
5.2.2 Apparatus and Procedure.....	156
5.2.3 Analysis	157
5.3 Results and Discussion	160
5.3.1 Experimental Results.....	160
5.3.2 Data Regression	168
5.3.3 Thermodynamic Consistency Test	171
5.3.4 Effect of Solvent on VLE Methylcyclohexane and Toluene System.....	173
5.4 Conclusions	175
5.5 References	176
Chapter 6 Conclusions and Recommendations.....	178
6.1 Conclusions	178
6.2 Recommendations for Future Work	181
Abstract	182
List of Publications.....	183

List of Figures

Figure 1.1. T-xy and equilibrium diagram for binary system having minimum boiling azeotrope (ethanol-water).....	27
Figure 1.2. T-xy and equilibrium diagram for binary system having maximum boiling azeotrope (nitric acid-water).....	28
Figure 1.3. T-xy and equilibrium diagram for binary system having minimum-boiling heteroazeotrope (butanol – water).....	30
Figure 2.1. (a) yx diagram (●) experimental data [20] (—) NRTL model data (b) Txy diagram for THF-water system at 1 atm pressure (■) Tx data (●)Ty experimental data [20] (—) NRTL model data using Aspen Plus	41
Figure 2.2. Extractive distillation flow diagram.....	43
Figure 2.3. Effect of E/F and reflux ratio on the distillate stream THF composition (X_D).....	49
Figure 2.4. (a) Effect of the total number of stages (N_T) on the distillate purity (X_D) (b) Effect of binary feed stage (N_{FF}) on X_D , Q_R and Q_C for DMSO as a solvent.....	50
Figure 2.5. (a) Effect of the total number of stages (N_T) on the distillate purity (X_D) (b) Effect of binary feed stage (N_{FF}) on X_D , Q_R and Q_C for ethylene glycol as a solvent	50
Figure 2.6 (a) Effect of the total number of stages (N_T) on the distillate purity (X_D) (b) Effect of binary feed stage (N_{FF}) on X_D , Q_R and Q_C for glycerol as a solvent	51
Figure 2.7. (a) Effect of the total number of stages (N_T) on the distillate purity (X_D) (b) Effect of binary feed stage (N_{FF}) on X_D , Q_R and Q_C for 1, 2-propanediol as a solvent.....	51
Figure 2.8. Effect of solvent feed stage (N_{EF}) with respect to the total number of stages (N_T) on the distillate composition (X_D) for DMSO as a solvent.....	52
Figure 2.9. The optimal design flowsheet of the extractive distillation system with DMSO as a solvent	55
Figure 2.10. SRDC temperature profile	56
Figure 2.11 The composition profiles of the extractive distillation column with DMSO as a solvent .	57
Figure 2.12. Pressure swing distillation flow diagram.....	60
Figure 2.13. Effect of reflux ratio (RR_1) for LPC of fully heat integrated THF-water PSD on the RR_2 , Q_{C2} and Q_{R2}	66
Figure 2.14. The optimal steady-state design flowsheets of the pressure swing distillation system.....	69

Figure 3.1. VLE diagram of HNO ₃ /water/H ₂ SO ₄ binary and ternary system with experimental and estimated data.	85
Figure 3.2. Process flow diagram of distillation column sequence for dehydration of dilute nitric acid	88
Figure 3.3. Schematic representations of the input and output to any stage n of the multistage distillation column.....	90
Figure 3.4. Sequential iterative procedure for optimization of design parameters for ED of nitric acid water system	93
Figure 3.5. Effect of the total number of stages (N _T) on distillate purity (X _D) for (a) PDC (b) EDC (c) SRDC	96
Figure 3.6. Effect of E/F ratio on (a) Distillate purity (X _D) with different reflux ratios (b) X _D , Q _R and Q _C of EDC column of nitric acid dehydration ED system.	101
Figure 3.7. Effect of Mass Reflux Ratio (RR) on X _D , Q _R and Q _C of the EDC column of nitric acid dehydration ED system	102
Figure 3.8. Effect of binary mixture feed location (N _{FF}) on X _D , Q _R and Q _C of (a) PDC and (b) SRDC of nitric acid dehydration ED system.....	103
Figure 3.9. (a) Effect of solvent feed stage (N _{EF}) and (b) Effect of binary mixture feed location (N _{FF}) on the X _D , Q _R and Q _C of EDC of nitric acid dehydration ED system.	104
Figure 3.10. Effect of solvent feed temperature (T _{EF}) on X _D , Q _R and Q _C of the EDC of nitric acid dehydration ED system	105
Figure 3.11. Optimal design flow sheet of distillation column sequence for dilute nitric acid dehydration ED system with sulphuric acid as solvent.....	107
Figure 3.12 Temperature and composition profile for EDC	109
Figure 3.13 Temperature and composition profile for SRDC column	111
Figure 4.1. Schematic diagram of experimental vapour-liquid equilibrium setup; (A) electric heater, (B) boiling chamber, (C) Cottrell tube, (E) equilibrium chamber, (D) drain valve, (F) feed point, (G) condensate receiver, (H) liquid chamber, (I) liquid sampling point, (J) condenser, (K) to vacuum pump, (L) magnetic stirrer, (M) mixing chamber, (N) coolant in, (O) coolant out, (P) temperature sensor, (Q) vapour condensate sampling point.	122
Figure 4.2. Calibration curve for the water (1) + ethanol (2) system with refractive index (n _D) versus mole fraction of ethanol (x ₂); (◆) measured values at 298.15 K, (—) polynomial equation.	126

Figure 4.3. Calibration curve for the water (1) + ethanol (2) system with density (ρ) versus mole fraction of ethanol (x_2); (\blacklozenge) measured values at 298.15 K, (---) polynomial equation.	127
Figure 4.4. Isobaric vapour-liquid equilibrium data of the binary system of water (1) + ethanol (2) at 94.5 kPa. (\circ) this work, (---) solid line estimated by NRTL model	129
Figure 4.5. Isobaric y-x' diagram for the system of water (1) ethanol (2) + calcium chloride (3) at 94.5 kPa; (\circ) salt free, (\blacksquare) 5 %, (\blacktriangle) 10 % and (\bullet) 15 % w/w salt; solid line correlated by eNRTL model, x', liquid phase mole fraction (salt-free basis); y, vapour phase mole fraction.....	133
Figure 4.6. Isobaric y-x' diagram for the system of water (1) ethanol (2) + zinc chloride (3) at 94.5 kPa; (\circ) salt free, (\blacksquare) 5 %, (\blacktriangle) 10 % and (\bullet) 15 % w/w salt; solid line correlated by eNRTL model, x', liquid phase mole fraction (salt-free basis); y, vapour phase mole fraction.....	134
Figure 4.7. Isobaric y-x' diagram for the system of water (1) ethanol (2) + lithium bromide (3) at 94.5 kPa; (\circ) salt free, (\blacksquare) 5 %, (\blacktriangle) 10 % and (\bullet) 15 % w/w salt; solid line correlated by eNRTL model, x', liquid phase mole fraction (salt-free basis); y, vapour phase mole fraction.....	135
Figure 4.8. Relative volatility (α_{21}) for the system of water (1) ethanol (2) + calcium chloride (3) at 94.5 kPa; (\circ) salt free, (\blacksquare) 5 %, (\blacktriangle) 10 % and (\bullet) 15 % w/w salt; solid line correlated by eNRTL model, x', liquid phase mole fraction (salt-free basis).	143
Figure 4.9. Relative volatility (α_{21}) for the system of water (1) ethanol (2) + zinc chloride (3) at 94.5 kPa; (\circ) salt free, (\blacksquare) 5 %, (\blacktriangle) 10 % and (\bullet) 15 % w/w salt; solid line correlated by eNRTL model, x', liquid phase mole fraction (salt-free basis).	143
Figure 4.10. Relative volatility (α_{21}) for the system of water (1) ethanol (2) + lithium bromide (3) at 94.5 kPa; (\circ) salt free, (\blacksquare) 5 %, (\blacktriangle) 10 % and (\bullet) 15 % w/w salt; solid line correlated by eNRTL model, x', liquid phase mole fraction (salt-free basis).	144
Figure 4.11. Isobaric y-x' diagram for water (1) ethanol (2) + salt (3) system, (\circ) salt free, (\blacktriangle) 15 % ZnCl ₂ , and (\bullet) 15 % CaCl ₂ w/w salt (this study), (\square) 16.7 % CaCl ₂ w/w salt [24], (Δ) 0.04 molar concentration of MgCl ₂ [14] x', liquid phase mole fraction (salt-free basis); y, vapour phase mole fraction.....	145
Figure 4.12. Isobaric y-x' diagram for water (1) ethanol (2) + salt (3) system, (\circ) salt free, (\blacksquare) 15 % ZnCl ₂ , and (\bullet) 15 % CaCl ₂ w/w salt, (\blacktriangle) 15 % LiBr w/w salt x', liquid phase mole fraction (salt-free basis); y, vapour phase mole fraction.....	146
Figure 4.13. EDC column using CaCl ₂ as an entrainer.....	147

Figure 5.1. Calibration curve for the methylcyclohexane (1) + toluene (2) system with refractive index (n_D) versus mole fraction of methylcyclohexane (x_1); (■) measured values at 298.15 K, (—) polynomial equation.....	157
Figure 5.2. Calibration curve for the methylcyclohexane (1) + anisole (2) system with refractive index (n_D) versus mole fraction of methylcyclohexane (x_1); (■) measured values at 298.15 K, (—) polynomial equation.....	158
Figure 5.3. Calibration curve for the methylcyclohexane (1) + NEP (2) system with refractive index (n_D) versus mole fraction of methylcyclohexane (x_1); (■) measured values at 298.15 K, (—) polynomial equation.....	158
Figure 5.4. Calibration curve for the toluene (1) + NEP (2) system with refractive index (n_D) versus mole fraction of toluene (x_1); (■) measured values at 298.15 K, (—) polynomial equation.	159
Figure 5.5. Calibration curve for the toluene (1) + anisole (2) system with refractive index (n_D) versus mole fraction of toluene (x_1); (■) measured values at 298.15 K, (—) polynomial equation.	159
Figure 5.6. Txy diagram for methylcyclohexane (1) + toluene (2) at 92 kPa. (●) T-x experimental (■) T-y experimental; (- - -) NRTL, (—) Wilson, (...) UNIQUAC model.	164
Figure 5.7. Txy diagram for methylcyclohexane (1) + anisole (2) at 92 kPa. (●) T-x experimental (■) T-y experimental; (- - -) NRTL, (—) Wilson, (...) UNIQUAC model.	165
Figure 5.8. Txy diagram for methylcyclohexane (1) + NEP (2) at 92 kPa. (●) T-x experimental (■) T-y experimental; (- - -) NRTL, (—) Wilson, (...) UNIQUAC model.	166
Figure 5.9. Txy diagram for toluene (1) + NEP (2) at 92 kPa. (●) T-x experimental (■) T-y experimental; (- - -) NRTL, (—) Wilson, (...) UNIQUAC model.	167
Figure 5.10. Txy diagram for toluene (1) + anisole (2) at 92 kPa. (●) T-x experimental (■) T-y experimental; (- - -) NRTL, (—) Wilson, (...) UNIQUAC model.	168
Figure 5.11. Effect on VLE for the system methylcyclohexane (1) + toluene (2) with different entrainers. (●) Experimental value without entrainer, (—) calculated by NRTL model without entrainer, (***), calculated by NRTL model with anisole, (- - -) calculated by NRTL model with NEP.	174

List of Tables

Table 2.1. Basis of economics and equipment sizing	44
Table 2.2. Binary interaction parameter estimated by UNIFAC	45
Table 2.3. Comparison of designs of EDC at various operating pressures	47
Table 2.4. Economic optimization results for EDC.....	53
Table 2.5. Economic optimization results for SRDC.....	53
Table 2.6. Optimized design parameters with TAC of THF-Water extractive distillation system for various solvents.....	54
Table 2.7 Economic analysis results for THF-water ED with and without heat integration	59
Table 2.8. Estimated effect of pressure on azeotropic composition for THF-water system using ASPEN simulations.....	62
Table 2.9. THF-water PSD economic optimization results for N_{T1} (LPC at 1 atm and HPC at 5 atm)	63
Table 2.10. THF-water PSD economic optimization results for N_{T2} (LPC at 1 atm and HPC at 5 atm)	63
Table 2.11. THF-water PSD optimization results with various operating pressure of HPC.....	64
Table 2.12. Economic analysis results for THF-water ED and PSD with and without heat integration	70
Table 3.1. Coefficients of extended Antoine equation ^a of pure components [14].....	78
Table 3.2. Redlich-Kwong equation of state parameters [14].....	78
Table 3.3. Coefficients of liquid molar density model equations [14]	78
Table 3.4. Coefficients of dielectric constant equation ^a [14]	80
Table 3.5. Coefficients of ideal gas heat capacity model equation ^a [14].....	81
Table 3.6. Coefficients of heat of vaporization model equations [14].....	81
Table 3.7. Average Absolute Deviation (AAD) between Experimental Data and Model Data.....	86
Table 3.8. Molecule-molecule binary interaction parameter for ENRTL-RK thermodynamic model obtained using regression of experimental data.....	86
Table 3.9. Molecule-electrolyte binary interaction parameter for ENRTL-RK thermodynamic model obtained using regression of experimental vle data	86
Table 3.10. Equations for equipment sizing and economics analysis.....	89
Table 3.11. Economic optimization for PDC of nitric acid dehydration ED system for the different total number of stages (N_{T1})	97


Table 3.12. Economic optimization for EDC of nitric acid dehydration ED system for the different total number of stages (N_{T2})	98
Table 3.13. Economic Optimization of SRDC of nitric acid dehydration ED system for the different total number of stages (N_{T3})	99
Table 3.14. Detail TAC calculations for complete of nitric acid dehydration ED system.....	112
Table 4.1. Specification of the chemicals used in experiments.....	121
Table 4.2. Experimental values of density (ρ) and refractive index (n_D), mole fractions of ethanol (x_2) for water (1) + ethanol (2) mixture at 298.15 K. ^a	124
Table 4.3. Polynomial equation for calibration curves	127
Table 4.4. Isobaric vapour-liquid equilibrium data for temperature T, liquid phase mole fraction x_i , and vapour phase mole fraction y_i and relative volatility α for the binary system of water (1) + ethanol (2) at 94.5 kPa	128
Table 4.5. Isobaric ternary vapour-liquid equilibrium data for temperature T, liquid phase mole fraction salt-free basis x' , x_1 and x_2 are the mole fractions (on salt basis) of water and ethanol, respectively, liquid phase mass fraction of salt z, vapour phase mole fraction y, activity coefficient γ , relative volatility α_{21} for water (1) ethanol (2) + calcium chloride (3) at 94.5 kPa. ^a	130
Table 4.6. Isobaric ternary vapour-liquid equilibrium data for temperature T, liquid phase mole fraction salt-free basis x' , x_1 and x_2 are the mole fractions (on salt basis) of water and ethanol, respectively, liquid phase mass fraction salt z, vapour phase mole fraction y, activity coefficient γ , relative volatility α for water (1) ethanol (2) + zinc chloride (3) at pressure of 94.5 kPa. ^a	131
Table 4.7. Isobaric ternary vapour-liquid equilibrium data for temperature T, liquid phase mole fraction salt-free basis x' , x_1 and x_2 are the mole fractions (on salt basis) of water and ethanol, respectively, liquid phase mass fraction of salt z, vapour phase mole fraction y for water (1) ethanol (2) + lithium bromide (3) at pressure of 94.5 kPa. ^a	132
Table 4.8. Parameters of the extended Antoine equation ^a of pure components [31].....	136
Table 4.9. Coefficients of dielectric constant equation ^a	138
Table 4.10. Coefficients of ideal gas heat capacity model equation ^a	139
Table 4.11. Coefficients of heat of vaporization model equations	139
Table 4.12. Binary interaction parameter for the eNRTL Model	140
Table 4.13. The root-mean-square deviation (RMSD) for the equilibrium temperature (T) and vapour phase mole fraction (y_1) for the eNRTL model	140

Table 4.14. Preliminary EDC column configuration	147
Table 4.15. Preliminary stream results for EDC column	148
Table 5.1. Detailed specification of chemicals used.....	156
Table 5.2. Fitted polynomial equation for calibration curves.....	160
Table 5.3. Vapour-liquid equilibrium data for the binary system of methylcyclohexane (1) + toluene (2) temperature T in K, liquid phase mole fraction (x_1), vapour phase mole fraction (y_1), activity coefficients (γ_i) and relative volatility (α_{12}) at 92.0 kPa.....	161
Table 5.4. Vapour-liquid equilibrium data for the binary system of methylcyclohexane (1) + anisole (2) temperature T in K, liquid phase mole fraction (x_1), vapour phase mole fraction (y_1), activity coefficients (γ_i) and relative volatility (α_{12}) at 92.0 kPa.....	161
Table 5.5. Vapour-liquid equilibrium data for the binary system of methylcyclohexane (1) + NEP (2) temperature T in K, liquid phase mole fraction (x_1), vapour phase mole fraction (y_1), activity coefficients (γ_i) and relative volatility (α_{12}) at 92.0 kPa.....	162
Table 5.6. Experimental VLE data for the binary system of toluene (1) + NEP (2) temperature T in K, liquid phase mole fraction (x_1), vapour phase mole fraction (y_1), activity coefficients (γ_i) and relative volatility (α_{12}) at 92.0 kPa.	162
Table 5.7. Experimental VLE data for the binary system of toluene (1) + anisole (2) temperature T in K, liquid phase mole fraction (x_1), vapour phase mole fraction (y_1), activity coefficients (γ_i) and relative volatility (α_{12}) at 92.0 kPa.....	163
Table 5.8. Parameters of the extended Antoine equation.....	169
Table 5.9. Regressed binary interaction parameters of the NRTL, UNIQUAC, and Wilson models and RMSD and AAD.....	171
Table 5.10. Van Ness thermodynamic consistency test results	172
Table 5.11. Estimated parameters of extended Redlich-Kister's model for infinite dilution test	173
Table 5.12. Infinite dilution consistency check results for binary VLE systems	173

List of Symbols

x_2'	Mole fractions of component i in the liquid phase on salt-free basis
x_i	Mole fractions of component i in the liquid phase
y_i	Mole fractions of component i in the vapour phase
y_i^{exp}	Experimental mole fraction of component i in vapour phase
y_i^{cal}	Calculated mole fraction of component i in vapour phase
T	Equilibrium temperature
T_i^{exp}	Experimental temperature
T_i^{cal}	Temperature calculated by ENRTL model
P	Total pressure in the equilibrium system
P_i^s	Saturated vapour pressure of pure component i at equilibrium temperature
u	Standard uncertainties
z_3	Mass fraction of salts in the liquid phase
γ_i	Activity coefficient of component i
α_{21}	Relative volatility of ethanol to water
ρ	Density
n_D	Refractive index

Synopsis

	Synopsis of the Thesis to be submitted to the Academy of Scientific and Innovative Research for Award of the Degree of Doctor of Philosophy in Sciences/ Engineering
Name of the Candidate	Pravin Devram Ghuge
Degree Enrollment No. &Date	20EE18J26015 Date: 04/01/2018
Laboratory	CSIR-NCL, Pune
Title of the Thesis	Development of Energy Efficient Distillation Configurations for Separation of Binary Azeotropic systems
Research Supervisor/ Co-supervisor	Dr. Nilesh A. Mali

Introduction:

The process of mixing liquids is a fascinating and significant economic activity that has shaped our world in countless ways. It is commonly used to create new products or improve the quality of existing ones, such as gasoline blending or mixing reactants in chemical reactors. Mixing occurs spontaneously when two miscible liquids are put into contact, and its rate can be increased by applying a stirring. But conversely, separating the liquid mixture into its pure components is quite challenging without any external interference [1]. Several possible technologies are feasible to perform separation either by individual technique or using combination of techniques, such as membrane separations, extraction, distillation, adsorption, etc. [2]. Distillation is the most preferred unit operation in process industry for separating liquid mixtures.

Distillation has a distinct processing advantage, such as high throughput, handling a wide range of feed concentrations, and producing high-purity products. It is a mature and well-established technology in terms of design, operation, and control [3]. Although this is an old and mature technology in the chemical process industry, it does have some challenges to overcome, as mentioned below:

High energy consumption: Distillation columns are responsible for more than 90% of the total energy used in separations in chemical process industries worldwide. Hence, energy-efficient distillation configurations are needed to reduce fuel consumption and operating costs.

Formation of an azeotrope: An azeotrope is a mixture of chemical components that have the same composition in the liquid and vapor phases and are in equilibrium with each other. Azeotrope is also known as a constant boiling mixture. This non-ideal azeotropic behaviour in two different chemical components occurs due to their molecular interactions, either repulsion or attraction. Repulsion increases the effective vapor pressures of the components at a given temperature, which leads to the formation of the minimum boiling azeotrope. In this case, azeotrope will boil at a lower temperature than the other components of the mixture. In some systems, molecular attraction decreases the component's resulting vapor pressures, leading to the formation of a maximum-boiling azeotrope. In this case, azeotrope will boil at a higher temperature than the boiling points of the other components present in the mixture.

Statement of the Problem:

When the azeotropic condition occurs, there is no change in the liquid and vapor compositions from tray to tray in a distillation column. Therefore, an azeotrope acts as a distillation boundary. This phenomenon makes it impossible to get a sharp separation of the feed mixture using conventional distillation. Hence, various advanced distillation techniques are required to separate such mixtures. Each separation technique has its pros and cons. It may be possible to achieve the separation with the desired purity by using one or more separation methods; however, the most appropriate separation method should be selected based on the economics of the overall system. It was reported in the literature that the azeotropic distillation process required almost 30 to 40% more energy in comparison to Extractive Distillation (ED) and Pressure Swing Distillation (PSD) in most of the cases [2]. The performance of ED and PSD for separating azeotropic systems varies from system to system; hence, both are competitive with each other for separating the azeotropic system.

Various solvents have been reported in the literature for the extractive distillation of some binary azeotropic systems. However, due to a lack of a common basis for comparison, determining a better solvent in terms of operating and capital costs with the desired product purity was difficult. There was an insufficient or missing built-in binary interaction parameter in the Aspen Plus simulator

for many component pairs, which may led to improper simulation and an unreliable conceptual design of the process.

In the present work, novel and advanced energy-efficient distillation configurations are developed for the separation of various binary azeotropic systems with the following objectives:

- Evaluation of various possible novel entrainers for altering the azeotropic/close-boiling behaviour of the systems through experimental VLE analysis
- Development of a thermodynamic model and its validation for new entrainer systems using experimental VLE data.
- Conceptualization, optimization, and modelling of a pressure swing and enhanced extractive distillation system for industrial applications
- Development of an energy-saving configuration by adopting heat integration
- Development of an optimization approach for the conceptual design of an advanced distillation configuration, starting from essential VLE data, thermodynamic activity coefficient model, sensitivity analysis, and then techno-economic optimization of design parameters.

Methodology and Results:

Chapter 2. Separation of Tetrahydrofuran (THF)-Water Mixture,

Part I- Using Extractive Distillation with Various Entrainers.

Part II- Pressure Swing Distillation (PSD) and Heat Integration.

In this work, extractive and pressure-swing distillation methods are analyzed in detail through steady state ASPEN Plus simulations to propose the most economic method for separation of equimolar mixture of THF-Water. Various solvents were evaluated and DMSO was identified as the most appropriate solvent, as it gave minimum Total Annual Cost (TAC) for desired purity. In case of pressure swing distillation, various pressure ranges were explored to achieve minimum TAC. Configurations for extractive and pressure swing distillation with heat integration were also worked out. The optimum designs of extractive and pressure swing distillation with and without heat integration were compared on a common basis of feed conditions and purity constraints. Results indicate that TAC of extractive distillation with heat integration is 5.2 % less than that of PSD with partial heat integration.

Chapter 3. Extractive Distillation Configuration for dilute Nitric Acid Dehydration Using Sulphuric Acid as a Solvent

In this work, an extractive distillation configuration for dehydration of dilute nitric acid is proposed with sulphuric acid as a solvent. Thermodynamic modeling of vapor-liquid-equilibrium of binary and ternary systems of nitric acid/water/sulphuric acid was carried out using eNRTL-RK (Electrolyte Non Random Two Liquid) thermodynamic property method in the Aspen plus process simulator. The model performance was validated by comparing the experimental data with the estimated data by eNRTL-RK model and found to be in good agreement. The thermodynamic model is then used for developing a triple column extractive distillation sequence, comprising pre-concentrating column, extractive distillation column and solvent recovery column. The configuration is designed, simulated and optimized to concentrate dilute nitric acid using sulphuric acid as a solvent to break the nitric acid water azeotrope. The operating and structural parameters of the distillation configuration are optimized simultaneously with an objective of minimizing energy consumption and Total Annual Cost (TAC) overall configuration.

Chapter 4. Effect of Various Salts on Isobaric Vapor-Liquid Equilibrium in Separation of the Azeotropic Mixture of Ethanol + Water

In this work, different salts are explored as potential entrainers for extractive distillation of ethanol-water mixture. Calcium chloride (CaCl_2), lithium bromide (LiBr) and zinc chloride (ZnCl_2) salts were explored as possible entrainers for breaking the minimum boiling azeotrope of ethanol and water. Isobaric vapor-liquid equilibrium (VLE) data for the binary systems of water + ethanol and ternary system of water + ethanol + calcium chloride, water + ethanol + lithium bromide and water + ethanol + zinc chloride were measured at a constant pressure of 94.5 kPa. The effect of salts on the relative volatility of ethanol to water as well as on the vapor phase mole fractions of ethanol were also studied experimentally. From the experimental results, it was observed that with addition of salts, the azeotropic point of the ethanol and water system can be eliminated. Salting out effects in case of calcium chloride was more than that of lithium bromide and zinc chloride salts. The results obtained in this work showed that calcium chloride could be a better choice for separation of the water + ethanol azeotrope. Electrolyte nonrandom two-liquid (eNRTL) model was used to correlate the experimental VLE data. The model prediction with the regressed parameters was found in well agreement with the

experimental data. The experimental data obtained in this work was found thermodynamically consistent using van Ness test.

Chapter 5. Isobaric VLE Measurements and Modeling of Binary Systems of Methylcyclohexane with Toluene, Anisole, and NEP at 92 kPa.

Methylcyclohexane and toluene are the close-boiling components; anisole and n-ethyl-2-pyrrolidone (NEP) were explored as separating agents for the extractive distillation of this mixture. The influence of anisole and NEP on the VLE behaviour of the system was analyzed. The isobaric vapor-liquid equilibrium (VLE) data for the binary systems of methylcyclohexane + toluene, methylcyclohexane + anisole, methylcyclohexane + NEP, toluene + anisole, and toluene + NEP were measured at 92.0 kPa. The NRTL, UNIQUAC, and Wilson thermodynamic activity coefficient models were used in the regression of experimental data to obtain the binary interaction parameters. All three models are able to predict the experimental VLE behaviour. The Van Ness and infinite dilution tests confirmed the thermodynamic consistency of the experimental VLE data. Since NEP and anisole both exhibit shift in relative volatility and NEP shows larger shift as compared to anisole and thus it can be effective extractive agent for separating methylcyclohexane and toluene systems. The results show that the obtained binary interaction parameter can be used to simulate and optimize extractive distillation configurations for **separating the** mixture of methylcyclohexane and toluene.

Conclusions:

- An approach for conceptual distillation design was developed, starting from the generation of VLE data, thermodynamic modelling and its validation, sensitivity analysis of design parameters, and techno-economic optimization.
- For the minimum boiling THF–water azeotropic system, the optimum design of ED and PSD with and without HI was developed systematically using techno-economic optimization with minimum TAC as an objective function.
- It was found that, extractive distillation using DMSO as an entrainer with heat integration requires 5.2% less TAC than PSD with partial heat integration; hence, ED with DMSO as solvent appears to be a better option economically.

- Thermodynamic modelling was done and validated for the nitric acid/water/sulphuric acid system using the eNRTL-RK model, which agreed with the experimental VLE data reported in literature.
- Sulphuric acid was found to be a suitable solvent for dehydrating nitric acid, which leads to nitric acid purity of up to 99.99 percent by mass using a triple-column extractive distillation configuration.
- The isobaric VLE data for ethanol + water + calcium chloride, zinc chloride, and lithium bromide were determined, and an eNRTL model was found suitable to correlate the experimental data.
- It was found that, calcium chloride could be the better choice for separating ethanol and water as it showed a more significant salting-out effect for ethanol.
- NEP (n-ethyl-2-pyrrolidone) and anisole were explored experimentally as novel entrainers for the separation of methylcyclohexane and toluene, and NEP was found to be a suitable entrainer.

References:

- [1] Doherty, M.F. and Malone, M.F., 2001. *Conceptual design of distillation systems*. McGraw-Hill.
- [2] Luyben WL, Chien I-L. Design and control of distillation systems for separating azeotropes. John Wiley & Sons; 2011.
- [3] Kiss, A.A., 2013. *Advanced distillation technologies: design, control and applications*. John Wiley & Sons.

Publications:

- [1] **Ghugre, P.D.**, Mali, N.A. and Joshi, S.S., 2021. Effect of CaCl₂ and ZnCl₂ salts on isobaric vapor-liquid equilibrium in separation of the azeotropic mixture of ethanol+ water. *Fluid Phase Equilibria*, 537, p.113000.
- [2] **Ghugre, P.D.**, Mali, N.A. and Joshi, S.S., 2020. Extractive distillation configuration for nitric acid dehydration using sulfuric acid as a solvent. *Industrial & Engineering Chemistry Research*, 59(13), pp.6183-6193.

[3] **Ghuge, P.D.**, Mali, N.A. and Joshi, S.S., 2017. Comparative analysis of extractive and pressure swing distillation for separation of THF-water separation. *Computers & Chemical Engineering*, 103, pp.188-200.

[4] Mali, N.A., Yadav, S.S., **Ghuge, P.D.** and Joshi, S.S., 2017. Vapor–Liquid Equilibrium Data for Binary Mixtures of Dimethyl Carbonate with Methyl Acetate, Ethyl Acetate, n-Propyl Acetate, Isopropyl Acetate, n-Butyl Acetate, and Isoamyl Acetate at 93.13 kPa. *Journal of Chemical & Engineering Data*, 62(12), pp.4356-4363.

[5] **Ghuge, P.D.**, Mali, N.A. and Sirsam, R.S., 2018. Study of the effect of operating parameters on the extractive distillation of isopropyl alcohol–water mixture using dimethyl Sulphoxide as an entrainer. *Indian Chemical Engineer*, 60(2), pp.141-161.

Chapter 1

Introduction

Chapter 1 Introduction

1.1 Introduction

The process of mixing liquids is a fascinating and significant economic activity that has shaped our world in countless ways. It is commonly used to create new products or improve the quality of existing ones, such as gasoline blending or mixing reactants in chemical reactors. When two miscible liquids are combined, they mix spontaneously, though stirring and shaking can speed up the process. However, separating the liquid mixture into its pure components is quite challenging and requires external interference [1]. Various techniques, such as membrane separation, extraction, distillation, and adsorption, can be used either individually or in combination to perform the separation [2]. Among these, distillation is the most preferred unit operation in the process industry for separating liquid mixtures.

Distillation is a highly efficient process with several advantages, including high throughput, the ability to handle a wide range of feed concentrations, and the production of high-purity products. It is a well-established and mature technology with regards to design, operation, and control [3]. However, despite being an old and mature technology in the chemical process industry, there are still some challenges that need to be addressed, as mentioned below:

High energy consumption: Distillation columns are responsible for more than 90 % of the total energy used in separations in chemical process industries worldwide. Hence, energy-efficient distillation configurations are needed to reduce fuel consumption and operating costs.

Formation of an azeotrope: Azeotropes is a mixture of chemical components with the same composition in the liquid and vapour phases and are in equilibrium. Since distillation relies on distinct compositional differences between the liquid and vapour phases, the existence of this phenomenon means that simple distillation procedures cannot be employed to complete separation.

1.2 Azeotropy

The formation of azeotrope was first reported by Dalton in 1802 [1]. Wade and Merriman (1911) first introduced the term "azeotrope" to assign mixtures having maximum or minimum boiling points [3]. The word azeotrope is derived from the ancient Greek words meaning "no change on boiling" [1].

Azeotrope is also known as a constant boiling mixture. This non-ideal azeotropic behaviour in two different chemical components occurs due to either repulsion or attraction of molecular interactions forces exist between them. The chemical industry often deals with many component types that result in azeotropes. The manufacturing of tetrahydrofuran, tert-amyl methyl ether, vinyl acetate, methyl acetate, isopropanol and several other products are typical examples.

Azeotropes do not form if the components have the same essential molecules and structural makeup. In this case, the molecular interaction is very minimal. Propane, butane, pentane, and other hydrocarbon mixtures are notable examples. Such mixtures frequently exhibit almost constant relative volatilities and phase equilibrium behaviour close to ideal. The mixture that does not form azeotropes is called a "zeotropic" mixture.

1.3 Types of Azeotrope

Azeotrope can be a minimum or maximum boiling point relative to the boiling points of the pure components. Depending on the number of phases, they can also be categorized as homogeneous or heterogeneous azeotropes. Azeotropes occur in various systems, such as binary, ternary and multicomponent mixtures.

1.3.1 Minimum Boiling Azeotrope

In minimum boiling azeotropic systems, the presence of distinct functional groups leads to repulsive forces between the components in the mixture. The intermolecular force between like molecules (A-A and B-B) is more potent than unlike molecules (A-B), i.e. repulsion is more between the unlike molecule. This repulsive force enhances the effective vapour pressures of the components at a given temperature and can lead to a minimum boiling azeotrope. If the azeotrope boils at a temperature lower than the boiling point of the pure components, it means a positive deviation from Raoult's law or ideality [1-3]. Alternatively, it is known as a positive azeotrope. Approximately 90 % of all azeotropes fall under this category [2]. For example, the ethanol-water system has stronger repulsion because the CH₃-CH₂ end of the ethanol molecule differs significantly from the OH end of the water molecule. The system becomes more nonideal, and a minimum boiling azeotrope arises. Figure 1.1 presents T-xy and the equilibrium diagram for the minimum boiling azeotropic system.

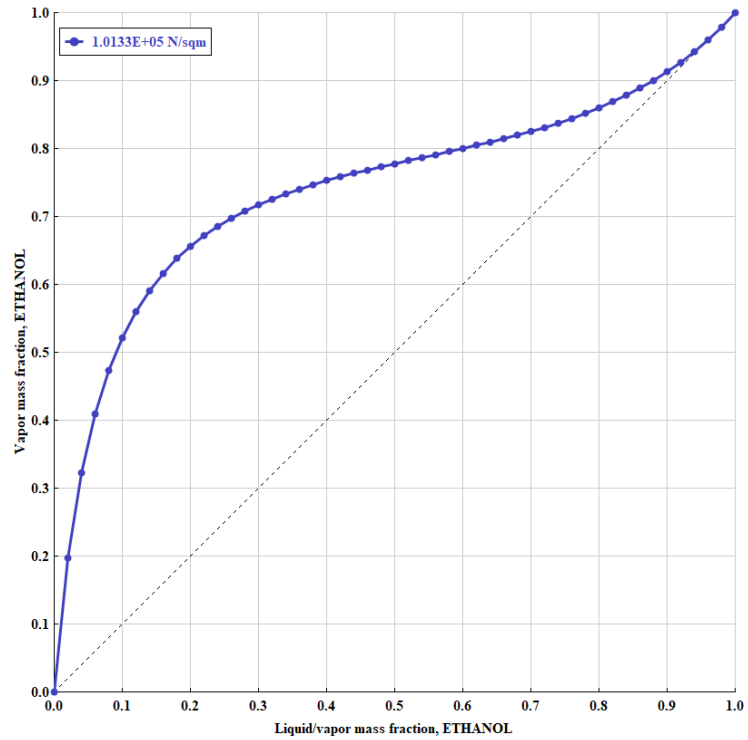
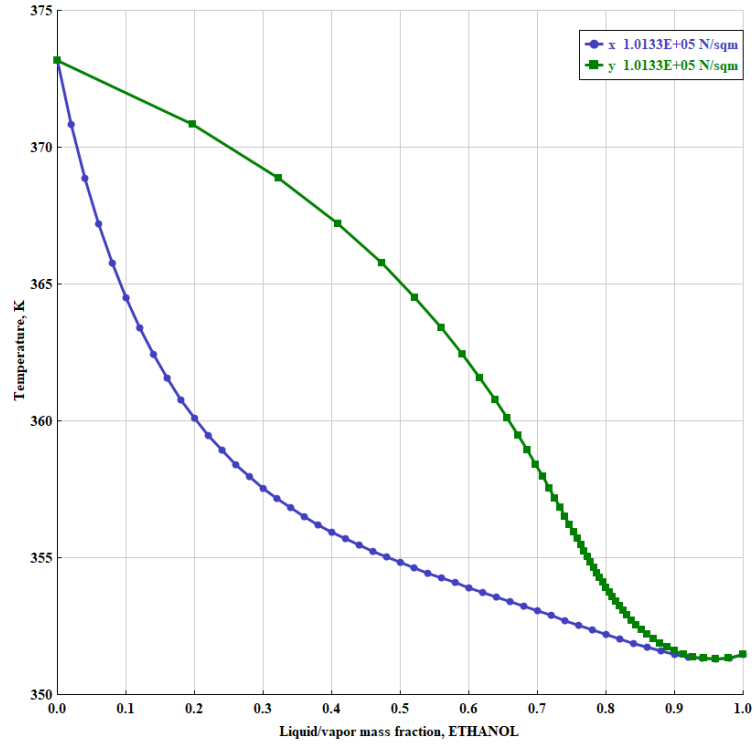


Figure 1.1. T-xy and equilibrium diagram for binary system having minimum boiling azeotrope (ethanol-water)

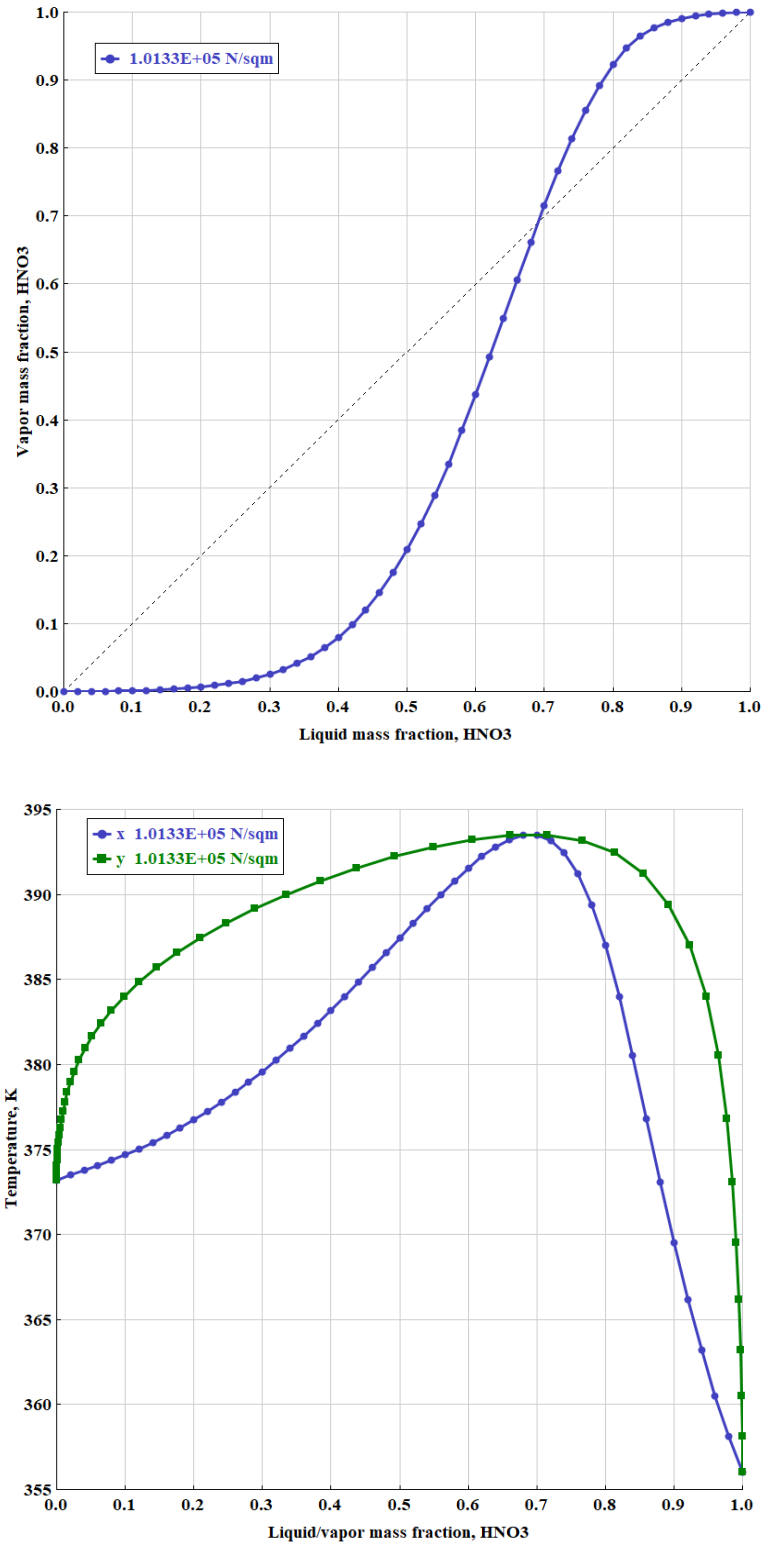


Figure 1.2. T-xy and equilibrium diagram for binary system having maximum boiling azeotrope (nitric acid-water)

1.3.2 Maximum Boiling Azeotrope

In some chemical mixtures, molecules attract each other instead of repulse. The attraction between different (unlike) molecules (A-B) is more potent than the like molecule. These results in maximum boiling azeotropes because the molecular attraction reduces the components' effective vapour pressures, which mean a negative deviation from Raoult's law or ideality. Maximum boiling azeotrope will boil at a higher temperature than the boiling point of pure components. Alternatively, it is known as a negative azeotrope [2, 3]. Figure 1.1 presents T-xy and the equilibrium diagram for the maximum boiling azeotrope.

Examples: Nitric acid-water, n-dimethyl acetamide-acetic acid, acetone-chloroform and formic acid-water.

1.3.3 Homogeneous Azeotrope

If the mixture's constituent has an azeotrope completely miscible or only one liquid phase exists is called a homogeneous azeotrope. Homogeneous azeotrope may be minimum boiling point azeotrope or maximum boiling point azeotrope.

Examples: Ethanol-water, THF-water, acetone-methanol and IPA-water etc.

1.3.4 Heterogeneous Azeotrope

If more than one liquid phase is present, the azeotrope is heterogeneous. Consider the example of n-butanol and water systems. The repulsion between the $\text{CH}_3\text{-CH}_2\text{-CH}_2$ end of n-butanol and the OH end of the water is more. These form a heterogeneous minimum boiling azeotrope with two liquid phases in equilibrium with a vapour phase [2]. Heterogeneous binary azeotropes can be separated without the use of a separating agent. By exploiting the liquid-liquid phase separation, a decanter can produce high-purity products by feeding the two resulting liquid phases to two separate columns.

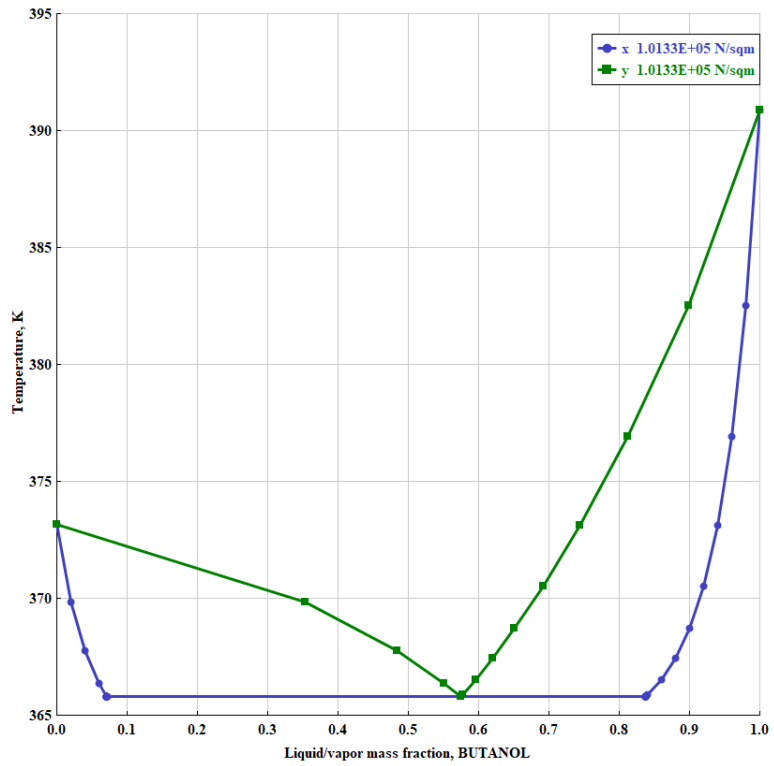
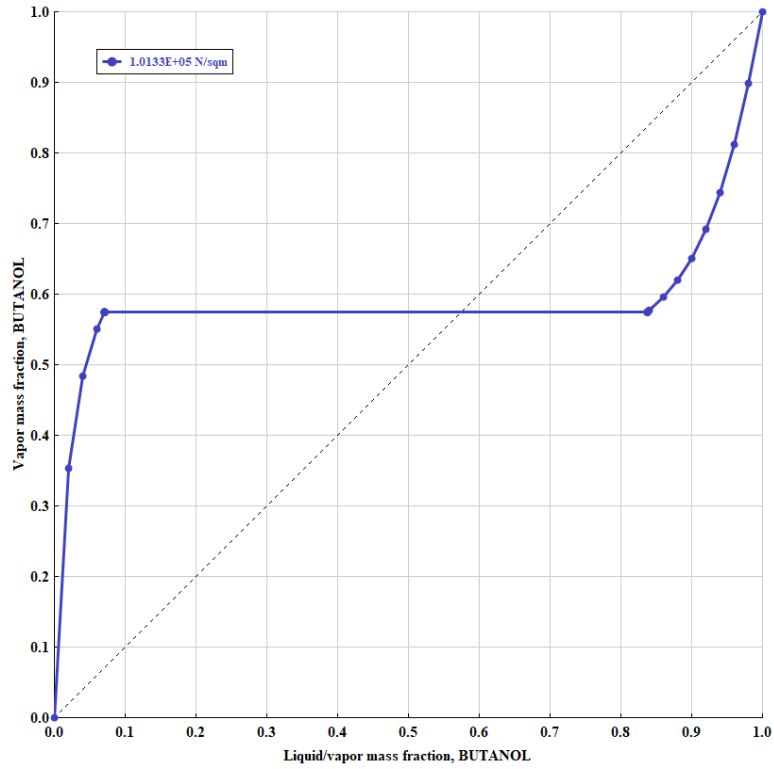


Figure 1.3. T-xy and equilibrium diagram for binary system having minimum-boiling heteroazeotrope (butanol – water)

1.4 Different Methods for Separation of Azeotrope

Since there are different types of azeotrope occurring because of the variety of physical properties of components so; there will be many design methods to achieve separation. The separation methods of the azeotropic mixture are divided into categories depending on the addition of differentiating agents, that is, with or without the addition of an entrainer. Multiple methods may be used to separate homogeneous binary azeotropes of either minimum boiling or maximum boiling.

1.4.1 Using Membrane

If a semipermeable membrane is placed between the vapour and liquid phases, this alters the vapour-liquid equilibrium (VLE) and allows the separation of the constituents in the mixture. This method is known as pervaporation (PV), which comprises of the passage of feed components across a membrane and, subsequently the evaporation at various rates downstream. At high throughput, pervaporation is likely to be costly in terms of both investment and processing costs [5, 6].

1.4.2 Azeotropic Distillation

Adding a light entrainer into the system, so that other azeotropes can form which assist in separation is one of the ways to separate mixtures containing an azeotrope. There are two key characteristics of this supplementary azeotrope; first, the minimum temperatures of all ternary systems should be azeotropic temperature for one additional azeotrope. Second, this azeotrope should be heterogeneous so the separation can be done using simple decanter system. In heterogeneous distillation, a third component called a light entrainer or solvent is added to form a minimum boiling heterogeneous azeotrope, which splits into two liquid phases in the decanter, one liquid phase from the feed to the first column and the other liquid phase from the recovery column. In order to produce a high purity product at the bottom, the recovered entrainer shall be recycled into the first column, while the lighter component and the entrainer shall be supplied into the second column. Some drawbacks associated with this method such as distillation boundaries, a high degree of nonlinearity, multiple steady states, etc. Furthermore, the entrainer must go through the top of the column resulting in significant energy consumption.

1.4.3 Pressure Swing Distillation

The content of the azeotrope varies remarkably with pressure in many mixtures (called pressure-sensitive azeotropes), and the azeotrope may even be eliminated. This phenomenon may be utilized to separate azeotropic mixtures using pressure swing distillation (PSD) without adding a separating agent. A pressure-sensitive azeotrope in a binary mixture moves the distillation boundary, allowing it to be adopted or, sometimes, eliminated at a different pressure. In this a double-column system operating at different pressure is used to achieve the desired separation. For the minimum boiling azeotropic system, the fresh binary mixture feed is mixed with a recycled distillate stream from the second column operating at higher pressure to form the mixed feed stream to the first column operating at lower pressure. The distillate streams, having compositions close to the azeotropic composition at lower pressure, are fed to the second column. The distillate stream of the second column operating at high pressure, containing nearly azeotropic composition at high pressure, is recycled to the low-pressure column. The shift in azeotropic composition at different pressure will help to separate the azeotropic binary mixtures. The pure products are withdrawn from the bottom streams. Pressure swing distillation is applicable only when the azeotropic composition is sensitive to pressure

1.4.3 Extractive Distillation

The binary mixture is put into the extractive distillation column (EDC) over one of the intermediate stages of an extractive distillation system. A few levels above the binary feed mixture stage, the heavier or higher boiling solvent is injected simultaneously. No more azeotrope is introduced to the original mixture by the solvent addition. The extractive distillation column is divided into three subsections due to the different locations where solvent and binary feed are fed, including a rectifying section above the solvent feed stage, an extractive section between the binary feed stage and the solvent feed stage, and a stripping section below the binary feed stage. The heavy solvent causes the light component to rise upward in the column and is recovered as a distillate in practically pure form. The bottom of the EDC is where intermediate boiling and heavy solvent are collected and then transferred to the solvent recovery distillation column (SRDC) for further separation. Based on their high relative volatility, medium boiling and heavy solvent may be separated simply in SRDC. The

distillate is made up entirely of the light component, and the heavy solvent at the bottom of the column is recycled to the EDC.

To achieve complete separation of azeotropic mixtures, various alternative ways are proposed to achieve sharp separation, including extractive distillation, azeotropic distillation and pressure swing distillation. Choosing a distillation method that leads to high product purity with minimum energy consumption and total annual cost (TAC) is always preferred. In most cases, extractive distillation is found to be a better option for the separation of the binary azeotropic mixture than pressure swing distillation (PSD) [7,8] and azeotropic distillation (AD) [9-12] as it leads to less energy requirement for the given separation. Azeotropic distillation has some disadvantages, such as the generation of two liquid phases, formation of an additional ternary azeotrope, multiple steady states, and higher energy requirement, which can be overcome by using the extractive distillation method [9, 10, 13]. PSD can be used only for azeotropic systems where azeotropic compositions are pressure sensitive. In addition, azeotrope composition sensitivity should be sufficient to reduce the recycle flows and the column sizes. The extractive distillation technique is the most preferable over the other one due to its lower energy requirement, flexibility in entrainer selection, simple operation and high-purity product [14].

1.5 Statement of the Problem

When the azeotropic condition occurs in a distillation column, there is no change in the liquid and vapor compositions from tray to tray. This makes it hard to get a sharp separation of the feed mixture using conventional distillation, as an azeotrope acts as a distillation boundary. Therefore, more advanced distillation techniques are required to separate such mixtures.

Several separation methods can be used to obtain the necessary purity, but the most appropriate method should be chosen depending on the entire system's economics. Extractive distillation (ED) and pressure swing distillation (PSD) have been shown to be competitive methods for separating azeotropic systems, and they require 30% to 40% less energy than azeotropic distillation [2]. However, the ability of ED or PSD to separate azeotropic systems varies from system to system.

Various solvents have been reported in the literature for the extractive distillation of some binary azeotropic systems. However, determining a best solvent in terms of operating and capital costs with the desired product purity has proven difficult due to a lack of a common basis for comparison.

Also, the Aspen Plus simulator does not have a built-in binary interaction parameter for many component pairs, leading to improper simulation and unreliable conceptual design of the process. In this work, advanced energy-efficient distillation configurations were developed to separate difficult binary azeotropic and systems that cannot be separated using simple distillation.

The focus of this project is to develop advanced and novel distillation configurations that are both energy-efficient and effective in separating various binary azeotropic systems. These systems are often challenging to separate using simple distillation methods, requiring more complex and innovative approaches. Through our research, we aim to address this challenge by exploring a range of distillation configurations and developing new solutions that can improve separation efficiency while reducing energy consumption. By doing so, we hope to contribute to the development of more sustainable and efficient separation processes across a range of industries. To optimize the conceptual design of an advanced distillation system, consider essential VLE data, a thermodynamic activity coefficient model, sensitivity analysis, and techno-economic optimization of design parameters. The data helps determine optimal operating conditions, while a model accounts for non-ideal behavior. Sensitivity analysis identifies critical parameters, and techno-economic optimization balances separation performance and equipment cost.

The **objectives** of the project are:

- Evaluation of various possible novel entrainers for altering the azeotropic/close-boiling behaviour of the systems through experimental VLE analysis
- Development of a thermodynamic model and its validation for new entrainer systems using experimental VLE data.
- Conceptualization, optimization, and modelling of a pressure swing and enhanced extractive distillation system for industrial applications
- Development of an energy-saving configuration by adopting heat integration
- Development of an optimization approach for the conceptual design of an advanced distillation configuration, starting from VLE data, activity coefficient model, sensitivity analysis, and techno-economic parameters.

1.6 Structure of Thesis

Chapter 2 analyses extractive and pressure-swing distillation methods through steady-state ASPEN Plus simulations to propose the most economical method for separating an equimolar mixture of THF-Water. DMSO was identified as the most appropriate solvent for extractive distillation, and various pressure ranges were explored for pressure swing distillation to achieve minimum TAC. The optimum designs of extractive and pressure swing distillation with and without heat integration were compared on a common basis of feed conditions and purity constraints.

Chapter 3 proposes an extractive distillation configuration using sulfuric acid as a solvent for dehydrating maximum boiling nitric acid water system. Nitric acid / water / sulfuric acid binary and ternary systems' vapour-liquid equilibrium was thermodynamically modelled utilizing the eNRTL-RK (Electrolyte Non-Random Two Liquid-Redlich Kwong) thermodynamic property method in the Aspen Plus process simulator. The model performance was validated by comparing the experimental data with the data estimated by the eNRTL-RK model. The development of a triple-column extractive distillation sequence, consisting of a pre-concentrating column, an extractive distillation column, and a solvent recovery column, is then carried out. The configuration is designed, simulated and optimized to concentrate dilute nitric acid using sulphuric acid as a solvent to break the nitric acid water azeotrope. The operational and structural distillation configuration parameters are optimized to reduce energy consumption and total annual cost (TAC) of the overall configuration.

In Chapter 4, calcium chloride (CaCl_2), lithium bromide (LiBr) and zinc chloride (ZnCl_2) salts were explored as possible entrainers for breaking the minimum boiling azeotrope of ethanol and water. Isobaric vapor-liquid equilibrium (VLE) data for the binary systems of water + ethanol and ternary system of water + ethanol + calcium chloride/lithium bromide and zinc chloride were measured at a constant pressure of 94.5 kPa. The effect of salts on the relative volatility of ethanol to water as well as on the vapor phase mole fractions of ethanol were also studied experimentally. Electrolyte nonrandom two-liquid (eNRTL) model was used to correlate the experimental VLE data. The experimental data obtained in this work was validated using Van Ness thermodynamic consistency test.

Chapter 5 analyzed the influence of anisole and NEP on the VLE behaviour of methylcyclohexane and toluene low relative volatility system. The isobaric vapor-liquid equilibrium (VLE) data for the binary systems of methylcyclohexane + toluene, methylcyclohexane + anisole,

methylcyclohexane + NEP, toluene + anisole, and toluene + NEP were measured at 92.0 kPa. The NRTL, UNIQUAC, and Wilson thermodynamic activity coefficient models were used in the regression of experimental data to obtain the binary interaction parameters. The Van Ness and infinite dilution tests were used to confirm the thermodynamic consistency of the experimental VLE data.

1.7 Reference

- [1] M.F. Doherty, and M.F., Malone, Conceptual design of distillation systems. McGraw-Hill, 2001.
- [2] W.L. Luyben, Distillation Systems for Separating Design and Control of Distillation Systems for Separating, 2016
- [3] A.A. Kiss, Advanced Distillation Technologies: design, control and applications, John Wiley & Sons 2013.
- [4] S. Widagdo, W.D. Seider, Azeotropic Distillation, AIChE J. 42 (1996) 96–130.
- [5] T. Mahdi, A. Ahmad, M.M. Nasef, A. Ripin, State-of-the-art technologies for separation of azeotropic mixtures, Sep. Purif. Rev. 44 (2015) 308–330.
- [6] R. Smith, Chemical Process Design and Integration, John Wiley & Sons Ltd. 2005.
- [7] W.L. Luyben, Comparison of extractive distillation and pressure-swing distillation for acetone-methanol separation, Ind. Eng. Chem. Res. 47 (2008) 2696–2707.
- [8] W.L. Luyben, Comparison of extractive distillation and pressure-swing distillation for acetone/chloroform separation, Comput. Chem. Eng. 50 (2013) 1–7.
- [9] A.A. Kiss, D.J.P.C. Suszwalak, Enhanced bioethanol dehydration by extractive and azeotropic distillation in dividing-wall columns, Sep. Purif. Technol. 86 (2012) 70–78.
- [10] A. Meirelles, S. Weiss, H. Herfurth, Ethanol dehydration by extractive distillation, J. Chem. Technol. Biotechnol. 53 (1992) 181–188.

- [11] S. Arifin, I.L. Chien, Design and control of isopropyl alcohol dehydration via homogeneous azeotropic distillation using dimethyl sulfoxide as extractive agent, *AIChE Annu. Meet. Conf. Proc.* (2006) 790–803.
- [12] Y.C. Chen, B.Y. Yu, C.C. Hsu, I.L. Chien, Comparison of heteroazeotropic and extractive distillation for the dehydration of propylene glycol methyl ether, *Chem. Eng. Res. Des.* 111 (2016) 184–195.
- [13] R.P. Brito, Optimization of the design and operation of extractive distillation processes, *Sep. Sci. Technol.* 50 (2015) 2238–2247.
- [14] Z. Lei, C. Li, B. Chen, Extractive distillation: a review, *Sep. Purif. Rev.* 32 (2003) 121-21

Chapter 02

Comparative Analysis of Extractive and Pressure Swing Distillation for Separation of THF-Water Separation

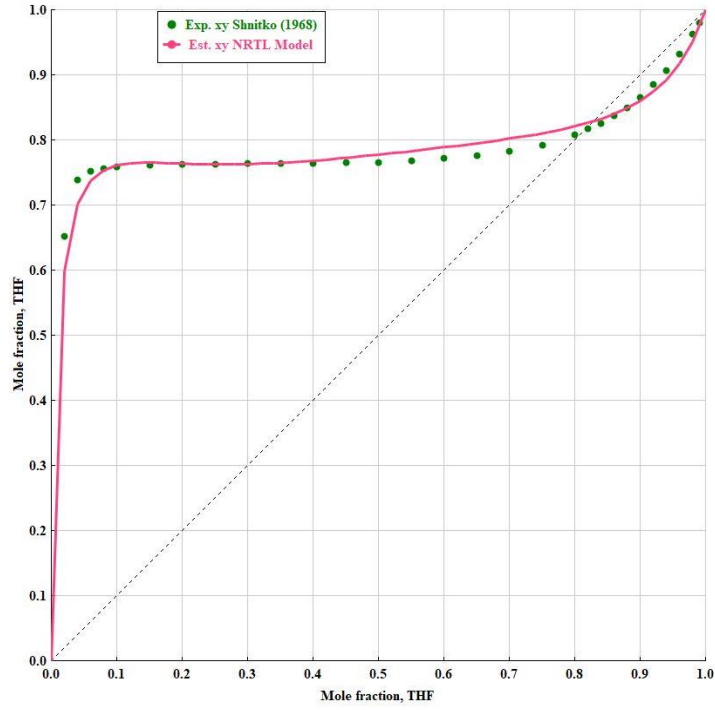
Chapter 2 Comparative Analysis of Extractive and Pressure Swing Distillation for Separation of THF-Water Separation

Abstract

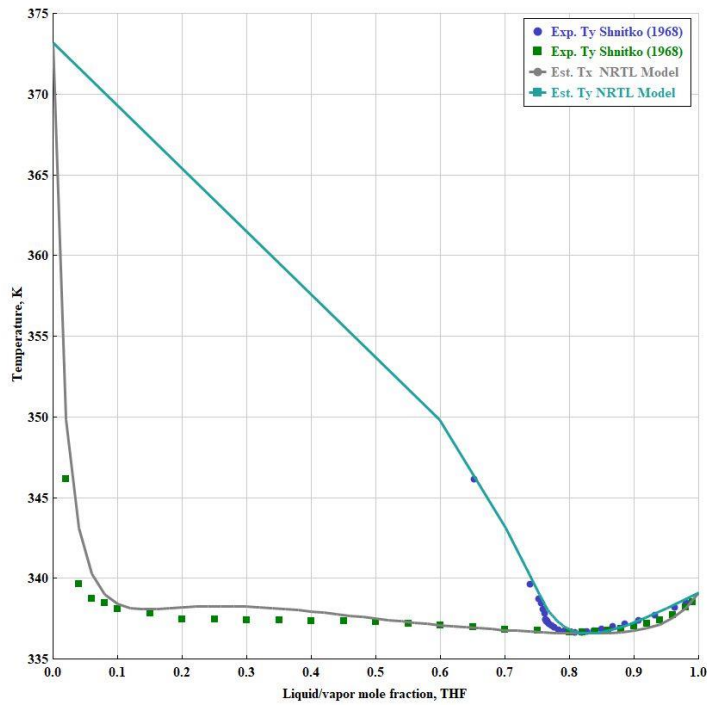
In the present work, extractive and pressure-swing distillation methods are analyzed in detail through steady-state ASPEN Plus simulations to propose the most economical method for separating the equimolar mixture of THF-Water. Various solvents were evaluated, and DMSO was identified as the most appropriate solvent, as it gave minimum total annual cost (TAC) for desired purity. In the case of pressure swing distillation, various pressure ranges were explored to achieve minimum TAC. Configurations for extractive and pressure swing distillation with heat integration were also worked out. The optimum designs of extractive and pressure swing distillation with and without heat integration were compared on a common basis of feed conditions and purity constraints. Results indicate that the TAC of extractive distillation with heat integration is 5.2 % less than that of PSD with partial heat integration.

2.1 Introduction

Tetrahydrofuran (THF) is an industrially useful organic solvent widely used in adhesives, polymer, paint and pharmaceutical industries. THF (65.97 °C) forms a minimum boiling homogeneous azeotrope with water (100 °C) at atmospheric pressure and 63.43 °C with the azeotropic composition of 95.09 wt. % (82.87 mol %) of THF, as shown in Figures 2.1 (a) and (b). Thus, it is impossible to separate the THF-water mixture by conventional distillation. Hence, various distillation techniques must be considered for azeotropic mixture separation, such as pressure swing distillation (PSD) and extractive distillation (ED). Each separation technique may have pros and cons for separating an azeotropic system. It may be possible to achieve the separation with desired purity by using one or more separation methods; however, the most appropriate separation method should be selected based on operating cost and the economics of the overall system.



(a)



(b)

Figure 2.1. (a) yx diagram (●) experimental data [20] (—) NRTL model data (b) Txy diagram for THF-water system at 1 atm pressure (■) Tx data (●)Ty experimental data [20] (—) NRTL model data using Aspen Plus

Several authors have performed comparative studies of pressure swing and extractive distillation for various minimum and maximum azeotropic systems. W. L. Luyben [1, 2] studied the separation of minimum boiling acetone-methanol system and maximum boiling acetone-chloroform systems through steady-state simulations. He found that extractive distillation was more suitable than pressure swing distillation in terms of capital cost and energy consumption for both these cases. Similar studies were carried out for the separation of equimolar di-n-propyl ether and n-propyl alcohol system [3], isopropyl alcohol and diisopropyl ether [4] and methanol and chloroform [5] by pressure swing distillation and extractive distillation. All these studies found pressure swing distillation more economical than extractive distillation in terms of the total annual cost of the complete system for the respective azeotropic system. The various other reported studies [6-8] indicate that extractive and pressure swing distillation performance for separation of the azeotropic system varies from system to system. Hence, both are competitive for separating azeotropic systems for which azeotropic compositions are pressure-sensitive.

In this chapter, the extractive and pressure swing distillation methods are compared for separating THF from water. So far, no published data directly compares these two techniques for THF-water separation. The extractive distillation system considered here comprised of extractive distillation column (EDC) and solvent recovery distillation column (SRDC). Pressure swing distillation system comprised of two column configurations operating at different pressures. Four different solvents were evaluated for extractive distillation to develop the most optimum configuration.

In contrast, six different pressure ranges were analyzed for pressure swing distillation to arrive at the best pressure range. Configurations with partial and full heat integration were also analyzed for extractive and pressure swing distillation. Minimum total annual cost (TAC) was taken as the decision-making criterion for both analyses.

2.2 THF-Water Separation Using Extractive Distillation

In an extractive distillation system, the binary mixture is fed at one of the intermediate stages of the extractive distillation column (EDC). At the same time, the heavy or higher boiling solvent is

added at a few stages above the binary feed mixture stage. The addition of solvent does not introduce any additional azeotrope with the original mixture. Due to the different feed locations of solvent and binary feed, the extractive distillation column is divided into three subsections, as shown in Figure 2.2, which are rectifying section above the solvent feed stage, the extractive section in between the binary feed stage and the solvent feed stage; and stripping section, below the binary feed stage. Heavy solvent alters the relative volatility of the binary mixture and causes THF to move upward in the column and is recovered as a distillate in almost pure form. In contrast, water and heavy solvent are collected from the bottom of the EDC, which is sent to the solvent recovery distillation column (SRDC) for further separation.

In SRDC, simple binary separation of water and the heavy solvent is achieved based on the high relative volatility between them. Pure water is recovered as the distillate, and the heavy solvent from the bottom of the column is then recycled to the EDC. Usually, a cooler is placed in the recycled loop between the two columns to reduce the solvent feed temperature. A small amount of solvent is lost along with the water stream, balanced by adding the pure solvent through the solvent makeup stream.

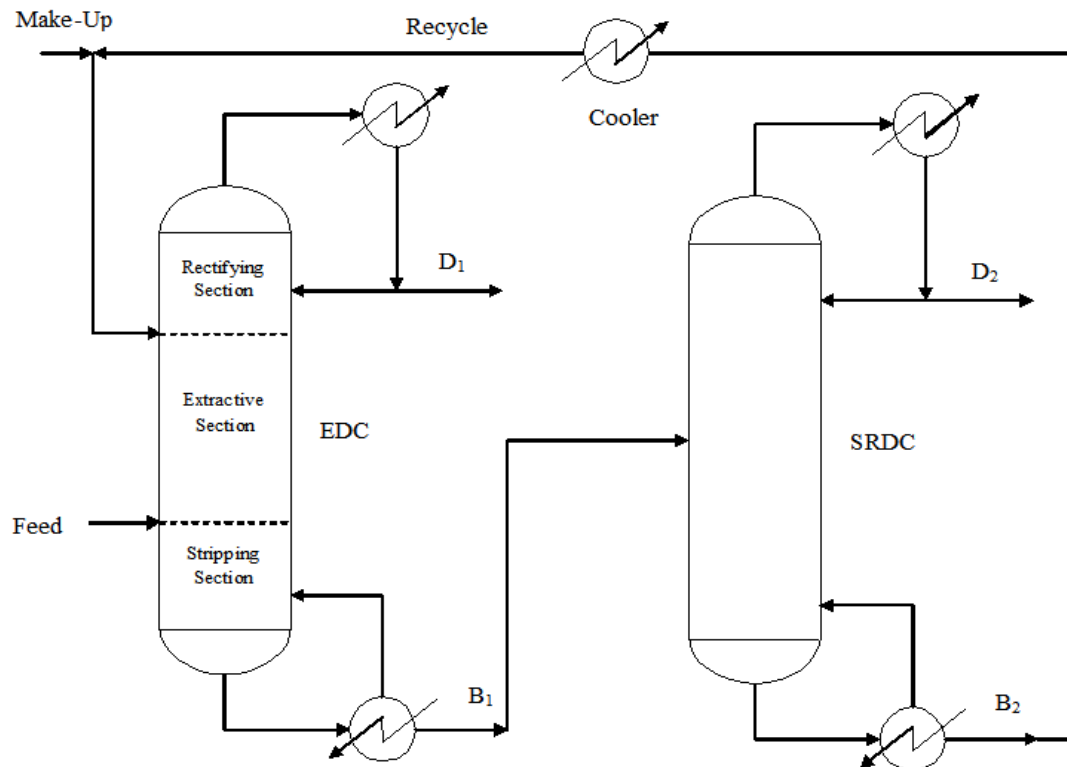


Figure 2.2. Extractive distillation flow diagram

An extractive distillation's separation performance depends on the solvent's influence on the VLE of the binary mixture to be separated. Several authors proposed various solvents for separating the THF-water mixture based on their simulation or experimental analysis. Xu and Wang [9, 10] used the 1,2- propanediol to separate THF-water. Using rigorous simulation in the HYSYS simulator and experimental analysis of batch extractive distillation system, they found that 1,2- propanediol was a suitable solvent for this separation. Gomez and Gil [11] simulated the dehydration of THF through extractive distillation by taking 100 kmol/h of azeotropic feed as a basis. Authors claimed purity of 99.95 mole % of THF could be achieved with glycerol as a solvent compared to the other two solvents considered 1,2-propanediol and 1,4-butanediol. Fan et al. [12], in their simulation work, used ethylene glycol as an entrainer for the separation of 90 wt % THF and 10 wt % water with a feed rate of 3000 kg/h. They reported a purity of 99.9 wt % THF from the distillate of the EDC.

Zhang et al. [13] developed vapour liquid equilibrium (VLE) data for THF + water + solvent ternary system at atmospheric pressure with 1,2-propanediol and DMSO as solvents. They found that DMSO is a more capable solvent for breaking THF-water azeotrope than 1,2-propanediol as the less amount of DMSO needed to achieve the separation. Deorukhkar et al. [14] performed experiments on pilot distillation setup in batch, semi-batch and continuous modes with DMSO and 1, 2-propanediol as solvents. They proposed the DMSO as a better solvent than 1, 2-propanediol.

It was found from the literature that several solvents were reported for the dehydration of THF based on models and tests. Due to the lack of a standard comparison method, it is challenging to determine which system is optimum for a whole extractive distillation system, including the solvent recovery column, in terms of operational and capital expenses. Hence, this section identified the most suitable solvent for separating THF-water by taking a basis of equimolar feed and a target purity of 99.99 mole % for THF and water. Both capital and operating costs were estimated and presented in the form of TAC of the complete extractive distillation system with various reported solvents.

2.2.1 Basis of Economical Analysis

All economic calculations to determine TAC were performed according to the equations listed in Table 2.1, taken from Luyben and Chien [15]. Total annual cost (TAC) is the addition of total

annual operating cost and total capital cost divided by the payback period. In calculating the capital cost, only the cost of major pieces of equipment in the distillation system like column shell, reboiler and condenser was considered, and the cost of reflux drums, pump and valves was neglected as it would be very negligible as compared to the cost of column and heat exchangers. The “Tray Sizing” functions with the sieve tray in the Aspen Plus simulator was used to determine the diameter of the columns. The height of the column was assumed to be 20 % more than the required height for the trays, and a typical distance of 0.61 m between the trays was considered. As per ASPEN Plus distillation model (RADFRAC) notation, the first stage is considered a condenser, while the last stage is a reboiler.

2.2.2 Simulation Analysis of Extractive Distillation System

In this section, the extractive distillation column and solvent recovery column were simulated simultaneously for the separation of the THF-water mixture with four solvents, DMSO, 1,2-propanediol (1,2-PDO), glycerol and ethylene glycol to achieve required purity. These simulation results will form a basis for direct comparison among various solvents to determine the best minimum TAC. The equimolar feed composition of THF and water (50 mole % of THF and 50 mole % of water) with a flow rate of 100 kmol/h was taken as the basis for the simulation. The product purity specification of both the components was set to be at 99.99 mole % of THF and 99.99 mole % of water in the distillate of the EDC and SRDC, respectively.

Table 2.1. Basis of economics and equipment sizing

Column Diameter (D): Aspen tray sizing

Height (H) of a distillation column,

$$H = 1.2 \times 0.61 \times (N_s - 2) \quad (\text{D and H are in meters})$$

$$\text{Column shell cost (\$)} = 17640 \times (D)^{1.066} \times (H)^{0.802}$$

Condenser:

$$\text{Area (m}^2\text{), } A_c = \frac{Q_c}{U_c \times \Delta T_{lm}}$$

$$\text{Heat transfer coefficient (} U_c \text{)} = 0.852 \text{ kW/m}^2\text{K}$$

$$\text{Capital cost (\$)} = 7296 (A_c)^{0.65}$$

Reboiler:

$$\text{Area (m}^2\text{), } A_r = \frac{Q_r}{U_r \times \Delta T_{lm}}$$

Heat transfer coefficient (U_r) = 0.568 kW/m²K

$$\text{Capital cost (\$)} = 7296 (A_r)^{0.65}$$

Cooler:

$$\text{Area (m}^2\text{), } A_{\text{cooler}} = \frac{Q_{\text{cooler}}}{U_{\text{cooler}} \times \Delta T_{lm}}$$

Heat transfer coefficient (U_{cooler}) = 0.852 kW/m²K

$$\text{Capital cost (\$)} = 7296 (A_{\text{cooler}})^{0.65}$$

Energy costs:

LP steam (433 K) = \$7.72 per GJ

MP steam (457 K) = \$8.22 per GJ

HP steam (537 K) = \$9.88 per GJ

$$\text{TAC} = \frac{\text{Capital cost}}{\text{Payback period}} + \text{Energy cost}$$

Payback period = 3 years

The activity coefficient model NRTL was used to consider the non-ideality of the liquid phase and ideal vapour phase behaviour was assumed. The NRTL built-in binary interaction parameters available in the Aspen data bank were used for the simulation. In contrast, for the component pairs THF-glycerol and THF-1,2-propanediol, for which no ASPEN built-in interaction parameters were available, the parameters were estimated through the UNIFAC group contribution method and are given in Table 2.2.

Table 2.2. Binary interaction parameter estimated by UNIFAC

Component i	THF	THF
Component j	Glycerol	1, 2-Propanediol
A _{ij}	0	0
A _{ji}	0	0
B _{ij}	1298.88	819.92
B _{ji}	75.5122	-41.7627

C _{ij}	0.3	0.3
-----------------	-----	-----

This chapter extensively explains a simulation study of extractive distillation using DMSO as the solvent to explain the simulation technique. While deciding the operating pressure of the columns, it was ensured that cooling water could be used as a utility with an outlet temperature of 305 K. Operating EDC at higher pressure would lead to an increase in reboiler temperature and hence, the operating cost, as high-pressure steam will be required as a utility in the reboiler. According to Luyben [16], commonly used heuristics for distillation column pressure selection do not always give an optimum column pressure for the separation under consideration. Hence, the TAC of the extractive distillation column at various operating pressures was estimated to find out a suitable EDC pressure with a constraint of having the difference between cooling water return temperature and reflux drum temperature to be at least 20 K ($\Delta T_{lm} \geq 20$ K). The pressure was varied from 2 atm and was restricted to 0.65 atm as below 0.65 atm pressure ΔT_{lm} goes below 20 K. The designs were obtained through detailed sensitivity analysis of various operating parameters with a fixed number of stages, and the results are given in Table 2.3.

According to the findings in table 2.3, greater operating pressures are associated with a considerable rise in the column's TAC. Capital cost increases for below atmospheric column pressures as vacuum distillation operation demands bigger column diameters and condensers. However, it decreases the operating cost as, at reduced pressures, relative volatility improves, which leads to smaller reflux ratios and reboiler duties. In the present system, a similar effect was observed for EDC at reduced pressures, but no significant reduction in TAC was observed. Also, an additional capital and operating cost for the vacuum pump will further reduce the TAC advantage of reduced column pressure operation. Hence, in this case, it was decided to go ahead with atmospheric pressure for the EDC.

It was proposed to operate the solvent recovery column under vacuum to reduce the reboiler temperature and, subsequently, the required utility steam pressure. If the operating pressure is lower than 0.15 atm, the condenser would need chilled water as a cooling utility, consequently increasing the operating cost. Hence, SRDC was proposed to be operated at 0.15 atm since cooling water can be used as a cooling utility in the condenser of the column.

Table 2.3. Comparison of designs of EDC at various operating pressures

Parameters	EDC Operating Pressure						
	2 atm	1.5 atm	1 atm	0.9 atm	0.8 atm	0.7 atm	0.65 atm
N_T	21	21	21	21	21	21	21
D (m)	0.84	0.63	0.66	0.67	0.68	0.69	0.70
H (m)	13.90	13.90	13.90	13.90	13.90	13.90	13.90
RR	1.71	0.44	0.38	0.36	0.34	0.32	0.31
E/F	0.55	0.35	0.25	0.25	0.25	0.25	0.25
Q_R (kW)	1491.6	853.7	750.3	731.1	711.7	691.4	680.80
A_R (m ²)	85.88	58.83	30.28	27.56	25.02	22.61	21.44
Q_C (kW)	1071.5	581.9	573.4	568.1	563.7	559.8	558.07
A_C (m ²)	22.00	14.48	19.73	21.57	24.14	27.92	30.56
Total capital (10 ⁶ \$)	0.3079	0.2336	0.2107	0.2112	0.2133	0.2175	0.2209
Total operating (10 ⁶ \$/yr)	0.3531	0.1913	0.1681	0.1638	0.1595	0.1549	0.1525
TAC (10 ⁶ \$/yr)	0.4558	0.2691	0.2384	0.2342	0.2306	0.2274	0.2262

The various design variables in the extractive distillation system which need to be determined for optimum performance are listed below.

- Solvent to feed ratio (E/F)
- Total number of stages of EDC (N_{T1}) and SRDC (N_{T2})
- Binary mixture feed stage (N_{FF}) for EDC
- Solvent feed stage location (N_{EF})
- Temperature of solvent feed (T_{EF})
- Molar reflux ratio of EDC (RR_1) and SRDC (RR_2)
- Feed stage location of SRDC (N_{F2}).

All these design variables were optimized to achieve the specified purity with minimum TAC. Sensitivity analysis was used to investigate the effect of all these parameters on the columns' product

purities and heat duties. It is possible to achieve the desired purity with some minimum reflux ratio value, below which purity drops and above which purity does not improve significantly but increases the reboiler duty unnecessarily. Thus, for a distillation column, there will be multiple values of molar reflux ratio for which desired purity can be achieved. However, there will be a unique value of molar reflux ratio for which purity is matched, and the reboiler duty is minimum. Hence, the present analysis considers the molar reflux ratio the design variable. For each combination of total stage number and feed stage locations, the molar reflux ratio value for which purity constraint is matched with minimum reboiler duty was worked out. In the present simulation analysis, the molar reflux ratio was estimated through the Design Spec feature of the ASPEN simulator for both columns. The temperature of solvent feed (T_{EF}) was found to significantly affect the distillate purity and the reboiler duty of EDC for different reflux ratios. From the sensitivity analysis results, the solvent feed temperature (T_{EF}) was fixed at 60 °C, which is in good agreement with the suggestion of Knight and Doherty [17] for solvent feed temperature.

The EDC's most essential design variables are solvent-to-feed ratio (E/F) and molar reflux ratio (RR), directly affecting product purity and energy consumption. The effect of solvent-to-feed molar ratio (E/F) and reflux ratio (RR_1) on the distillate THF mole composition (X_D) of EDC with $N_{T1} = 21$ can be seen from the sensitivity analysis results shown in Figure 2.3. It was observed that at higher reflux ratios (RR_1) and solvent to feed ratios (E/F), the mole fractions of THF in the distillate are higher because, at higher values of solvent to feed ratio, the dilution of the solvent caused by the reflux is less which helps to increase the distillate purity. At a fixed value of molar reflux ratio (say $RR_1=0.4$), solvent to feed molar ratio (E/F) of 0.25 or higher was required to achieve the desired purity of THF, which is almost constant beyond this value, as shown in Figure 2.3. The reboiler duty (Q_R) increases significantly with the solvent to feed molar ratio (E/F) value. Thus, an optimal E/F value could be 0.25 because at this value desired purity of THF is achieved with minimum reboiler duty.

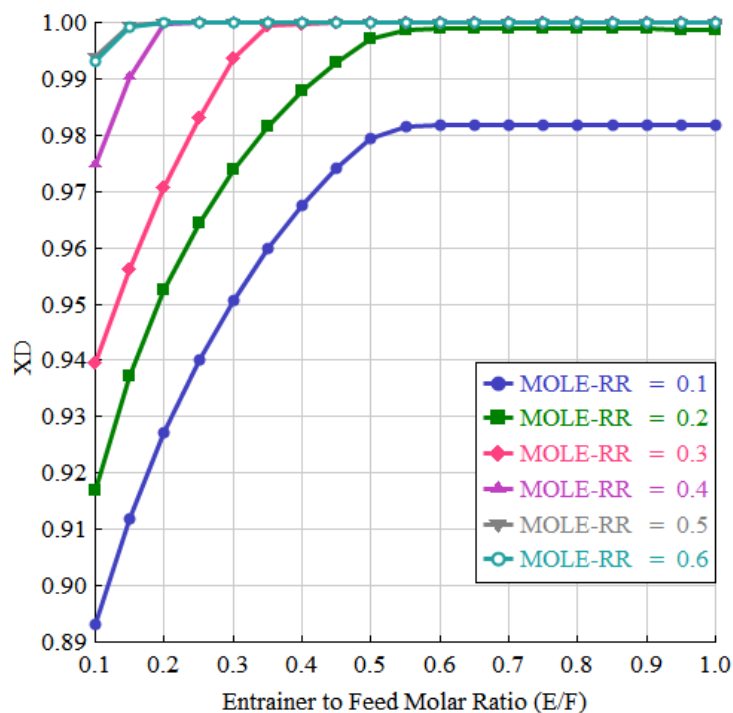
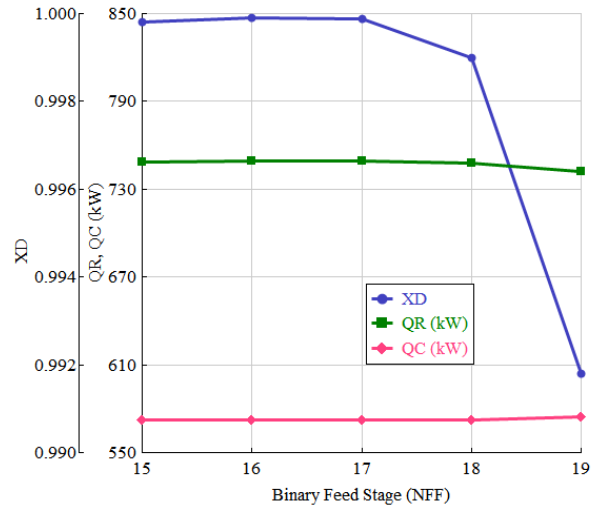
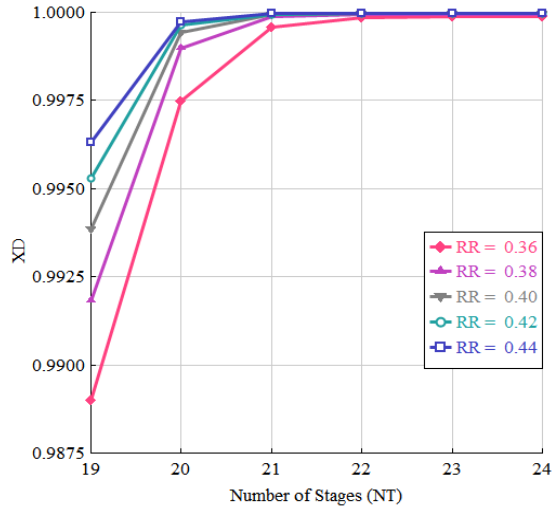


Figure 2.3. Effect of E/F and reflux ratio on the distillate stream THF composition (X_D)

Adding trays in the distillation column improves the separation capacity of the column. However, it also increases the capital cost, so finding an optimum number of stages in EDC and SRDC is crucial. The preliminary value of N_{T1} and N_{FF} was fixed by the sensitivity analysis of the various parameters to achieve the specified product purity with minimum energy consumption. The effect of the varying total number of stages (N_T) on distillate purity (X_D) for each solvent case is shown in Figures 2.4 (a) to 2.7 (a). It was seen that, at $N_T = 21$, the desired product purity ($X_D = 0.9999$) was obtained. Beyond this, the composition of distillate does not change significantly concerning the N_T for the DMSO, ethylene glycol and glycerol as solvents. In the case of the 1, 2-propanediol as a solvent, a similar effect was observed at $N_T = 22$.

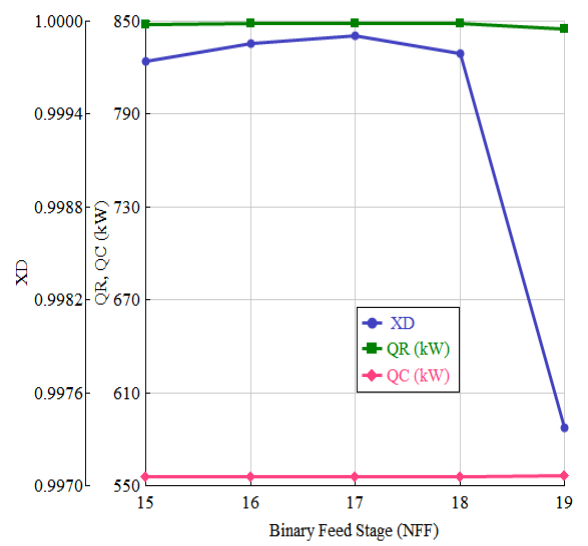
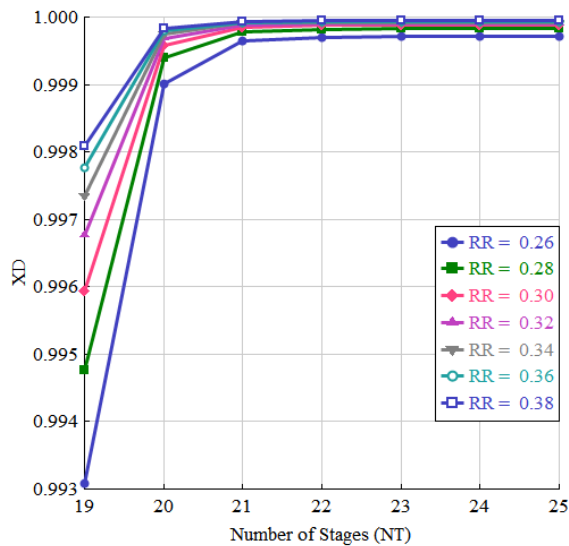
Effect binary feed stage (N_{FF}) on X_D , Q_R and Q_C is shown in Figure 2.4 (b) to 2.7 (b) for each solvent case, and it can be observed that the desired product purity was achieved when the binary mixture is fed at stage $N_{FF} = 17$ with minimum energy consumption. Table 2.4 shows the economic optimization results for EDC having DMSO as a solvent. Similarly, optimum N_{T1} and N_{FF} values for each solvent case were obtained.



(a)

(b)

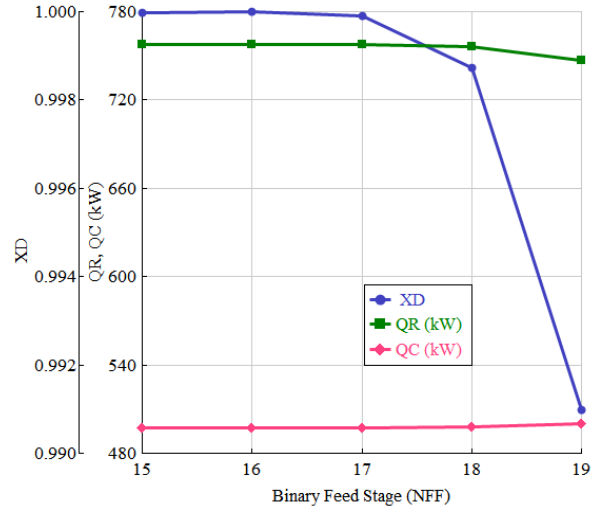
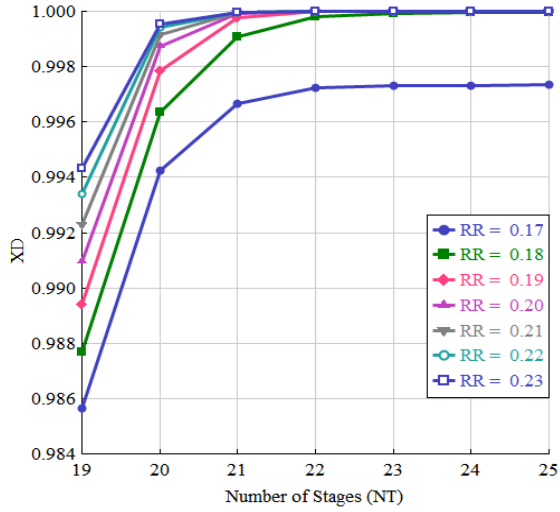
Figure 2.4. (a) Effect of the total number of stages (N_T) on the distillate purity (X_D) (b) Effect of binary feed stage (N_{FF}) on X_D , Q_R and Q_C for DMSO as a solvent



(a)

(b)

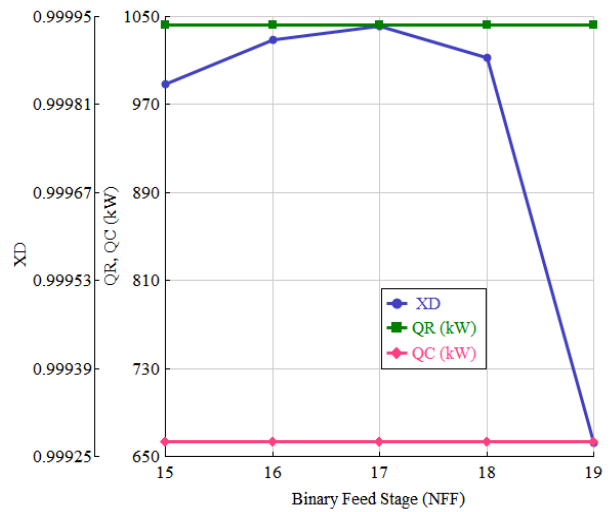
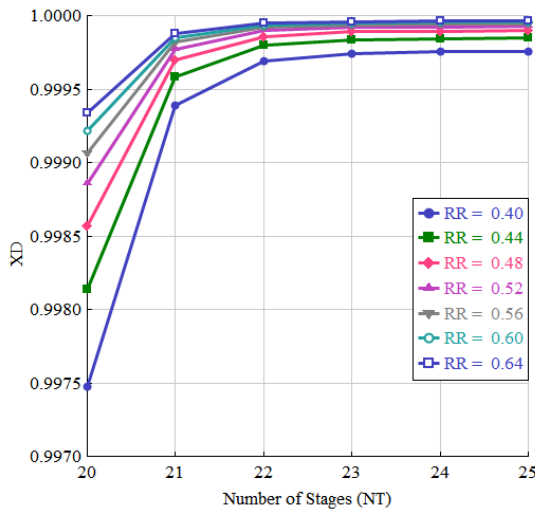
Figure 2.5. (a) Effect of the total number of stages (N_T) on the distillate purity (X_D) (b) Effect of binary feed stage (N_{FF}) on X_D , Q_R and Q_C for ethylene glycol as a solvent



(a)

(b)

Figure 2.6 (a) Effect of the total number of stages (N_T) on the distillate purity (X_D) (b) Effect of binary feed stage (N_{FF}) on X_D , Q_R and Q_C for glycerol as a solvent



(a)

(b)

Figure 2.7. (a) Effect of the total number of stages (N_T) on the distillate purity (X_D) (b) Effect of binary feed stage (N_{FF}) on X_D , Q_R and Q_C for 1, 2-propanediol as a solvent

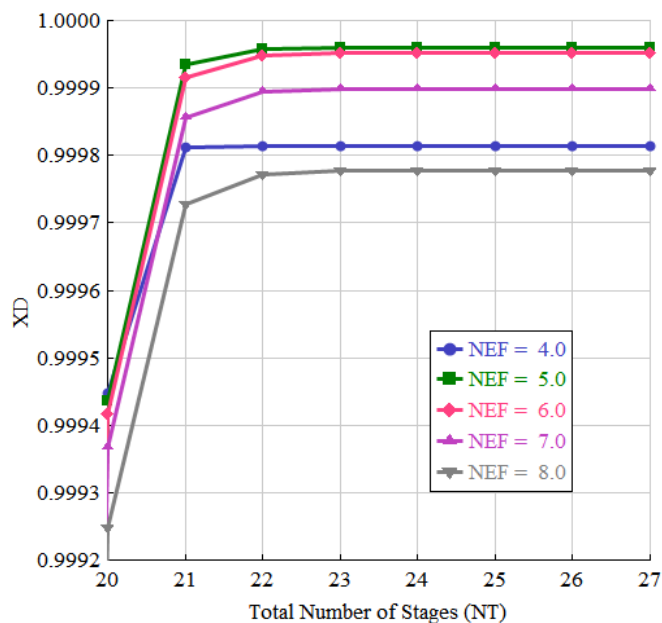


Figure 2.8. Effect of solvent feed stage (N_{EF}) with respect to the total number of stages (N_T) on the distillate composition (X_D) for DMSO as a solvent

The solvent feed stage number (N_{EF}) was optimized to achieve the desired purity with minimum energy consumption. The effect of the total number of stages (N_T) and solvent feed stage (N_{EF}) on the distillate composition (X_D) was plotted by using sensitivity analysis of EDC and is shown in Figure 2.8. From this plot, it was observed that at $N_{EF} = 5$, the maximum purity in the distillate was achieved concerning the different N_T .

The details of economic optimization results for the DMSO solvent are summarized in Table 2.4. The first total number of EDC (N_{T1}) stages was varied to find optimum stages by keeping the SRDC (N_{T2}) stages constant. In each case, the optimum binary mixture feed stage (N_{FF}), solvent feed stage (N_{EF}), solvent to feed ratio and molar reflux ratio were obtained by minimizing the TAC of the system. Table 2.4 shows that, for simulation case 2, minimum TAC was obtained with 21 total stages and a solvent flow rate of 25 kmol/hr ($E/F = 0.25$). For the SRDC, optimum stages were found by varying its stages and keeping the number of stages in the EDC constant at optimum value 21 to obtain minimum TAC. It can be observed from Table 2.5 for case 7, having a total number of stages 14 with the feed stage location (N_{F2}) at 6 and a molar reflux ratio of 0.1, giving the minimum TAC. The steady-state design flowsheet with optimal operating conditions, reboiler and condenser duties, detail stream information and column diameter is given in Figure 2.9 (a).

Table 2.4. Economic optimization results for EDC

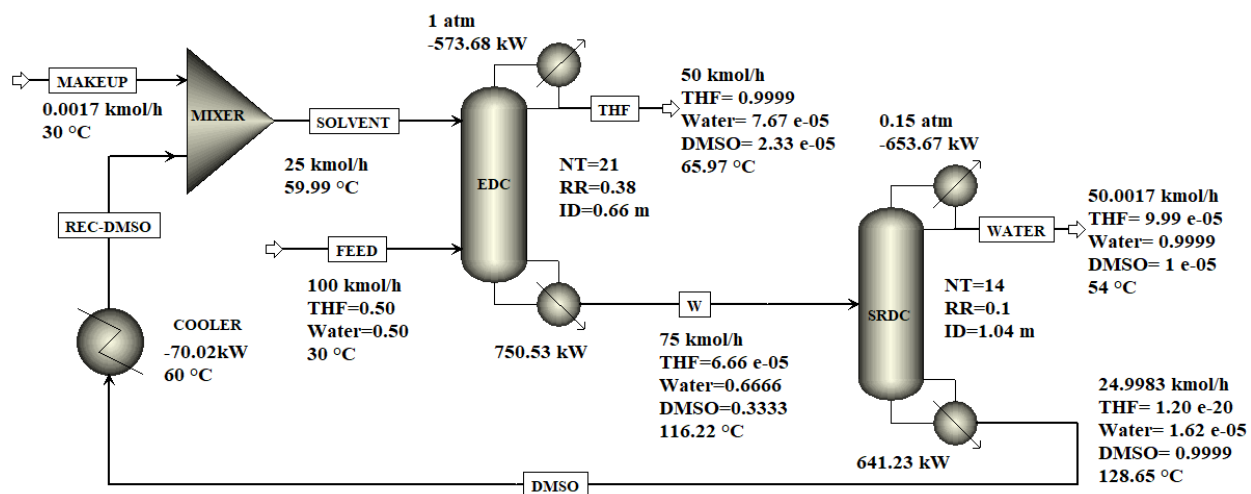
Parameter	Case 1	Case 2	Case 3	Case 4	Case 5
N_{T1}	19	21	23	25	27
N_{T2}	14	14	14	14	14
E/F (optimum)	0.25	0.25	0.25	0.2	0.2
N_{FF} (optimum)	16	17	19	21	23
N_{EF} (optimum)	5	5	5	5	5
D (m)	0.70	0.66	0.66	0.66	0.66
RR_1 (optimum)	0.56	0.38	0.38	0.40	0.40
Q_{R1} (kW)	821.4	750.5	746.8	744.9	744.6
Q_{C1} (kW)	644.5	573.7	570.0	581.5	581.2
Q_{cooler} (kW)	70	70	70	56	56
Total capital (10^6 \$)	0.4786	0.4729	0.4799	0.4849	0.4924
Total operating (10^6 \$)	0.3277	0.3118	0.3110	0.3104	0.3104
TAC (10^6 \$ /yr)	0.4872	0.4695	0.4710	0.4721	0.4745

Table 2.5. Economic optimization results for SRDC

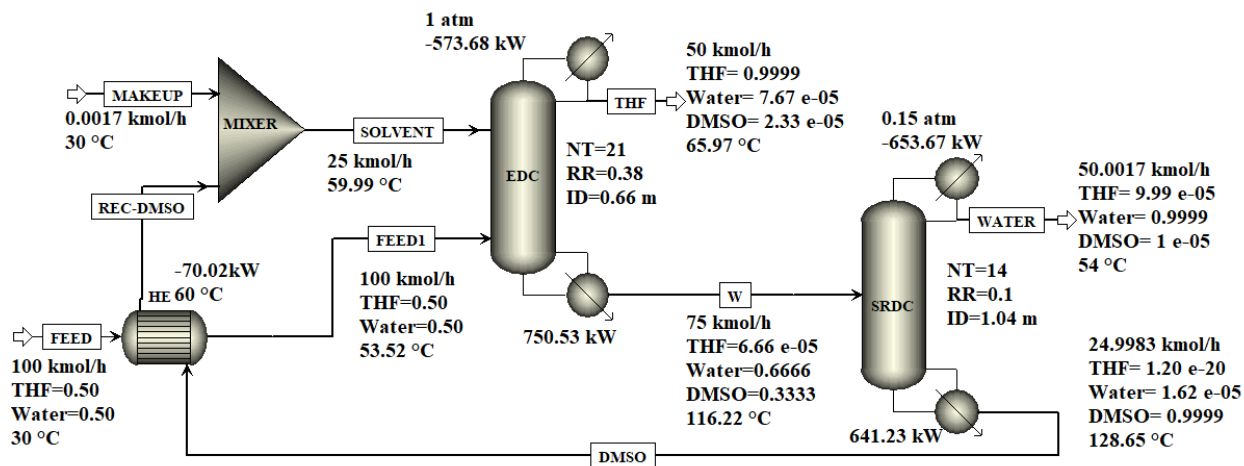
Parameter	Case 6	Case 7	Case 8	Case 9
N_{T2}	12	14	16	18
N_{T1}	21	21	21	21
RR_2 (optimum)	0.13	0.1	0.08	0.08
E/F (optimum)	0.25	0.25	0.25	0.25
N_{F2} (optimum)	5	6	7	7
D_2 (m)	1.05	1.04	1.03	1.03
Q_{R2} (kW)	659.0	641.2	629.3	629.4
Q_{C2} (kW)	671.5	653.7	641.8	641.8
Total capital (10^6 \$)	0.4628	0.4729	0.4837	0.4969
Total operating (10^6 \$)	0.3161	0.3118	0.3092	0.3091
TAC (10^6 \$ /yr)	0.4703	0.4695	0.4704	0.4748

Table 2.6. Optimized design parameters with TAC of THF-Water extractive distillation system for various solvents

Parameter	DMSO		Ethylene Glycol		Glycerol		1,2-PDO	
	EDC	SRDC	EDC	SRDC	EDC	SRDC	EDC	SRDC
N_T	21	14	21	12	21	8	22	12
RR	0.38	0.1	0.34	0.08	0.20	0.05	0.60	0.11
E/F	0.25	-	0.5	-	0.25	-	0.6	-
N_{FF}	17	6	17	7	17	4	17	7
D (m)	0.66	1.04	0.65	0.91	0.61	0.96	0.73	0.97
H (m)	13.92	8.78	13.90	7.32	13.89	4.39	14.63	7.32
Q_R (kW)	750.5	641.2	846.2	628.9	757.3	719.4	1042.8	637.7
A_R (m ²)	30.29	36.18	37.54	26.90	29.45	44.41	47.90	45.00
Q_C (kW)	573.7	653.7	553.3	641.8	496.9	624.0	663.3	659.6
A_C (m ²)	19.73	34.64	19.04	34.00	17.10	33.06	22.82	34.95
Q_{cooler} (kW)	70.0		185.5		261.3		263.1	
A_{cooler} (m ²)	1.48		3.61		3.58		5.35	
Capital (10 ⁶ \$)	0.4729		0.4481		0.4271		0.5210	
Operating (10 ⁶ \$/yr)	0.3118		0.3385		0.3744		0.3765	
TAC (10 ⁶ \$ /yr)	0.4695		0.4878		0.5167		0.5502	

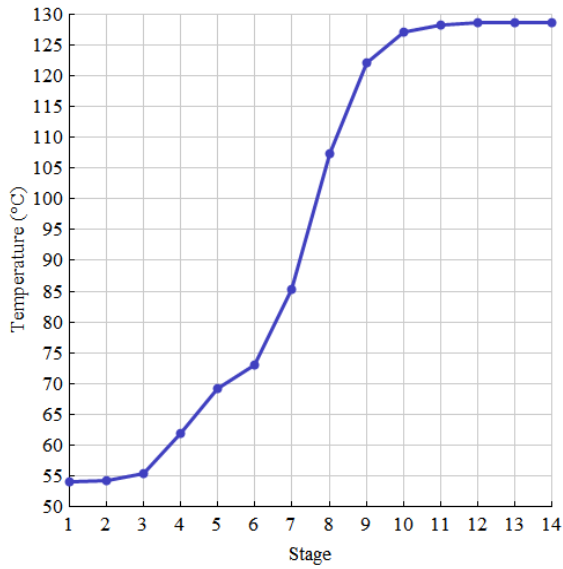


(a) Configuration without heat integration

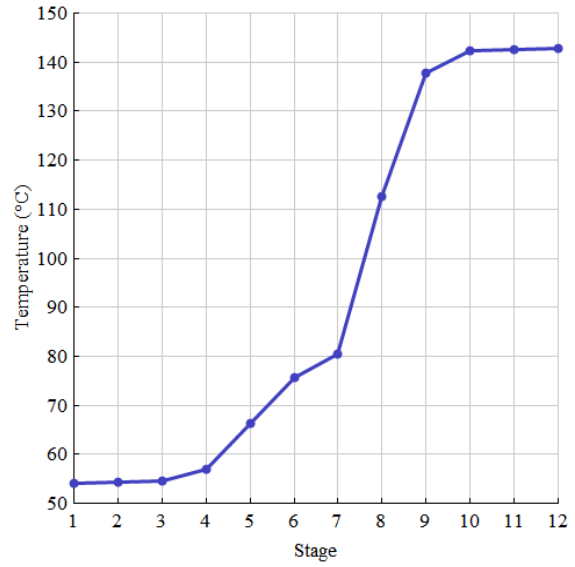


(b) Configuration with thermal heat integration

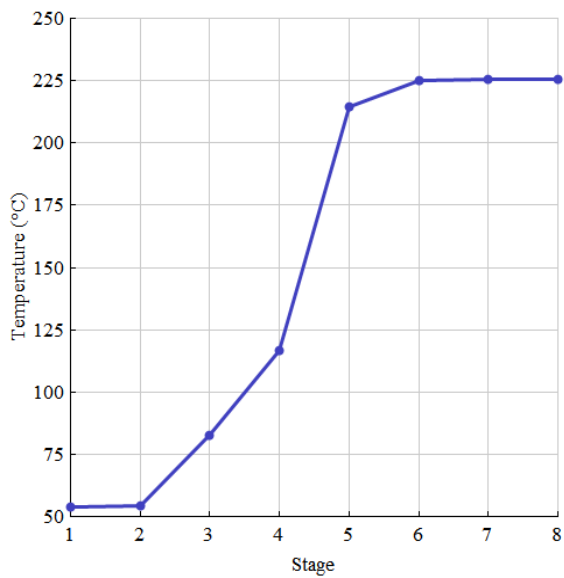
Figure 2.9. The optimal design flowsheet of the extractive distillation system with DMSO as a solvent



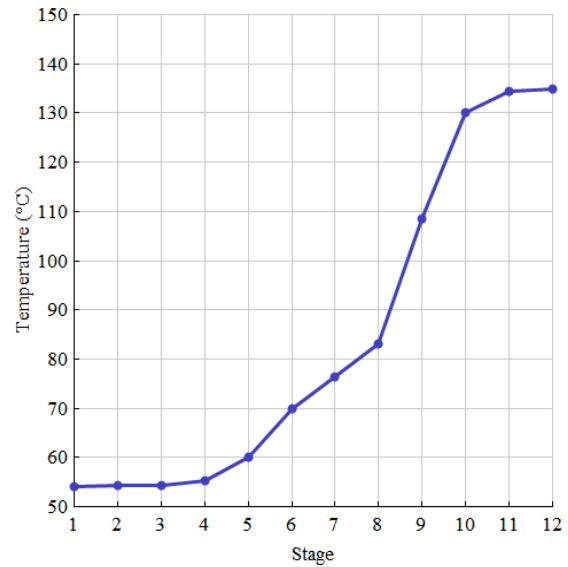
(a) DMSO as a solvent



(b) Ethylene glycol as a solvent



(c) Glycerol as a solvent



(d) 1, 2-propanediol as a solvent

Figure 2.10. SRDC temperature profile

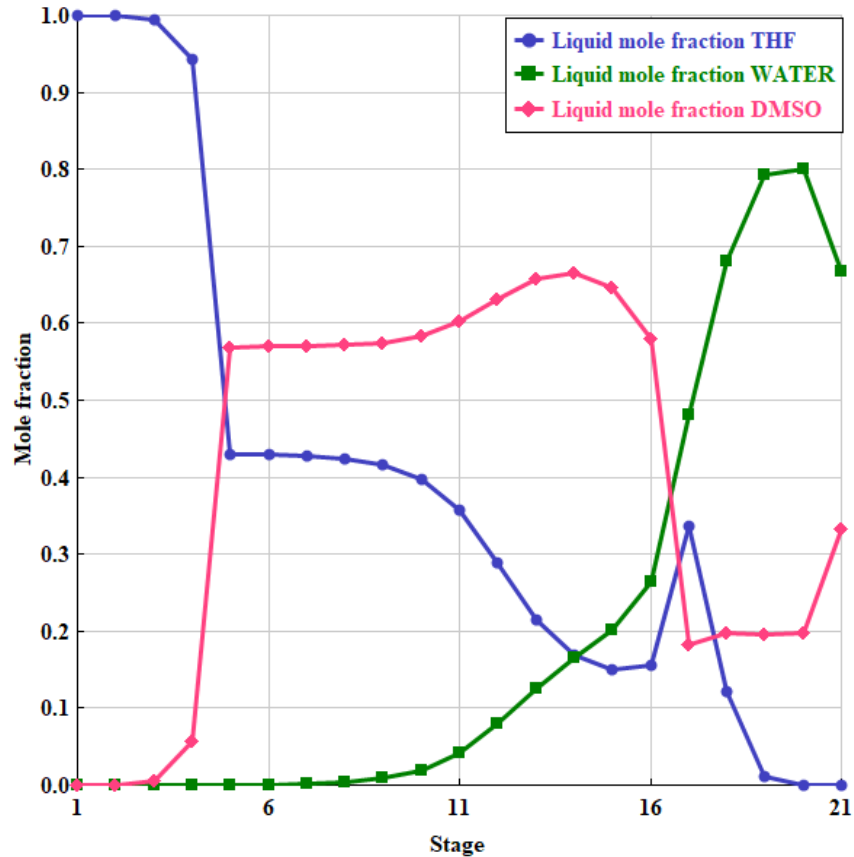


Figure 2.11 The composition profiles of the extractive distillation column with DMSO as a solvent

The complete simulation of extractive distillation systems with Ethylene glycol, Glycerol and 1, 2- propanediol (1, 2-PDO) as a solvent to achieve desired purity with minimum TAC was performed in a similar manner as explained above for the THF-water-DMSO system. The temperature profile of SRDC in each solvent case is shown in Figure 2.10. The composition profile of the ED column can be seen in Figure 2.11. The solvent is fed into stage 5 while the binary feed is introduced on stage 17. The main objective of extractive distillation is to remove water from the rectifying section, and it appears that this goal has been achieved. The binary feed condition, operating pressures of both columns and required purity specifications of both product streams were kept the same for direct comparison purposes. The optimized operating conditions, reboiler and condenser duties, the diameter of the columns and TAC of the complete extractive distillation system for the respective solvent are summarized in Table 2.6. These results show that the total operating cost and TAC required for the THF-water-DMSO system are less than all

other solvent systems. So, it is concluded that DMSO is the best solvent among all considered solvents for separating equimolar THF-water mixture by extractive distillation in terms of energy consumption and TAC.

2.2.3 Heat Integration for Extractive Distillation

Heat integration in the extractive distillation can be achieved by utilizing the heat from the bottom stream of the solvent recovery column in a heat exchanger to preheat the feed solution. The bottom stream of SRDC contains almost pure high boiling solvent, which is recycled to the EDC. Preheating the feed solution will reduce the reboiler duty of EDC and hence, the TAC.

The total number of stages (N_T) and purity specifications of the product stream were the same for the system without thermal integration. The other parameters were optimized similarly in the previous case to obtain the optimal design of extractive distillation with heat integration. By utilizing the heat from the bottom stream in the SRDC, the temperature of the feed increases up to 53.52 °C, which leads to a reduction in the reboiler duty of the extractive distillation column from 750.53 kW to 683.89 kW. The flowsheet with heat integration is shown in Figure 2.9. (b). Table 2.7 shows a 3.44 % reduction in TAC and a 4.80 % reduction in operating cost in extractive distillation with thermal integration compared to the design without thermal heat integration.

Table 2.7 Economic analysis results for THF-water ED with and without heat integration

Parameter	ED without HI		ED with HI	
	C ₁	C ₂	C ₁	C ₂
NT	21	14	21	14
D (m)	0.66	1.03	0.66	1.03
H (m)	13.90	8.78	13.90	8.78
Q _R (kW)	750.53	641.23	683.69	641.23
A _R (m ²)	30.29	36.18	27.59	36.18
Q _C (kW)	573.67	653.66	577.02	653.66
A _C (m ²)	19.73	34.64	19.85	34.64
Q _{HE} (kW)		70.02		70.02
A _{HE} (m ²)		1.48		1.67
Capital (10 ⁶ \$)	0.2202	0.2527	0.2175	0.2527
Operating (10 ⁶ /y)	0.1682	0.1437	0.1532	0.1437
TAC (10 ⁶ \$ /y)	0.2416	0.2279	0.2257	0.2279
Capital (10 ⁶ \$)		0.4729		0.4702
Operating (10 ⁶ \$/y)		0.3118		0.2969
TAC (10 ⁶ \$ /y)		0.4695		0.4536

2.3 Pressure Swing Distillation (PSD)

In pressure swing distillation, two columns are operated at different pressures, as shown in Figure 2.11. For the minimum boiling azeotropic system, the fresh binary mixture feed is mixed with a recycled distillate stream (D₂) from the second column operating at higher pressure (P₂) to form the mixed feed stream to the first column operating at lower pressure (P₁). The distillate streams (D₁), having compositions close to the azeotropic composition at pressure P₁, is fed to the second column. The distillate stream of the second column (D₂), containing nearly azeotropic composition at pressure P₂, is recycled back to the low-pressure column (LPC). The shift in azeotropic composition at different pressure will help to separate the azeotropic binary mixtures. The pure products are withdrawn from the bottom streams B₁ and B₂.

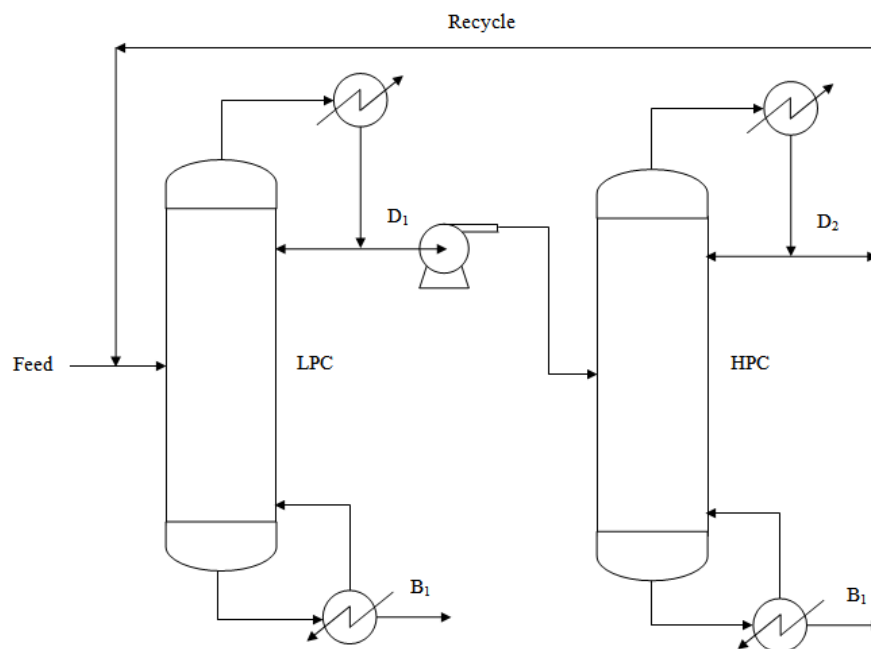


Figure 2.12. Pressure swing distillation flow diagram

Abu-Eishah and Luyben [18] explored the partial heat integration of PSD for the THF-water system through simulations by taking the azeotropic feed composition and pressure $P_1 = 1$ atm and $P_2 = 7.8$ atm. Luyben [19] extended the work of Abu-Eishah and Luyben [18] to a fully heat-integrated configuration that minimizes energy consumption. In both design cases, the authors did not consider the TAC of the overall pressure swing distillation system. There is no sufficient literature data on the optimum design of PSD design based on TAC. Hence, in this section, the complete optimized design of PSD for separating the equimolar THF-water mixture is worked out.

2.3.1 Simulation Analysis of Pressure Swing Distillation System

The steady-state Aspen Plus simulator with the RadFrac model and NRTL property package with built-in binary interaction parameter was used to simulate the PSD system. The PSD analysis used the same feed circumstances and product purity restrictions as those used for the extractive distillation system in the preceding section. The distillate composition of LPC is the azeotropic composition at low pressure, while the distillate composition of HPC is the azeotropic composition at high pressure. Recycle flow rates were estimated by the system's total material and component balance.

2.3.2 Selection of Pressure and N_T for Columns

The effect of pressure on the azeotropic point and the boiling point of both components estimated using ASPEN simulations are given in Table 2.8. It can be observed that the azeotropic composition of the THF-water system shifts significantly with the moderate change in pressure. More significant shifts in the azeotropic composition with pressure will reduce the recycle flow rate and hence, the reboiler duties of the columns. So, a higher pressure will be preferred in HPC, but it would lead to a high utility temperature requirement for the reboiler. The operating pressure of LPC was set at atmospheric pressure. LPC did not prefer the vacuum which would demand expensive chilled utility for the condenser operation. Atmospheric pressure operation allows LPC to use cooling water with a temperature of around 305 K as a utility in the condenser.

The pressure of the HPC was chosen by optimizing the flowsheet at two levels. In the first level, for the assumed HPC pressure, the number of stages was optimized such that TAC for the overall separation system obtained was the minimum. In the second level, the TAC of the overall system for various operating pressure for the HPC were compared, and the pressure with minimum TAC was taken as the optimum pressure for the HPC. The economic optimization result for HPC operating at 5 atm is summarized in Tables 2.9 and 2.10. First, the number of LPC (N_{T1}) stages varied from 12 to 15 while keeping the stages in the HPC (N_{T2}) the same. Then the number of HPC (N_{T2}) stages varied from 14 to 17 while keeping N_{T1} the same to determine the minimum TAC. The Design Spec function was used to fix the optimum reflux ratio to achieve the specified purity of the product streams. Sensitivity analysis results obtained the feed location of both columns to minimize the heat duties of the columns. The results indicate that LPC having $N_T = 13$ with a feed stage at 10 and HPC having $N_T = 16$ with a feed stage at 7 gives minimum TAC for the complete pressure swing distillation system.

Table 2.8. Estimated effect of pressure on azeotropic composition for THF-water system using ASPEN simulations

Pressure (atm)	Boiling point of water ($^{\circ}\text{C}$)	Boiling point of THF ($^{\circ}\text{C}$)	Boiling temperature of azeotrope ($^{\circ}\text{C}$)	Azeotrope (mole fraction of THF)
0.1	46.06	8.9	8.74	0.9551
0.5	81.67	46.09	44.74	0.8732
0.8	93.88	59.26	57.17	0.8437
1	100.02	65.97	63.43	0.8287
2	120.69	89.03	84.54	0.7775
3	134.05	104.32	98.20	0.7442
4	144.16	116.11	108.54	0.7190
5	152.41	125.86	116.98	0.6986
6	159.43	134.25	124.14	0.6814
7	165.57	141.65	130.41	0.6666
8	171.05	148.31	135.99	0.6535
9	176.01	154.38	141.04	0.6418
10	180.55	159.97	145.67	0.6312
11	184.75	165.16	149.93	0.6215

With fixed pressure of 1 atm and a number of stages of 13 in LPC, the optimum pressure of HPC was fixed in such a way that the TAC of the overall system will be the minimum. HPC at various pressures was simulated, similar to that for 5 atm pressure, and the results are summarized in Table 2.11, which includes heat duties, sizing, operating cost, capital cost and TAC of both columns for various HPC pressures. The results show that the minimum total operating cost and TAC has obtained at HPC pressure 10 atm. Further, an increase in HPC pressure above 10 atm would require expensive high-pressure steam, which will increase the operating cost and, consequently, the TAC of the system. The optimal steady-state design flowsheet of the pressure swing distillation system with HPC at 10 atm pressure is shown in Figure 2.13 (a).

Table 2.9. THF-water PSD economic optimization results for N_{T1} (LPC at 1 atm and HPC at 5 atm)

Parameters	Case 1	Case 2	Case 3	Case 4
N_{T1}	12	13	14	15
N_{T2}	16	16	16	16
N_{F1} (optimal)	9	10	11	12
RR_1 (optimal)	0.22	0.21	0.21	0.20
D_1 (m)	0.96	0.95	0.95	0.95
Q_{R1} (kW)	1411.3	1401.3	1394.0	1388.5
Q_{C1} (kW)	1437.8	1427.7	1420.5	1415.0
Total capital cost (10^6 \$)	0.4880	0.4934	0.4990	0.5047
Total operating cost (10^6 \$)	0.5800	0.5778	0.5761	0.5749
TAC (10^6 \$ /yr)	0.7427	0.7423	0.7425	0.7431

Table 2.10. THF-water PSD economic optimization results for N_{T2} (LPC at 1 atm and HPC at 5 atm)

Parameters	Case 5	Case 6	Case 7	Case 8
N_{T1}	13	13	13	13
N_{T2}	14	15	16	17
N_{F2} (optimal)	6	6	7	8
RR_2 (optimal)	0.30	0.28	0.27	0.26
D_2 (m)	0.77	0.77	0.77	0.76
Q_{R2} (kW)	1199.2	1186.4	1177.4	1172.8
Q_{C2} (kW)	901.2	888.4	879.4	874.8
Total capital cost (10^6 \$)	0.4857	0.4892	0.4934	0.4973
Total operating cost (10^6 \$)	0.5827	0.5798	0.5778	0.5768
TAC (10^6 \$ /yr)	0.7446	0.7429	0.7423	0.7425

Table 2.11. THF-water PSD optimization results with various operating pressure of HPC.

Parameters	Case 1		Case 2		Case 3		Case 4		Case 5		Case 6	
	C ₁	C ₂	C ₁	C ₂	C ₁	C ₂	C ₁	C ₂	C ₁	C ₂	C ₁	C ₂
Pressure (atm)	1	3	1	5	1	8	1	9	1	10	1	11
N _T	13	16	13	16	13	16	13	16	13	16	13	16
N _F (optimal)	11	9	10	7	11	8	10	8	10	8	11	8
RR (optimal)	0.20	0.35	0.21	0.27	0.21	0.29	0.22	0.29	0.22	0.29	0.22	0.31
D (m)	1.12	1.04	0.95	0.77	0.86	0.66	0.85	0.64	0.83	0.63	0.82	0.63
H (m)	8.05	10.23	8.05	10.25	8.05	10.25	8.05	10.25	8.05	10.25	8.05	10.25
Q _R (kW)	1995	1888	1401	1177	1151	966	1108	935	1074	912	1048	899
A _R (m ²)	56.54	59.83	39.50	60.95	32.46	47.83	31.30	55.78	30.38	67.14	29.66	17.71
Q _C (kW)	2039	1622	1428	879	1171	619	1128	573	1093	536	1065	513
A _C (m ²)	75.77	28.69	53.07	12.12	43.53	6.98	41.91	6.15	40.63	5.52	39.59	5.12
Total capital (10 ⁶ \$)	0.6173		0.4934		0.4240		0.4242		0.4300		0.3599	
Total operating(10 ⁶ \$)	0.8699		0.5778		0.4865		0.4695		0.4565		0.4907	
TAC (10 ⁶ \$ /y)	1.0757		0.7423		0.6279		0.6109		0.5999		0.6107	

2.3.3 Heat Integration of Pressure Swing Distillation

In pressure swing distillation, energy consumption can be further reduced by heat integration of both columns. From Figure 2.13 (a) for the PSD of the THF/water mixture, it can be observed that the condenser duty of HPC is 535.5 kW with a top vapour temperature of 418.8 K. The reboiler duty of LPC is 1074.3 kW with a bottom boiling liquid temperature of 370.7 K, which indicates that heat integration is possible for this system as the temperature difference between the top vapour of HPC and boiling liquid of LPC is almost 48.1 K, which is suitable for the heat integration.

The design of a heat integration system can be done in two modes such as partial heat integration and full heat integration. For designing both options of heat integration for PSD, the total number of stages and product purity of both columns were kept the same as that obtained for the PSD without heat integration in section 3.2. All other parameters were optimized accordingly.

2.3.3.1 Partial Heat Integration

In the Partial heat integration system, the condenser duty (Q_{C2}) of the HPC and reboiler duty (Q_{R1}) of the LPC are not equal. Therefore, an auxiliary reboiler (AR) is provided to compensate for the LPC's heat requirement. In PSD configuration, given in Fig 2.13 (a), the condenser duty of the HPC is not equal to the reboiler duty of the LPC; hence the auxiliary reboiler of duty $Q_{AR} = 538.74$ kW will be required to meet the heat requirement of the LPC. The complete design flowsheet PSD with partial heat integration is given in Figure 2.13 (b).

2.3.3.2 Full Heat Integration

In full heat integration, the condenser duty (Q_{C2}) of the HPC is set exactly equal to the reboiler duty (Q_{R1}) of the LPC, and thus auxiliary reboiler is not required. The complete design flowsheet for PSD with full heat integration is given in Figure 2.13 (c). By adjusting the reflux ratio (RR_2) of the HPC, the Design Spec feature in Aspen Plus was utilized to set both duties to equal amounts. LPC's reflux ratio (RR_1) was varied to minimize energy consumption. Desired

product purity was achieved by varying the bottom flow rate of the respective columns. The effect of reflux ratio (RR_1) on the RR_2 , Q_{C2} and Q_{R2} is shown in Figure 2.12. It shows that the optimum reflux ratio (RR_1) was 0.12, for which minimum condenser duty was $Q_{C2} = 1025.5$ kW and corresponding reboiler duty and reflux ratio were $Q_{R2} = 1414.2$ kW and $RR_2 = 1.26$, respectively.

The cost analysis data and optimum design parameters for three alternatives are given in Table 2.12. The TAC of the partially heat-integrated process is 0.4786 \$/y, and the full heat-integrated process is 0.4874 \$/y. The results show that about 20.2 % and 18.8 % reduction in TAC was achieved by the PSD with partial and full heat integration, respectively, compared to the PSD without heat integration. For THF-Water PSD, the partial heat integration configuration is more attractive than the PSD with full heat integration and without heat integration in terms of TAC.

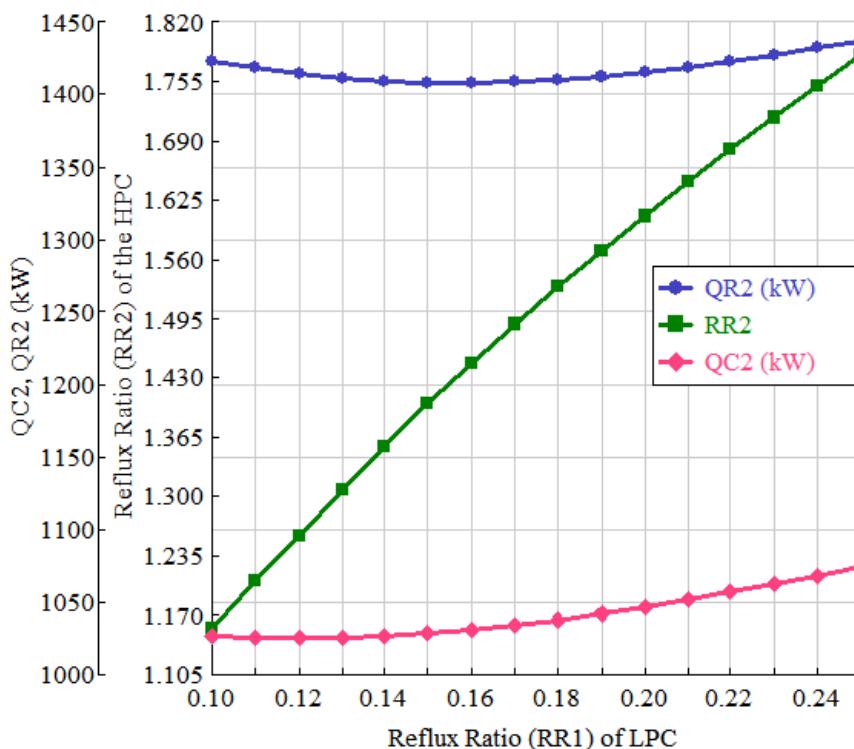
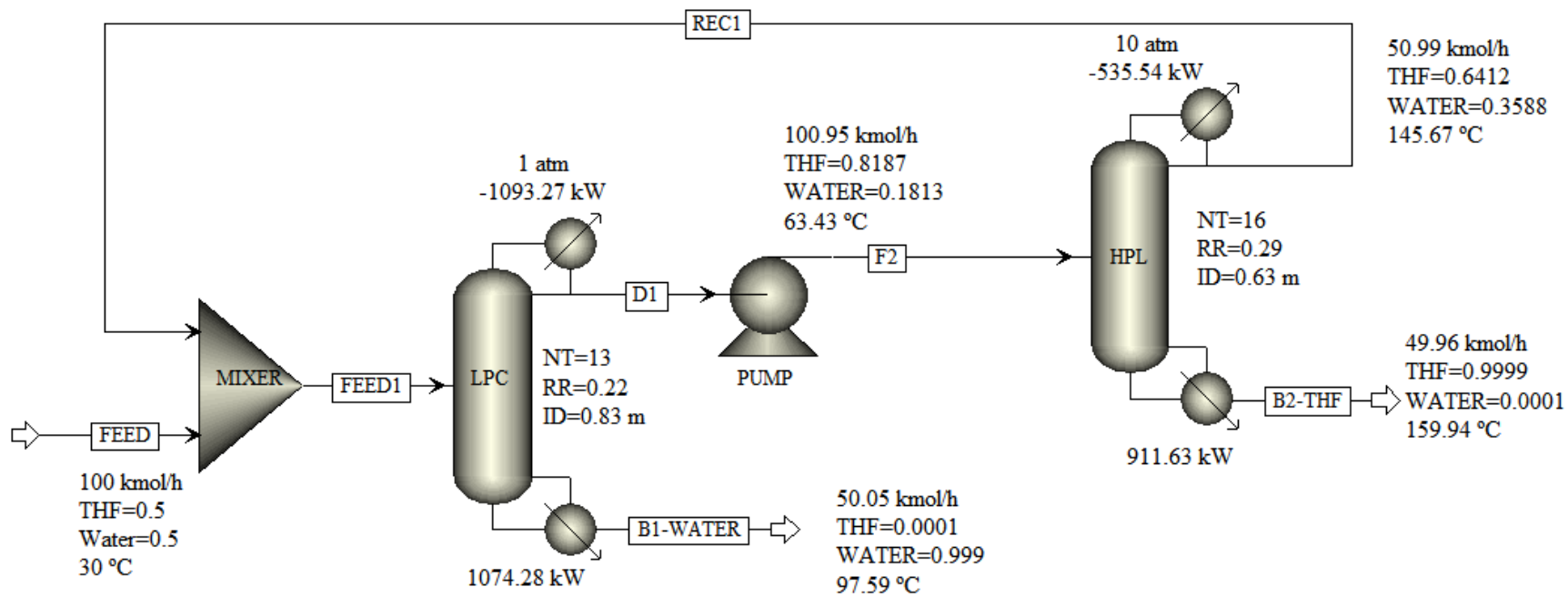
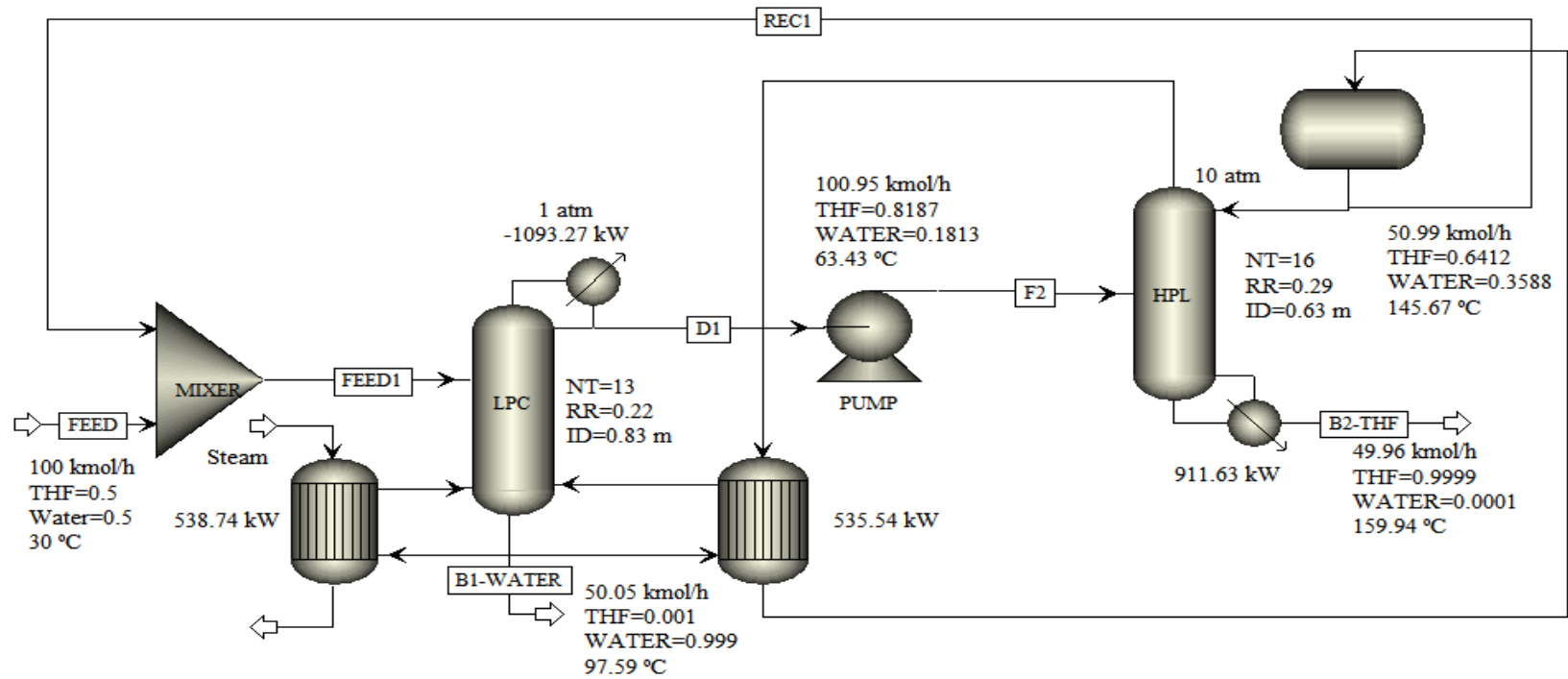


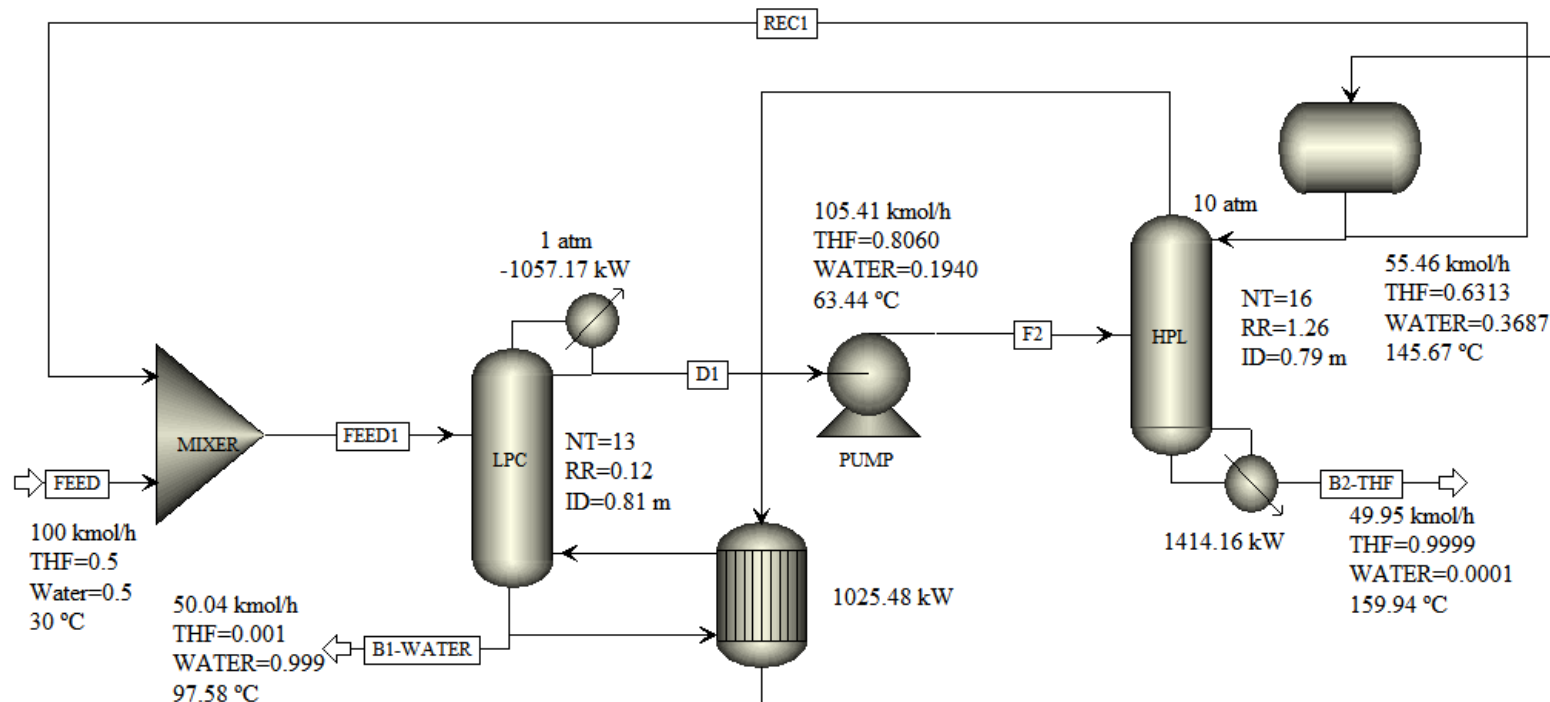
Figure 2.13. Effect of reflux ratio (RR_1) for LPC of fully heat integrated THF-water PSD on the RR_2 , Q_{C2} and Q_{R2}



(a) THF-water PSD without heat integration



(b) THF-water PSD with partial heat integration



(c) THF-water PSD with full heat integration

Figure 2.14. The optimal steady-state design flowsheets of the pressure swing distillation system

Table 2.12. Economic analysis results for THF-water ED and PSD with and without heat integration

Parameter	ED without HI		ED with HI		PSD without HI		PSD partial HI		PSD with fully HI	
	C ₁	C ₂	C ₁	C ₂	C ₁	C ₂	C ₁	C ₂	C ₁	C ₂
NT	21	14	21	14	13	16	13	16	13	16
D (m)	0.66	1.03	0.66	1.03	0.83	0.63	0.83	0.63	0.81	0.79
H (m)	13.90	8.78	13.90	8.78	8.05	10.25	8.05	10.25	8.05	10.25
Q _R (kW)	750.53	641.23	683.69	641.23	1074.3	911.63	535.54	911.63	1025.5	1414.5
A _R (m ²)	30.29	36.18	27.59	36.18	30.38	67.14	15.14	67.14	28.99	104.14
Q _C (kW)	573.67	653.66	577.02	653.66	1093.3	535.54	1093.3	-	1057.2	-
A _C (m ²)	19.73	34.64	19.85	34.64	40.63	5.52	40.63	-	39.28	-
Q _{HE} (kW)	70.02		70.02		-		538.74		-	
A _{HE} (m ²)	1.48		1.67		-		15.23		-	
Capital (10 ⁶ \$)	0.2202	0.2527	0.2175	0.2527	0.2255	0.2045	0.2439	0.1823	0.2195	0.2382
Operating (10 ⁶ /y)	0.1682	0.1437	0.1532	0.1437	0.2407	0.2158	0.1207	0.2158	-	0.3348
TAC (10 ⁶ \$ /y)	0.2416	0.2279	0.2257	0.2279	0.3159	0.2840	0.2020	0.2766	0.0732	0.4142
Capital (10 ⁶ \$)	0.4729		0.4702		0.4300		0.4263		0.4577	
Operating (10 ⁶ \$/y)	0.3118		0.2969		0.4565		0.3365		0.3348	
TAC (10 ⁶ \$ /y)	0.4695		0.4536		0.5999		0.4786		0.4874	

2.4 Comparison of Extractive Distillation and PSD for THF-Water Separation

The most optimum designs of extractive distillation for THF-water separation were compared with the most optimum design of PSD. The optimized design parameters, with economical analysis of both extractive distillation and pressure swing distillation, are given in Table 2.12. Reduction in TAC can be observed with heat integration in both designs. Results indicate that heat integration in extractive distillation leads to a 3.4 % reduction in TAC, which is mainly because of saving in operating costs. Partial and full heat integration in the case of PSD results in a 20.2 % and 18.8 % reduction in TAC, respectively, compared to the basic configuration without heat integration. PSD configuration with partial heat integration is more economical than full heat integration because capital cost increases significantly in the case of a full heat integrated system because of increased heat transfer area requirement for both column reboilers and higher HPC diameter. Extractive distillation with heat integration requires 5.2 % less TAC than PSD with partial heat integration.

2.5 Conclusion

In this chapter, steady-state simulation of extractive and pressure swing distillation for the separation of equimolar THF-water binary mixture was investigated in detail. Designs of extractive distillation systems with various solvents were worked out and evaluated economically. DMSO was the best solvent for extractive distillation of THF-water separation as it gave minimum TAC to achieve product purity. For Pressure swing distillation, LPC pressure was fixed at 1 atm, and various operating pressures for HPC were analyzed. It was found that HPC with 10 atm pressure gave minimum TAC. The design of steady-state extractive and pressure swing distillation with heat integration was also a workout.

As the basis, in terms of feed conditions and constraints in terms of product purity were the same for the simulation analysis; the optimum configuration of extractive distillation with and without thermal integration by using DMSO as the solvent was directly compared with the most optimum configuration of PSD with and without heat integration. Results indicate that extractive distillation with and without heat integration gives a 24.4 % and 21.7 % reduction in the TAC and 34.96 % and 31.70 % in the operating cost over the PSD without heat integration. The TAC of extractive distillation with heat integration is 5.2 % less than that of PSD with partial heat integration. Hence, extractive distillation with DMSO as solvent is a better option economically for separating an equimolar THF-water mixture.

2.6 References

- [1] W.L. Luyben, Comparison of extractive distillation and pressure-swing distillation for acetone-methanol separation, *Ind. Eng. Chem. Res.* 47 (2008) 2696–2707.
- [2] W.L. Luyben, Comparison of extractive distillation and pressure-swing distillation for acetone/chloroform separation, *Comput. Chem. Eng.* 50 (2013) 1–7.
- [3] E. Lladosa, J.B. Montón, M.C. Burguet, Separation of di-n-propyl ether and n-propyl alcohol by extractive distillation and pressure-swing distillation: Computer simulation and economic optimization, *Chem. Eng. Process. Process Intensif.* 50 (2011) 1266–1274.
- [4] H. Luo, K. Liang, W. Li, Y. Li, M. Xia, C. Xu, Comparison of pressure-swing distillation and extractive distillation methods for isopropyl alcohol/diisopropyl ether separation, *Ind. Eng. Chem. Res.* 53 (2014) 15167–15182.
- [5] E. Hosgor, T. Kucuk, I.N. Oksal, D.B. Kaymak, Design and control of distillation processes for methanol-chloroform separation, *Comput. Chem. Eng.* 67 (2014) 166–177.
- [6] B. Yu, Q. Wang, C. Xu, Design and control of distillation system for methylal/methanol separation. Part 1: Extractive distillation using DMF as an entrainer, *Ind. Eng. Chem. Res.* 51 (2012) 1281–1292.
- [7] B. Yu, Q. Wang, C. Xu, Design and control of distillation system for methylal/methanol separation. Part 2: Pressure swing distillation with full heat integration, *Ind. Eng. Chem. Res.* 51 (2012) 1293–1310.
- [8] H.M. Wei, F. Wang, J.L. Zhang, B. Liao, N. Zhao, F. Xiao, W. Wei, Y.H. Sun, Design and control of dimethyl carbonate-methanol separation via pressure-swing distillation, *Ind. Eng. Chem. Res.* 52(2013) 11463–11478.
- [9] S. Xu, H. Wang, A new entrainer for separation of tetrahydrofuran-water azeotropic mixture by extractive distillation, *Chem. Eng. Process. Process Intensif.* 45 (2006) 954–958.
- [10] S. Xu, H. Wang, Separation of tetrahydrofuran-water azeotropic mixture by batch extractive distillation process, *Chem. Eng. Res. Des.* 84 (2006) 478–482.

- [11] P.A. Gomez, I.D. Gil, Simulation of the tetrahydrofuran dehydration process by extractive distillation, *Latin American Applied Research* 39 (2009) 275–284.
- [12] Z. Fan, X. Zhang, W. Cai, F. Wang, Design and Control of Extraction Distillation for Dehydration of Tetrahydrofuran, *Chem. Eng. Technol.* 36 (2013) 829–839.
- [13] Z.G. Zhang, D.H. Huang, M. Lv, P. Jia, D.Z. Sun, W.X. Li, Entrainer selection for separating tetrahydrofuran/water azeotropic mixture by extractive distillation, *Sep. Purif. Technol.* 122 (2014) 73–77.
- [14] O.A. Deorukhkar, B.S. Deogharkar, Y.S. Mahajan, Purification of tetrahydrofuran from its aqueous azeotrope by extractive distillation: Pilot plant studies, *Chem. Eng. Process. Process Intensif.* 105 (2016) 79–91.
- [15] W.L. Luyben, I. L. Chien, *Design and control of distillation systems for separating azeotropes*, John Wiley & Sons, 2011.
- [16] W.L. Luyben, Distillation column pressure selection, *Sep. Purif. Technol.* 168 (2016) 62–67.
- [17] J.R. Knight, M.F. Doherty, Optimal Design and Synthesis of Homogeneous Azeotropic Distillation Sequences, *Ind. Eng. Chem. Res.* 28 (1989) 564–572.
- [18] S.I. Abu-Eishah, W.L. Luyben, Design and Control of a Two-Column Azeotropic Distillation System, *Ind. Eng. Chem. Process Des. Dev.* 24 (1985) 132–140.
- [19] W.L. Luyben, Design and control of a fully heat-integrated pressure-swing azeotropic distillation system, *Ind. Eng. Chem. Res.* 47 (2008) 2681–2695.
- [20] V.A. Shnitko, and V.B. Kogan, Liquid-vapor equilibrium in the systems tetrahydrofuran-water and tetrahydrofuran-ethylene glycol and a method for dehydration of tetrahydrofuran. *J. Appl. Chem. USSR*, 4 (6) (1968) 1236-1242.

Chapter 03

Extractive Distillation Configuration

for Nitric Acid Dehydration

Using Sulphuric Acid as a Solvent

Chapter 3 Extractive Distillation Configuration for Nitric Acid Dehydration

Using Sulphuric Acid as a Solvent

Abstract

In this work, an extractive distillation configuration for the dehydration of nitric acid is proposed with sulphuric acid as a solvent. Thermodynamic modelling of vapour-liquid-equilibrium of binary and ternary systems of nitric acid (HNO₃)/water/sulphuric acid was carried out using eNRTL-RK (Electrolyte Non-Random Two Liquid) thermodynamic property method in the Aspen Plus process simulator. The model performance was validated by comparing the experimental data with the estimated data by the eNRTL-RK model and found to be in good agreement. The thermodynamic model is then used for developing a triple-column extractive distillation sequence comprising a pre-concentrating column, extractive distillation column and solvent recovery column. The configuration is designed, simulated and optimized to concentrate dilute nitric acid using sulphuric acid as a solvent to break the nitric acid water azeotrope. The operating and structural parameters of the distillation configuration are optimized simultaneously to minimize energy consumption and total annual cost (TAC) overall configuration.

3.1 Introduction

Concentrated nitric acid (HNO₃) is widely used in the nitration process as a nitrating agent, in the oxidation process as the oxidizing agent and various other agrochemical and explosive industries processes. Ammonium nitrate required in fertilizer industries is produced from concentrated nitric acid. There is a significant requirement for concentrated nitric acid worldwide from various process industries for a wide range of applications. Processes utilizing concentrated nitric acid lead to an effluent of dilute nitric acid, typically in the range of 15 - 20 mass % nitric acids, which needs to be concentrated and recycled to the process to improve the overall economy of the plant [1]. However, the concentration of nitric acid by conventional distillation process is difficult due to the formation of a maximum boiling azeotrope with water. The azeotropic temperature is 120 °C which is higher than that of the boiling point of pure water (100 °C) and nitric acid (83 °C) at atmospheric pressure, as shown in Figure 3.1 (a)

The extractive distillation method is widely used for separating azeotropic systems. It has good energy efficiency and high product purity with low total annual cost (TAC) compared to other distillation configurations dealing with azeotropic or closed boiling systems [2, 3]. In the case of dehydration of the nitric acid, magnesium nitrate and sulphuric acid are proposed as extracting agents for extractive distillation in the literature [1, 4]. Vailiancourt [5] commented that magnesium nitrate is a less efficient extractive entrainer than sulphuric acid as it requires a higher number of stages and reflux ratio and ultimately leads to higher energy consumption and quantity of entrainer to achieve the same separation. The feasibility of using sulfuric acid to dehydrate spent nitric acid is already reported [5]. Also, industrial-scale application of sulfuric acid for dehydrating nitric acid was reported by Thomas et al. [6]

The present work reports an optimized extractive distillation configuration for the dehydration of nitric acid using sulphuric acid as a solvent. To the best of our knowledge, detailed parametric analysis for extractive distillation configuration for the dehydration of nitric acid using sulphuric acid as a solvent is not available in the open literature. Thermodynamic modelling of the system plays a vital role while designing any distillation configuration using a process simulator. The present work addresses the crucial aspects of distillation modelling viz, thermodynamic modelling of phase equilibrium and detailed process simulation analysis with cost analysis. The development of distillation configuration for the dehydration of dilute nitric acid is divided into two parts. In the first part, the thermodynamic modelling of nitric acid (HNO_3) / water / sulphuric acid three component system using reported experimental binary and ternary vapour-liquid-equilibrium (VLE) data is performed. The binary interaction parameters for e-NRTL (Electrolyte Non-Random Two Liquid) model are generated using this data in the Aspen data regression system (DRS). In the second part, the design and optimization of the complete extractive distillation scheme for the dehydration of nitric acid are performed using the thermodynamic model developed in the first section with the objective of minimizing the total annual cost (TAC) of the overall distillation configuration.

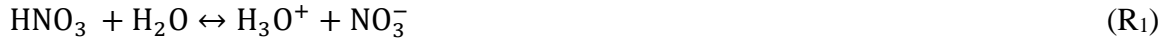
3.2 Thermodynamic Framework

Electrolyte Non-Random Two Liquid (eNRTL) model can be represented as eNRTL-SR and eNRTL-RK. The eNRTL-SR model considers the symmetric reference state for ions as pure

fused salts in the case of the mixed salt system or a pure liquid in the case of a mixed solvent system. The eNRTL-RK model considers infinite dilution in an aqueous solution that is the unsymmetric reference state. Wang et al. [7] reported the suitability of the thermodynamic eNRTL model with symmetric reference to describe the HNO₃-water-sulphuric acid three components system. The model parameters were inadequate to estimate the experimental vapour-liquid-equilibrium behaviour of the HNO₃/water/sulphuric acid three components system reported by Ellis and Thwaites [8]. Hence, the present work estimates interaction parameters using the eNRTL-RK activity coefficient model with experimental vapour-liquid-equilibrium data to predict binary and ternary vapour-liquid phase equilibrium behaviour. The details of the thermodynamic modeling are discussed in this section.

3.2.1 Chemical Reactions

The equilibrium reaction of partial dissociation of HNO₃ in a single step, H₂SO₄ dissociation in two-step reactions and the formation of hydronium ion in the aqueous solution were defined in the chemistry tab of the Aspen Plus simulator. These reactions are given below,



3.2.2 Vapour-Liquid Equilibrium (VLE)

Vapour-liquid equilibrium relationship is represented by the following equation [9],

$$y_i \Phi_i^V P = \gamma_i^S x_i \Phi_i^S P_i^S \exp \left[\frac{V_i(P - P_i^S)}{RT} \right] \quad (1)$$

Where x_i and y_i are the liquid and vapour phase mole fractions of component i , respectively, p and represents the total pressure of the system and the vapour pressure of the pure component i , the vapour pressure of the pure component was calculated using the extended Antoine equations by retrieving its coefficients from the Aspen Plus as given in Table 3.1.

Table 3.1. Coefficients of extended Antoine equation^a of pure components [14]

Parameters	C ₁	C ₂	C ₃	C ₄	C ₅	C ₆	C ₇	C ₈	C ₉
HNO ₃	170.14	-10078	0	0	-22.769	2.73 e ⁻⁰⁵	2	231.55	376.1
H ₂ O	73.649	-7258.2	0	0	-7.3037	4.1653 e ⁻⁰⁶	2	273.16	647.1
H ₂ SO ₄	14.422	-9757.7	0	0	2.3632	3.27 e ⁻¹⁹	6	283.14	603.2

$${}^a \ln p_i^s = C_{1i} + \frac{C_{2i}}{T+C_{3i}} + C_{4i}T + C_{5i} \ln T + C_{6i} T^{C_{7i}} \text{ for } C_{8i} \leq T \leq C_{9i} \text{ Where } P \text{ is in N/m}^2 \text{ and } T \text{ is in K.}$$

The fugacity coefficient (Φ_i) for component i in the mixture is calculated using the Redlich-Kwong equation of state. The critical pressure (P_c), critical temperature (T_c) and acentric factor (Ω) required in the Redlich- Kwong equations of state parameters are given in Table 3.2.

Table 3.2. Redlich-Kwong equation of state parameters [14]

Parameters	T _c (K)	P _c (N/m ²)	Ω
HNO ₃	520	6.8901e ⁰⁶	0.7144
H ₂ O	647.096	2.2064 e ⁰⁷	0.3449
H ₂ SO ₄	924	6.4 e ⁰⁶	0.9070

Liquid molar volume (V_i) for component i at temperature, T and saturation pressure, P_i^s obtained from the liquid molar density (ρ_i^l) calculated by the relationship given below in equation (2),

$$V_i = 1/\rho_i^l \quad (2)$$

The liquid molar density of component i is calculated using the coefficients of respective model equations as given in Table 3.3.

Table 3.3. Coefficients of liquid molar density model equations [14]

Parameters	C ₁	C ₂	C ₃	C ₄	C ₅	C ₆	C ₇
HNO ₃ ^a	1.5895	0.2304	520	0.1933	0	231.55	373.2
H ₂ O ^b	17.863	58.606	-95.396	213.89	-414.26	273.16	647.1
H ₂ SO ₄ ^c	1.4986	0.2653	924	0.2713	0	283.46	610

$${}^a \rho_i^l = C_{1i}/C_{2i}^{1+(1-T/C_{3i})^{C_{4i}}} \text{ for } C_{6i} \leq T \leq C_{7i}$$

$${}^b \rho_i^l = C_{1i} + C_{2i}\tau^{0.35} + C_{3i}\tau^{2/3} + C_{4i}\tau + C_{5i}\tau^{4/3}, \tau = 1 - \frac{T}{T_c}$$

$$c_{p_i}^l = \rho_{ci} + C_{1i}\tau^{0.35} + \sum_{m=2}^{nTerms} C_{mi}\tau^{m-1}; \tau = 1 - T/T_{ci}$$

The exponential term in equation (1) is called a pointing correction, and it can be assumed to be one at low pressure. The liquid phase activity coefficient is represented by γ_i can be calculated from the electrolyte non-random two-liquid model.

3.2.3 eNRTL-RK Activity Coefficient Model

The activity coefficient of component i is obtained from the partial derivative of the G^E/RT with respect to n_i given as the following equation [9]

$$\ln\gamma_i = \left[\frac{\partial(nG^E/RT)}{\partial n_i} \right]_{T,P,n_j \neq i} \quad (3)$$

The liquid phase activity coefficient is represented by γ_i can be calculated using the most versatile electrolyte non-random two-liquid model proposed by Chen et al.[10] and Mock et al.[11] based on the two assumptions, such as local electro-neutrality and like ion repulsion. Excess Gibbs free energy is given as,

$$\frac{G_m^*E}{RT} = \frac{G_m^*E,PDH}{RT} + \frac{G_m^*E,Born}{RT} + \frac{G_m^*E,lc}{RT} \quad (4)$$

This can leads to,

$$\ln\gamma_i^* = \ln\gamma_i^{*PDH} + \ln\gamma_i^{*Born} + \ln\gamma_i^{*lc} \quad (5)$$

Where G_m^*E,PDH represents the long-range interaction contribution with the Pitzer-Debye-Huckel model equation [12, 13] for multicomponent electrolyte is,

$$\frac{G_m^*E,PDH}{RT} = -(\sum_i x_i) \left(\frac{1000}{M_s} \right)^{1/2} \left(\frac{4A_\phi I_x}{\rho} \right) \ln(1 + \rho I_x^{1/2}) \quad (6)$$

Where ρ is the closest approach parameter, A_ϕ is the Debye–Huckel parameter, and I_x is the ionic strength given by eq. (7) and (8),

$$A_\phi = \frac{1}{3} \left(\frac{2\pi N_A d_s}{1000} \right)^{1/2} \left(\frac{Q_e^2}{\epsilon_s kT} \right)^{3/2} \quad (7)$$

$$I_x = \frac{1}{2} \sum_i z_i^2 x_i \quad (8)$$

Where x_i is the mole fraction of component i , M_s represents the molecular weight of solvent, N_A is the Avogadro's number, d_s is the mass density of the solvent, Q_e electron charge, T temperature, k is the Boltzmann constant, z_i is charge number of an ion, the dielectric constant of the solvent represented by ϵ_s .

Activity coefficient is,

$$\ln \gamma_i^{*PDH} = - \left(\frac{1000}{M_s} \right)^{1/2} A_\phi \left[\left(\frac{2z_i^2}{\rho} \right) \ln(1 + \rho I_x^{1/2}) + \frac{z_i^2 I_x^{1/2} - 2I_x^{3/2}}{1 + \rho I_x^{1/2}} \right] \quad (9)$$

The Born equations [13] are represented by the following equations

$$\frac{G_m^{*E,Born}}{RT} = \frac{Q_e^2}{2kT} \left(\frac{1}{\epsilon_s} - \frac{1}{\epsilon_w} \right) \sum_i \frac{x_i z_i^2}{r_i} 10^{-2} \quad (10)$$

$$\ln \gamma_i^{*Born} = \frac{Q_e^2}{2kT} \left(\frac{1}{\epsilon_s} - \frac{1}{\epsilon_w} \right) \frac{z_i^2}{r_i} 10^{-2} \quad (11)$$

Where Q_e is the electron charge, r_i is the Born radius, and ϵ_w is the dielectric constant of pure water. Each component's dielectric constants for thermodynamic modelling are given in Table 3.4.

Table 3.4. Coefficients of dielectric constant equation^a [14]

Parameters	A	B	C
HNO ₃	19	0	298.15
H ₂ O	78.54	31989.4	298.15
H ₂ SO ₄	101	0	298.15

$${}^a \epsilon = A + B \left(\frac{1}{T} - \frac{1}{C} \right)$$

$G_m^{*E,lc}$ represents the excess Gibbs energy obtained from short-range interaction modelled with local composition activity coefficient model NRTL equation. In a generalized version, the electrolyte system comprising cation (c), anion (a), and molecular species (m) may be stated as,

$$\frac{G_m^{*E,lc}}{nRT} = \sum_m n_m \left(\frac{\sum_i X_i G_{im} \tau_{im}}{\sum_i X_i G_{im}} \right) + \sum_c z_c n_c \left(\frac{\sum_{i \neq c} X_i G_{ic} \tau_{ic}}{\sum_{i \neq c} X_i G_{ic}} \right) + \sum_a z_a n_a \left(\frac{\sum_{i \neq a} X_i G_{ia} \tau_{ia}}{\sum_{i \neq a} X_i G_{ia}} \right) \quad (12)$$

$$X_i = C_i x_i = C_i \left(\frac{n_i}{n} \right), i = m, c, a \quad (13)$$

$$n = \sum_i n_i = \sum_m n_m + \sum_c n_c + \sum_a n_a \quad (14)$$

$$G_{ij} = \exp(\alpha_{ij} \tau_{ij}) \quad (15)$$

Where α_{ij} is the non-randomness factor. τ_{ij} represents the binary energy interaction parameter given as follows,

For molecule- molecule τ_{ij} is,

$$\tau_{ij} = c_{ij} + \frac{d_{ij}}{T} \quad (16)$$

For molecule- electrolyte τ_{ij} is,

$$\tau_{ij} = c_{ij} + \frac{d_{ij}}{T} + e_{ij} \left[\frac{T_{ref}-T}{T} + \ln \left(\frac{T}{T_{ref}} \right) \right] \quad (17)$$

T_{ref} is the reference temperature, and c_{ij} , d_{ij} , and e_{ij} are adjustable parameters generated by regression of the vapour-liquid equilibrium data using Aspen Plus. Other physical characteristics of the essential components, like ideal gas heat capacity and heat of vaporizations, were acquired by extracting the coefficients of corresponding equations from the Aspen Plus [14], as shown in Tables 3.5 and 3.6.

Table 3.5. Coefficients of ideal gas heat capacity model equation^a [14]

Parameters	C ₁	C ₂	C ₃	C ₄	C ₅	C ₆	C ₇
HNO ₃	33440	70500	1041	44700	473	100	1500
H ₂ O	33363	26790	2610.5	8896	1169	100	2273.15
H ₂ SO ₄	40240	109500	943	83700	393.8	100	1500

$${}^a C_{p,i}^1 = C_{1i} + C_{2i}T + C_{3i}T^2 + C_{4i}T^3 + C_{5i}T^4 \text{ for } C_{6i} \leq T \leq C_{7i}$$

Table 3.6. Coefficients of heat of vaporization model equations [14]

Parameters	C ₁	C ₂	C ₃	C ₄	C ₅	C ₆	C ₇	C ₈
HNO ₃ ^a	7.0604e ⁺⁰⁷	0.6929	0	0	0	231.55	359.15	
H ₂ O ^a	5.66e ⁺⁰⁷	0.6120	-0.6257	0.0399	0	273.16	647.1	

H ₂ SO ₄ ^b	18.3153	0.2065	0.7616	-0.5762	578	4	280	578
---	---------	--------	--------	---------	-----	---	-----	-----

$${}^a\Delta_{\text{vap}}H_i = C_{1i}(1 - T_{ri})^{C_{2i}+C_{3i}T_{ri}+C_{4i}T_{ri}^2+C_{5i}T_{ri}^3} \text{ for } C_{6i} \leq T \leq C_{7i}; T_{ri} = \frac{T}{T_{ci}}$$

$${}^b\ln(\Delta_{\text{vap}}H_i) = C_{1i} + \sum_{m=2}^n C_{mi} T_r^{m-2} \ln(1 - T_r); T_r = T/T_C$$

Where $\Delta_{\text{vap}}H_i$ is heat of vapourization at T, T_{ri} and T_{ci} are reduced and the critical temperature of component i in Kelvin, respectively.

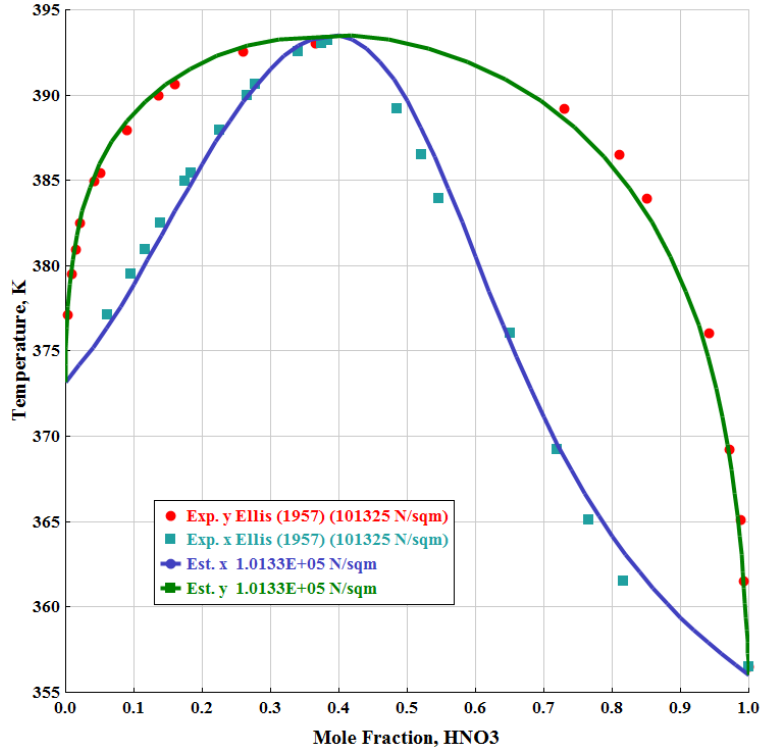
3.2.4 Data for Regression

The binary interaction parameters of molecule-molecule and molecule-electrolyte pairs, given in Tables 3.8 and 3.9, are obtained by regression of the experimental VLE data of binary and ternary system taken from literature in the Aspen DRS using eNRTL-RK thermodynamic model. The data regression system used the maximum likelihood objective function with the Britt-Luecke algorithm and Deming Initialization method. The non-randomness factor was fixed at 0.3 for all molecule-molecule pairs, while it was set at 0.2 for molecule-electrolyte and electrolyte-electrolyte pairs [10, 11].

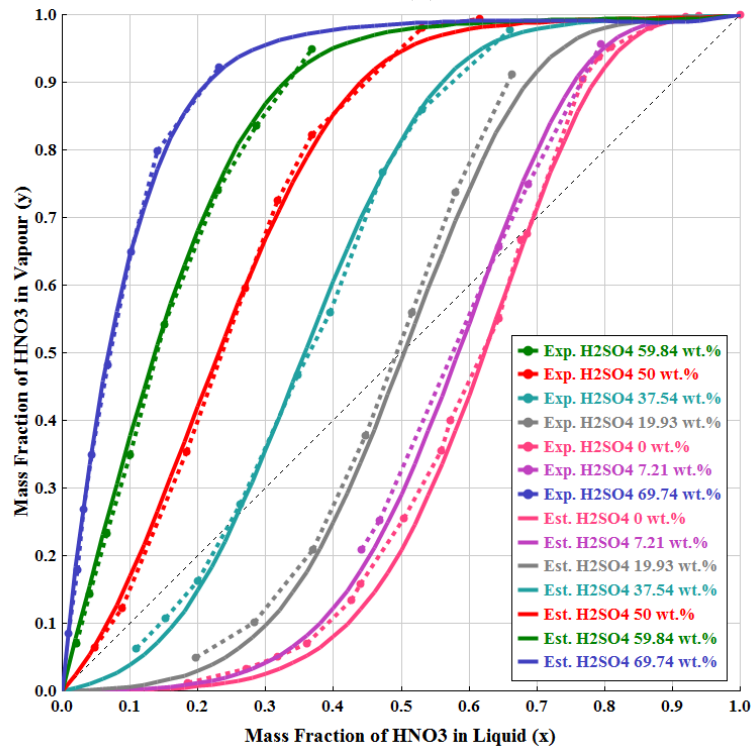
The various data sets in the literature for binary and ternary HNO₃/water/sulphuric acid systems cover the different operating pressure ranges. Ellis and Thwaites [8] reported binary and ternary T-x,y data for HNO₃/water pair and HNO₃/water/H₂SO₄ system at atmospheric pressure. The T-x,y data for HNO₃/water binary system with varying pressure, such as 79993 Pa, 59995 Pa, 101325 Pa, was determined by Potier [15], and at pressure 13332 Pa, 26664 Pa, 46663 Pa was reported by Rivenq[16]. Boublik and Kuchynka [17] reported the experimental T-x,y data at different pressure such as 26664 Pa, 101325 Pa, 6666 Pa, 53329 Pa and 13332.2 Pa. Area consistency test was applied to all the binary equilibrium data to find out the consistent thermodynamic data. Thermodynamically consistent data sets proposed by Ellis and Thwaites [8] are used for the regression exercise to determine binary interaction parameters. While performing the regression using the eNRTL model for the ternary system of HNO₃/water/H₂SO₄, initially, all possible molecule-molecule, molecule-electrolyte and electrolyte-electrolyte interaction parameters, including water-H₂SO₄ pair were considered. However, it was found that the eNRTL model needs to fit better into the experimental data and show significant deviation from the experimental data. It was also not predicting the azeotropic compositions well. Hence, the regression exercise was completed without the water-H₂SO₄ molecule-molecule interaction

parameter. However, their interaction is considered via molecule-electrolyte pairs of (water- H_3O^+ , HSO_4^- and water- H_3O^+ , SO_4^{2-}). The selection of interaction parameters was validated from previously reported literature about the eNRTL parameters regression comprising water- H_2SO_4 pair. It was found that the H_2SO_4 -water pair molecule-molecule interaction parameters were not considered [18, 19], which validates the selection of the interaction parameters for the present investigation.

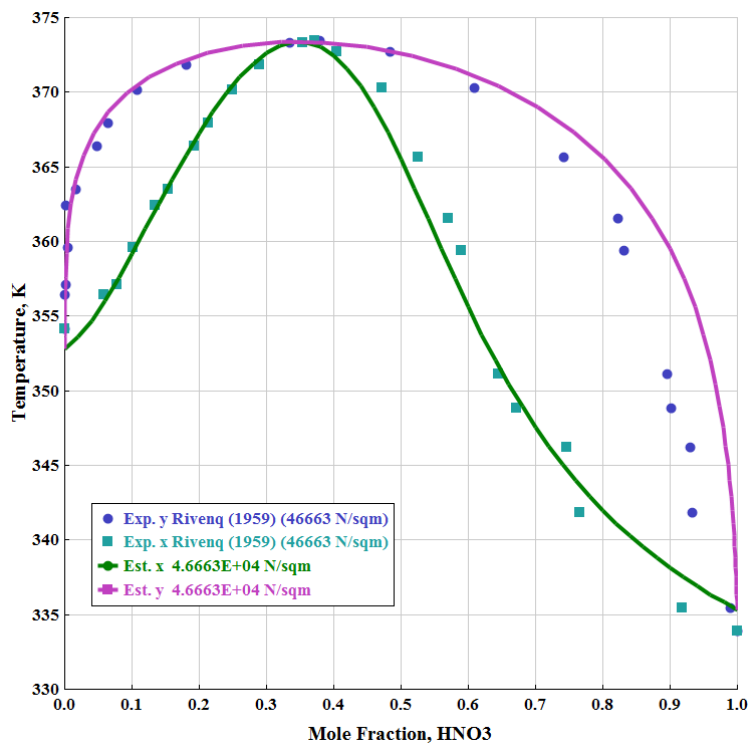
Model parameters were validated by plotting the experimental data of Ellis and Thwaites [8], Potier [15], and Rivenq [16], with the estimated data based on the regressed parameters simultaneously. Estimated VLE data with the regressed parameters shows a good agreement with experimental data reported in the literature, as shown in Figure 3.1 (a), (b), (c) and (d) and Table 3.7. As shown in Figure 3.1 (a), the azeotropic behaviour of the HNO_3 and water system predicted by the model is well in agreement with the experimental data on the phase equilibrium diagram. The plot of the vapour-liquid-equilibrium diagram with ternary experimental data of Ellis and Thwaites[8] and estimated data from the model parameter was drawn on solvent-free basis composition on both axes and varying solvent concentration from 0 to 69.74 mass % at atmospheric pressure as shown the Figure 3.1 (b). It can also be seen that more than 50 mass % composition of H_2SO_4 is required to eliminate the azeotrope of the HNO_3 and water. Thus, it could be confirmed that estimated binary interaction parameters, given in Tables 3.8 and 3.9 from the regression, can predict the experimental equilibrium behaviour of the system accurately and is suitable for further modelling and simulation of the extractive distillation process.



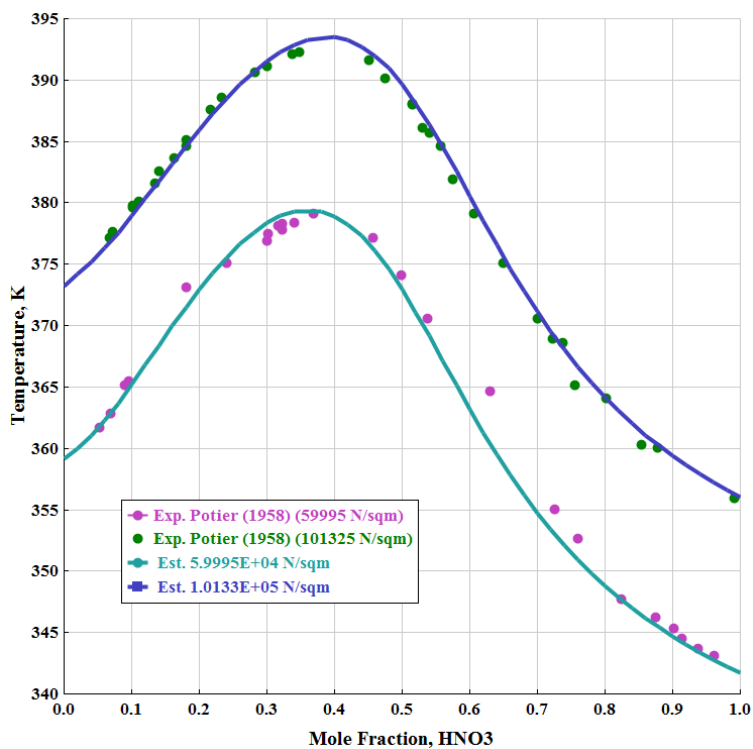
(a)



(b)



(c)



(d)

Figure 3.1. VLE diagram of HNO₃/water/H₂SO₄ binary and ternary system with experimental and estimated data.

Table 3.7. Average Absolute Deviation (AAD) between Experimental Data and Model Data

Pressure (N/m ²)	ΔT	Δy	Reference
101325	0.0020	0.1451	7
46663	0.0029	0.3171	15
59995	0.0028	-	14
10133	0.0387	-	14

$AAD = \frac{1}{k} \sum_{i=1}^k \left| \frac{Z_i - Z_{M_i}}{Z_{M_i}} \right|$ Where Z_i is the regressed or estimated property value, Z_{M_i} is the corresponding experimental or measured value and k is the total number of data points.

Table 3.8. Molecule-molecule binary interaction parameter for ENRTL-RK thermodynamic model obtained using regression of experimental data

Component i	Component j	A_{ij}	B_{ij}	$\alpha_{ij}=\alpha_{ji}$	τ_{ij} (at 298.15 K)
HNO ₃	Water	10.52	-4890.22	0.3	-5.88
Water	HNO ₃	-12.11	4407.67		2.67
HNO ₃	H ₂ SO ₄	3.43	0	0.3	3.43
H ₂ SO ₄	HNO ₃	-2.24	0		-2.24

3.3 Extractive Distillation Configuration

Table 3.9. Molecule-electrolyte binary interaction parameter for ENRTL-RK thermodynamic model obtained using regression of experimental vle data

Component i	Component j	C_{ij}	D_{ij}	E_{ij}	τ_{ij} (298.15 K)
HNO ₃	H ₃ O ⁺ , NO ₃ ⁻	3.74	997.76	-184.27	7.09
H ₃ O ⁺ , NO ₃ ⁻	HNO ₃	-3.50	-350.78	-16.88	-4.67
Water	H ₃ O ⁺ , NO ₃ ⁻	8.62	370.77	-73.45	9.86
H ₃ O ⁺ , NO ₃ ⁻	Water	-5.13	-437.18	5.65	-6.59
HNO ₃	H ₃ O ⁺ , HSO ₄ ⁻	0.07	-58.61	6.27	-0.13
H ₃ O ⁺ , HSO ₄ ⁻	HNO ₃	0.25	-30.27	37.54	0.15
Water	H ₃ O ⁺ , HSO ₄ ⁻	-0.31	-394.07	4.12	-1.64
H ₃ O ⁺ , HSO ₄ ⁻	Water	-0.91	-507.84	4.41	-2.62
HNO ₃	H ₃ O ⁺ , SO ₄ ⁻²	-4.67	-200.02	1840.15	-5.34

$\text{H}_3\text{O}^+, \text{SO}_4^{-2}$	HNO_3	-9.74	4878.19	5841.71	6.62
Water	$\text{H}_3\text{O}^+, \text{SO}_4^{-2}$	-27.64	-6721.32	275.15	-50.18
$\text{H}_3\text{O}^+, \text{SO}_4^{-2}$	Water	4.79	1159.76	326.40	8.68
H_2SO_4	$\text{H}_3\text{O}^+, \text{HSO}_4^-$	29.34	341.73	651.87	30.48
$\text{H}_3\text{O}^+, \text{HSO}_4^-$	H_2SO_4	-15.31	-8.50	3971.22	-15.33
H_2SO_4	$\text{H}_3\text{O}^+, \text{NO}_3^-$	-5.43	-1.52	-1.75	-5.44
$\text{H}_3\text{O}^+, \text{NO}_3^-$	H_2SO_4	-4.46	-1.75	-1.72	-4.47

In this section, the design, simulation and optimization of the complete nitric acid dehydration by extractive distillation configuration are performed using sulphuric acid as a solvent, using the eNRTL-RK thermodynamic model, with the binary interaction parameters obtained in the previous section. This work considers a feed stream with 20 mass % dilute HNO_3 at 100 kg/h mass flow rate at 298 K and 1 atm pressure as a design basis. As it is very dilute, it must first be concentrated to the azeotropic composition in a pre-concentrating distillation column (PDC) before sending it to the extractive distillation column (EDC). The process flowsheet for the complete distillation sequence is shown in Figure 3.2. As nitric acid and water form a maximum boiling azeotrope at 120 °C and at about 68 mass % of nitric acid concentration, a mixture containing nearly azeotropic composition is obtained from the bottom (B1) of the PDC. In contrast, pure water is obtained from the top of the PDC as a distillate (D1).

The azeotropic mixture, obtained from the bottom stream of the PDC, is fed to one of the intermediate stages of the EDC column. The concentrated sulphuric acid (98 mass %) is fed as a solvent at an appropriate stage above the azeotropic feed stage. The added solvent alters the relative volatility of the components such that azeotrope breaks and pure nitric acid is recovered from the top of the EDC column as a distillate (D₂). The mixture of water and sulphuric acid obtained from the bottom (B₂) of the EDC is sent directly to the solvent recovery distillation column (SRDC), where sulphuric acid is recovered from the bottom stream (B₃) is recycled to the EDC column as a recycle stream. A cooler is placed in the recycle loop before the solvent gets recycled to the EDC to maintain the desired solvent feed temperature. The minute quantity of solvent lost from the distillate streams, D₂ and D₃ of the EDC and SRDC, respectively, is balanced using the makeup stream.

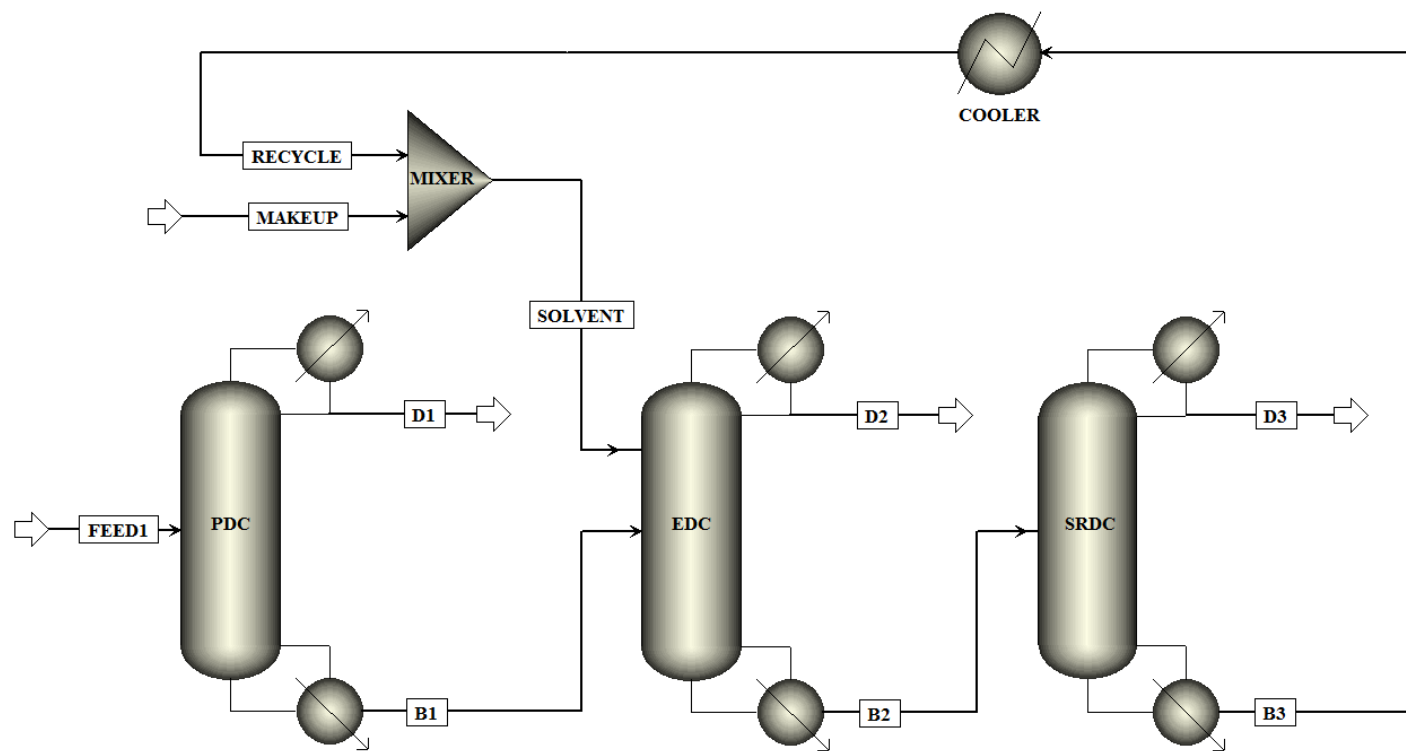


Figure 3.2. Process flow diagram of distillation column sequence for dehydration of dilute nitric acid

3.3.1 Basis for TAC Analysis

Table 3.10. Equations for equipment sizing and economics analysis

1. Diameter (D): from the ASPEN packing sizing option

2. Height (H): of a packed distillation column,

$$H \text{ (m)} = 1.2 \times \text{HETP} \times (N_T - 2)$$

Where N_T -number of stages of the column

3. Column Capital Cost:

$$\text{Column cost}(\$) = (\text{M\&S}/280) \times 937.636 \times D^{1.066} \times H^{0.802} \times (2.18 + F_c)$$

4. Heat Exchanger (HE) Capital Cost:

$$\text{Heat exchanger cost}(\$) = (\text{M\&S}/280) \times 474.668 \times A^{0.65} \times (2.29 + F_c)$$

5. Area of HE (both Condenser and Reboiler):

$$A = Q / (U \times \Delta T_{lm})$$

Heat-transfer coefficient (U) for condenser = 0.852 (kW/ m²K)

Heat-transfer coefficient (U) for reboiler = 0.568 (kW/ m²K)

6. Utility Cost:

LP steam (433 K) = \$7.72 /GJ

MP steam (457 K) = \$8.22 /GJ

HP steam (537 K) = \$9.88 /GJ

Cooling water = \$0.354 /GJ

Chilled water = \$4.43 /GJ

7. Total Annual Cost (TAC):

$$\text{TAC} = \frac{\text{Capital Cost}}{\text{Payback Period}} + \text{Energy Cost}$$

Payback period = 3 years

Total operating hours = 8000 hrs.

The economic evaluation of the extractive distillation system is done in terms of total annual cost (TAC). The diameter of a distillation column is determined by the ‘Packing Sizing’ function of the Aspen Plus simulator using the “Durapak” glass structure packing of standard dimension available in the Aspen. The basis of economics and equipment sizing and costing equations are summarized in Table 3.10, which are based on Douglas [20] and Luyben[3] other costs, such as pumps, valves and pipes, are neglected as a minor fraction of total equipment cost. 2.21 Marshal and Swift index (M&S) [22] value considered for all the calculations equals to 1431.7.

3.3.2 Simulation Analysis and Economic Optimization

Rigorous simulation of extractive distillation of nitric acid dehydration system is performed using Aspen Plus simulator with *Radfrac* distillation model. This model performs rigorous calculations comprising solving mass balance, equilibrium relationship, summation equation, and enthalpy balance equations, generally known as MESH equations added into the Supporting Information document. The numerical solution was obtained by simultaneously solving MESH equations at each stage of the distillation column with the Broyden quasi-Newton method. The MESH equations are applied and solved for each stage of the distillation column and each component to obtain the rigorous solution in the Aspen Plus simulator.

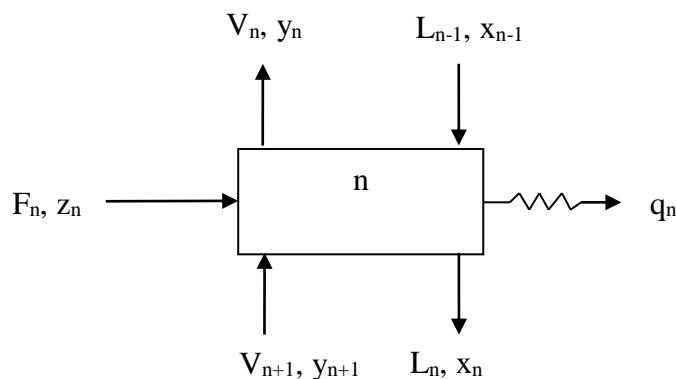


Figure 3.3. Schematic representations of the input and output to any stage n of the multistage distillation column.

Mass Balance Equation: The mass balance equation for any component i on any stage n of the multistage distillation column given as,

Overall mass balance equation,

$$F_n + V_{n+1} + L_{n-1} = V_n + L_n \quad (18)$$

Component balance equation,

$$F_n z_n + V_{n+1} y_{n+1} + L_{n-1} x_{n-1} = V_n y_n + L_n x_n \quad (19)$$

Equilibrium relationship: vapour-liquid equilibrium relationship for component i is given as,

$$y_i = K_i x_i \quad (20)$$

Where K is the chemical equilibrium constant.

Heat (Energy) Balance Equation:

$$F_n H_{F,n} + V_{n+1} H_{V,n+1} + L_{n-1} H_{L,n-1} \pm q_n = V_n H_{V,n} + L_n H_{L,n} \quad (21)$$

Summation Equation: summation of mole fractions in the liquid and vapour phase should be unity.

$$\sum x_{i,n} = \sum y_{i,n} = 1 \quad (22)$$

Where

F_n - feed flow into stage n.

V_n - vapour flow leave from the stage n.

V_{n+1} - vapour flow added to stage n, from the below stage n+1.

L_n - liquid flow leaves from stage n.

L_{n-1} - liquid flow added to stage n from the above stage n-1.

z - mole fractions of component i in the feed stream;

x - mole fractions of component i in the liquid phase;

y - mole fractions of component i in the vapour phase;

H - specific enthalpy.

q_n - heat added or removed from the given stage n.

The distillate purity of nitric acid and water obtained from the respective columns was set at 99.99 mass %. The design specification was used to achieve the desired purity of the product by varying the distillate mass flow rate or the reflux ratio of the respective columns. Sensitivity analysis [23, 24] was used to determine the effect of various operating parameters on the purity of the product, reboiler and condenser duty of the column and to minimize the column's total annual cost (TAC).

The various design variables in the extractive distillation systems, which need to be determined for optimum performances are listed below. All these parameters were optimized based on the minimum reboiler duty and TAC to achieve the desired purity product.

- Total number of stages (N_T)
- Solvent to feed ratio (E/F)
- Feed stage location (N_F)
- Solvent feed stage location (N_{EF})
- Solvent feed temperature (T_{EF})
- Mass reflux ratio (RR)

The sequential iterative optimization procedure, as discussed below and shown in Figure 3.4, is used to optimize all the above design parameters,

- (1) Select the column pressure.
- (2) Select the respective column's total number of stages (N_T) to achieve desired purity.
- (3) Select the binary feed stage location (N_F) and solvent feed stage location (N_{FS}).
- (4) Select the entrainer to feed (E/F) ratio and solvent feed temperature (T_{EF}).
- (5) Vary the reflux ratio and distillate rate to meet desired product purity of the respective column.
- (6) Use sensitivity analysis to determine the optimal range of the N_T , E/F, N_{EF} , N_{FS} , T_{EF} and RR with optimal Q_R and Q_C .
- (7) Return to step 4 and change E/F until TAC is minimized.
- (8) Return to step 3 and change N_{FF} and N_{FS} until TAC is minimized.
- (9) Return to step 2 and change N_T until TAC is minimized.
- (10) Repeat the steps from 7 to 9 to get TAC minimized.

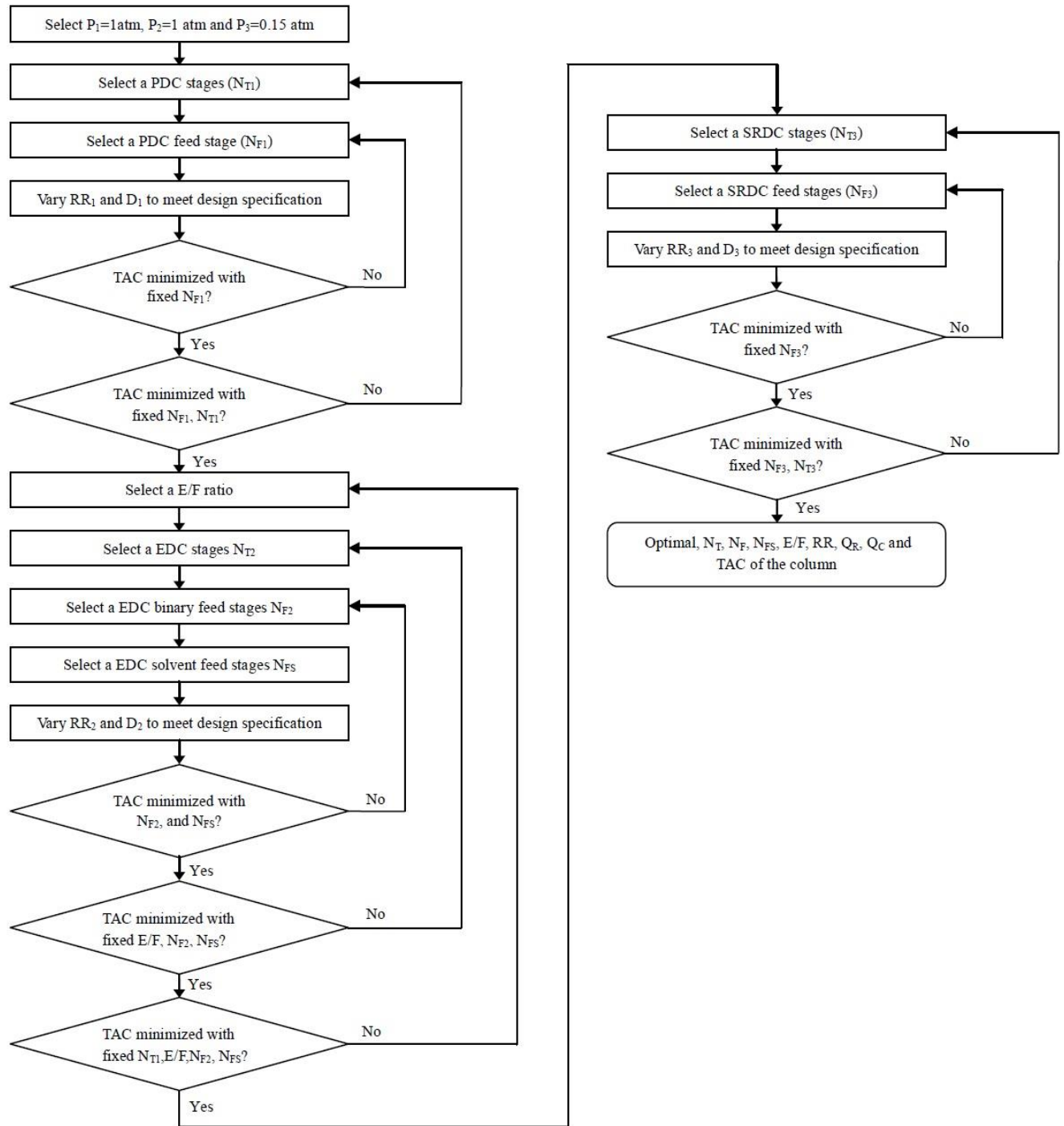


Figure 3.4. Sequential iterative procedure for optimization of design parameters for ED of nitric acid water system

3.4 Result and Discussion

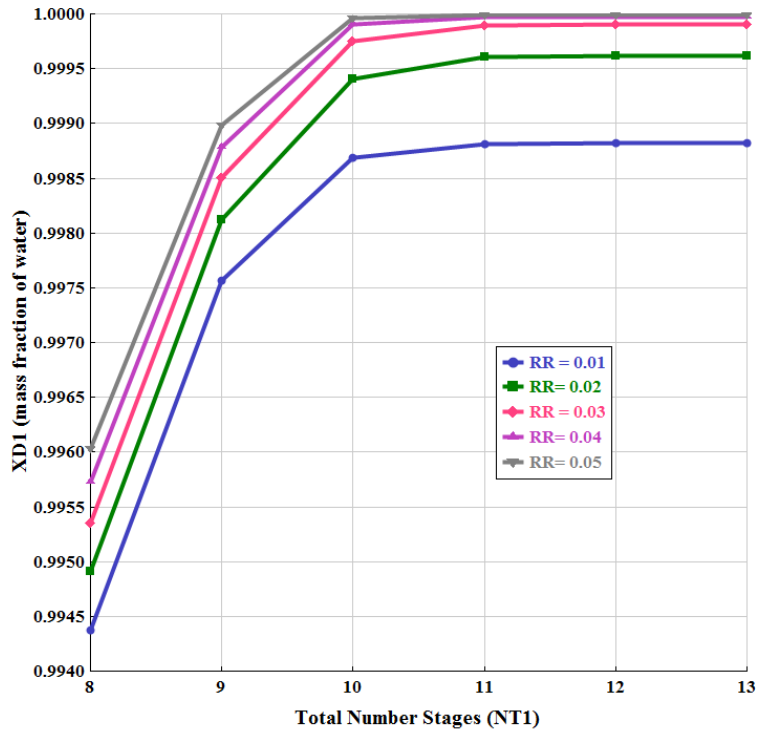
3.4.1 Operating Pressure for Column

It was chosen to operate both PDC and EDC columns at atmospheric pressure. In the case of SRDC, vacuum conditions are preferred as operation at atmospheric pressure will demand high-temperature utility to operate the reboiler due to the higher boiling point of sulphuric acid. Below 0.15 atm pressure condenser needs a chilled utility which consequently increases the TAC of the column significantly because of increased operating cost. Hence, operating the SRDC column at 0.15 atm pressure is suitable.

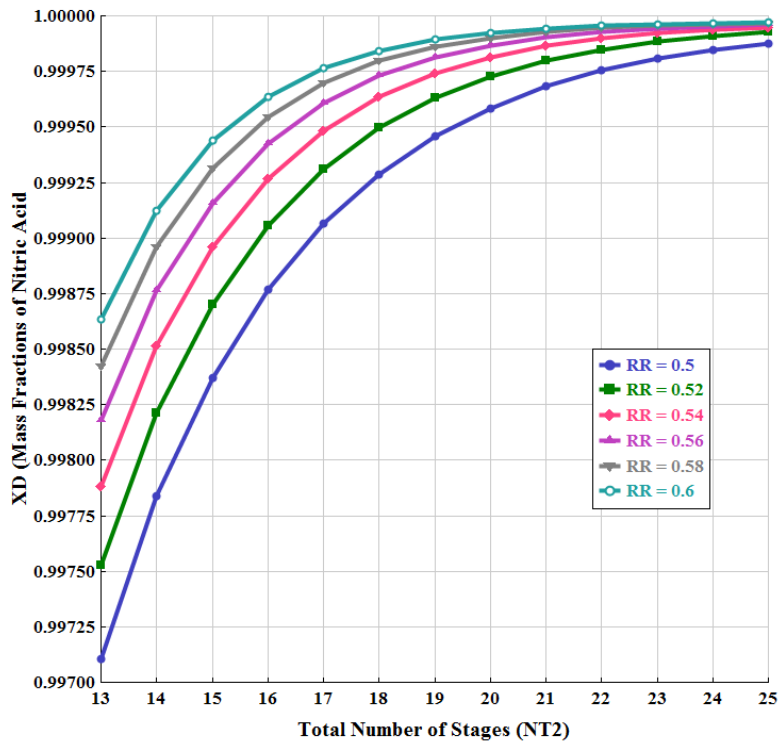
3.4.2 Selection of Number of Stages (N_T)

The selection of a total number of stages is a crucial design parameter in the extractive distillation system, as it directly influences the TAC and the purity of the product. N_T 's effect on the distillate product's purity is analyzed through the results obtained from sensitivity analysis by plotting the N_T versus distillate purity (X_D) at different mass reflux ratios. The effect of variation in the number of stages on the TAC was determined by estimating the TAC of the column to achieve the desired purity. In the case of the PDC, the distillate product is water. It can be observed in Figure 3.5. (a) the desired purity of the product in the distillate is attained if the number of stages of the PDC column is greater than or equal to 10 with a mass reflux ratio (RR) greater than 0.04. TAC of the PDC column was estimated for different N_T in the range of 9 to 13, as shown in Table 3.11. It is concluded from the results obtained in Table 3.11 that PDC with 10 stages have minimum TAC and can be considered as the optimum number of stages for the PDC column.

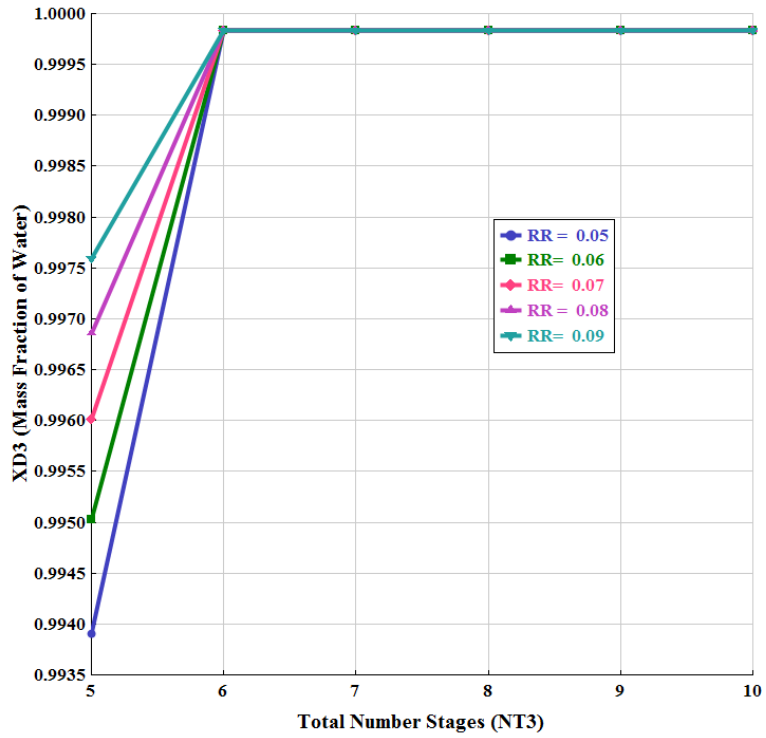
In the case of EDC, desired product purity of nitric acid was achieved after the $N_T = 20$ and mass RR greater than 0.58, as shown in Figure 3.5 (b). The estimated TAC for the EDC for total stages from 16 to 22 indicates a minimum TAC at $N_T = 20$, as shown in Table 3.12. Similarly, for SRDC, as seen in Figure 3.5 (c), the desired distillate purity was achieved at $N_T = 6$. After that, the distillate concentration is almost constant irrespective of the increasing number of stages. Having additional stages beyond this point increases the capital cost. TAC of the SRDC column was estimated for the total number of stages from 6 to 10, as shown in Table 3.13, and it was confirmed that a minimum TAC is obtained for $N_T = 6$.



(a)



(b)



(c)

Figure 3.5. Effect of the total number of stages (N_T) on distillate purity (X_D) for (a) PDC (b) EDC (c) SRDC

Table 3.11. Economic optimization for PDC of nitric acid dehydration ED system for the different total number of stages (N_{TI})

N_{TI}	9	10	11	12	13
Pressure (P_1) (atm)	1	1	1	1	1
RR_1 (optimum)	0.140	0.040	0.029	0.022	0.020
N_{FF} (optimum)	3	4	5	5	6
D (m)	0.2117	0.2064	0.2058	0.2055	0.2054
H (m)	3.36	3.84	4.32	4.8	5.28
Q_R (kW)	89.19	84.73	84.23	83.94	83.84
A_R	3.98	3.78	3.76	3.74	3.74
Q_C (kW)	50.87	46.41	45.91	45.62	45.52
A_C	0.88	0.80	0.79	0.79	0.78
Total capital ($10^3\$$)	58.97	58.56	59.99	61.48	63.04
Total operating ($10^3\$/y$)	20.50	19.46	19.34	19.27	19.25
TAC ($10^3\$/y$)	40.16	38.98	39.34	39.77	40.26

Table 3.12. Economic optimization for EDC of nitric acid dehydration ED system for the different total number of stages (N_{T2})

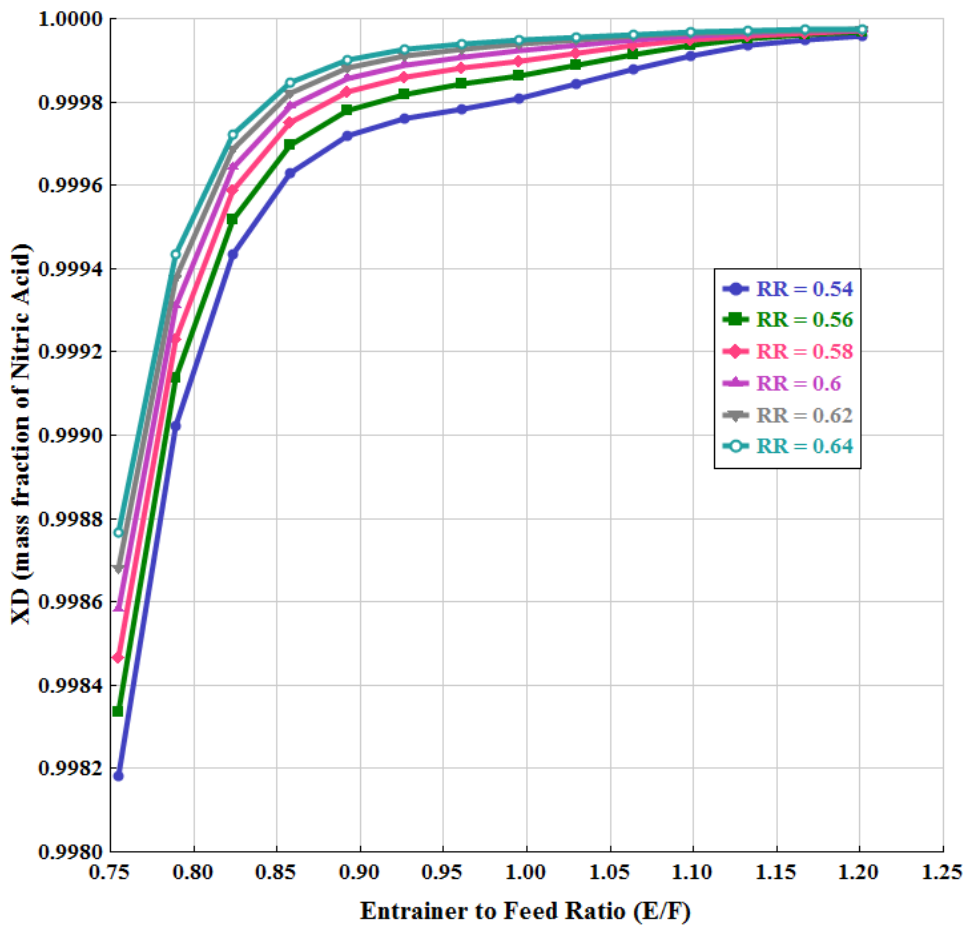
N_{T2}	16	17	18	19	20	21	22
Pressure (P_2) (atm)	1	1	1	1	1	1	1
RR_2 (optimum)	0.75	0.69	0.64	0.61	0.58	0.56	0.55
N_{FF} (optimum)	6	6	6	6	6	6	6
N_{FS} (optimum)	4	5	5	5	5	5	5
D (m)	0.0335	0.0326	0.0318	0.0314	0.0309	0.0306	0.03
H (m)	6.72	7.20	7.68	8.16	8.64	9.12	9.60
Q_R (kW)	1.93	1.76	1.62	1.54	1.46	1.40	1.36
A_R	0.05	0.04	0.04	0.04	0.04	0.04	0.03
Q_C (kW)	4.90	4.73	4.59	4.51	4.42	4.37	4.33
A_C	0.11	0.11	0.11	0.10	0.10	0.10	0.10
Total capital ($10^3\$$)	8.75	8.68	8.63	8.68	8.71	8.80	8.91
Total operating ($10^3\$/y$)	0.60	0.55	0.51	0.48	0.46	0.44	0.43
TAC ($10^3\$/y$)	3.51	3.44	3.39	3.38	3.36	3.38	3.40

Table 3.13. Economic Optimization of SRDC of nitric acid dehydration ED system for the different total number of stages (N_{T3})

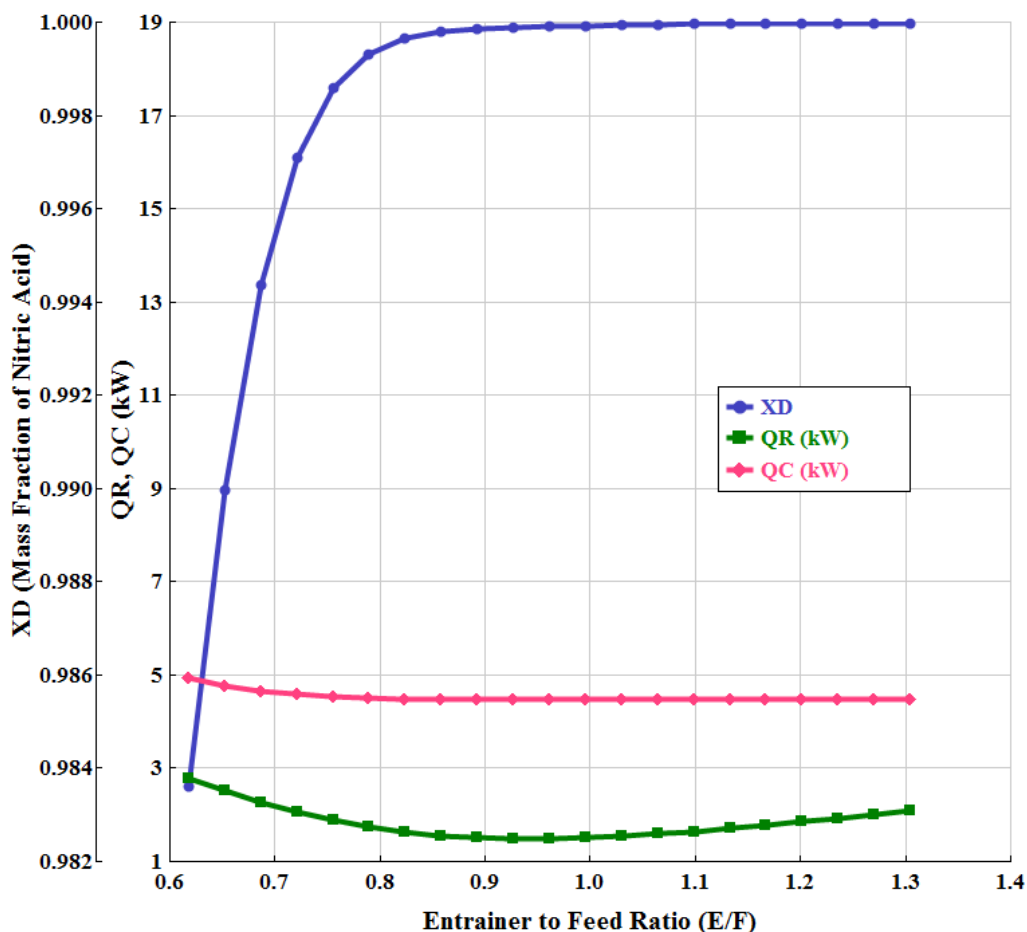
N_{T3}	6	7	8	9	10
Pressure (atm)	0.15	0.15	0.15	0.15	0.15
RR ₃ (optimum)	0.05	0.05	0.05	0.07	0.05
N _{FF} (optimum)	3	3	3	5	3
D (m)	0.1243	0.1241	0.1241	0.1243	0.1241
H (m)	1.92	2.40	2.88	3.36	3.84
Q _R (kW)	11.86	11.82	11.82	11.86	11.82
A _R (m ²)	0.76	0.76	0.76	0.76	0.76
Q _C (kW)	6.48	6.44	6.44	6.48	6.44
A _C	0.34	0.34	0.34	0.34	0.34
Total capital (10 ³ \$)	22.80	23.85	24.92	26.02	26.95
Total operating (10 ³ \$/y)	3.44	3.43	3.43	3.44	3.43
TAC (10 ³ \$/y)	11.04	11.38	11.74	12.11	12.41

3.4.3 Selection of Solvent to Feed (E/F) Ratio

Solvent-to-feed (E/F) mass ratio is one of the most critical design parameters in designing of EDC column, which directly affects the heating and cooling duties as well as distillate product purity, as shown in Figures 3.6 (a) and (b). The effect of the E/F ratio on the distillate purity was studied through sensitivity analysis. The plot of the E/F ratio versus distillate purity (X_D) with varying reflux ratios is shown in Figure 3.6 (a). It is observed that at desired purity of the distillate product is attained around an E/F ratio value of greater than 0.95 and a reflux ratio value of 0.6. A higher reflux ratio needs a higher E/F ratio due to dilution caused by a reflux stream at a higher RR. Hence, the optimum value for E/F is 1 with an optimum reflux ratio of 0.58, which leads to the desired purity with minimum energy consumption.



(a)



(b)

Figure 3.6. Effect of E/F ratio on (a) Distillate purity (X_D) with different reflux ratios (b) X_D , Q_R and Q_C of EDC column of nitric acid dehydration ED system.

In conventional distillation higher value of reflux, ratio gives higher purity with less number of stages. However, in the case of the EDC column, a higher RR value causes dilution of the solvent stream extractive section of the column and affects the purity of the top product. So, the optimum reflux ratio was determined by plotting the X_D , Q_R and Q_C versus mass reflux ratio (RR) with all other parameters constant, as shown in Figure 3.7. The desired distillate purity is attained between a reflux ratio of 0.56 to 3.10 and continuously decreases after an RR of 3.10. It can also be observed that a higher reflux ratio increases the reboiler and condenser duty sharply. Hence, the mass RR is fixed at the lower side, which is at 0.58 in this case which achieved the desired purity with minimum energy consumption.

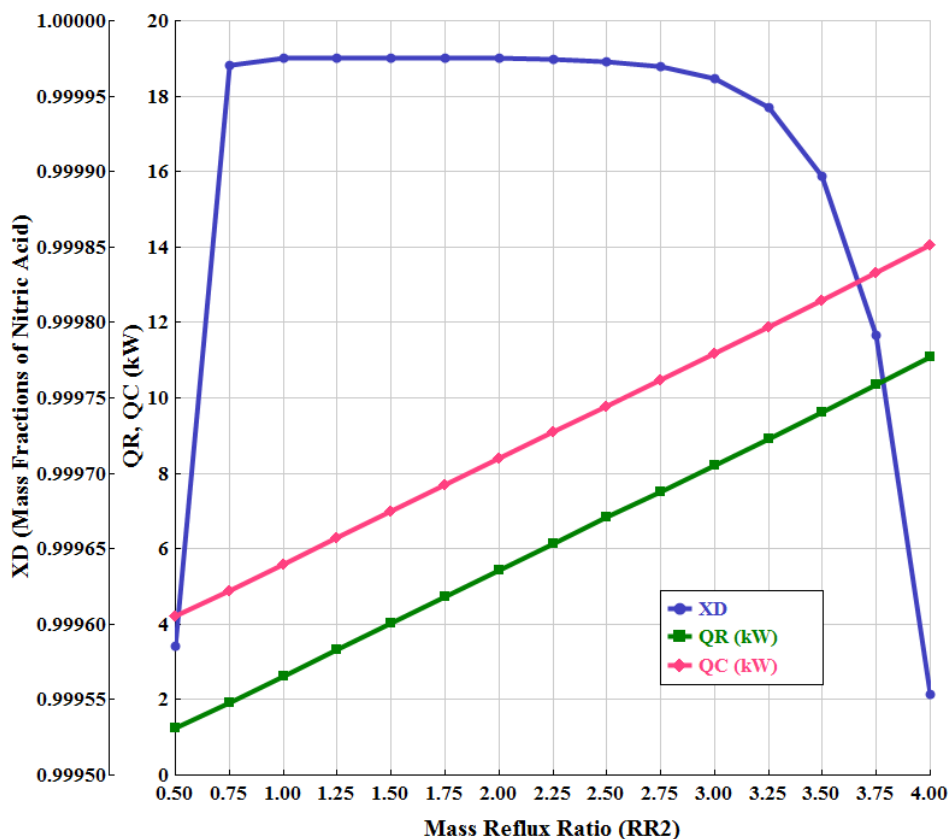
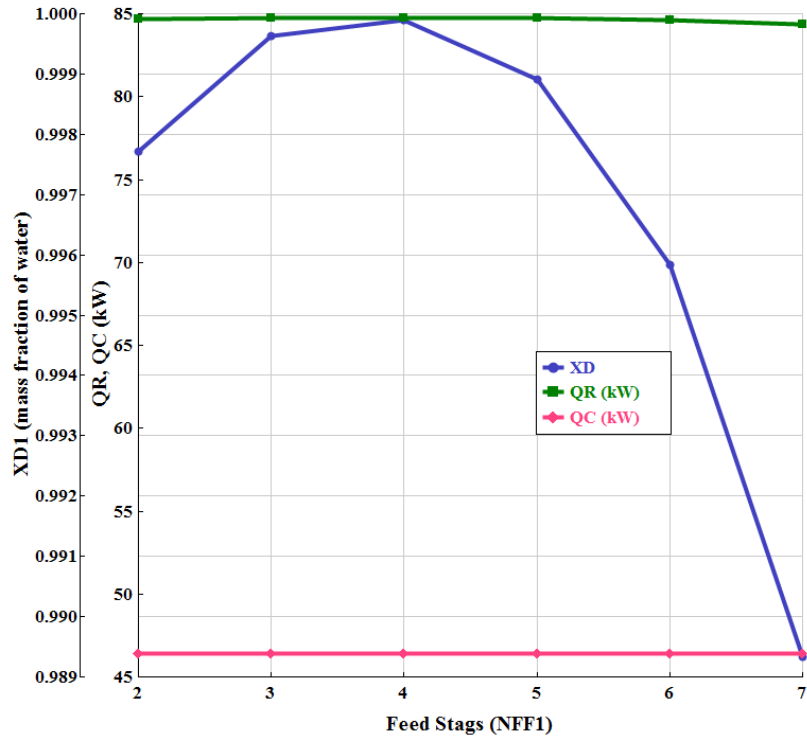


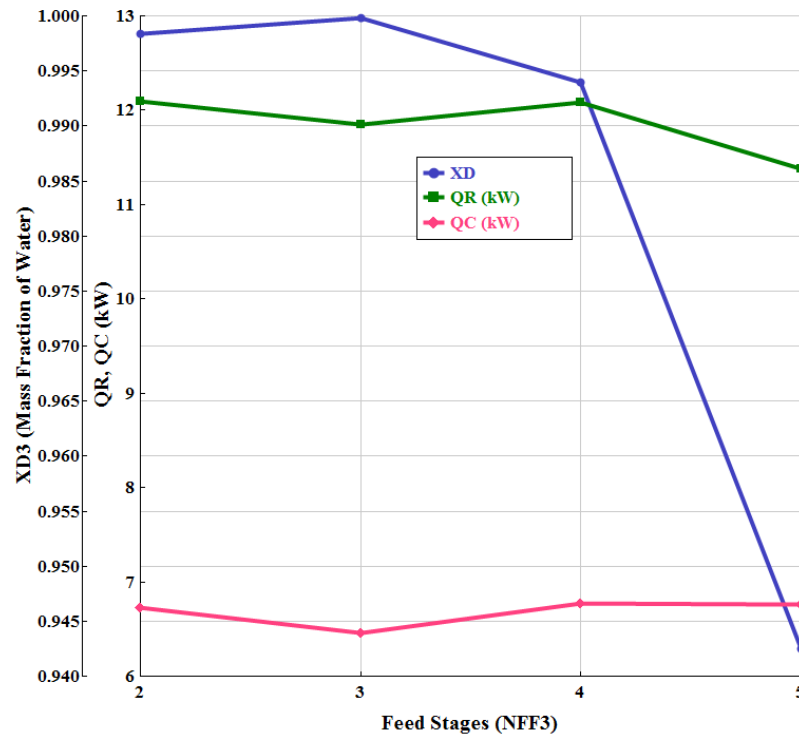
Figure 3.7. Effect of Mass Reflux Ratio (RR) on X_D , Q_R and Q_C of the EDC column of nitric acid dehydration ED system

3.4.4 Binary Mixture Feed Stage (N_{FF}) and Solvent Feed Stage (N_{EF})

While choosing the optimal total numbers of stages, the optimal binary feed stage (N_{FF}) and solvent feed stage (N_{EF}) locations are determined for the desired distillate purity with lower energy consumption. The effect of binary mixture feed location (N_{FF}) on the distillate purity (X_D), reboiler (Q_R) and condenser (Q_C) duty is shown in Figure 3.8 (a) and (b) for PDC and SRDC, respectively. It was found that feed stage location at 4 and 3 gives desired distillate purity with minimum reboiler and condenser duty in the case of PDC and SRDC, respectively. In the case of the EDC column, the binary feed stage is fixed at $N_{FF} = 6$ and above. In contrast, the solvent feed stage is fixed at $N_{EF} = 5$ as it gives the desired mass fractions of nitric acid in the distillate of the column with the lowest reboiler and condenser duty, as shown in Figure 3.9 (a) and (b) which results in the reduction in the TAC as given in Table 3.12.

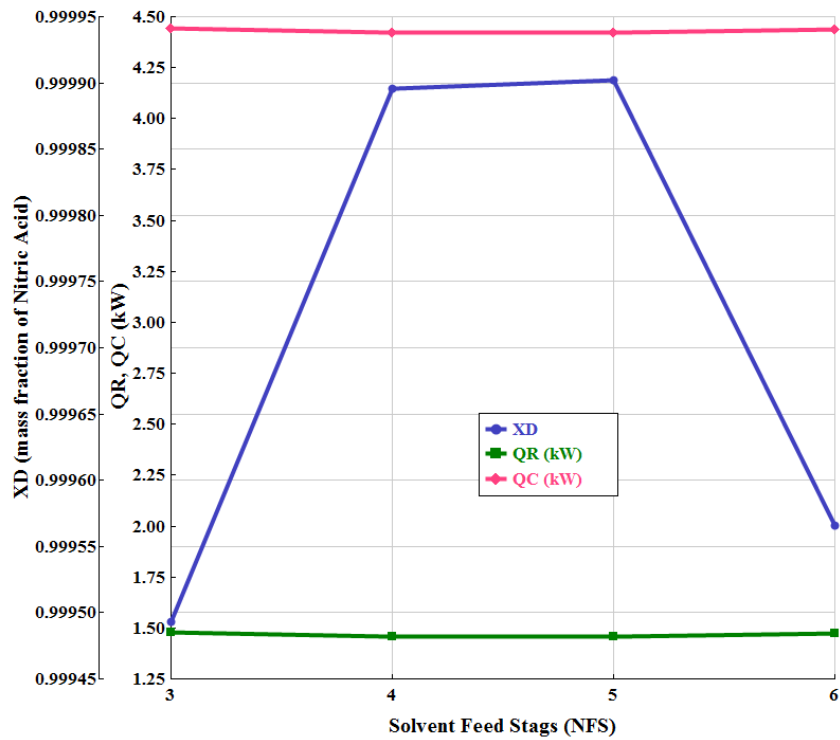


(a)

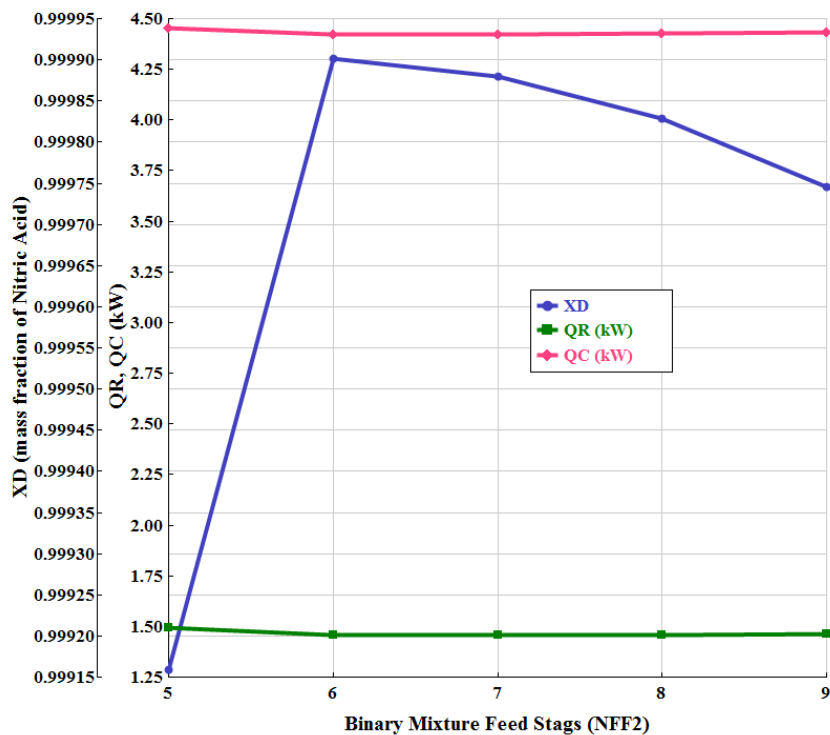


(b)

Figure 3.8. Effect of binary mixture feed location (N_{FF}) on X_D , Q_R and Q_C of (a) PDC and (b) SRDC of nitric acid dehydration ED system



(a)



(b)

Figure 3.9. (a) Effect of solvent feed stage (N_{EF}) and (b) Effect of binary mixture feed location (N_{FF}) on the X_D , Q_R and Q_C of EDC of nitric acid dehydration ED system.

3.4.5 Solvent Feed Temperature (T_{EF})

The effect of solvent feed temperature on the distillate purity and the energy consumption is also determined, as shown in Figure 3.10. It is observed that as solvent temperature increases beyond the top temperature of the column, the purity of the product decreases significantly. Therefore, the solvent feed temperature is kept at 5 to 15 °C below the top temperature of the EDC column, which agrees with the general rule for selecting the solvent feed temperature proposed by Knight and Doherty [25]. In this case, the solvent temperature has been kept at 350 K, at which desired purity product is obtained with optimum reboiler and condenser duty.

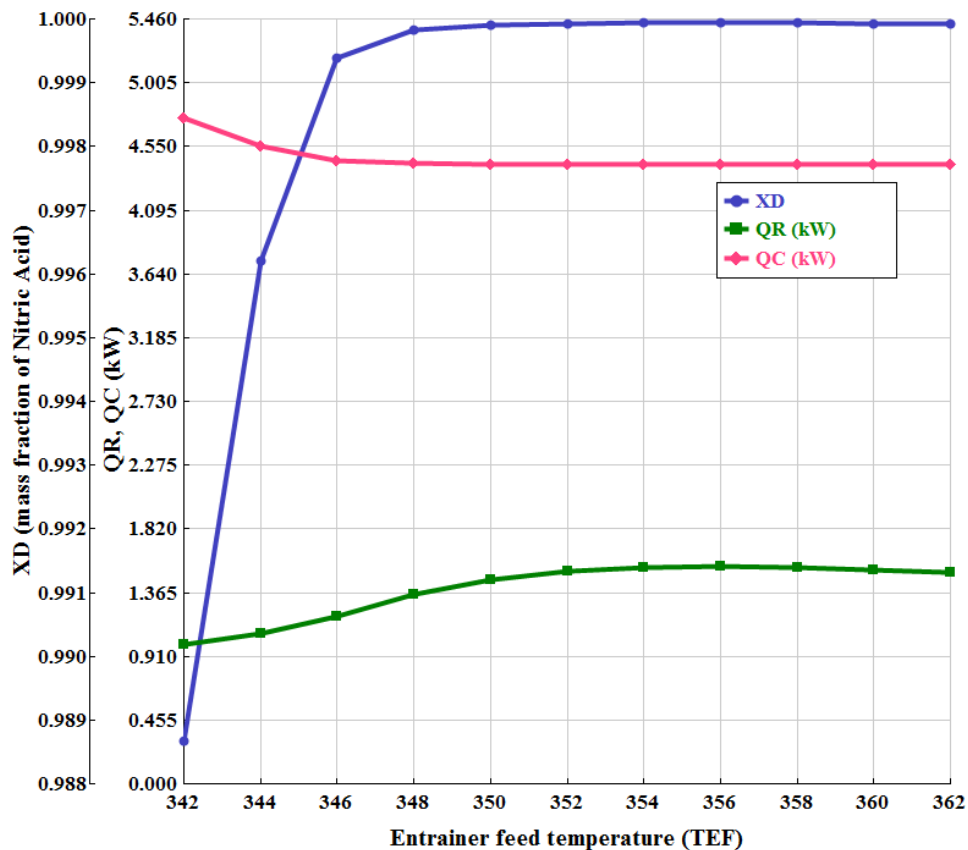


Figure 3.10. Effect of solvent feed temperature (T_{EF}) on X_D , Q_R and Q_C of the EDC of nitric acid dehydration ED system

3.4.6 Complete Conceptual Design of Proposed of Nitric Acid Dehydration ED System Configuration

Triple column extractive distillation process flowsheet containing pre-concentration (PDC), extractive (EDC) and solvent recovery (SRDC) columns for nitric acid dehydration using sulphuric acid as an extractive solvent with optimized parameters is shown in Figure 3.11. With the optimized operating and structural parameters, a purity of 99.99 mass % for nitric acid in distillate (D₂) from the extractive column and purity of 99.99 mass % for water from the distillate (D₁) of PDC and up to 99.98 mass % from the distillate (D₃) of SRDC column is achievable. Thus, sulphuric acid can be considered an excellent extractive solvent for the dehydration of nitric acid. According to the results obtained from the simulation, the E/F mass ratio around 1.0 is appropriate for desired product purity. A very minute quantity of sulphuric acid gets lost from the distillate streams due to its high boiling point, which needs to be balanced by a makeup stream added to the recycle loop of the system. The detailed TAC calculation of the extractive distillation configuration is given in Table 3.14. The overall TAC of the system is around $\$53.82 \times 10^3/\text{y}$. Figures 3.12 and 3.13 provide temperature and composition profiles for EDC and SRDC columns, respectively. The azeotropic feed is introduced on stage 6. It was observed that the objective of extractive distillation is achieved by preventing water from entering the rectifying section.

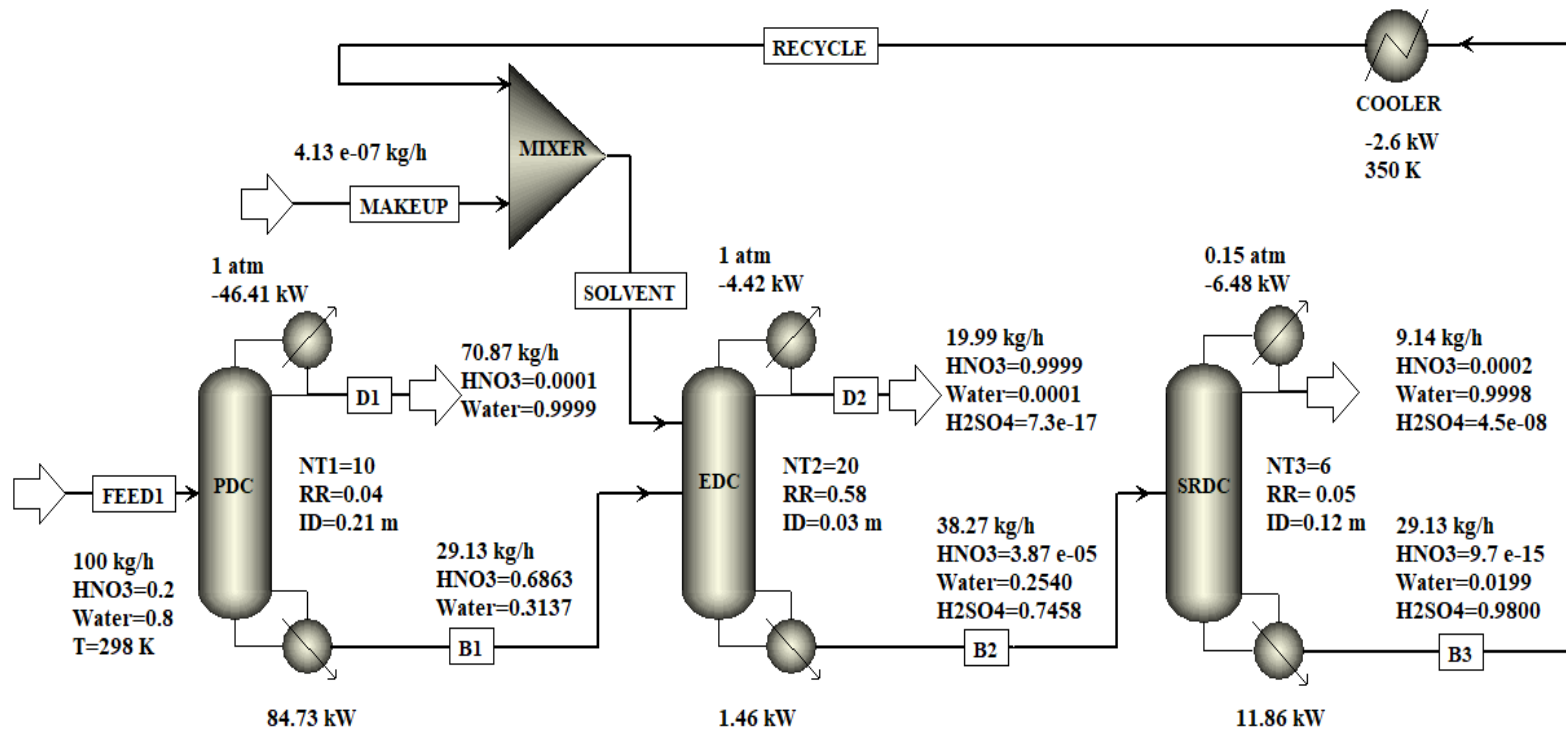
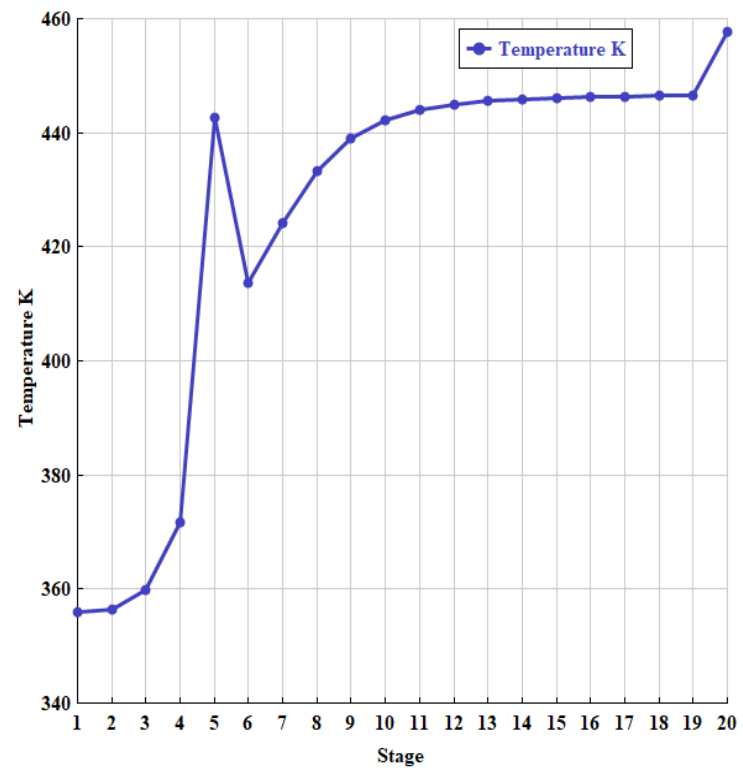


Figure 3.11. Optimal design flow sheet of distillation column sequence for dilute nitric acid dehydration ED system with sulphuric acid as solvent



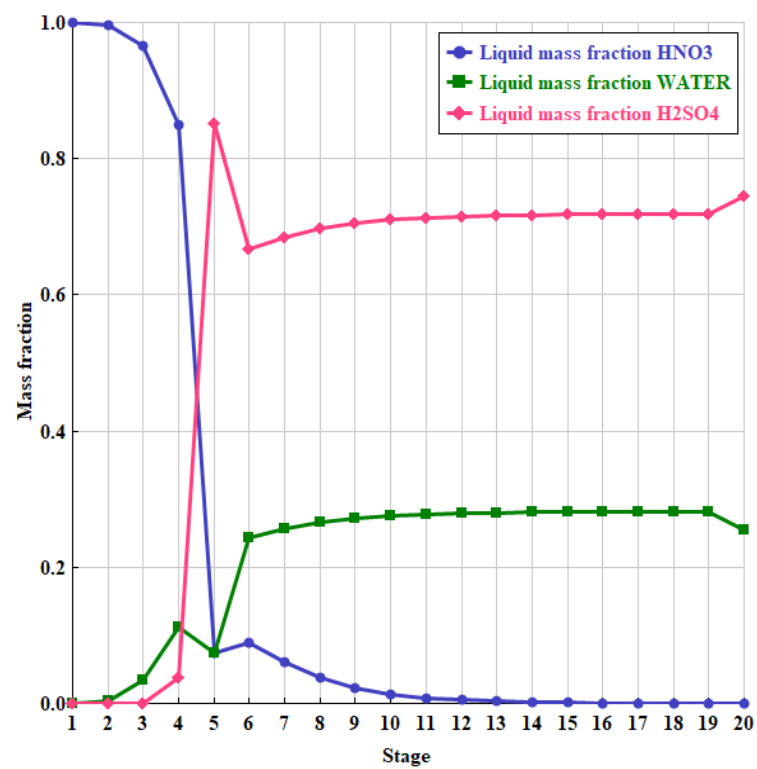
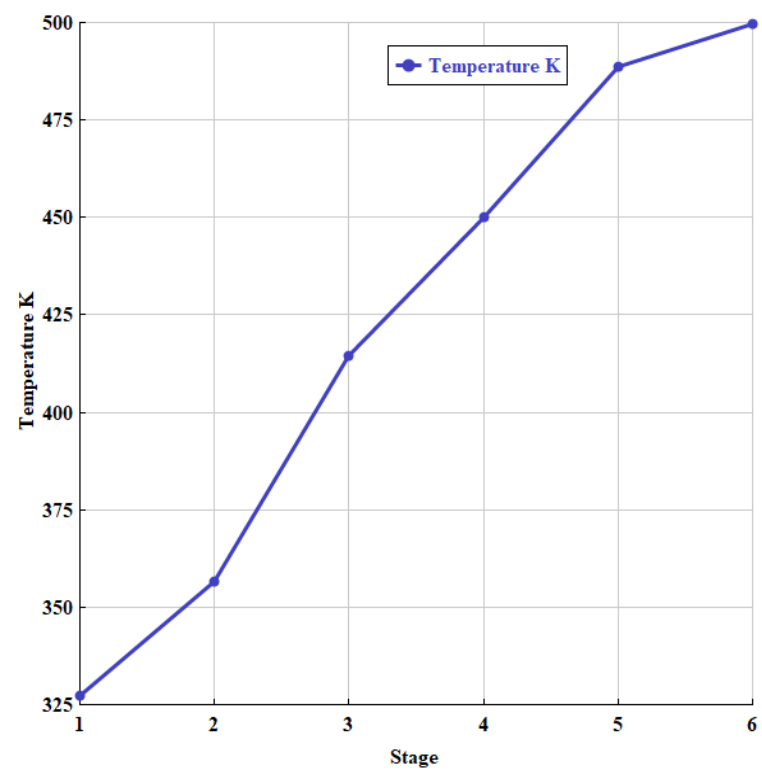


Figure 3.12 Temperature and composition profile for EDC



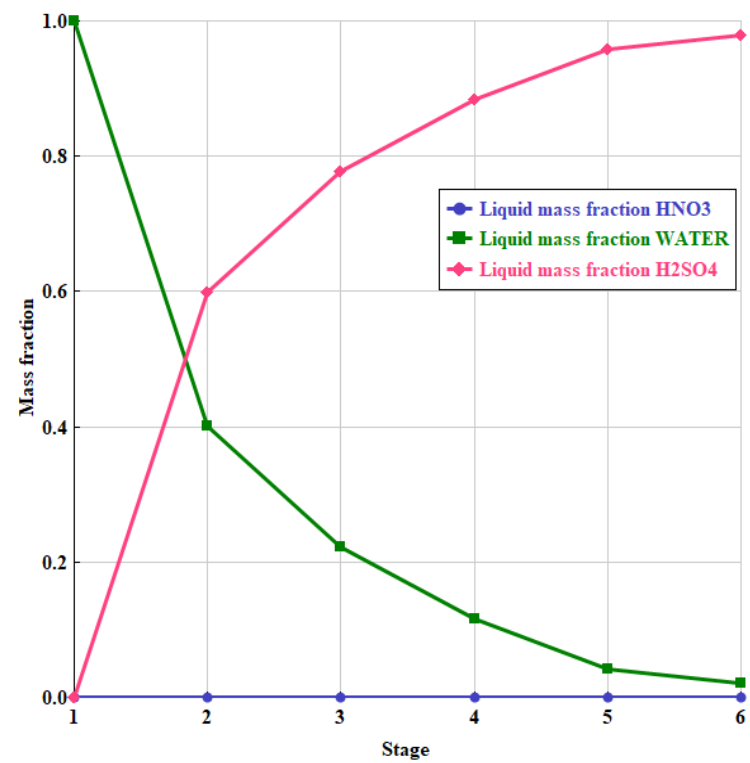


Figure 3.13 Temperature and composition profile for SRDC column

Table 3.14. Detail TAC calculations for complete of nitric acid dehydration ED system

Parameter	PDC	EDC	SRDC
Pressure (atm)	1	1	0.15
RR (optimum)	0.04	0.58	0.05
N _{FF} (optimum)	4	6	3
N _{FS} (optimum)	-	5	-
T _{FF} (feed temperature) (K)	298	393.52	393.52
T _{FS} (solvent temperature) (K)	-	350	-
N _T	10	20	6
D (m)	0.21	0.03	0.12
H (m)	3.84	8.64	1.92
Q _R (kW)	84.73	1.46	11.86
A _R (m ²)	3.78	0.04	0.76
Cost reboiler (10 ³ \$)	30.46	1.51	10.75
Q _C (kW)	46.41	4.42	6.48
A _C (m ²)	0.80	0.10	0.34
Cost condenser (10 ³ \$)	11.09	2.91	6.37
Q _{cooler} (kW)	-	2.58	-
A _{cooler} (m ²)	-	0.03	-
Cost cooler(10 ³ \$)	-	1.31	-
Column shell cost (10 ³ \$)	17.00	4.30	5.68
Capital cost (10 ³ \$)	58.56	10.02	22.80
Energy cost (10 ³ \$/yr)	19.46	0.46	3.44
Total capital cost (10 ³ \$)		91.37	
Total energy cost (10 ³ \$/y)		23.36	
TAC (10 ³ \$/y)		53.82	

3.5 Conclusions

Thermodynamic modelling and extractive distillation configuration design for nitric acid dehydration with sulphuric acid as a solvent has been presented in this work. Thermodynamic modelling of binary and ternary systems of HNO₃/water/sulphuric acid vapour-liquid-equilibrium data using the eNRTL-RK model has been done in the Aspen Plus data regression system. Validation of the thermodynamic model with the regressed parameters was performed by plotting the equilibrium diagrams using the experimental literature data and the model estimated data. It was found that the estimated value shows good agreement with the experimental values. Hence, the determined eNRTL-RK model parameters suit the simulation work comprising nitric acid, water and sulphuric acid.

The design and optimization of the continuous distillation column sequence comprising a preconcentrating column, extractive distillation column and solvent recovery column for dilute nitric acid dehydration using sulphuric acid as a solvent was performed systematically. The optimal parameters were obtained by optimizing the minimum energy consumption and Total Annual cost (TAC). With a solvent-to-feed ratio value of 1, sulphuric acid is a suitable solvent for the dehydration of nitric acid, leading to purity up to 99.99 mass %.

3.6 References

- [1] J.G. Sloan, The Extractive Distillation Process for Nitric Acid Concentration Using Magnesium Nitrate. *Adv. Chem. Ser.* 155 (1976) 128–142.
- [2] P.D. Ghuge, N.A. Mali, S.S. Joshi, Comparative analysis of extractive and pressure swing distillation for separation of THF-water separation, *Comput. Chem. Eng.* 103 (2017) 188–200.
- [3] W.L. Luyben, Comparison of extractive distillation and pressure-swing distillation for acetone/chloroform separation, *Comput. Chem. Eng.* 50 (2013) 1–7.
- [4] R.T. Jubin, R.M. Counce, W.D. Holland, W.S. Groenier, E.D. North, A Simplified Process for the Extractive Distillation of Nitric Acid, *Ind. Eng. Chem. Res.* 26 (1987) 990–997.
- [5] J. A. Vailiancourt, Use of magnesium nitrate in extractive distillation of nitric acid. *Adv. Chem. Ser.* 155 (1976) 143–149.
- [6] T.L. Guggenheim, R.R. Odle, J. Pace, Process design and operational controls to safeguard strong nitric acid recovery systems, *ACS Symp. Ser.* 1155 (2013) 185–202.
- [7] M. Wang, H. Kaur, C. C. Chen, Thermodynamic modeling of HNO₃-H₂SO₄-H₂O ternary system with symmetric electrolyte NRTL model. *AIChE J.* 63 (2017), 3110–3117.
- [8] S. R. M. Ellis, J. M. Thwaites, Vapour–liquid equilibria of nitric acid–water–sulfuric acid mixtures, *J. Appl. Chem.* 7 (1957), 152–160.
- [9] J.M. Smith, H.C. Van Ness *Introductio to chemical engineering thermodynamics*, McGraw-Hill, New York. 1975
- [10] C.C. Chen, H.I. Britt, J.F. Boston, L.B. Evans Local composition model for excess Gibbs energy of electrolyte systems, part I. Single solvent, single completely dissociated electrolyte systems. *AIChE J.* 28 (1982) 588–596.

- [11] B. Mock, L.B. Evans, C. -C Chen, Thermodynamic representation of phase equilibria of mixed-solvent electrolyte systems, *AIChE J.* 32 (1986) 1655–1664.
- [12] K. S. Pitzer, Electrolytes. From dilute solutions to fused salts. *J. Am. Chem. Soc.* 102 (1980) 2902–2906.
- [13] C.C. Chen, Y. Song, Generalized electrolyte-NRTL model for mixed-solvent electrolyte systems, *AIChE J.* 50 (2004) 1928–1941.
- [14] Aspen Properties V8.4. Burlington, MA: Aspen Technology, 2013.
- [15] J. Potier, Ebullometric study of the $\text{HNO}_3\text{-H}_2\text{O}$ system. *J. Sci. Phys. (Algier)* 4 (1958) 99.
- [16] Rivenq, F. Boiling point diagrams of water- HNO_3 mixtures under reduced pressure. *Bull. Soc. Chim. France.* (1959) 822.
- [17] T. Boublik, K. Kuchynka, Balance liquid-vapour XXII. Dependence of composition of azeotropic mix of system nitric acid-water pressure. *Coll. Czech. Chem. Commun.* 25 (1960) 579–582.
- [18] H. L. Que, Y. H. Song, C. C. Chen, Thermodynamic modelling of the sulfuric acid-water-sulfur trioxide system with the symmetric electrolyte NRTL model. *J. Chem. Eng. Data.* 2011, 56, 963–977.
- [19] G. Li, E. Asselin, Z. Li, Process simulation of sulfuric acid recovery by azeotropic distillation: Vapor-liquid equilibria and thermodynamic modeling, *Ind. Eng. Chem. Res.* 53 (2014) 11794–11804.
- [20] J. M. Douglas, *Conceptual Design of Chemical Processes*, McGraw-Hill, New York. 1988.
- [21] X. You, I. Rodriguez-Donis, V. Gerbaud, Investigation of Separation Efficiency Indicator for the Optimization of the Acetone-Methanol Extractive Distillation with Water, *Ind. Eng. Chem. Res.* 54 (2015) 10863–10875.

- [22] Y. Cao, M. Li, Y. Wang, T. Zhao, X. Li, Z. Zhu, Y. Wang, Effect of feed temperature on economics and controllability of pressure-swing distillation for separating binary azeotrope, *Chem. Eng. Process. Process Intensif.* 110 (2016) 160–171.
- [23] G. Li, P. Bai, New operation strategy for separation of ethanol-water by extractive distillation. *Ind. Eng. Chem. Res.* 51, (2012) 2723–2729.
- [24] X. You, J. Gu, C. Peng, W. Shen, H. Liu, Improved Design and Optimization for Separating Azeotropes with Heavy Component as Distillate through Energy-Saving Extractive Distillation by Varying Pressure, *Ind. Eng. Chem. Res.* 56 (2017) 9156–9166.
- [25] J. R. Knight, M. F. Doherty, Optimal design and synthesis of homogeneous azeotropic distillation sequences. *Ind. Eng. Chem. Res.* 28 (1989) 564–572.

Chapter 04

*Effect of CaCl₂, ZnCl₂ and LiBr salts
on Isobaric Vapour-liquid Equilibrium
in Separation of the Azeotropic
Mixture of Ethanol + Water*

Chapter 4 Effect of CaCl₂, ZnCl₂ and LiBr salts on Isobaric Vapour-liquid Equilibrium in Separation of the Azeotropic Mixture of Ethanol + Water

Abstract

The present work analyzes the potential of calcium chloride (CaCl₂), zinc chloride (ZnCl₂) and lithium bromide (LiBr) salts as entrainer for breaking the minimum boiling azeotrope of ethanol and water. Isobaric vapour-liquid equilibrium (VLE) data for the binary systems of water + ethanol and ternary system of water + ethanol + calcium chloride, water + ethanol + zinc chloride and water + ethanol + lithium bromide (LiBr) were measured at a constant pressure of 94.5 kPa. The effect of salts on the relative volatility of ethanol to water as well as on the vapour phase mole fractions of ethanol, were also studied experimentally. According to the results of experiments, salts can be added to the ethanol and water system to eliminate the azeotropic point. Salting out effects in the case of calcium chloride was more than that of zinc chloride and lithium bromide salts. The results of this study suggested that calcium chloride would be a more practical option for separating the water and ethanol azeotrope. The electrolyte non-random two-liquid (eNRTL) model was used to correlate the experimental VLE data. The model prediction with the regressed parameters agreed well with the experimental data. The experimental data obtained in this work was thermodynamically consistent using the van Ness test.

4.1 Introduction

Ethanol has a wide range of applications in the chemical industry. It can be used as a solvent, reactant or intermediate in producing various paints, perfumes, medicines and food products [1]. Ethanol is a suitable feedstock for producing various renewable chemicals and products. Nowadays, anhydrous ethanol is used as a fuel additive [2]. The production of anhydrous ethanol by conventional distillation technique is complex due to the formation of a minimum boiling azeotrope of the ethanol-water mixture at atmospheric pressure. At azeotropic conditions, liquid and vapour phase compositions are equal, leading to equal relative volatility; hence, conventional distillation is not helpful in purifying the products beyond azeotropic

compositions. Advanced distillation techniques [3], such as extractive, azeotropic, and pressure-swing distillations, are required to deal with azeotropic mixture separations.

Extractive distillation technique is the most preferable over the other one due to its lower energy requirement, flexibility in entrainer selection, simple operation and high-purity product in case of ethanol dehydration [4]. It is reported that salts are an effective entrainer in altering the vapour-liquid equilibrium behaviour of the azeotropic mixture so that the azeotrope formation can be eliminated. Most salts have very low volatility; thus, they are not vaporized in the extractive distillation process, which results in high-purity distillate products and low energy consumption [5]. Salts are the preferred entrainer in extractive distillation due to their low cost and toxicity. The lower entrainer-to-feed ratio leads to less salt required to achieve the separation in the extractive distillation compared to that with the organic solvent as the entrainer [6]. Extractive distillation process using potassium acetate [5, 7, 8], calcium chloride [6, 9-13], and magnesium chloride [14] as an entrainer was studied to obtain the anhydrous ethanol. Salts are added at the appropriate location at the top of the extractive distillation column, which alters the relative volatility so that a light component is obtained as a distillate and salt with other components is obtained as the bottom product [5]. Thus, salts have good potential to be considered entrainer, instead of conventional organic solvents, in the extractive distillation process.

The VLE data of the binary azeotropic system with the addition of the entrainer has great importance in the design of the extractive distillation process. For extractive distillation with salts, information on the change in the VLE behaviour of the system due to the presence of salts, specifically the change in the vapour phase composition of the mixed solvent system, is essential. The experimental VLE data is helpful in understanding if the given entrainer can break the azeotrope or not during the selection of the entrainer. Also, while designing of extractive distillation system, it is necessary to develop a thermodynamic model with appropriate parameters for simulation analysis. The accurate experimental VLE data is necessary for regression of the thermodynamic model parameters.

VLE data is reported in the literature for some salts having the capability to break the azeotrope of the ethanol-water system, which includes potassium acetate [15-18], strontium

bromide [19, 20], calcium nitrate [21], cobalt II chloride [22], and potassium and sodium iodide [23]. Isobaric VLE data for the ethanol-water system containing calcium chloride at a constant mass concentration of 16.7 wt % was reported by Nishi [24] at atmospheric pressure, and with 0.974 mol/kg salt at 12.3 kPa pressure was reported by Meyer [25], VLE data at a constant temperature of 298.15 K were reported by Mishima [26]. To the best of our knowledge, VLE data for varying concentrations of calcium chloride at constant pressure still needed to be reported in the literature. No literature on ethanol + water + zinc chloride is reported in the NIST literature database.

The current study aims to investigate how different calcium chloride, zinc chloride, and lithium bromide salt concentrations affect the behaviour of ethanol and azeotropic water systems. This work uses isobaric vapour-liquid equilibrium data for the binary system of ethanol + water, the ternary system of ethanol + water + calcium chloride, ethanol + water + zinc chloride and ethanol + water + lithium bromide was determined at 94.5 kPa. The effects of varying concentrations of salts on the phase equilibrium behaviour of the ethanol + water azeotropic system were discussed. The van Ness test checked the thermodynamic consistency of the obtained experimental VLE data. The eNRTL model was used to correlate the experimental VLE data.

4.2 Experimental

4.2.1 Materials

Changshu Hongsheng Fine Chemical Co. Ltd. supplied ethanol with a mass fraction of 0.999. The mass fraction of ethanol was 0.999, and no impurities were detected by gas chromatography. Calcium chloride was supplied by Thermo Fisher Scientific India Pvt. Ltd. Zinc chloride and lithium bromide was supplied by Loba Chemie Pvt. Ltd. The moisture content of salts was determined by Karl Fisher titration. The mass fraction of water was below 0.006. Ethanol and salts were used without further purification. The deionized water (conductivity less than 1.0 $\mu\text{S cm}^{-1}$) was generated using an ultrapure water system provided by Siemens. Specifications of chemicals used in the experiments are listed in Table 4.1.

Table 4.1. Specification of the chemicals used in experiments

Name	CAS No.	Source	Purity	Analysis method
Ethanol	64-17-5	Changshu Hongsheng Fine Chemical Co., Ltd.	0.999	GC ^a
Calcium chloride	10043-52-4	Thermo Fisher Scientific India Pvt. Ltd	≥0.98	KF ^b
Zinc chloride	7646-85-7	Loba Chemie Pvt. Ltd.	≥0.98	KF ^b
Lithium bromide	7550-35-8	Loba Chemie Pvt. Ltd.	≥0.98	KF ^b

^a GC = gas chromatography.

^b KF = Karl Fisher titration.

4.2.2 Experimental Apparatus and Procedure

The glass dynamic circulation VLE apparatus used to generate the vapour-liquid equilibrium data for binary and ternary systems is schematically shown in Figure 4.1. A detailed description of the VLE apparatus and its working was reported earlier for generating the VLE data of various binary systems [27-29]. In the present work, ternary solutions with constant salt concentrations of 5, 10, and 15 mass percentages and varying concentrations of ethanol were prepared gravimetrically using an electronic weighing balance with an accuracy of ± 0.0001 g. The solution was stirred well, using a magnetic stirrer, until all salts were completely dissolved; approximately 330 ml solution was fed into the boiling chamber of the VLE apparatus to find out its VLE data. The chilled water circulation was given to the condenser (J).

At the time of determination of this experimental data, the local atmospheric pressure varied slightly between 95 to 96 kPa. Thus we have used the vacuum pump provided by KNF, Germany (Model number SC920G), which ensures a constant pressure of 94.5 kPa with an accuracy of ± 0.1 kPa throughout the experiment, slightly below the local atmospheric pressure. The condenser vent valve (K) was connected to a vacuum pump. The heating to the boiling chamber (B) was started, and vapour and liquid were allowed to flow into the equilibrium chamber (E) through the Cottrell pump (C). Due to gravity force, liquid flowed back into the mixing chamber (M). Vapours were allowed to condense into the condenser (J) and flow back to the mixing chamber via the vapour holding chamber (G), which gets recycled back to the boiling chamber so that continuous recirculation of vapour and liquid was achieved in the still.

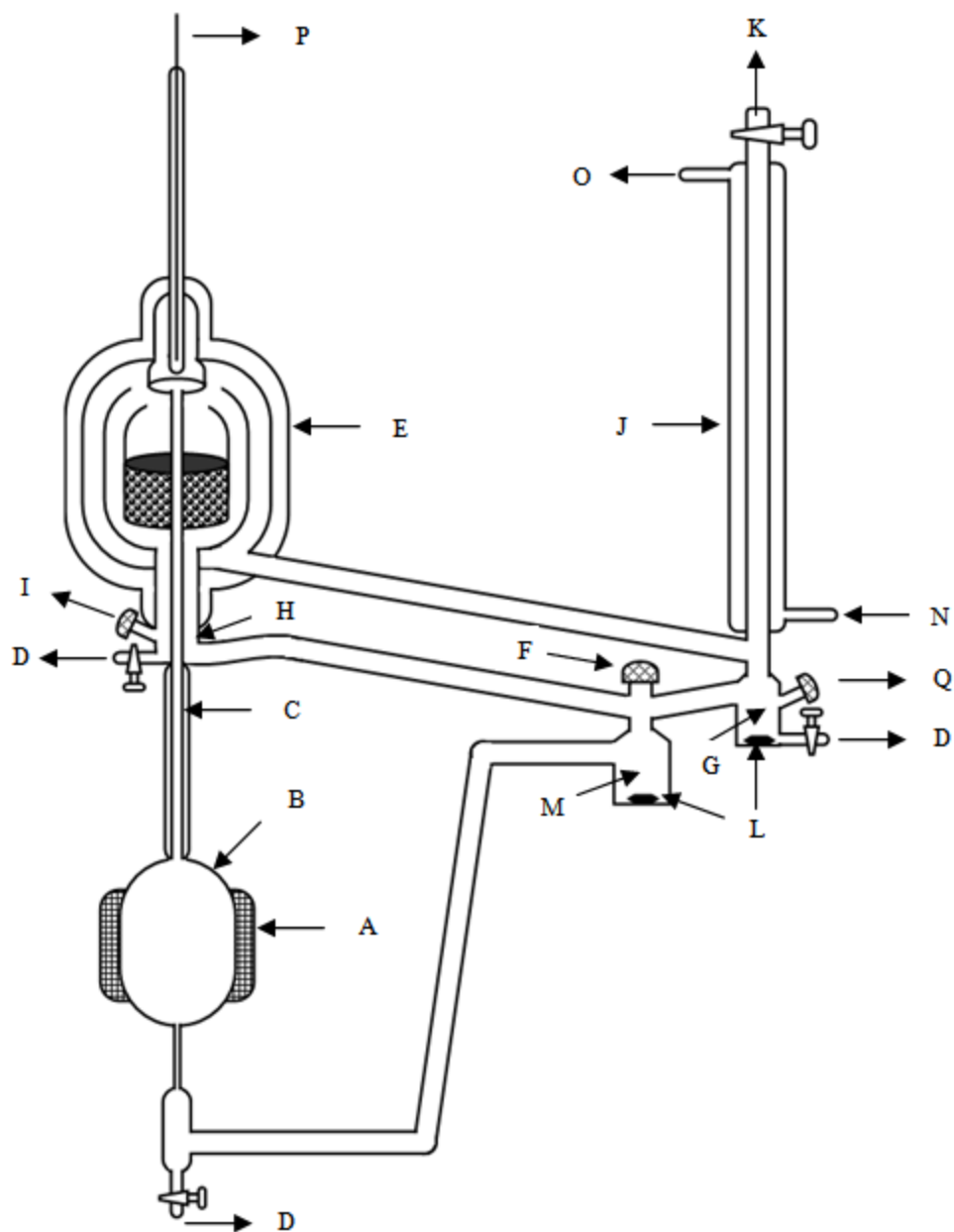


Figure 4.1. Schematic diagram of experimental vapour-liquid equilibrium setup; (A) electric heater, (B) boiling chamber, (C) Cottrell tube, (E) equilibrium chamber, (D) drain valve, (F) feed point, (G) condensate receiver, (H) liquid chamber, (I) liquid sampling point, (J) condenser, (K) to vacuum pump, (L) magnetic stirrer, (M) mixing chamber, (N) coolant in, (O) coolant out, (P) temperature sensor, (Q) vapour condensate sampling point.

Once the equilibrium condition was reached, the temperature of the equilibrium chamber was recorded using the handheld thermometer provided by Wika, India (Model CTH 7000) with an

accuracy of ± 0.01 K and a very small quantity of sample was taken from the sampling port to analyze the composition. The same experimental process was repeated to obtain the VLE data of various feed compositions with different salt concentrations.

4.2.3 Analysis

The standard samples of ethanol-water binary mixtures covering the whole composition range from pure ethanol to pure water were prepared gravimetrically, and densities and refractive indices were measured at 298.15 K, as given in Table 4.2. The density meter provided by Rudolph Research Analytical, USA (Model number 2911 plus) was used to measure density with an accuracy of 0.0001. The refractometer from Atago, Japan (Model-RX-7000i) was used to measure the refractive index with an accuracy of ± 0.0001 and a resolution of 0.00001. The calibration curves for density (ρ) and refractive index (n_D) versus mole fraction of ethanol are plotted; experimental data is also compared with the literature in Figures 4.2 and 4.3. The findings indicate a strong correlation between experimental and literature data collected at 25 °C. The appropriate polynomial equation was fitted to the data, and the respective calibration equation was generated in Table 4.3. These equations were used to estimate the compositions of ethanol by measuring the density or refractive index of the sample. Estimating the composition of ethanol at higher concentrations using the refractive index was difficult due to the lower difference in the refractive indices of the samples at higher concentrations of ethanol. It was found that the estimation accuracy using density measurement was more even at higher ethanol concentrations. Hence, the binary system of ethanol and water density measurements was preferred to obtain the compositions.

In the case of the ternary system of ethanol, water and salt, the vapour phase composition was analyzed using the density measurement. Salts are highly non-volatile; do not appear in the vapour phase. The liquid phase composition was estimated using material balance calculations across the VLE apparatus. Due to salt's extremely low volatility, it was anticipated that the salt content in the liquid phase would be the same as that of the initially delivered feed.

Table 4.2. Experimental values of density (ρ) and refractive index (n_D), mole fractions of ethanol (x_2) for water (1) + ethanol (2) mixture at 298.15 K. ^a

x_2	$\rho/\text{g}\cdot\text{cm}^{-3}$	n_D
0.000	0.9970	1.3324
0.020	0.9883	1.3354
0.042	0.9803	1.3388
0.076	0.9702	1.3438
0.090	0.9658	1.3458
0.121	0.9576	1.3495
0.143	0.9513	1.3517
0.165	0.9445	1.3537
0.207	0.9316	1.3562
0.240	0.9222	1.3578
0.282	0.9108	1.3593
0.318	0.9008	1.3603
0.362	0.8898	1.3612
0.416	0.8767	1.3620
0.478	0.8639	1.3625
0.532	0.8535	1.3628
0.615	0.8396	1.3629
0.690	0.8271	1.3626
0.780	0.8140	1.3621
0.802	0.8115	1.3619
0.861	0.8006	1.3613
0.885	0.8003	1.3610
0.894	0.7993	1.3609
0.944	0.7928	1.3602
1.000	0.7855	1.3594

^a standard uncertainty $u(T) = 0.01$ K, $u(\rho) = 0.0001$, $u(n_D) = 0.0001$

The ternary solution prepared with a known concentration of each component is called feed solution (f). Once the complete recirculation was achieved in the VLE still, the feed solution is constituted in three forms boiling mixture, vapour and liquid. The solution in the boiler is mainly a boiling mixture (b). Vapour mixture (v) exists in the gaseous state before condensation or in the liquid state after condensation in the vapour sampling chamber. Liquid mixture (l) exists

mainly in the flow path between the equilibrium and mixing chambers. So the component mass balance equations are represented as,

$$W_{b,1} = W_{f,1} - W_{v,1} \quad (1)$$

$$W_{b,2} = W_{f,2} - W_{v,2} \quad (2)$$

$$W_{b,3} = W_{f,3} \quad (3)$$

Where w is the mass,

The salt weights added to the feed solution remain in the boiling mixture. As salts are highly non-volatile, the vapour phase contains only a pure solvent or a binary mixture. Thus the mass of each component in the vapour mixture (w_v) is calculated as,

$$w_{v,1} = \left(\frac{y_1 M_1}{y_1 M_1 + y_2 M_2} \right) V \rho \quad (4)$$

$$w_{v,2} = \left(\frac{y_2 M_2}{y_1 M_1 + y_2 M_2} \right) V \rho \quad (5)$$

The mole fractions for components 1 and 2 in the vapour phase are y_1 and y_2 , respectively. The molecular weights of components 1 and 2 are M_1 and M_2 , respectively. V and ρ are the volume and density of the vapour, and mass fractions of the salt ($z_{b,3}$) are calculated as,

$$z_{b,3} = \left(\frac{w_{b,3}}{w_{b,1} + w_{b,2} + w_{b,3}} \right) \quad (6)$$

Mole fractions of more volatile component (2) on salt-free basis is,

$$x'_{b,2} = \frac{w_{b,2}/M_2}{w_{b,1}/M_1 + w_{b,2}/M_2} \quad (7)$$

Mole fractions of more volatile component (2) on salt-free basis is,

$$x'_{l,2} = \frac{x'_{b,2} - \beta'_n y_2}{1 - \beta'_n} \quad (8)$$

Where β'_n represents the molar vapour to liquid circulation ratio on salt-free basis, liquid concentration on salt basis is calculated as,

$$x_{l,1} = \frac{x'_{l,1}}{x'_{l,1} + x'_{l,2} + \left(\frac{z_{l,3}}{1-z_{l,3}}\right) \left(\frac{x'_{l,1}M_1 + x'_{l,2}M_2}{M_3}\right)} \quad (9)$$

$$x_{l,2} = \frac{x'_{l,2}}{x'_{l,1} + x'_{l,2} + \left(\frac{z_{l,3}}{1-z_{l,3}}\right) \left(\frac{x'_{l,1}M_1 + x'_{l,2}M_2}{M_3}\right)} \quad (10)$$

Where $x'_{l,1} = 1 - x'_{l,2}$

Experiments for ethanol and water without the addition of salts were performed to validate the method for estimation of liquid phase composition using the material balance. In these experiments, the liquid phase composition was estimated by a material balance calculation and was compared with the values obtained by density measurements. The absolute standard deviation calculated and analyzed liquid phase composition was less than 0.005.

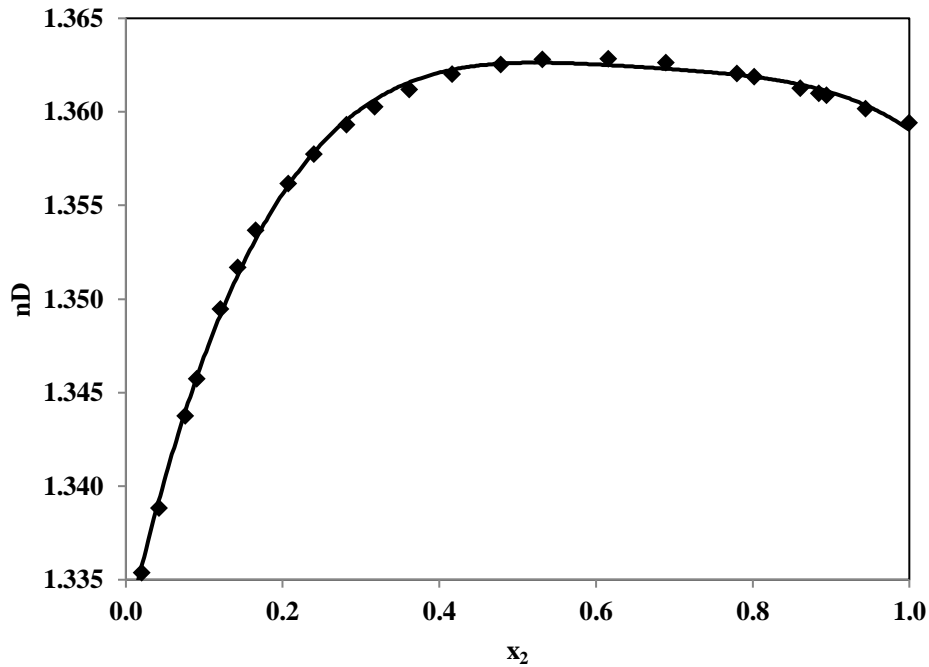


Figure 4.2. Calibration curve for the water (1) + ethanol (2) system with refractive index (n_D) versus mole fraction of ethanol (x_2); (◆) measured values at 298.15 K, (—) polynomial equation.

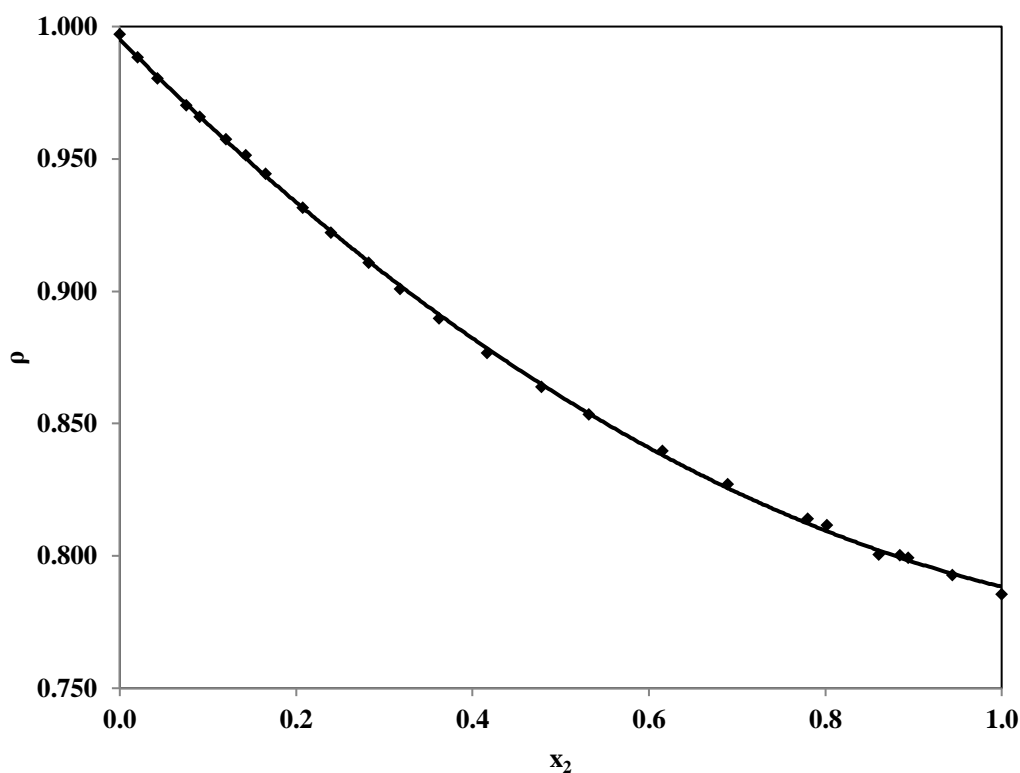


Figure 4.3. Calibration curve for the water (1) + ethanol (2) system with density (ρ) versus mole fraction of ethanol (x_2); (\blacklozenge) measured values at 298.15 K, (—) polynomial equation.

Table 4.3. Polynomial equation for calibration curves

	Figure	Polynomial Equation	R^2
RI	Figure 4.2	$y = -0.156x^4 + 0.416x^3 - 0.418x^2 + 0.185x + 1.332$	0.999
Density	Figure 4.3	$y = 0.125x^2 - 0.332x + 0.995$	0.999

4.3 Results and Discussion

4.3.1 Experimental Data

The binary VLE data for the water (1) + ethanol (2) system was produced at 94.5 kPa in order to validate the VLE still that is currently being utilized in this study, and it is listed in 4. 4. x_i and y_i are the mole fractions of component i in liquid and vapour phase, respectively. T is the equilibrium temperature. The experimental data obtained in this work agrees with the data

estimated by the NRTL model using the Aspen Plus simulator with in-built binary interaction parameters. Experimental data also agree with literature data, as shown in Figure 4.4. The average absolute deviation of equilibrium temperature was 0.15 K, and vapour composition was 0.0037 between the experimental and estimated VLE data by the NRTL model.

Table 4.4. Isobaric vapour-liquid equilibrium data for temperature T, liquid phase mole fraction x_i , and vapour phase mole fraction y_i and relative volatility α for the binary system of water (1) + ethanol (2) at 94.5 kPa

T/K	x_2	y_2	ΔT^b	Δy^c	α_{21}
349.66	1.000	1.000	0.09	0.000	
349.62	0.958	0.955	0.02	0.000	0.923
349.58	0.879	0.882	0.00	-0.002	1.031
349.68	0.786	0.807	0.04	0.002	1.136
350.42	0.614	0.708	0.01	-0.001	1.528
351.49	0.472	0.646	-0.15	0.000	2.043
352.27	0.363	0.609	-0.06	-0.002	2.735
353.27	0.262	0.574	0.03	-0.005	3.789
354.40	0.188	0.539	0.17	-0.008	5.056
356.14	0.124	0.485	0.37	-0.009	6.652
358.39	0.079	0.412	0.59	-0.006	8.143
363.65	0.036	0.263	-0.14	0.007	9.636
367.00	0.018	0.160	-0.41	0.009	10.404
371.20	0.000	0.000	0.00	0.000	

^a Standard uncertainty u are $u(x_i)=u(y_i)=0.005$, $u(T)=0.01K$, $u(P)=0.1$ kPa

^b $\Delta T = T^{cal} - T^{exp}$

^c $\Delta y_2 = y_2^{cal} - y_2^{exp}$

The isobaric VLE data for the ternary system of water (1) + ethanol (2) + calcium chloride (3), water (1) + ethanol (2) + zinc chloride and (3) water (1) + ethanol (2) + lithium bromide (3) were measured at 94.6 kPa. The data was generated for all salts for the concentration of 0.05, 0.10, and 0.15, by mass, in each experimental run which is listed in Tables 4.5 - 4.7, respectively, where, x'_2 is the mole fractions of ethanol in the liquid phase on the salt-free basis,

y_2 is the mole fraction of ethanol in the vapour phase, w_3 is the mass fractions of salt in the liquid phase, x_1 and x_2 are the mole fractions (on salt basis) of water and ethanol, respectively. T is the equilibrium temperature, Y_i is the experimental activity coefficient of component i , α_{21} is the relative volatility of ethanol (2) to water (1) estimated by using the following equation,

$$\alpha_{21} = \frac{y_2/x_2'}{y_1/x_1'} \quad (11)$$

Where x_i' (salt-free basis) and y_i are mole fractions of component i in the liquid and vapour phase, respectively.

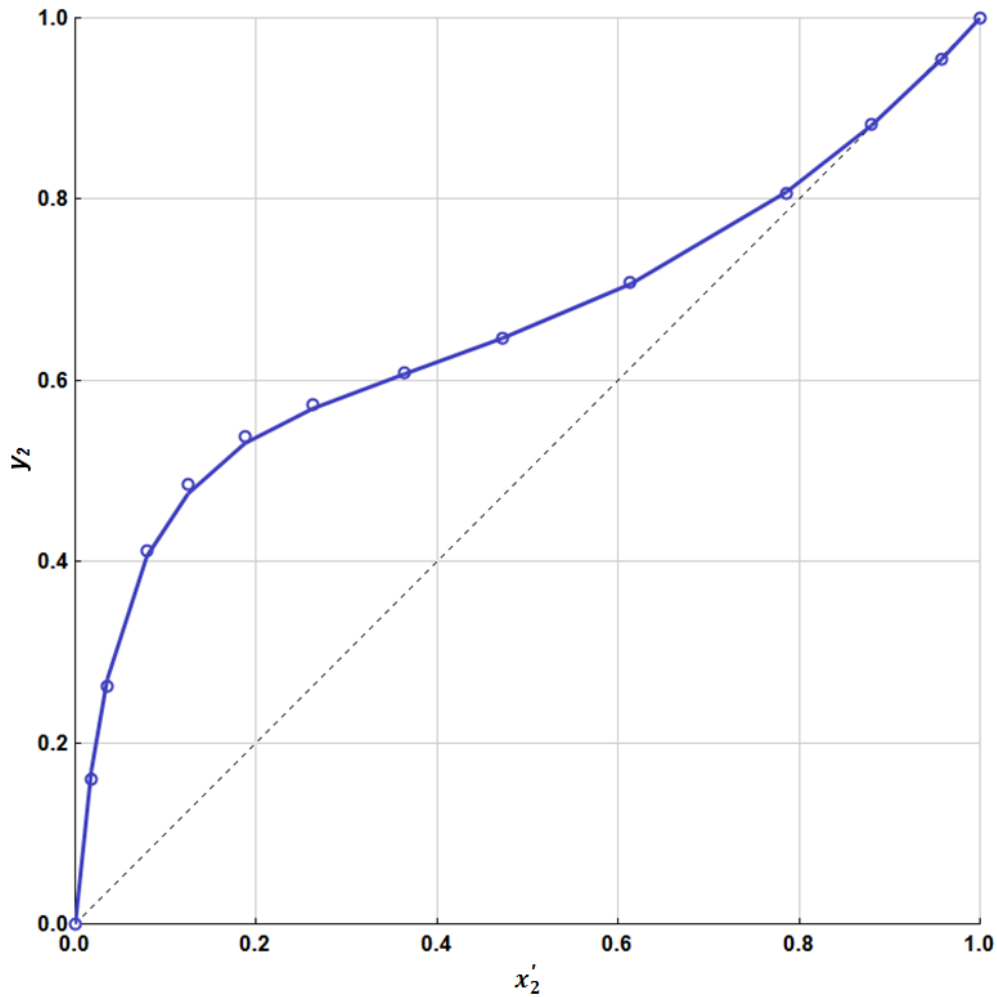


Figure 4.4. Isobaric vapour-liquid equilibrium data of the binary system of water (1) + ethanol (2) at 94.5 kPa. (\circ) this work, (—) solid line estimated by NRTL model

Table 4.5. Isobaric ternary vapour-liquid equilibrium data for temperature T, liquid phase mole fraction salt-free basis x' , x_1 and x_2 are the mole fractions (on salt basis) of water and ethanol, respectively, liquid phase mass fraction of salt z , vapour phase mole fraction y , activity coefficient γ , relative volatility α_{21} for water (1) ethanol (2) + calcium chloride (3) at 94.5 kPa. ^a

z_3 (mass %)	T/K	x'_2	x_1	x_2	y_2	γ_1	γ_2	α_{21}
Around 5 %								
5.17	349.97	1.000	0.000	0.978	1.000		0.989	
5.17	349.92	0.880	0.118	0.862	0.920	1.519	1.036	1.567
5.11	350.01	0.757	0.238	0.743	0.849	1.414	1.107	1.797
5.16	350.31	0.605	0.388	0.595	0.764	1.342	1.231	2.106
5.16	350.79	0.472	0.520	0.465	0.699	1.251	1.419	2.603
5.16	351.58	0.362	0.629	0.358	0.655	1.150	1.678	3.342
5.16	352.48	0.273	0.718	0.270	0.614	1.090	2.012	4.224
4.53	353.60	0.199	0.793	0.197	0.575	1.041	2.480	5.443
5.15	355.12	0.136	0.855	0.134	0.530	1.003	3.160	7.180
5.16	357.66	0.082	0.909	0.081	0.448	1.002	4.030	9.130
5.16	362.77	0.036	0.955	0.036	0.297	0.998	4.941	11.147
5.17	371.43	0.000	0.991	0.000	0.000	0.993		
Around 10 %								
10.32	350.46	1.000	0.000	0.954	1.000		0.970	
10.32	350.21	0.879	0.116	0.842	0.939	1.145	1.046	2.098
10.33	350.27	0.775	0.216	0.745	0.885	1.146	1.116	2.235
10.31	350.55	0.604	0.382	0.583	0.802	1.110	1.283	2.652
10.31	350.85	0.471	0.513	0.456	0.740	1.076	1.502	3.200
10.30	351.30	0.362	0.620	0.352	0.694	1.031	1.801	4.003
10.29	351.90	0.273	0.708	0.266	0.655	0.995	2.202	5.065
10.29	352.97	0.198	0.783	0.193	0.612	0.974	2.713	6.369
10.29	354.41	0.135	0.846	0.132	0.560	0.965	3.448	8.149
10.29	357.09	0.081	0.900	0.079	0.484	0.958	4.482	10.630
10.33	362.71	0.036	0.945	0.035	0.320	0.967	5.416	12.611
10.32	372.04	0.000	0.982	0.000	0.000	0.971		
Around 15 %								
15.47	351.11	1.000	0.000	0.929	1.000		0.946	
15.45	351.04	0.879	0.113	0.821	0.955	0.811	1.030	2.914
15.44	350.98	0.775	0.212	0.727	0.912	0.854	1.119	3.006
15.44	351.03	0.603	0.375	0.571	0.838	0.891	1.317	3.389
15.43	351.14	0.470	0.504	0.447	0.782	0.893	1.571	4.034
15.43	351.41	0.361	0.611	0.345	0.729	0.907	1.888	4.771
15.42	351.83	0.272	0.699	0.261	0.688	0.903	2.324	5.893
15.42	352.70	0.197	0.773	0.190	0.650	0.886	2.925	7.548
15.41	353.99	0.134	0.836	0.130	0.604	0.882	3.804	9.844
15.40	356.29	0.081	0.890	0.078	0.520	0.918	4.998	12.386
15.42	363.66	0.035	0.936	0.034	0.348	0.893	5.903	14.870
15.47	373.31	0.000	0.971	0.000	0.000	0.928		

^a Standard uncertainty u are $u(x_i) = u(y_i) = 0.005$, $u(x'_2) = 0.005$, $u(T) = 0.01\text{K}$, $u(P) = 0.1\text{ kPa}$

Table 4.6. Isobaric ternary vapour-liquid equilibrium data for temperature T, liquid phase mole fraction salt-free basis x' , x_1 and x_2 are the mole fractions (on salt basis) of water and ethanol, respectively, liquid phase mass fraction salt z , vapour phase mole fraction y , activity coefficient γ , relative volatility α for water (1) ethanol (2) + zinc chloride (3) at pressure of 94.5 kPa. ^a

z_3 (mass %)	T (K)	x'_2	x_1	x_2	y_2	γ_1	γ_2	α_{21}
Around 5 %								
5.17	349.99	1.000	0.000	0.982	1.000		0.988	
5.17	349.87	0.881	0.117	0.866	0.895	2.012	1.009	1.152
5.17	350.01	0.778	0.219	0.765	0.813	1.907	1.033	1.244
5.16	350.65	0.607	0.388	0.598	0.714	1.605	1.134	1.621
5.16	351.42	0.472	0.522	0.466	0.661	1.373	1.309	2.184
5.16	352.29	0.363	0.630	0.359	0.621	1.230	1.543	2.870
5.16	353.09	0.274	0.719	0.271	0.588	1.134	1.881	3.793
5.15	354.25	0.199	0.793	0.197	0.553	1.066	2.321	4.967
5.15	358.31	0.082	0.911	0.081	0.434	1.002	3.798	8.595
5.16	363.02	0.036	0.957	0.036	0.284	1.006	4.756	10.639
5.16	371.41	0.000	0.993	0.000	0.000	0.994		
Around 10 %								
10.31	350.41	1.000	0.000	0.963	1.000		0.972	
10.31	350.13	0.881	0.115	0.850	0.903	1.827	1.008	1.267
10.32	350.27	0.777	0.216	0.752	0.823	1.786	1.035	1.330
10.33	350.71	0.606	0.382	0.589	0.724	1.543	1.147	1.706
10.31	351.40	0.472	0.515	0.459	0.667	1.349	1.323	2.246
10.30	352.14	0.363	0.622	0.354	0.631	1.203	1.580	3.007
10.29	353.23	0.274	0.711	0.268	0.595	1.108	1.895	3.908
10.28	354.35	0.199	0.785	0.195	0.558	1.049	2.335	5.076
10.28	355.86	0.136	0.849	0.133	0.515	1.005	2.982	6.754
10.28	358.42	0.082	0.903	0.080	0.437	0.992	3.815	8.716
10.29	363.54	0.036	0.949	0.035	0.286	0.983	4.711	10.776
10.31	371.50	0.000	0.985	0.000	0.000	0.990		
Around 15 %								
15.02	350.98	1.000	0.000	0.944	1.000		0.951	
15.44	350.82	0.881	0.113	0.833	0.898	1.871	0.976	1.196
15.45	350.78	0.777	0.211	0.738	0.820	1.773	1.011	1.309
15.44	351.19	0.607	0.376	0.579	0.717	1.556	1.114	1.641
15.43	351.82	0.472	0.507	0.453	0.664	1.339	1.295	2.215
15.44	352.76	0.363	0.614	0.350	0.617	1.219	1.506	2.826
15.42	353.66	0.274	0.702	0.265	0.585	1.117	1.830	3.741
15.42	354.75	0.199	0.777	0.193	0.553	1.043	2.283	4.990
15.42	356.42	0.136	0.840	0.132	0.505	1.002	2.869	6.512
15.41	358.83	0.082	0.894	0.079	0.429	0.990	3.691	8.446
15.42	363.69	0.036	0.940	0.035	0.274	0.995	4.469	10.096
15.45	371.92	0.000	0.976	0.000	0.000	0.975		

^a Standard uncertainty u are $u(x_i) = u(y_i) = 0.005$, $u(x'_2) = 0.005$, $u(T) = 0.01\text{K}$, $u(P) = 0.1\text{ kPa}$

Table 4.7. Isobaric ternary vapour-liquid equilibrium data for temperature T, liquid phase mole fraction salt-free basis x' , x_1 and x_2 are the mole fractions (on salt basis) of water and ethanol, respectively, liquid phase mass fraction of salt z , vapour phase mole fraction y for water (1) ethanol (2) + lithium bromide (3) at pressure of 94.5 kPa. ^a

z_3 (mass %)	T (K)	x'_2	x_1	x_2	y_2	y_1	y_2	α_{21}
Around 5 %								
5.16	350.33	1.000	0.000	0.972	1.000		0.977	
5.16	350.14	0.881	0.116	0.858	0.896	1.974	1.001	1.161
5.16	350.24	0.777	0.217	0.758	0.821	1.800	1.036	1.318
5.17	350.65	0.606	0.385	0.593	0.728	1.526	1.157	1.735
5.16	351.37	0.472	0.518	0.463	0.664	1.361	1.320	2.215
5.16	352.15	0.363	0.626	0.357	0.627	1.215	1.570	2.950
5.15	352.96	0.274	0.715	0.270	0.596	1.118	1.916	3.909
5.15	354.19	0.199	0.789	0.196	0.563	1.044	2.371	5.174
5.15	355.82	0.136	0.852	0.134	0.512	1.011	2.971	6.680
5.38	358.21	0.082	0.906	0.081	0.440	0.994	3.866	8.808
5.16	363.17	0.036	0.953	0.036	0.277	1.010	4.586	10.216
5.16	371.39	0.000	0.989	0.000	0.000	0.993		
Around 10 %								
10.31	372.07	0.000	0.977	0.000	0.000	0.969		
10.29	363.39	0.036	0.940	0.035	0.289	0.984	4.760	10.874
10.29	358.11	0.082	0.894	0.079	0.451	0.977	3.996	9.267
10.29	355.76	0.136	0.840	0.132	0.522	0.992	3.040	6.964
10.29	354.26	0.199	0.777	0.193	0.574	1.013	2.416	5.430
10.29	353.05	0.273	0.703	0.265	0.609	1.077	1.953	4.133
10.29	352.01	0.363	0.614	0.350	0.650	1.147	1.637	3.259
10.30	351.29	0.471	0.508	0.453	0.694	1.242	1.386	2.550
10.30	351.05	0.605	0.377	0.579	0.763	1.303	1.197	2.100
10.30	350.90	0.776	0.213	0.738	0.854	1.427	1.050	1.683
10.30	351.01	0.776	0.212	0.738	0.852	1.434	1.044	1.664
10.31	350.30	1.000	0.000	0.943	1.000		0.978	
Around 15 %								
15.44	351.08	1.000	0.000	0.912	1.000		0.948	
15.46	352.00	0.880	0.110	0.807	0.928	1.243	0.965	1.772
15.43	352.33	0.776	0.207	0.716	0.867	1.219	1.009	1.888
15.44	352.47	0.605	0.368	0.563	0.783	1.124	1.162	2.360
15.43	352.60	0.470	0.497	0.441	0.721	1.075	1.367	2.904
15.43	352.82	0.362	0.602	0.342	0.669	1.048	1.635	3.558
15.42	353.46	0.273	0.690	0.259	0.626	1.012	1.979	4.456
15.41	354.37	0.198	0.764	0.189	0.590	0.970	2.478	5.819
15.41	355.90	0.135	0.827	0.129	0.542	0.946	3.147	7.560
15.40	358.63	0.081	0.881	0.078	0.467	0.930	4.065	9.892
15.42	363.98	0.036	0.927	0.034	0.298	0.950	4.869	11.519

^a Standard uncertainty u are $u(x_i) = u(y_i) = 0.005$, $u(x'_2) = 0.005$, $u(T) = 0.01\text{K}$, $u(P) = 0.1\text{ kPa}$.

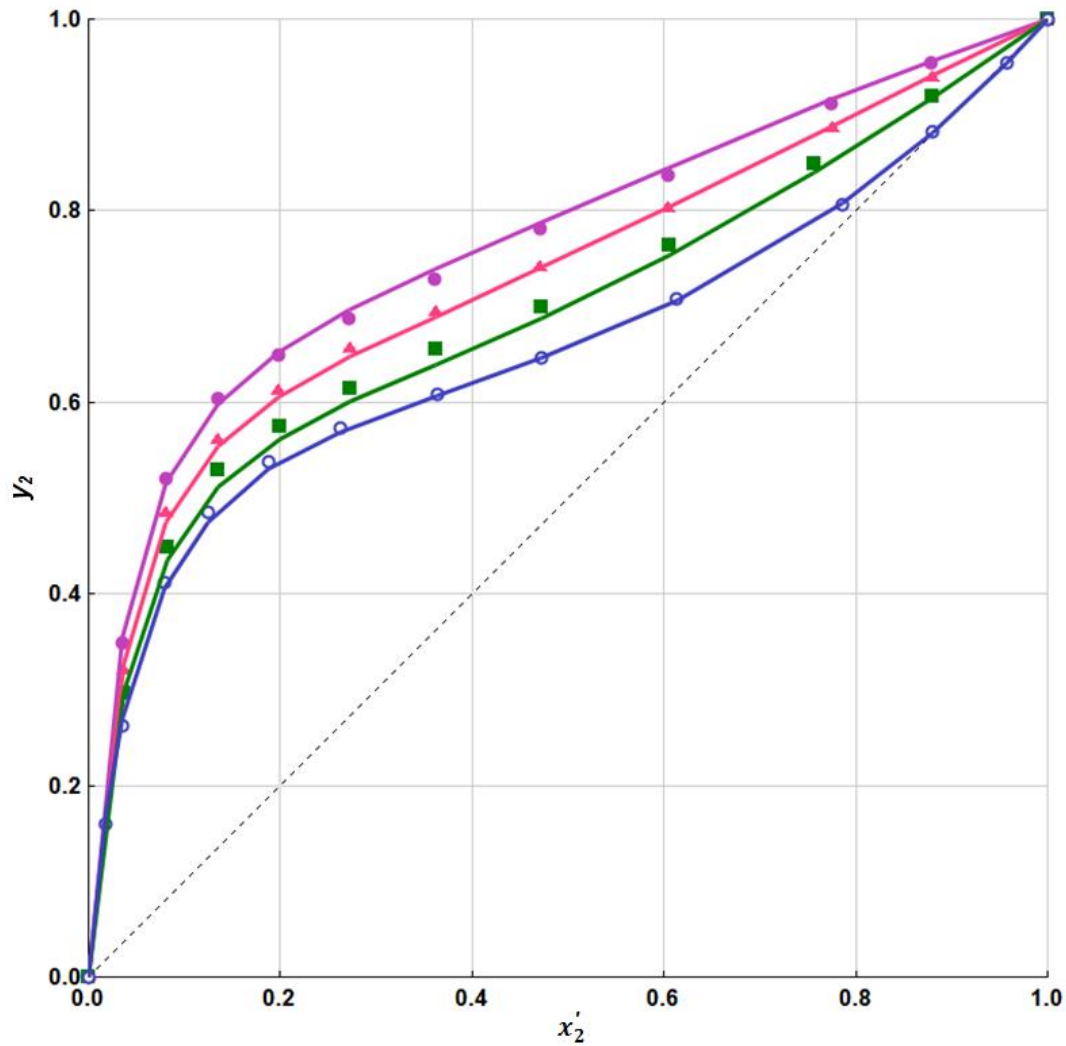


Figure 4.5. Isobaric y - x' diagram for the system of water (1) ethanol (2) + calcium chloride (3) at 94.5 kPa; (○) salt free, (■) 5 %, (▲) 10 % and (●) 15 % w/w salt; solid line correlated by eNRTL model, x' , liquid phase mole fraction (salt-free basis); y , vapour phase mole fraction.

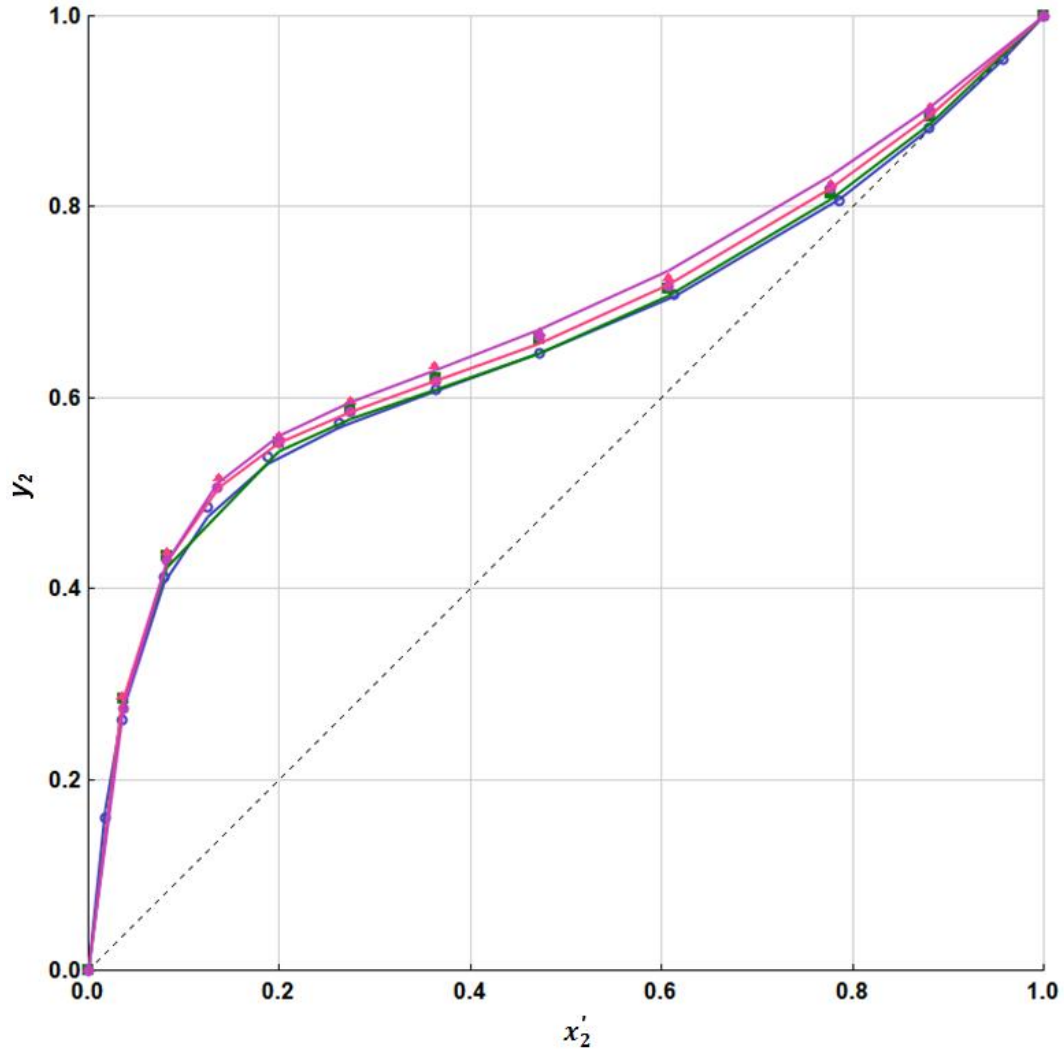


Figure 4.6. Isobaric y - x' diagram for the system of water (1) ethanol (2) + zinc chloride (3) at 94.5 kPa; (○) salt free, (■) 5 %, (▲) 10 % and (●) 15 % w/w salt; solid line correlated by eNRTL model, x' , liquid phase mole fraction (salt-free basis); y , vapour phase mole fraction.

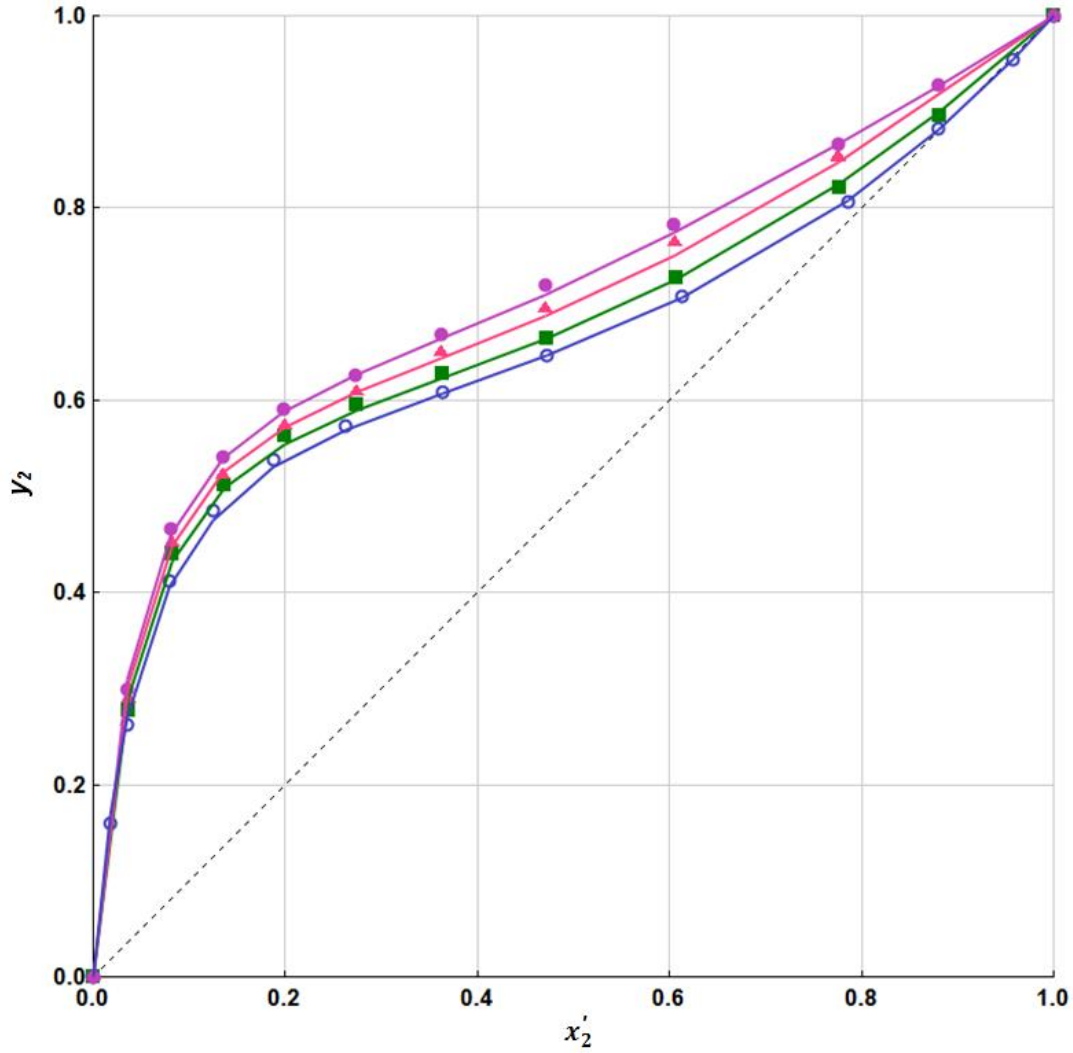


Figure 4.7. Isobaric y - x' diagram for the system of water (1) ethanol (2) + lithium bromide (3) at 94.5 kPa; (○) salt free, (■) 5 %, (▲) 10 % and (●) 15 % w/w salt; solid line correlated by eNRTL model, x' , liquid phase mole fraction (salt-free basis); y , vapour phase mole fraction.

4.3.2 Correlation of the VLE Data

Vapour-liquid phase equilibrium for component i can be expressed with following equation 12, [30]

$$y_i \Phi_i^V P = \gamma_i^S x_i \Phi_i^S P_i^S \exp \left[\frac{V_i (P - P_i^S)}{RT} \right] \quad (12)$$

Where liquid and vapour mole fractions of a more volatile component i are represented by x_i and y_i , respectively. P is the system pressure, and the exponential term represents the Poynting factor which is equal to one for the low-pressure system; thus above equation is simplified to,

$$y_i P = \gamma_i x_i P_i^S \quad (13)$$

Where P_i^S , is the saturation vapour pressure of the pure component i at temperature T , which can be calculated by extended Antoine equation,

$$\ln(P_i^S / \text{kPa}) = C_{1i} + \frac{C_{2i}}{T + C_{3i}} + C_{4i} T + C_{5i} \ln T + C_{6i} T^{C_{7i}} \quad \text{for } C_{8i} \leq T \leq C_{9i}$$

(14)

Where C_{1i} to C_{9i} are the coefficients of pure components i , C_{8i} and C_{9i} represents the temperature range limits, which were retrieved from the Aspen databank [31] and given in 4. 8.

Table 4.8. Parameters of the extended Antoine equation^a of pure components [31]

Parameters	C_1	C_2	C_3	C_4	C_5	C_6	C_7	C_8	C_9
ethanol	66.3962	-7122.3	0	0	-7.1424	2.9×10^{-6}	2	159.0	514
water	66.7412	-7258.2	0	0	-7.3037	4.2×10^{-6}	2	273.16	647.1

^a Where P is in kPa, and T is in K.

The Activity coefficient for a component i can be obtained by taking the partial derivative of the excess Gibbs free energy model with respect to n_i as follows [30]

$$\ln \gamma_i = \left[\frac{\partial (nG^E / RT)}{\partial n_i} \right]_{T, P, n_j \neq i} \quad (15)$$

The liquid phase activity coefficient (γ_i) can be calculated using the electrolyte non-random two-liquid model (e-NRTL) proposed by Chen et al. [32] and Mock et al.[33] for mixed solvent electrolyte systems based on two fundamental assumptions like ion repulsion and local electro-neutrality. The following equation gives the Excess Gibbs free energy model,

$$G_m^{*E}/RT = (G_m^{*E,PDH}/RT) + (G_m^{*E,Born}/RT) + (G_m^{*E,lc}/RT) \quad (16)$$

This can lead to,

$$\ln\gamma_i^* = \ln\gamma_i^{*PDH} + \ln\gamma_i^{*Born} + \ln\gamma_i^{*lc} \quad (17)$$

In multicomponent electrolyte systems, the long-range interaction contribution accounts with the Pitzer-Debye-Huckel (PDH) [34] formula, which can be represented by the following expression,

$$G_m^{*E,PDH}/RT = -(\sum_i x_i)(1000/M_s)^{1/2}(4A_\phi I_x/\rho) \ln(1 + \rho I_x^{1/2}) \quad (18)$$

Where x_i is the mole fraction of component i , M_s is the molecular weight of solvent, ρ is the closest approach parameter, A_ϕ is the Debye-Huckel parameter. is given by the following expression,

$$A_\phi = (1/3)(2\pi N_A d_s/1000)^{1/2}(Q_e^2/\epsilon_s kT)^{3/2} \quad (19)$$

And I_x is the ionic strength as given by,

$$I_x = (1/2)\sum_i x_i z_i^2 \quad (20)$$

Where N_A is the Avogadro's number, k is the Boltzmann constant, d_s is the mass density of solvent, ϵ_s is the dielectric constant of the solvent, Q_e is the electron charge, T is the temperature, z_i is charge number of ion, The expression for activity coefficient is given as,

$$\ln\gamma_i^{*PDH} = -(1000/M_s)^{1/2}A_\phi[(2z_i^2/\rho)\ln(1 + \rho I_x^{1/2}) + (z_i^2 I_x^{1/2} - 2I_x^{3/2})/(1 + \rho I_x^{1/2})] \quad (21)$$

The Born are equations represented by the following equations, [34]

$$G_m^{*E,Born}/RT = (Q_e^2/2kT)[(1/\epsilon_s) - (1/\epsilon_w)] \sum_i \frac{x_i z_i^2}{r_i} 10^{-2} \quad (22)$$

An expression derived for the activity coefficient of from born equation [35] is,

$$\ln\gamma_i^{*Born} = (Q_e^2/2kT)[(1/\epsilon_s) - (1/\epsilon_w)](z_i^2/r_i)10^{-2} \quad (23)$$

Where ϵ_w is the dielectric constant of water, r_i is the Born radius, dielectric constants for each component used for thermodynamic modeling are given in Table 4.9

Table 4.9. Coefficients of dielectric constant equation^a

Parameters	A	B	C
Ethanol	24.1113	12601.6	298.15
H ₂ O	78.54	31989.4	298.15

$$^a \epsilon = A + B \left(\frac{1}{T} - \frac{1}{C} \right)$$

The local interaction contribution excess Gibbs energy obtained with local composition NRTL equation. For electrolyte system containing molecular species (m), cation (c), and anion (a) can be expressed as follow,

$$\frac{G_m^{*E,lc}}{nRT} = \sum_m n_m \left(\frac{\sum_i X_i G_{im} \tau_{im}}{\sum_i X_i G_{im}} \right) + \sum_c z_c n_c \left(\frac{\sum_{i \neq c} X_i G_{ic} \tau_{ic}}{\sum_{i \neq c} X_i G_{ic}} \right) + \sum_a z_a n_a \left(\frac{\sum_{i \neq a} X_i G_{ia} \tau_{ia}}{\sum_{i \neq a} X_i G_{ia}} \right) \quad (24)$$

Where

$$X_i = C_i x_i = C_i \left(\frac{n_i}{n} \right), i = m, c, a \quad (25)$$

$$n = \sum_i n_i = \sum_m n_m + \sum_c n_c + \sum_a n_a \quad (26)$$

$$G_{ij} = \exp(\alpha_{ij} \tau_{ij}) \quad (27)$$

Where τ_{ij} is binary energy parameter and α_{ij} is the non-randomness factor, represent the binary energy interaction parameter

For molecule- molecule τ_{ij} is,

$$\tau_{ij} = c_{ij} + \frac{d_{ij}}{T} \quad (28)$$

For molecule- electrolyte τ_{ij} is,

$$\tau_{ij} = c_{ij} + \frac{d_{ij}}{T} + e_{ij} \left[\frac{T_{ref}-T}{T} + \ln \left(\frac{T}{T_{ref}} \right) \right] \quad (29)$$

Where T_{ref} is the reference temperature, c_{ij} , d_{ij} , and e_{ij} are adjustable parameters obtained from regression of the VLE data in Aspen Plus. Other physical properties of the components required, such as ideal gas heat capacity and heat of vaporizations, were obtained by retrieving the coefficients of the respective equation from the Aspen Plus [31], given Tables 4.10 and 4.11, respectively.

Table 4.10. Coefficients of ideal gas heat capacity model equation^a

Parameters	C ₁	C ₂	C ₃	C ₄	C ₅	C ₆
Ethanol	9014.18	214.071	-0.0839035	1.37327e ⁻⁰⁶	0	0
H ₂ O	33738.1	-7.01756	0.0272961	-1.66465e ⁻⁰⁵	4.2976e ⁻⁰⁹	-4.1696e ⁻¹³
Parameters	C ₇	C ₈	C ₉	C ₁₀	C ₁₁	
Ethanol	300	1318.4	33256	5.6902	1.5161	
H ₂ O	200	3000	33256	1.8978e ⁻¹³	9.2846	

$${}^a C_p^{ig} = C_{1i} + C_{2i}T + C_{3i}T^2 + C_{4i}T^3 + C_{5i}T^4 + C_{6i}T^5 \text{ for } C_{7i} \leq T \leq C_{8i}$$

$$C_p^{ig} = C_{9i} + C_{10i}T^{C_{11i}} \text{ for } T < C_{7i}$$

Table 4.11. Coefficients of heat of vaporization model equations

Parameters	$\Delta_{vap}H_i(T_1)$	T_1	a_i	b_i	T_{min}
Ethanol ^a	3.87698e ⁺⁰⁷	351.5	0.387894	0	159.1
H ₂ O ^a	4.06831e ⁺⁰⁷	373.2	0.310646	0	273.2

$${}^a \Delta_{vap}H_i(T) = \Delta_{vap}H_i(T_1) \left(\frac{1-T/T_{ci}}{1-T_1/T_{ci}} \right)^{a_i+b_i(1-T/T_{ci})} \text{ for } T > T_{min}$$

Where $\Delta_{vap}H_i(T_1)$ = Heat of vapoursization at reference temperature T_1

$\Delta_{vap}H_i(T)$ is heat of vaporization at temperature T , T_{ri} and T_{ci} are reduced and critical temperatures of component i , respectively.

The binary interaction parameters for the electrolyte-NRTL model are determined using experimental vapour-liquid equilibrium data in the Aspen data regression system (DRS) in Table

4.12. While performing the regression of the VLE data maximum likelihood principle was used as an objective function with the Deming initialization method and Britt-Luecke algorithm.

Table 4.12. Binary interaction parameter for the eNRTL Model

Component i	Component j	τ_{ij}	τ_{ij}	α_{ij}
ethanol	water	0.02	1.49	0.3
Water	CaCl ₂	12.23	-5.49	0.2
ethanol	CaCl ₂	27.26	-13.88	0.051
water	ZnCl ₂	10.30	-4.88	0.2
ethanol	ZnCl ₂	114.13	-57.16	0.012
water	LiBr	11.47	-5.45	0.2
ethanol	LiBr	55.0	--26.96	0.0275

Table 4.13. The root-mean-square deviation (RMSD) for the equilibrium temperature (T) and vapour phase mole fraction (y_1) for the eNRTL model

Salt	w_3 (%)	RMSD	
		y_1	T/K
Calcium Chloride	5	0.010	0.23
	10	0.005	0.15
	15	0.006	0.34
Zinc Chloride	5	0.008	0.24
	10	0.008	0.25
	15	0.009	0.44
Lithium Bromide	5	0.006	0.15
	10	0.007	0.24
	15	0.006	0.41

The root-mean-square deviation (RMSD) between the experimental and calculated values for the equilibrium temperature (T) and vapour phase mole fraction of ethanol (y_2) are expressed as follows,

$$\text{RMSD}(T_i) = \left(\sum_{i=1}^N (T_i^{\text{cal}} - T_i^{\text{exp}})^2 / N \right)^{0.5} \quad (30)$$

$$\text{RMSD}(y_i) = \left(\sum_{i=1}^N (y_i^{\text{cal}} - y_i^{\text{exp}})^2 / N \right)^{0.5} \quad (31)$$

The values for RMSD (y) and RMSD (T) are given in Table 4.13, which are less than 0.01 and 0.44 K, respectively. According to the calculated values of RMSD for equilibrium temperature and vapour phase mole fraction, the eNRTL model is suitable for the VLE analysis of the ternary system of water + ethanol + salts.

4.3.3 Thermodynamic Consistency Test

The thermodynamic consistency of all experimental results was examined using the van Ness test to ensure the accuracy of the VLE data acquired [36, 37]. The following is the Van Ness test equation

$$\Delta y = \frac{1}{N} \sum_{i=1}^N \Delta y_i = \frac{1}{N} \sum_{i=1}^N 100 |y_i^{\text{cal}} - y_i^{\text{exp}}| \quad (32)$$

N is the number of experimental the data and, y_i^{exp} and y_i^{cal} the mole fraction of component i in the vapour phase obtained experimentally and calculated by the eNRTL model, respectively. According to this method, the measured VLE data are to be thermodynamically consistent if Δy is less than one. The results obtained for van Ness test [36, 37] for Δy are 0.854, 0.413 and 0.473 for a system of water + ethanol + calcium chloride, 0.765, 0.672, 0.666 for the system of water + ethanol + zinc chloride, 0.462, 0.503, 0.414 for the system of water + ethanol + lithium bromide at a constant salt concentration of 0.05, 0.1 and 0.15 (mass fraction), respectively. As each value of Δy obtained for all the salt system are less than 1, it indicates that the experimental vapour-liquid equilibrium results obtained in this work are thermodynamic consistency.

4.3.4 Effect of Salts on Vapour-Liquid Equilibrium

The isobaric $y-x'$ and $-x$ diagrams for ternary systems of water + ethanol + calcium chloride, water + ethanol + zinc chloride, and water + ethanol + lithium bromide were included and plotted, respectively, to study the impact of salt concentration on the vapour-liquid equilibrium of the ethanol and water azeotropic system. It can be seen from these figures that the equilibrium curve intersects the diagonal line at the azeotropic point before the addition of the entrainer. As water is highly polar, the interaction between salt and water becomes much stronger with increasing salt concentration than between salt and ethanol. Thus ethanol concentration shifts from azeotropic composition to pure ethanol. As shown in Figure 4.5, the ethanol concentration in the vapour phase increases with the addition of the calcium chloride salt, this result in the upward shifting of the equilibrium curve with the addition of calcium chloride. As the content of calcium chloride increases, the degree of curve shift increases. It means that calcium chloride exhibited a stronger salting-out effect on ethanol, which leads to the complete elimination of the azeotropic point. On the other hand, zinc chloride and lithium bromide exhibited a significantly less salting-out effect on ethanol, resulting in a slight shift in azeotropic composition at higher concentrations of zinc chloride.

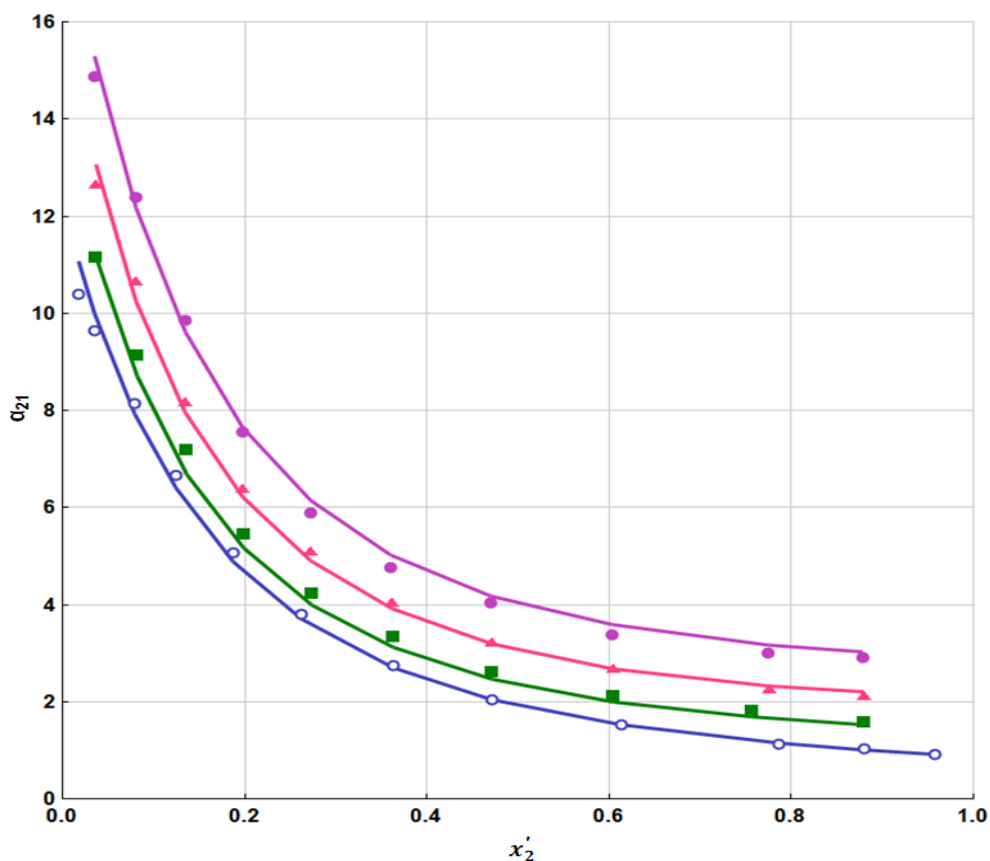


Figure 4.8. Relative volatility (α_{21}) for the system of water (1) ethanol (2) + calcium chloride (3) at 94.5 kPa; (○) salt free, (■) 5 %, (▲) 10 % and (●) 15 % w/w salt; solid line correlated by eNRTL model, x' , liquid phase mole fraction (salt-free basis).

The effects of all the salts on the relative volatility of ethanol to water are presented in Figs.8-10. The relative volatility can also express the separation ability for all salts. The higher the relative volatility better is the separation of the azeotrope. The calcium chloride salt could eliminate the azeotrope formed by ethanol and water, while zinc chloride could not help when the mass fraction of zinc chloride was up to 0.05; only a slight shift in azeotropic composition was observed in the case of zinc chloride as entrainer. Thus, calcium chloride can be a better entrainer choice than zinc chloride and lithium bromide in separating ethanol and water azeotropic systems.

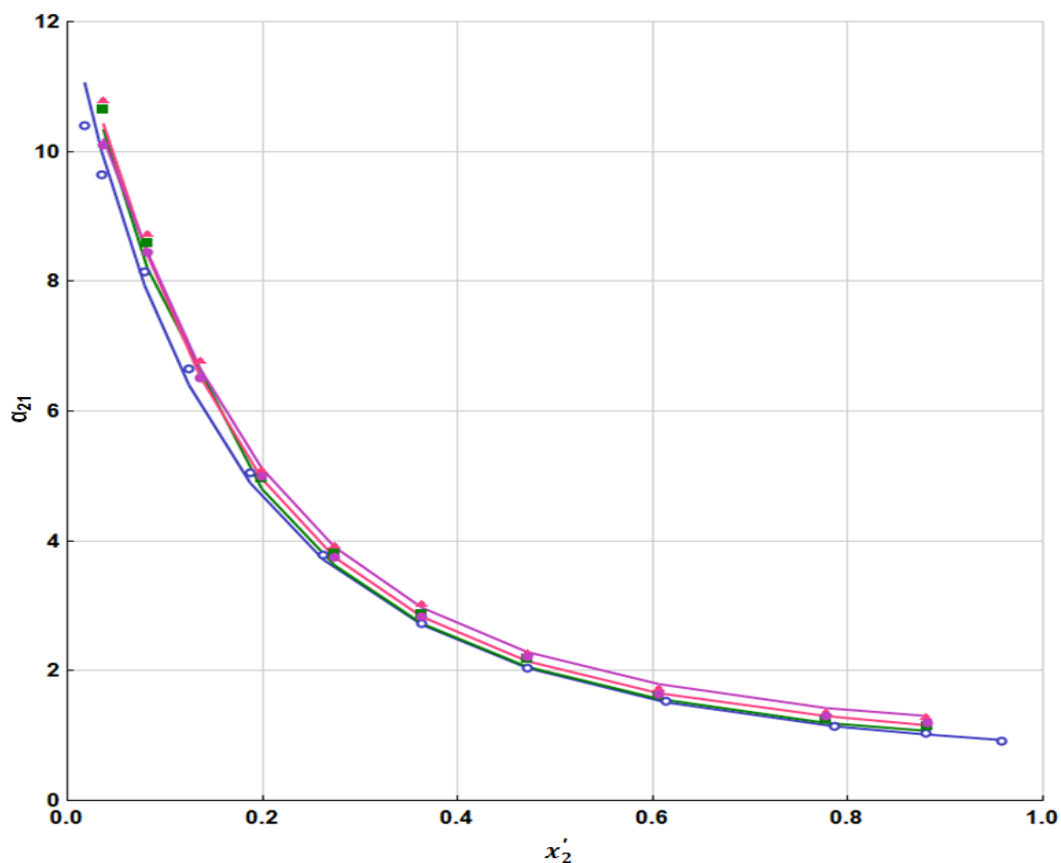


Figure 4.9. Relative volatility (α_{21}) for the system of water (1) ethanol (2) + zinc chloride (3) at 94.5 kPa; (○) salt free, (■) 5 %, (▲) 10 % and (●) 15 % w/w salt; solid line correlated by eNRTL model, x' , liquid phase mole fraction (salt-free basis).

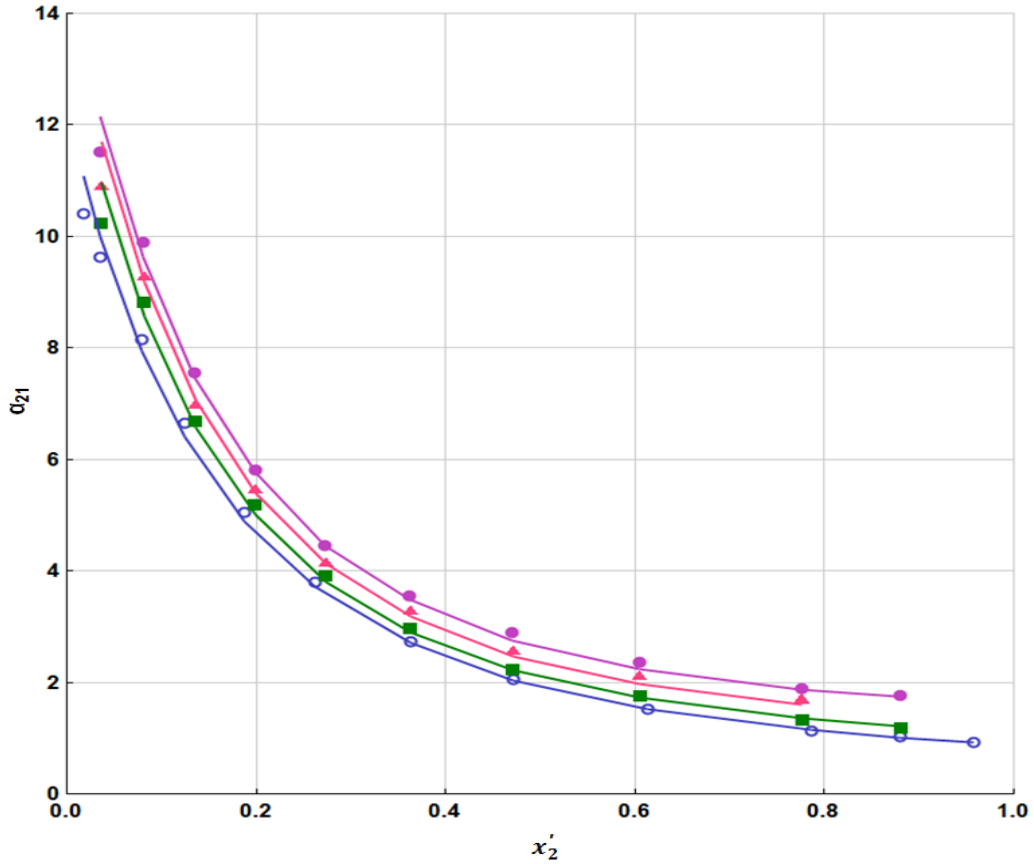


Figure 4.10. Relative volatility (α_{21}) for the system of water (1) ethanol (2) + lithium bromide (3) at 94.5 kPa; (○) salt free, (■) 5 %, (▲) 10 % and (●) 15 % w/w salt; solid line correlated by eNRTL model, x' , liquid phase mole fraction (salt-free basis).

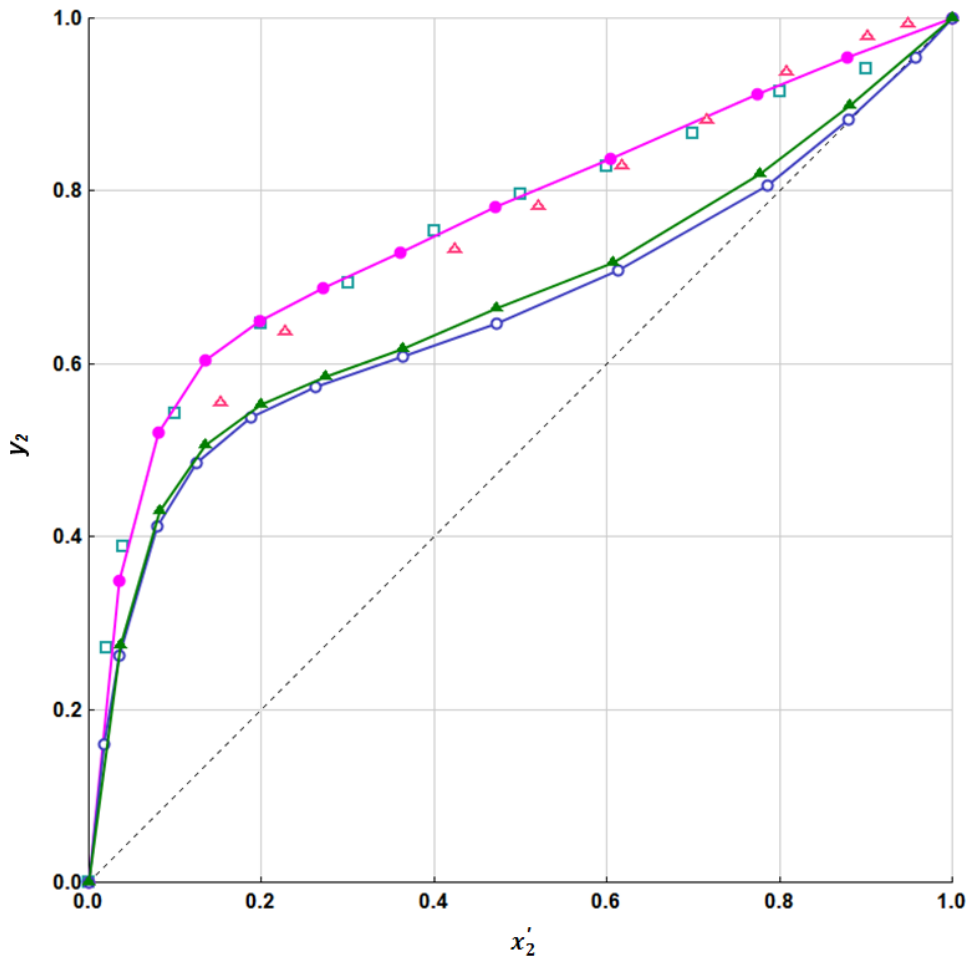


Figure 4.11. Isobaric y - x' diagram for water (1) ethanol (2) + salt (3) system, (\circ) salt free, (\blacktriangle) 15 % ZnCl_2 , and (\bullet) 15 % CaCl_2 w/w salt (this study), (\square) 16.7 % CaCl_2 w/w salt [24], (\triangle) 0.04 molar concentration of MgCl_2 [14] x' , liquid phase mole fraction (salt-free basis); y , vapour phase mole fraction.

For water+ ethanol+ salt ternary system equilibrium diagram is plotted for comparing the experimental data with literature data as shown in Fig 11; the result shows that experimental data is in good agreement with the literature data. It is observed that from Fig 12, the shift in equilibrium curve in the case of CaCl_2 was more as compared to ZnCl_2 and LiBr when all salts have the same concentration of 15 %, So it can be concluded that CaCl_2 will act as a good entrainer as compared to ZnCl_2 and LiBr for separation of ethanol + water azeotropic mixture.

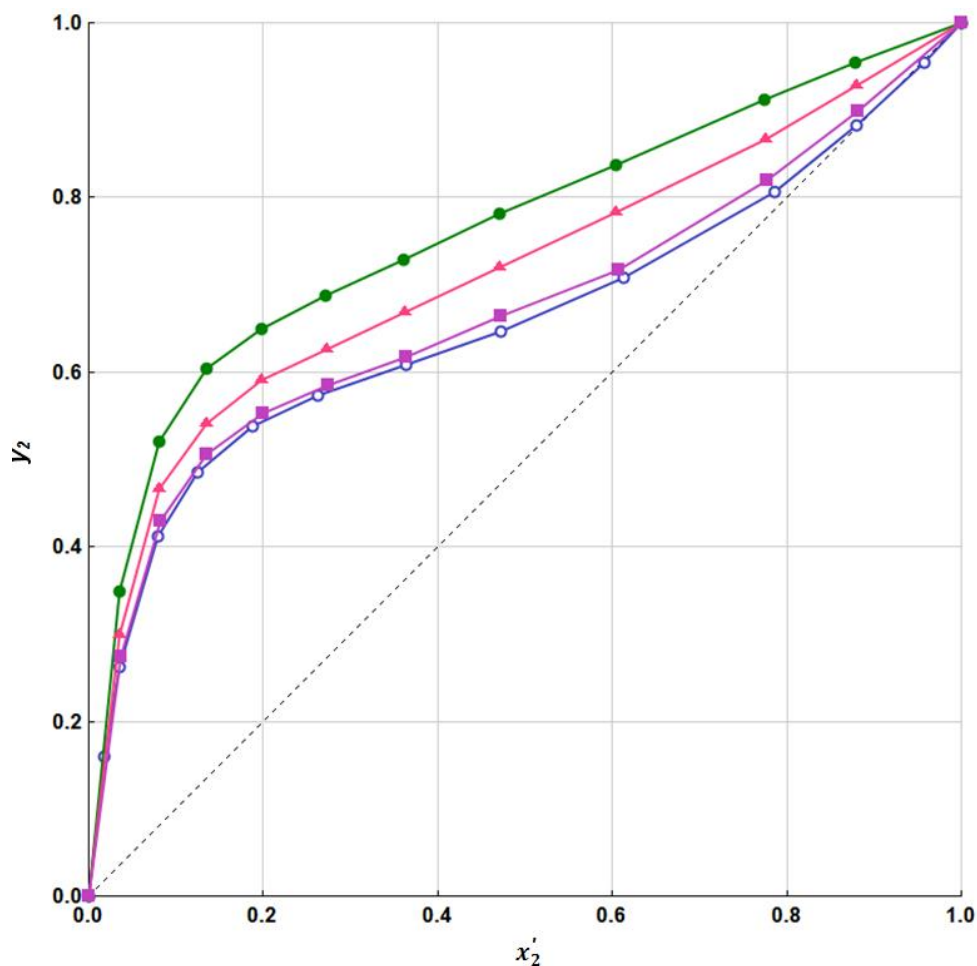


Figure 4.12. Isobaric y - x' diagram for water (1) ethanol (2) + salt (3) system, (\circ) salt free, (\blacksquare) 15 % ZnCl₂, and (\bullet) 15 % CaCl₂ w/w salt, (\blacktriangle) 15 % LiBr w/w salt x' , liquid phase mole fraction (salt-free basis); y , vapour phase mole fraction.

4.3.5 Extractive Distillation Configuration

An Extractive distillation configuration is proposed with CaCl₂ salt as an extractive entrainer and analyzed through the steady state simulations for feasibility of the separation of an ethanol and water mixture, as shown in Fig 13. The binary interaction parameter obtained in this work was utilized as the basis for the simulation. This method involves directly introducing the aqueous ethanol solution having 85 mole % of ethanol composition with a flow rate of 100 kmol/h at intermediate stage and salt with flow rate of 3.4 kmol/h fed at the top stage of the salt extractive distillation column, where the anhydrous ethanol is produced as a distillate. The operating conditions of the salt extractive distillation column utilized in the concentrated ethanol

feed process are also shown in Table 4.14. It was found that almost 99.9 mole % of ethanol was obtained from the distillate stream, as shown in Table 4.15. The salt distillation column's bottom product, essentially an aqueous solution containing calcium chloride, may be recovered using the evaporation system.

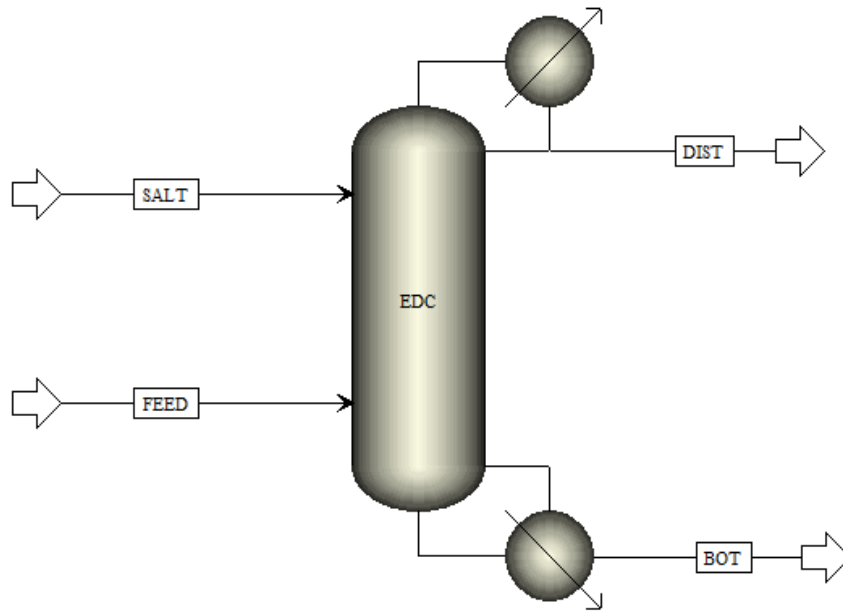


Figure 4.13. EDC column using CaCl_2 as an entrainer

Table 4.14. Preliminary EDC column configuration

Parameter	Value
NT	37
NT _s	2
NT _F	31
RR (molar)	0.4
S/F Molar ratio	0.034
P (atm)	1

Table 4.15. Preliminary stream results for EDC column

Parameter	Units	FEED	SALT	DIST	BOT
Temperature	C	78	75	78.35	156.08
Mole Flows	kmol/hr	100	3.4	85	18.4
Ethanol	mole fractions	0.85	0	0.9993	0.0031
Water		0.15	0	0.0007	0.8122
CaCl ₂		0	1	1.53E-26	0.1848

4.4 Conclusions

The isobaric vapour-liquid equilibrium (VLE) data for binary ethanol + water and ternary system of ethanol + water + calcium chloride and ethanol + water + zinc chloride and ethanol + water + lithium bromide with constant mass fractions of salts of 0.05, 0.1 and 0.15, respectively, were determined at 94.6 kPa. The experimental data was found to be thermodynamically consistent using the van Ness test. Comparing the experimental data of binary and ternary systems showed that the azeotropic point of the ethanol-water system shifts with the addition of salt. In the case of adding CaCl₂ and LiBr, complete elimination of azeotrope was observed.

In contrast, a slight shift in azeotropic point was observed in the case of ZnCl₂, so it can be concluded that CaCl₂ can be a better entrainer in separating ethanol and water using extractive distillation. After performing a preliminary design of the salt extractive distillation column, it was found that the distillate stream contained over 99.9 moles percent ethanol. The electrolyte non-random two-liquid (eNRTL) model was used to correlate the VLE for the ternary system of water + ethanol + CaCl₂/ ZnCl₂/LiBr result showed that the eNRTL model agreed well with experimental data.

4.5 References

- [1] I.D. Gil, A.M. Uyazán, J.L. Aguilar, G. Rodríguez, L.A. Caicedo, Separation of ethanol and water by extractive distillation with salt and solvent as entrainer: process simulation, *Brazilian J. Chem. Eng.* 25 (2008) 207–215.
- [2] R.A. Dagle, A.D. Winkelman, K.K. Ramasamy, V. L. Dagle, R.S. Weber, Ethanol as a renewable building block for fuels and chemicals, *Ind. Eng. Chem. Res.* 59 (2020) 4843-4853.
- [3] Z. Lei, B. Chen, Z. Ding, *Special distillation processes*, Elsevier, Amsterdam, 2005.
- [4] Z. Lei, C. Li, B. Chen, Extractive distillation: a review, *Sep. Purif. Rev.* 32 (2003) 121-213.
- [5] E.L. Ligeró, T.M.K. Ravagnani, Dehydration of ethanol with salt extractive distillation-a comparative analysis between processes with salt recovery, *Chem. Eng. Process.* 42 (2003) 543–552.
- [6] C.A.T. Cantero, G.L. Lopez, V.M. Alvarado, R.F. E. Jimenez, J.Y.R. Morales, E.M.S. Coronado, Control structures evaluation for a salt extractive distillation pilot plant: Application to bio-ethanol dehydration, *Energies.* 10 (2017) 1276.
- [7] R.A. Cook, W.F. Furter, Extractive distillation employing a dissolved salt as separating agent, *Can. J. Chem. Eng.* 46 (1968) 119-123
- [8] D. Schmitt, A. Vogelpohl, Distillation of ethanol-water solutions in the presence of potassium acetate, *Sep. Sci. Technol.* 18 (1983) 547–554.
- [9] D. Barba, V. Brandani, G. Di Giacomo, Hyperazeotropic ethanol salted-out by extractive distillation. Theoretical evaluation and experimental check. *Chem. Eng. Sci.* 40 (1985), 2287-2292.
- [10] R.T.P. Pinto, M.R. Wolf-Maciel, L. Lintomen, Saline extractive distillation process for ethanol purification, *Comp. Chem. Eng.* 24 (2000) 1689–1694.

- [11] M. Llano-Restrepo, J. Aguilar-Arias, Modeling and simulation of saline extractive distillation columns for the production of absolute ethanol, *Comp. Chem. Eng.* 27 (2003) 527–549.
- [12] M.A. Hussain, J.L. Anthony, P.H. Pfromm, Reducing the energy demand of corn-based fuel ethanol through salt extractive distillation enabled by electro dialysis. *AIChE J.* 58 (2012) 163-172.
- [13] R.B. Soares, F.L.P. Pessoa, M.F. Mendes, Dehydration of ethanol with different salts in a packed distillation column, *Process Saf. Environ. Prot.* 93 (2015) 147–153.
- [14] L. Zeng, and Z. Li, A new process for fuel ethanol dehydration based on modeling the phase equilibria of the anhydrous MgCl_2 + ethanol + water system. *AIChE J.* 61 (2015) 664-676.
- [15] D. Meranda, W.F. Furter, Vapours-liquid equilibrium data for system: Ethanol-water saturated with Potassium acetate, *Can. J. Chem. Eng.* 44 (1966) 298–300.
- [16] D. Meranda, W.F. Furter, Vapours-liquid equilibrium in alcohol-water systems containing dissolved acetate salts. *AIChE J.* 17 (1971) 38-42.
- [17] E. Vercher, R. Muñoz, A. Martinez-Andreu, Isobaric vapour-liquid equilibrium data for the ethanol-water-potassium acetate and ethanol-water-(potassium acetate/sodium acetate) systems, *J. Chem. Eng. Data.* 36 (1991) 274–277.
- [18] R.J. Zemp, A.Z. Francesconi, Salt effect on phase equilibria by a recirculating still, *J. Chem. Eng. Data.* 37 (1992) 313–316
- [19] M.A. Galan, M.D. Labrador, J.R. Alvarez, Salt effect in liquid-vapour equilibrium: ethanol-water system saturated with strontium bromide, barium nitrate, and strontium nitrate, *J. Chem. Eng. Data.* 25 (1980) 7–9.
- [20] E. Vercher, M.P. Peña, A. Martinez-Andreu, Isobaric vapours–liquid equilibrium data for the ethanol–water–strontium bromide system, *J. Chem. Eng. Data.* 39 (1994) 316–319.

- [21] H.M. Polka, J. Gmehling, Effect of calcium nitrate on the vapour-liquid equilibria of ethanol + water and 2-propanol + water, *J. Chem. Eng. Data.* 39 (1994) 621–624.
- [22] M.P. Peña, E. Vercher, A. Martinez-Andreu, Isobaric vapour-liquid equilibrium for ethanol+ water+ cobalt (ii) chloride. *J. Chem. Eng. Data.* 39 (1994) 763-766.
- [23] D. Meranda, W.F. Furter, Vapours-liquid equilibrium in alcohol-water systems containing dissolved halide salts and salt mixtures, *AIChE J.* 18 (1972) 111-116.
- [24] Y. Nishi, Vapour-liquid equilibrium relations for the system accompanied by hypothetical chemical reaction containing salt, *J. Chem. Eng. Japan.* 8 (1975) 187–191
- [25] T. Meyer, H.M. Polka, J. Gmehling, Low-pressure isobaric vapour-liquid equilibria of ethanol/water mixtures containing electrolytes. *J. Chem. Eng. Data.* 36 (1991) 340–342.
- [26] K. Mishima, Y. Iwai, S. Yamaguchi, H. Isonaga, Y. Arai, M. Hongo, Correlation of vapour-liquid equilibria of ethanol-water-calcium chloride and methanol-ethanol-calcium chloride systems at 25 °C. *Mem. Facul. Eng. Kyushu Univ.* 46 (1986) 407-433
- [27] N.A. Mali, S.S. Yadav, P.D. Ghuge, S.S. Joshi, Vapour-liquid equilibrium data for binary mixtures of dimethyl carbonate with methyl acetate, ethyl acetate, n-propyl acetate, isopropyl acetate, n-butyl acetate, and isoamyl acetate at 93.13 kPa, *J. Chem. Eng. Data.* 62 (2017) 4356-4363.
- [28] B.R. Bhoi, N.A. Mali, S.S. Joshi, Experimental analysis of vapour-liquid phase equilibria for the binary systems of diethyl carbonate with methyl, ethyl, isopropyl, n-butyl and isoamyl acetates at 95 kPa, *J. Chem. Thermodynamics.* 150 (2020) 106189.
- [29] N.A. Mali, P.K. Mali, A.P. Patil, S.S. Joshi, Vapours–liquid equilibrium data for binary mixtures of acetic acid+anisole, acetone+anisole, and isopropanol+anisole at pressure 96.15 kPa, *J. Chem. Eng. Data.* 62 (2017) 947 - 953.
- [30] J.M. Smith, H.C. Van Ness *Introductio to chemical engineering thermodynamics*, McGraw-Hill, New York. 1975.
- [31] Aspen Properties V8.4; Aspen Technology: Burlington, MA, 2013.

- [32] C.C. Chen, H.I. Britt, J.F. Boston, L.B. Evans Local composition model for excess Gibbs energy of electrolyte systems, part I. Single solvent, single completely dissociated electrolyte systems. *AIChE J.* 28 (1982) 588–596.
- [33] B. Mock, L.B. Evans, C.C. Chen, Thermodynamic representation of phase equilibria of mixed-solvent electrolyte systems, *AIChE J.* 32 (1986) 1655–1664.
- [34] K.S. Pitzer, Electrolytes. From dilute solution to fused salts, *J. Am. Chem. Soc.* 102 (1980) 2902-2906.
- [35] C.C. Chen, Y. Song, Generalized electrolyte-NRTL model for mixed-solvent electrolyte systems, *AIChE J.* 50 (2004) 1928–1941.
- [36] L. Xu, D. Xu, P. Shi, K. Zhang, X. Ma, J. Gao, Y. Wang, Salts effect on isobaric vapour-liquid equilibrium for separation of the azeotropic mixture allyl alcohol + water, *Fluid Phase Equilib.* 457 (2018) 11-17.
- [37] H.C. van Ness, S.M. Byer, R.E. Gibbs, Vapour-liquid equilibrium: Part I. An appraisal of data reduction methods, *AIChE J.* 19 (1973) 238-244.

Chapter 05

*Isobaric Vapour-Liquid Equilibrium
Measurements and Modeling of Binary
Systems of Methylcyclohexane with
Toluene, Anisole, and NEP at 92 kPa*

Chapter 5 Isobaric Vapour-Liquid Equilibrium Measurements and Modeling of Binary Systems of Methylcyclohexane with Toluene, Anisole, and NEP at 92 kPa

Abstract

Methylcyclohexane and toluene are challenging to separate by simple distillation; thus, anisole and NEP were explored as separating agents for the extractive distillation of this mixture. The influence of the anisole and NEP on the VLE behaviour of the system was analyzed. The isobaric vapour-liquid equilibrium (VLE) data for the binary systems methylcyclohexane + toluene, methylcyclohexane + anisole, toluene + anisole, methylcyclohexane + NEP, toluene + NEP were measured at 92.0 kPa. The NRTL, UNIQUAC, and Wilson thermodynamic activity coefficient models were used in the regression of experimental data to obtain the binary interaction parameters. All three activity coefficient models were able to correlate the experimental VLE behaviour. The Van Ness and the infinite dilution test confirmed the thermodynamic consistency of the experimental VLE data.

5.1 Introduction

Aromatic compounds are fundamental building blocks for creating synthetic rubber, plastic, fiber, and other materials [1]. The chemical industry's primary challenge is separating aromatic and non-aromatic mixtures. Due to numerous aromatic and non-aromatic components being close to boiling and showing azeotropic behaviour, conventional distillation is not a viable solution for this type of separation. Several solvent-based processes, such as liquid-liquid extraction, azeotropic distillation, and extractive distillation, can be used to achieve this. However, extractive distillation was often a better option when compared to alternative technologies [1].

A highly polar organic solvent called 1-Ethyl-2-pyrrolidinone (NEP) can be used in several industrial separation procedures due to its excellent physical characteristics, high boiling point, low volatility, and solubility [2]. Despite being used in numerous industrial applications, additional information on thermodynamic vapour-liquid equilibrium for systems generating binary combinations with NEP must be included in the literature. Anisole has been widely used

as an industrial solvent in distillation separation [3]. In this study, we investigated using NEP and anisole as extractive entrainers to separate the binary combination of methylcyclohexane and toluene.

The literature reports the isobaric VLE data for the binary system of methylcyclohexane + toluene at various constant pressures [4-9]. For the binary system of toluene + anisole [3], isobaric VLE data is presented at 101.325 kPa. NIST [10] data bank confirmed no isobaric VLE data for methylcyclohexane + anisole, methylcyclohexane + NEP, and toluene + NEP published in the literature. The VLE data for each component with both entrainers is necessary to derive the binary interaction parameter of the activity coefficient models, which is used in the design and modelling of distillation configurations to separate methylcyclohexane and toluene.

This study aims to examine potential entrainers on the VLE behaviour of methylcyclohexane and toluene systems for extractive distillation, including the effects of anisole and NEP. The isobaric VLE data for a binary mixture of methylcyclohexane + toluene, methylcyclohexane + anisole, toluene + anisole, methylcyclohexane + NEP, toluene + NEP were measured at 92.0 kPa. Van Ness test [11] and Infinite dilution test [12] can be applied to check the thermodynamic consistency of the experimental data. The measured VLE data was regressed by the nonrandom two-liquid (NRTL) [13], universal quasi-chemical (UNIQUAC) [14], and Wilson [15] thermodynamic activity coefficient model to obtain the binary interaction parameters.

The isobaric VLE data for a binary mixture of methylcyclohexane + toluene, methylcyclohexane + anisole, toluene + anisole, methylcyclohexane + NEP, toluene + NEP were measured at 92.0 kPa. Van Ness test [11] and Infinite dilution test [12] can be applied to check the thermodynamic consistency of the experimental data. The measured VLE data was regressed by the nonrandom two-liquid (NRTL) [13], universal quasi-chemical (UNIQUAC) [14], and Wilson [15] thermodynamic activity coefficient model to obtain the binary interaction parameters.

5.2 Experimental

5.2.1 Materials/Chemicals

Methylcyclohexane, toluene, anisole and NEP used in this work were analytical reagents purchased from commercial sources. All of these chemicals are used as it is without any further purification. The details of the reagents, such as CAS number, molecular weight, refractive index and purity, are listed in Table 5.1.

Table 5.1. Detailed specification of chemicals used

Component	CAS No.	Source	MW/g mol ⁻¹	purity	n _D at 298.15 K ^a	
					Exp	Lit
Methylcyclohexane	108-87-2	Loba Chemie Pvt. Ltd.	98.19	0.990	1.42052	1.42058 [6]
Toluene	108-88-3	Loba Chemie Pvt. Ltd.	92.14	0.998	1.49348	1.49413 [6]
Anisole	100-66-3	Loba Chemie Pvt. Ltd.	108.14	0.990	1.51440	1.5143 [3]
NEP	2687-91-4	Spectrochem Pvt. Ltd.	113.16	0.990	1.46427	

^aStandard uncertainties *u* for n_D measurements are *u* (n_D) = 0.0001, *u* (T) = 0.01 K.

5.2.2 Apparatus and Procedure

Glass dynamic circulation equipment operating at 92.0 kPa was used to determine the binary VLE data. We previously reported on the VLE apparatus's specifications and reliability [16, 17]. We used a vacuum pump SC920G Model from KNF, Germany, to maintain a consistent pressure of 92.0 kPa during the experimental runs. This pump validated the pressure of 92.0 kPa with an accuracy of 0.1 kPa throughout the experiments. During the experimental run, liquid and vapour phases continuously recirculated to attain equilibrium. The constant temperature reading confirmed the equilibrium condition for at least 30 to 60 min. The temperature at the equilibrium state was noted using a thermometer (CTH 7000 model) supplied by Wika, India, with an accuracy of ±0.01 K. A small sample of both vapour and liquid phases was withdrawn through a sampling knob using a glass syringe for analysis.

5.2.3 Analysis

The equilibrium compositions of the binary mixtures in vapour and liquid phases were measured with the help of refractive index measurement. The calibration curve for each binary system is generated by measuring the refractive index of gravimetrically prepared standard binary samples using an electronic weighing balance having an accuracy of $\pm 0.0001\text{g}$, covering the entire composition range. The refractive index for every standard sample was measured at 298.15 K using Atago, Japan (Model-RX-7000i), having an accuracy of ± 0.0001 and a resolution of 0.00001. Figures 5.1 to 5.5 show the calibration curves produced for each binary system. The second-order polynomial equation fitted to the refractive index vs mole fractions of more volatile components data for each binary pair is listed in Table 5.2. These equations back-calculate the mole fractions of more volatile components in each binary mixture from its refractive index of 298.15 K.

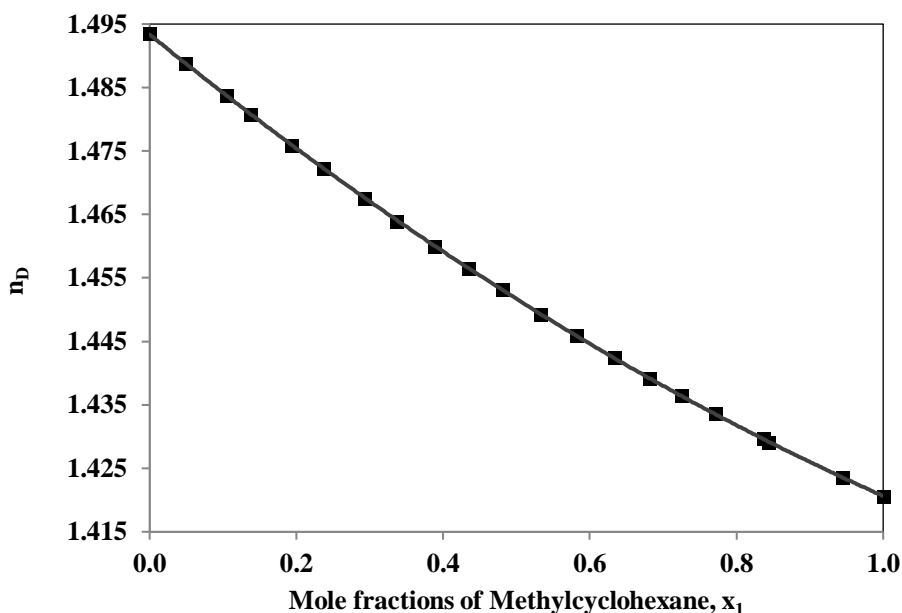


Figure 5.1. Calibration curve for the methylcyclohexane (1) + toluene (2) system with refractive index (n_D) versus mole fraction of methylcyclohexane (x_1); (■) measured values at 298.15 K, (—) polynomial equation.

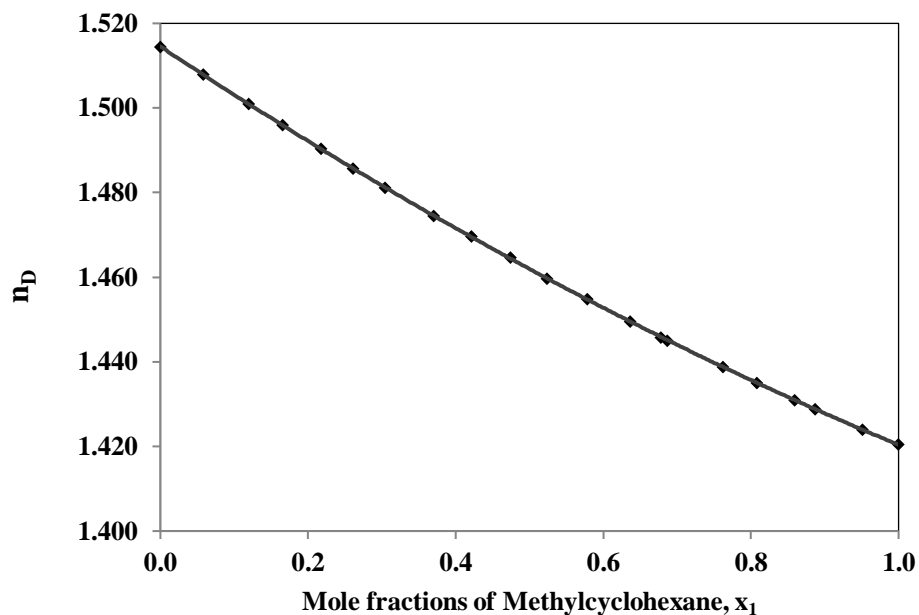


Figure 5.2. Calibration curve for the methylcyclohexane (1) + anisole (2) system with refractive index (n_D) versus mole fraction of methylcyclohexane (x_1); (■) measured values at 298.15 K, (—) polynomial equation.

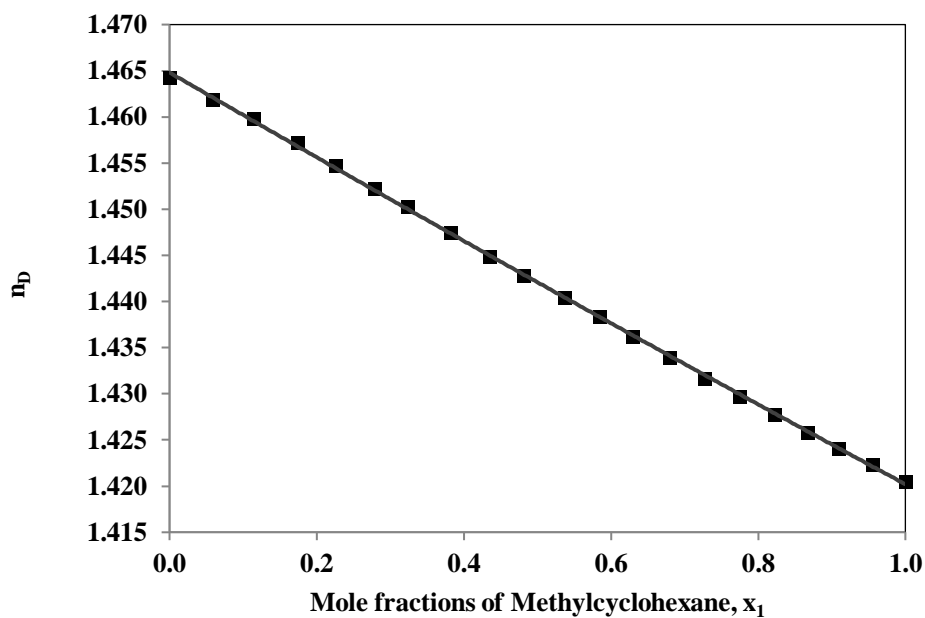


Figure 5.3. Calibration curve for the methylcyclohexane (1) + NEP (2) system with refractive index (n_D) versus mole fraction of methylcyclohexane (x_1); (■) measured values at 298.15 K, (—) polynomial equation.

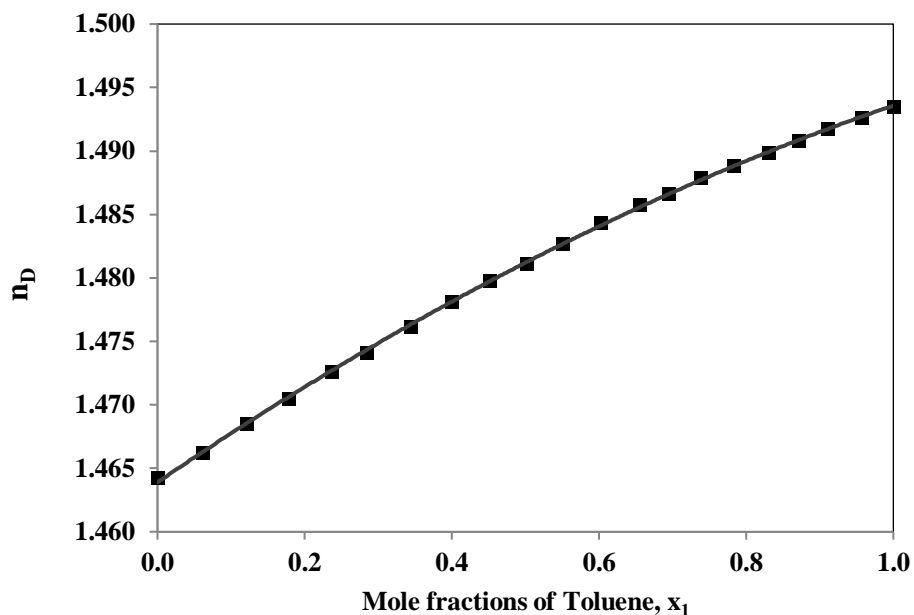


Figure 5.4. Calibration curve for the toluene (1) + NEP (2) system with refractive index (n_D) versus mole fraction of toluene (x_1); (■) measured values at 298.15 K, (—) polynomial equation.

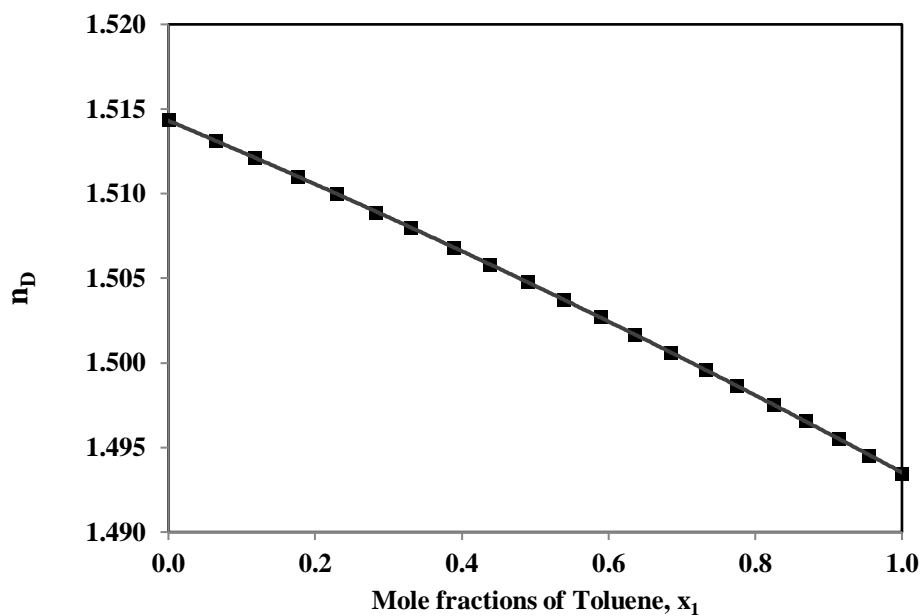


Figure 5.5. Calibration curve for the toluene (1) + anisole (2) system with refractive index (n_D) versus mole fraction of toluene (x_1); (■) measured values at 298.15 K, (—) polynomial equation.

Table 5.2. Fitted polynomial equation for calibration curves

System	Figure	Polynomial Equation	R ²
Methylcyclohexane (1) + Toluene (2)	Figure 5.1	$y = 0.0212x^2 - 0.0940x + 1.4933$	1.0000
Methylcyclohexane (1) + Anisole (2)	Figure 5.2	$y = 0.0220x^2 - 0.1161x + 1.5145$	1.0000
Methylcyclohexane (1) + NEP (2)	Figure 5.3	$y = 0.0017x^2 - 0.0463x + 1.4648$	0.9997
Toluene (1) + NEP (2)	Figure 5.4	$y = -0.0098x^2 + 0.0395x + 1.4639$	0.9997
Toluene (1) + Anisole (2)	Figure 5.5	$y = -0.0025x^2 - 0.0182x + 1.5143$	1.0000

5.3 Results and Discussion

5.3.1 Experimental Results

The isobaric vapour liquid equilibrium data for the binary mixtures of methylcyclohexane + toluene, methylcyclohexane + anisole, toluene + anisole, methylcyclohexane + NEP, toluene + NEP were measured at 92.0 kPa. Table 5.3 - 5.7 lists the measured VLE values, and Figure 5.6 - 5.10 displays Txy diagrams. Table 5.3 - 5.7 also includes relative volatility and activity coefficient information. The Txy plot in Figure 5.6 shows that the methylcyclohexane and toluene system exhibits a pinch towards pure methylcyclohexane due to decreased relative volatility values. Therefore, simple distillation to separate this binary combination requires a very high reflux ratio. Adding different stages also increases energy consumption and capital costs. Extractive distillation with the right entrainer may be a viable choice to separate this **low relative volatility** system. As shown in Figure 5.7 - 5.10, no azeotropic behaviour is observed between methylcyclohexane + anisole, methylcyclohexane + NEP, toluene + anisole and toluene + NEP, which indicates that they can be used as an entrainer in extractive distillation of methylcyclohexane and toluene.

Table 5.3. Vapour-liquid equilibrium data for the binary system of methylcyclohexane (1) + toluene (2) temperature T in K, liquid phase mole fraction (x_1), vapour phase mole fraction (y_1), activity coefficients (γ_i) and relative volatility (α_{12}) at 92.0 kPa.

$T(K)$	x_1	y_1	γ_1	γ_2	α_{12}
380.44	0.0000	0.0000		1.0008	
379.43	0.0433	0.0698	1.2553	1.0021	1.66
378.35	0.0954	0.1445	1.2147	1.0061	1.60
376.8	0.1891	0.2613	1.1564	1.0145	1.52
375.43	0.2895	0.3709	1.1137	1.0272	1.45
374.4	0.3817	0.4612	1.0810	1.0427	1.39
373.42	0.4827	0.5531	1.0538	1.0648	1.33
372.64	0.5828	0.6385	1.0301	1.0936	1.26
371.88	0.6922	0.7308	1.0143	1.1298	1.21
371.31	0.7911	0.8145	1.0054	1.1673	1.16
370.87	0.8941	0.9037	0.9995	1.2117	1.11
370.65	0.9494	0.9535	0.9994	1.2328	1.09
370.48	1.0000	1.0000	1.0000		

^aStandard uncertainties u are $u(x_1) = 0.001$, $u(y_1) = 0.001$, $u(T) = 0.1$ K, $u(P) = 0.1$ kPa.

Table 5.4. Vapour-liquid equilibrium data for the binary system of methylcyclohexane (1) + anisole (2) temperature T in K, liquid phase mole fraction (x_1), vapour phase mole fraction (y_1), activity coefficients (γ_i) and relative volatility (α_{12}) at 92.0 kPa.

$T(K)$	x_1	y_1	γ_1	γ_2	α_{12}
423.42	0.0000	0.0000		1.0002	
414.21	0.0357	0.2586	2.4023	0.9964	9.42
403.49	0.0959	0.4964	2.1934	0.9933	9.29
397.78	0.1417	0.6008	2.0598	0.9914	9.12
387.19	0.2875	0.7608	1.6772	1.0130	7.88
382.16	0.4205	0.8292	1.4267	1.0575	6.69
380.11	0.4923	0.8542	1.3265	1.1075	6.04
377.87	0.5897	0.8798	1.2123	1.2237	5.09
375.79	0.6956	0.9070	1.1222	1.3759	4.27
373.74	0.8086	0.9380	1.0573	1.5727	3.58
372.00	0.9062	0.9676	1.0223	1.7888	3.09
371.24	0.9529	0.9827	1.0090	1.9570	2.81
370.48	1.0000	1.0000	1.0000		

^aStandard uncertainties u are $u(x_1) = 0.001$, $u(y_1) = 0.001$, $u(T) = 0.1$ K, $u(P) = 0.1$ kPa

Table 5.5. Vapour-liquid equilibrium data for the binary system of methylcyclohexane (1) + NEP (2) temperature T in K, liquid phase mole fraction (x_1), vapour phase mole fraction (y_1), activity coefficients (γ_i) and relative volatility (α_{12}) at 92.0 kPa.

$T(K)$	x_1	y_1	γ_1	γ_2	α_{12}
370.48	1.0000	1.0000	1.0000		
371.57	0.9568	0.9920	1.0049	7.6607	5.60
372.24	0.9368	0.9891	1.0040	6.9252	6.12
373.45	0.8169	0.9833	1.1061	3.4716	13.20
375.07	0.7138	0.9796	1.2050	2.5274	19.25
376.18	0.6264	0.9773	1.3283	2.0531	25.68
379.02	0.4917	0.9716	1.5560	1.6716	35.37
384.11	0.3823	0.9635	1.7313	1.4292	42.65
389.56	0.2940	0.9529	1.9327	1.2945	48.58
408.01	0.1446	0.9044	2.3858	1.0840	55.96
431.14	0.0725	0.7883	2.5176	1.0255	47.64
442.11	0.0515	0.7062	2.5564	0.9989	44.27
486.77	0.0000	0.0000		1.0000	

^aStandard uncertainties u are $u(x_1) = 0.001$, $u(y_1) = 0.001$, $u(T) = 0.1$ K, $u(P) = 0.1$ kPa

Table 5.6. Experimental VLE data for the binary system of toluene (1) + NEP (2) temperature T in K, liquid phase mole fraction (x_1), vapour phase mole fraction (y_1), activity coefficients (γ_i) and relative volatility (α_{12}) at 92.0 kPa.

$T(K)$	x_1	y_1	γ_1	γ_2	α_{12}
380.44	1.0000	1.0000	1.0008		
381.48	0.9701	0.9991	1.0002	0.8119	34.22
383.01	0.9236	0.9976	1.0039	0.7951	34.38
386.41	0.8294	0.9937	1.0114	0.8131	32.44
389.58	0.7501	0.9892	1.0195	0.8379	30.51
393.49	0.6600	0.9821	1.0345	0.8755	28.26
399.86	0.5374	0.9670	1.0576	0.9310	25.22
408.25	0.4079	0.9407	1.0965	0.9632	23.03
416.1	0.3210	0.9089	1.1139	0.9827	21.10
432.55	0.2016	0.8135	1.0943	1.0046	17.27
458.39	0.0820	0.5488	1.0742	1.0029	13.62
465.91	0.0558	0.4352	1.0874	1.0005	13.04
486.75	0.0000	0.0000		1.0005	

^aStandard uncertainties u are $u(x_1) = 0.001$, $u(y_1) = 0.001$, $u(T) = 0.1$ K, $u(P) = 0.1$ kPa

Table 5.7. Experimental VLE data for the binary system of toluene (1) + anisole (2) temperature T in K, liquid phase mole fraction (x_1), vapour phase mole fraction (y_1), activity coefficients (γ_i) and relative volatility (α_{12}) at 92.0 kPa.

$T(K)$	x_1	y_1	γ_1	γ_2	α_{12}
380.44	1.0000	1.0000	1.0008		
381.66	0.9501	0.9833	0.9999	1.2220	3.09
382.62	0.9143	0.9709	0.9980	1.1989	3.13
385.06	0.8171	0.9352	1.0036	1.1496	3.23
387.71	0.7212	0.8959	1.0113	1.1070	3.33
390.55	0.6227	0.8496	1.0272	1.0746	3.42
394.09	0.5100	0.7859	1.0542	1.0486	3.53
397.56	0.4133	0.7175	1.0834	1.0336	3.61
401.55	0.3191	0.6326	1.1156	1.0217	3.67
406.87	0.2140	0.5041	1.1590	1.0152	3.73
414.48	0.1002	0.2959	1.2072	1.0062	3.77
418.37	0.0532	0.1754	1.2297	1.0024	3.79
423.42	0.0000	0.0000		1.0002	

^aStandard uncertainties u are $u(x_1) = 0.001$, $u(y_1) = 0.001$, $u(T) = 0.1$ K, $u(P) = 0.1$ kPa

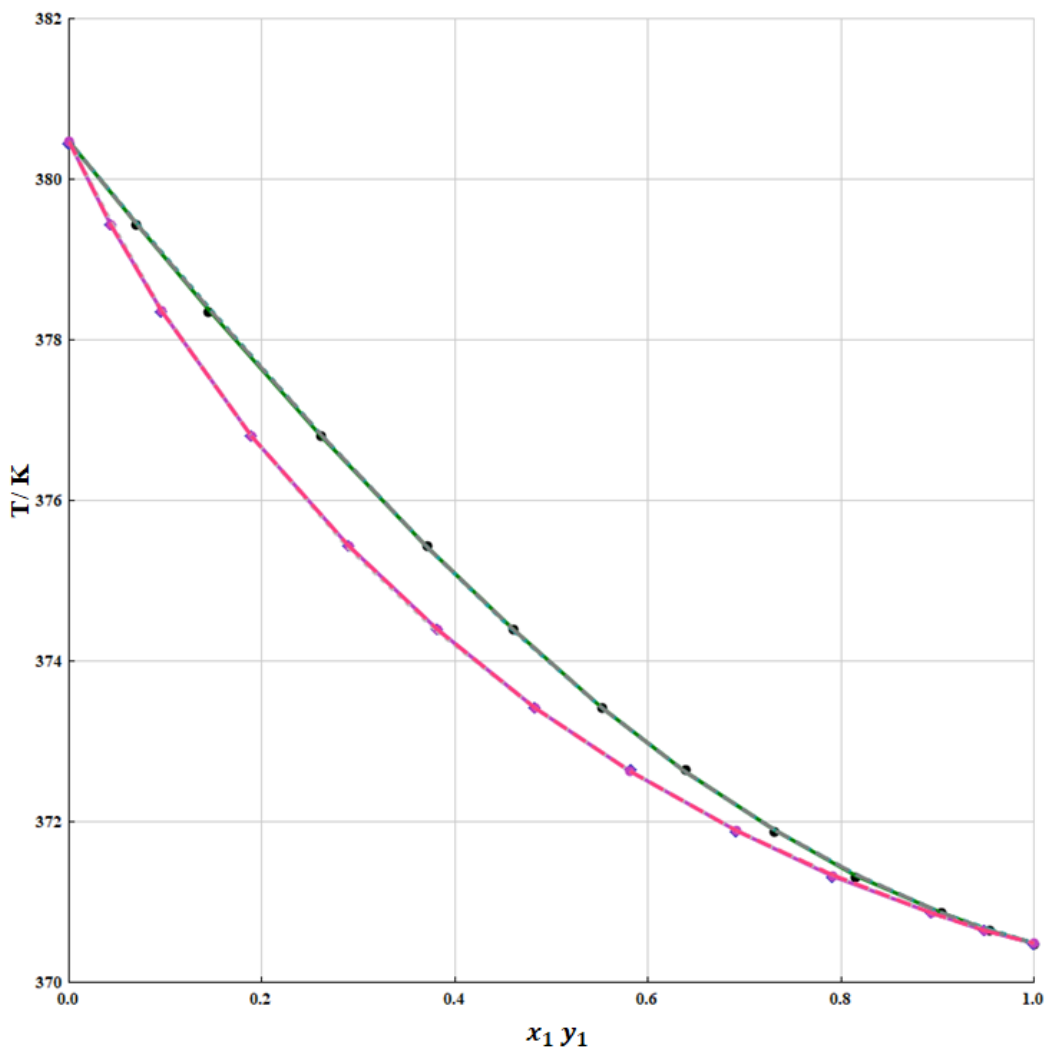


Figure 5.6. Txy diagram for methylcyclohexane (1) + toluene (2) at 92 kPa. (●) T-x experimental (■) T-y experimental; (- - -) NRTL, (—) Wilson, (...) UNIQUAC model.

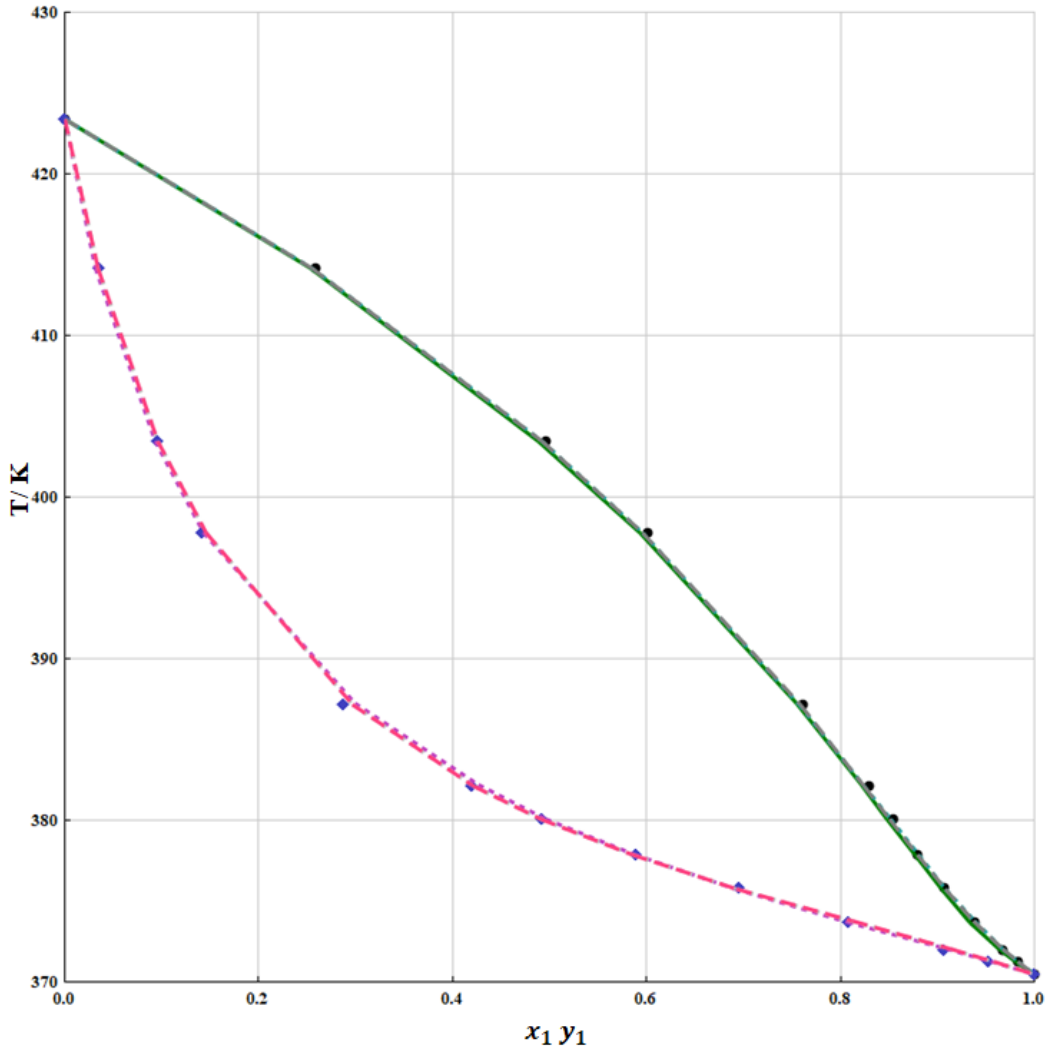


Figure 5.7. Txy diagram for methylcyclohexane (1) + anisole (2) at 92 kPa. (●) T-x experimental (■) T-y experimental; (- - -) NRTL, (—) Wilson, (...) UNIQUAC model.

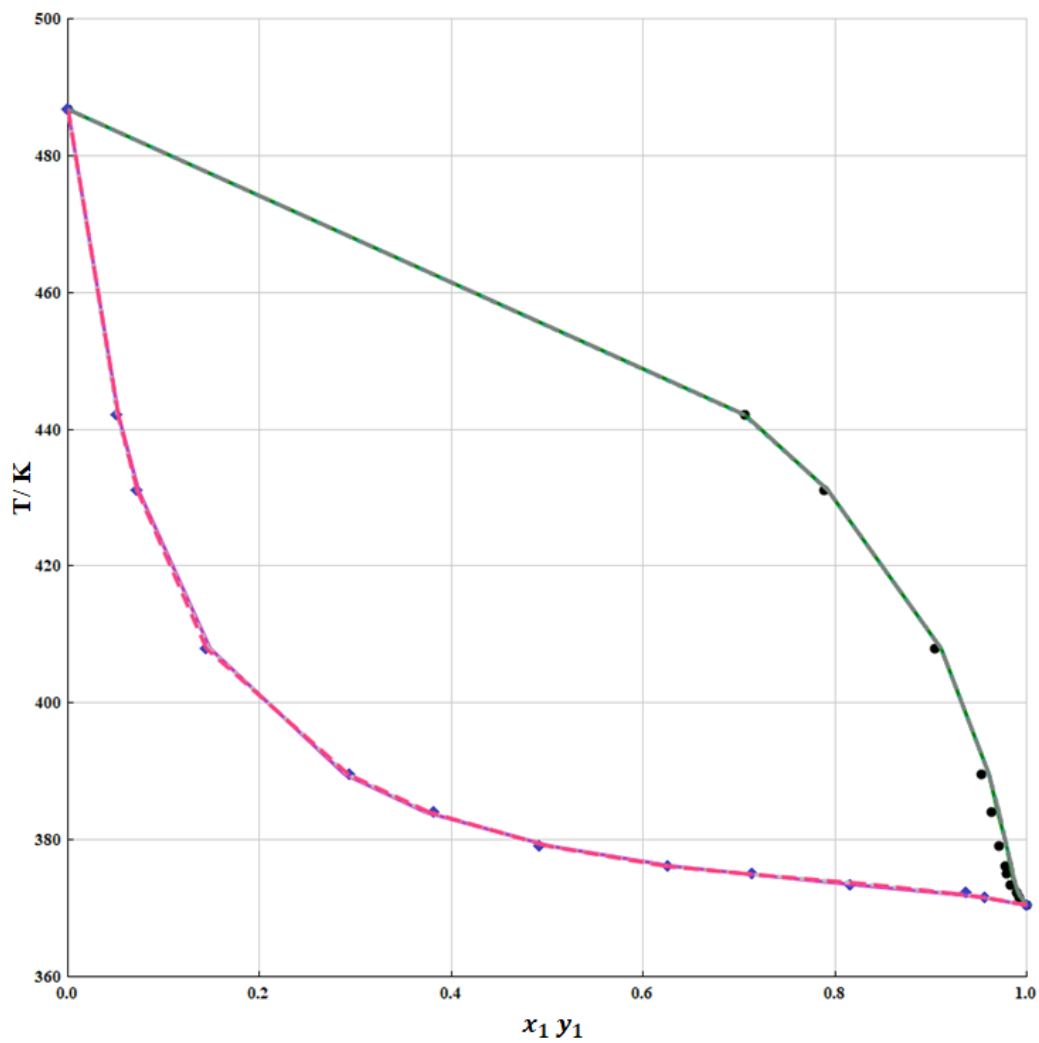


Figure 5.8. Txy diagram for methylcyclohexane (1) + NEP (2) at 92 kPa. (●) T-x experimental (■) T-y experimental; (- - -) NRTL, (—) Wilson, (...) UNIQUAC model.

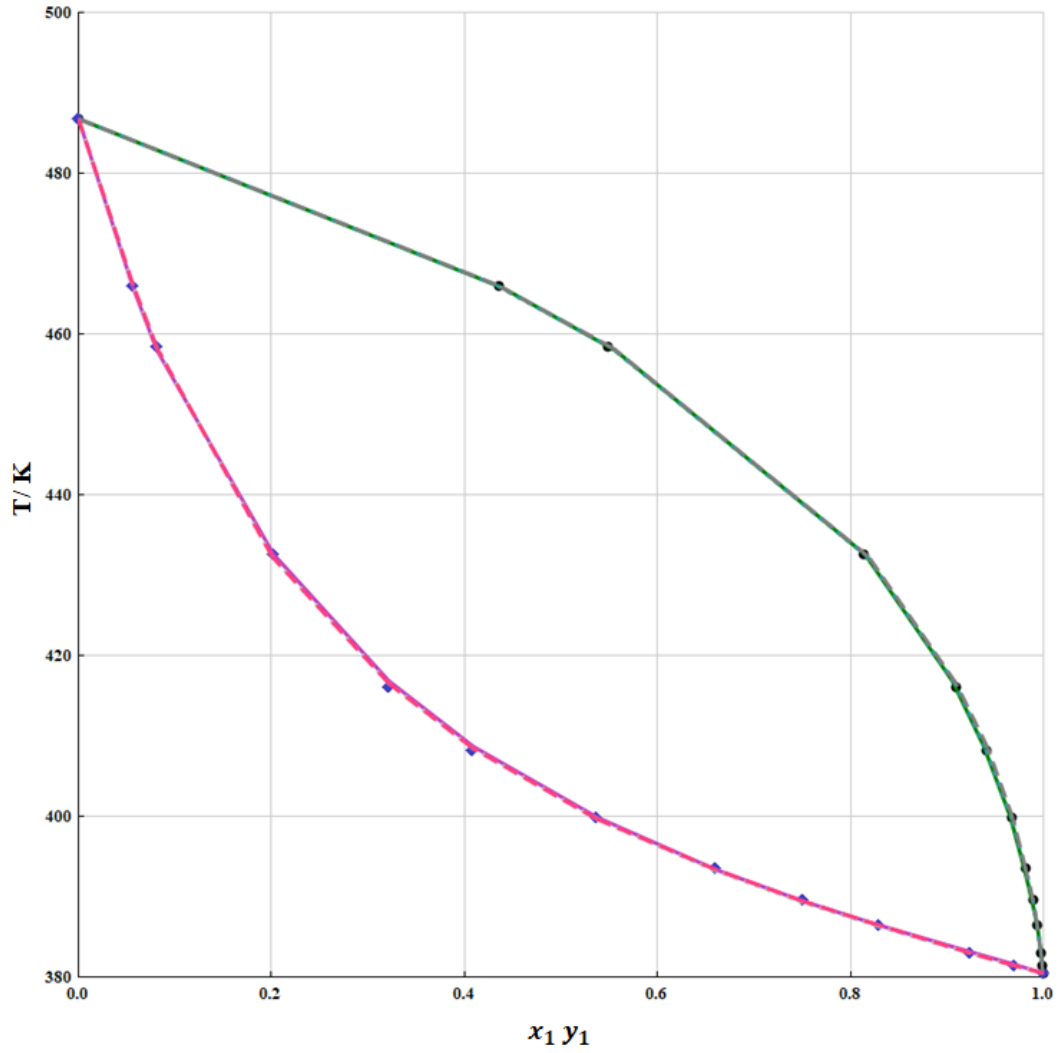


Figure 5.9. Txy diagram for toluene (1) + NEP (2) at 92 kPa(●) T-x experimental (■) T-y experimental; (- - -) NRTL, (—) Wilson, (...) UNIQUAC model.

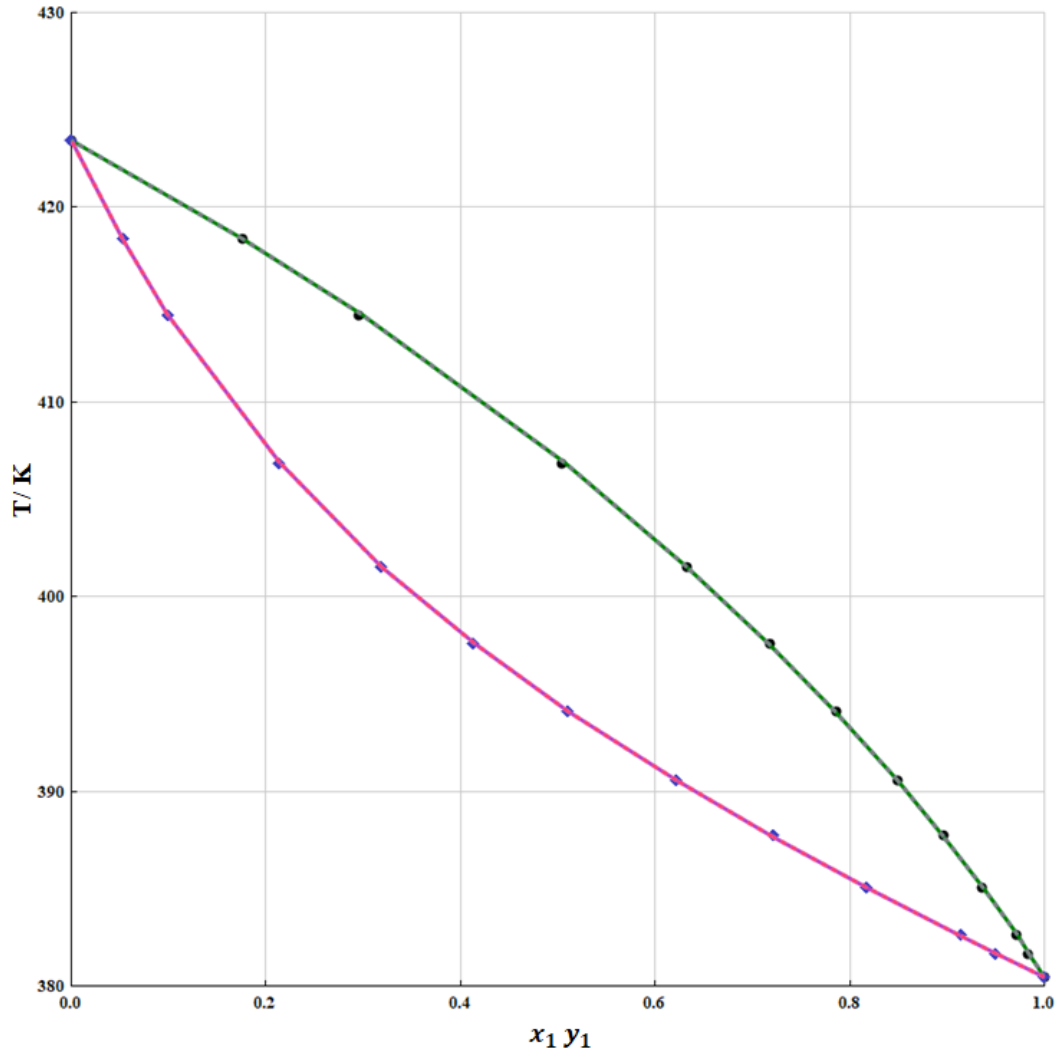


Figure 5.10. Txy diagram for toluene (1) + anisole (2) at 92 kPa. (●) T-x experimental (■) T-y experimental; (- - -) NRTL, (—) Wilson, (...) UNIQUAC model.

5.3.2 Data Regression

The relationship for vapour-liquid phase equilibrium of any binary mixture containing component i can be expressed by equation [18].

$$y_i \Phi_i^V P = \gamma_i^S x_i \Phi_i^S P_i^S \exp \left[\frac{V_i (P - P_i^S)}{RT} \right] \quad (1)$$

Liquid and vapour phase mole fractions for component i are denoted by x_i and y_i , respectively. P denotes the total pressure of the system. In this case, the exponential term

representing the Poynting factor is equal to one, as the experimental data was determined at low pressure. γ_i denotes to activity coefficient. The fugacity coefficients (Φ_i) for a component i in both the vapour phase and liquid phase is assumed to be unity due to low pressure; thus above equation is simplified to,

$$y_i P = \gamma_i x_i P_i^S \quad (2)$$

The saturated vapour pressure (P_i^S) at temperature T of any pure component i was determined by the extended Antoine equation,

$$\ln(P_i^S / \text{kPa}) = C_{1i} + \frac{C_{2i}}{T+C_{3i}} + C_{4i} T + C_{5i} \ln T + C_{6i} T^{C_{7i}} \quad \text{for } C_{8i} \leq T \leq C_{9i} \quad (3)$$

Where C_{1i} to C_{9i} are the parameters for the extended Antoine equation for pure components i , obtained from the Aspen physical property databank and are listed in Table 5.8, C_{8i} and C_{9i} show the limits of temperature range used in Eq.(3),

Table 5.8. Parameters of the extended Antoine equation

Parameter	C ₁	C ₂	C ₃	C ₄	C ₅	C ₆	C ₇	C ₈	C ₉
Methylcyclohexane	85.7762	-7080.8	0	0	-10.695	8.14E-06	2	146.58	572.1
Toluene	70.0372	-6729.8	0	0	-8.179	5.30E-06	2	178.18	591.75
Anisole	121.152	-9307.7	0	0	-16.693	0.014919	1	235.65	645.6
NEP	98.8222	-10022	0	0	-12.153	6.28E-06	2	266.7	736.1

The experimental isobaric VLE data were regressed by NRTL [13], UNIQUAC [14] and Wilson [15] thermodynamic model using the Aspen plus V10 data regression system; the obtained binary interaction for binary systems is given in Table 5.9. The regression of binary VLE data to the resulting binary interaction parameter was performed using the maximum likelihood objective function, which is defined as,

$$OF = \sum_{i=1}^N \left[\left(\frac{T_i^{exp} - T_i^{cal}}{\sigma_T} \right)^2 + \left(\frac{P_i^{exp} - P_i^{cal}}{\sigma_P} \right)^2 + \left(\frac{x_i^{exp} - x_i^{cal}}{\sigma_x} \right)^2 + \left(\frac{y_i^{exp} - y_i^{cal}}{\sigma_y} \right)^2 \right] \quad (4)$$

T, P, y and x denote the equilibrium temperature, pressure, and mole fractions in the vapour and liquid phases. σ stands for the standard deviation.

The deviation in experimental and calculated data can be calculated using the average absolute deviation (AAD) and root-mean-square deviations (RMSD) of equilibrium temperature (T) and vapour phase mole fraction (y) of a more volatile component using the following equations,

$$\text{RMSD } (T_i) = \left(\sum_{i=1}^N (T_i^{\text{cal}} - T_i^{\text{exp}})^2 / N \right)^{0.5} \quad (5)$$

$$\text{RMSD } (y_i) = \left(\sum_{i=1}^N (y_i^{\text{cal}} - y_i^{\text{exp}})^2 / N \right)^{0.5} \quad (6)$$

$$\text{AAD } (T_i) = \sum_{i=1}^N |T_i^{\text{cal}} - T_i^{\text{exp}}| / N \quad (7)$$

$$\text{AAD } (y_i) = \sum_{i=1}^N |y_i^{\text{cal}} - y_i^{\text{exp}}| / N \quad (8)$$

For all binary pairs, the calculated values for RMSD and AAD are listed in Table 5.9. RMSD (y), and AAD (y) values are lower than 0.005, whereas the values of RMSD (T) and AAD (T) are less than 0.26 and 0.18 respectively. According to these results, all three models can fit the experimental isobaric VLE data.

The relative volatility of binary mixture can be calculated as,

$$\alpha_{12} = \frac{y_1/x_1}{y_2/x_2} \quad (9)$$

Where y and x are mole fractions of the components in vapour and liquid phases, respectively

Table 5.9. Regressed binary interaction parameters of the NRTL, UNIQUAC, and Wilson models and RMSD and AAD

Model	Binary interaction parameters					Root mean square deviations		Average absolute deviations	
	A _{ij}	A _{ji}	B _{ij}	B _{ji}	C _{ij}	RMSD (y ₁)	RMSD (T/K)	AAD (y ₁)	AAD (T/K)
Methylcyclohexane (1) + Toluene (2)									
NRTL	-13.200	17.349	4784.370	-6210.06	0.3	0.001	0.012	0.001	0.009
UNIQUAC	0.476	-0.345	-135.479	53.103		0.001	0.015	0.001	0.012
Wilson	-11.982	9.023	4273.460	-3285.90		0.001	0.011	0.001	0.008
Methylcyclohexane (1) + Anisole (2)									
NRTL	10.762	1.996	-3434.270	-930.259	0.3	0.003	0.018	0.002	0.014
UNIQUAC	-5.745	0.794	1817.990	-129.914		0.003	0.019	0.002	0.014
Wilson	-3.081	-4.646	1175.880	1312.680		0.005	0.014	0.005	0.012
Methylcyclohexane (1) + NEP (2)									
NRTL	-12.071	7.612	5578.100	-3132.23	0.2	0.005	0.043	0.004	0.023
UNIQUAC	2.975	-1.849	-1474.150	827.448		0.005	0.039	0.004	0.022
Wilson	0.133	1.011	-163.241	-1088.32		0.005	0.032	0.004	0.022
Toluene (1) + NEP (2)									
NRTL	15.547	-0.900	-4842.540	-434.497	0.2	0.002	0.179	0.001	0.133
UNIQUAC	-9.293	1.432	3091.240	-238.566		0.002	0.219	0.001	0.181
Wilson	0.659	-23.206	117.011	8321.650		0.002	0.262	0.002	0.165
Toluene (1) + Anisole (2)									
NRTL	7.129	-5.332	-2769.150	2143.980	0.2	0.001	0.008	0.001	0.005
UNIQUAC	-2.460	2.051	985.898	-852.579		0.001	0.008	0.001	0.005
Wilson	2.519	-4.359	-1034.890	1675.970		0.001	0.008	0.001	0.005

5.3.3 Thermodynamic Consistency Test

The Van Ness test and infinite dilution test [11] were used in this study to verify the thermodynamic consistency of the observed VLE data for the binary system. Equation (10) and (11) defines the Van Ness test as,

$$\Delta y = \frac{1}{N} \sum_{i=1}^N \Delta y_i = \frac{1}{N} \sum_{i=1}^N 100 |y_i^{cal} - y_i^{exp}| \quad (10)$$

$$\Delta P = \frac{1}{N} \sum_{i=1}^N \Delta P_i = \frac{1}{N} \sum_{i=1}^N 100 \left| \frac{P_i^{cal} - P_i^{exp}}{P_i^{exp}} \right| \quad (11)$$

Where N consider the number of experimental data points, the superscripts “cal” and “exp” denotes values calculated using NRTL, UNIQUAC and Wilson thermodynamic activity coefficients model and determined experimentally. As seen from Table 5.10, the values obtained for Δy and ΔP are less than one, representing that the data obtained experimentally are thermodynamically consistent.

Table 5.10. Van Ness thermodynamic consistency test results

System	NRTL		UNIQUAC		Wilson	
	Δy_1	ΔP	Δy_1	ΔP	Δy_1	ΔP
Methylcyclohexane (1) + Toluene (2)	0.080	0.003	0.089	0.004	0.073	0.003
Methylcyclohexane (1) + Anisole (2)	0.201	0.004	0.201	0.005	0.462	0.004
Methylcyclohexane (1) + NEP (2)	0.448	0.009	0.442	0.008	0.397	0.008
Toluene (1) + NEP (2)	0.133	0.053	0.103	0.066	0.160	0.077
Toluene (1) + Anisole (2)	0.092	0.002	0.092	0.002	0.091	0.002

The infinite dilution test proposed by Kojima and co-workers [12] is used to test the thermodynamic consistency of the measured data, which is expressed as an equation,

$$I_1 = 100 \left| \frac{G^E/(x_1 x_2 RT) - \ln(\gamma_1/\gamma_2)}{\ln(\gamma_1/\gamma_2)} \right|_{x_1=0} \quad (12)$$

$$I_2 = 100 \left| \frac{G^E/(x_1 x_2 RT) - \ln(\gamma_2/\gamma_1)}{\ln(\gamma_2/\gamma_1)} \right|_{x_2=0} \quad (13)$$

Where,

$$\frac{G^E}{RT} = x_1 x_2 [c_1 + c_2(x_1 - x_2) + c_3(x_1 - x_2)^2 + c_4(x_1 - x_2)^3] \quad (14)$$

$$\ln\left(\frac{\gamma_1}{\gamma_2}\right) = d_1 + d_2(x_2 - x_1) + d_3(6x_1 x_2 - 1) + d_4(x_2 - x_1)(1 - 8x_1 x_2) \quad (15)$$

Equation (14) and (15) represents extended Redlich-Kister's equations, and their constant can be determined from the experimental values of α and β . The constants of Redlich-Kister's equations for all binary pairs are listed in Table 5.11.

In the infinite dilution consistency test, if the values for $I_1 < 30$ and $I_2 < 30$, the binary data set passes the consistency test. The results for I_1 and I_2 presented in Table 5.12 showed that experimental data measured for all binary systems passed the infinite dilution test, as the values obtained for I_1 and I_2 are less than 30 in each pair.

Table 5.11. Estimated parameters of extended Redlich-Kister's model for infinite dilution test

System	c_1	c_2	c_3	c_4	d_1	d_2	d_3	d_4
Methylcyclohexane (1) + Toluene (2)	0.229	-0.022	0.023	-0.025	-0.013	0.236	-0.019	0.005
Methylcyclohexane (1) + Anisole (2)	0.780	0.074	0.085	-0.028	0.132	0.849	0.042	-0.010
Methylcyclohexane (1) + NEP (2)	1.916	0.066	-0.212	0.580	-0.256	1.489	0.358	0.238
Toluene (1) + NEP (2)	0.006	-0.333	-0.078	0.200	0.146	-0.097	-0.020	0.017
Toluene (1) + Anisole (2)	0.202	-0.077	0.044	0.055	0.006	0.223	0.007	0.003

Table 5.12. Infinite dilution consistency check results for binary VLE systems

System	I_1	I_2
Methylcyclohexane (1) + Toluene (2)	21.18	12.85
Methylcyclohexane (1) + Anisole (2)	11.77	21.50
Methylcyclohexane (1) + NEP (2)	4.96	0.39
Toluene (1) + NEP (2)	28.83	16.97
Toluene (1) + Anisole (2)	18.41	1.25

5.3.4 Effect of Solvent on VLE Methylcyclohexane and Toluene System

In the case of methylcyclohexane and toluene systems, the equilibrium curve is very close to the diagonal line, as shown in Figure 11. Due to its **low relative volatility** points, its mixture cannot be separated using simple distillations and need enhanced distillation, such as extractive distillation with a suitable entrainer. For evaluation of the effect of entrainer such as anisole and NEP on the VLE behaviour of the methylcyclohexane + toluene system, we have

plotted the equilibrium diagram for methylcyclohexane + toluene system with and without the addition of the entrainers as shown in Figure 11. It was observed that both the entrainers can be able to shift the equilibrium curve from diagonal significantly. This means fewer stages are required to separate the methylcyclohexane and toluene using these entrainers. Also, relative volatility between the toluene and NEP is more which obviously reduce the solvent recovery cost during the extractive distillation operation. The equilibrium curve in the case of NEP shows a more significant deviation from the diagonal line than anisole, so it can be concluded that NEP can be a better extractive agent in separating methylcyclohexane and toluene systems.

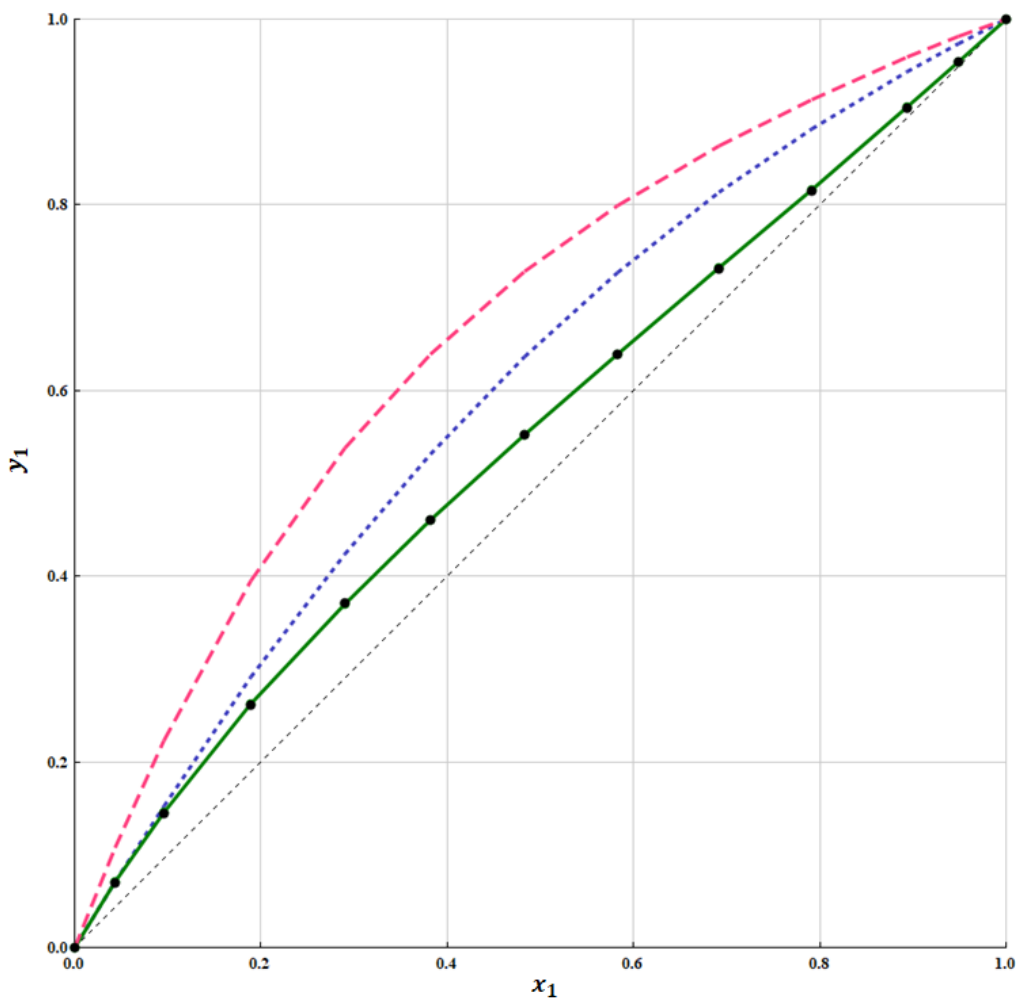


Figure 5.11. Effect on VLE for the system methylcyclohexane (1) + toluene (2) with different entrainers. (●) Experimental value without entrainer, (—) calculated by NRTL model without entrainer, (---) calculated by NRTL model with anisole, (- - -) calculated by NRTL model with NEP.

5.4 Conclusions

The isobaric experimental vapour-liquid equilibrium data for the binary systems consisting of methylcyclohexane + toluene, methylcyclohexane + anisole, toluene + anisole, methylcyclohexane + NEP, toluene + NEP were measured at 92.0 kPa. Then the experimental VLE data regressed to obtain the binary interaction parameters for NRTL, UNIQUAC and Wilson activity coefficient models. The RMSD and AAD values are reasonably low, indicating that all three models can predict the VLE behaviour of all binary systems. Infinite dilution and Van Ness tests for thermodynamic consistency were implemented to validate the consistency of the laboratory VLE results. NEP shows a more significant deviation from the diagonal line than anisole, so it can be concluded that NEP can be a better extractive agent in separating methylcyclohexane and toluene systems. Separating methylcyclohexane and using extractive distillation with anisole and NEP as entrainers is feasible. According to the results, extractive distillation configuration for separating difficult to separate combination of methylcyclohexane and toluene may be further optimized and simulated using the acquired binary interaction parameter.

5.5 References

- [1] K. Weissermel, and H.J. Arpe, Industrial Organic Chemistry, WILEY-VCH, (2003)
- [2] O. Karl, Rolf Dr. Pinkos, Hansjörg Nickel, Matthias Dr. Andreae, Roland Dr. Rossbacher, Philipp Dr. Eisenbarth, Patent, DE102004012751A1. Use of N-ethyl-2-pyrrolidone.
- [3] H. Li, S. Xia, F. Yan, Z. Yang, Y. Li, Fluid Phase Equilibria Isobaric (vapour + liquid) equilibria for three binary systems (toluene + anisole , n-butylbenzene + anisole , and guaiacol + anisole) at, 369 (2014) 109–114.
- [4] B.D. Quiggle, D. Ouiggle, Vapor-Liquid Equilibria Methylcyclohexane-Toluene Vapor-Liquid Equilibria of Methylcyclohexane-Toluene Mixtures, 743 (1937).
- [5] F. H. Garner, and R. T. W. Hall, Vapour liquid equilibria of C7hydrocarbonfurfural systems. I. Binary and ternary data for the system methylcyclohexane toluene furfural." J. Inst. Pet. 41(1955).
- [6] J. Weber, Vapor-Liquid Equilibria for System Methylcyclohexane-Toluene at Subatmospheric Pressures, Ind. Eng. Chem. 47 (1955) 55–55.
- [7] S. R. M. Ellis, and R. M. Contractor, Vapour-Liquid Equilibriums at Reduced Pressure Chem. Eng. Lond. 15 (1964) 10-13.
- [8] B. Tyminski, and A. Klepanska, Vapour-liquid equilibriums in the methylcyclohexane–toluene system, Inz. Chem. 7 (1977) 193.
- [9] J. Coca, J.J. Pis, Effect of Morpholine on Vapor-Liquid Equilibrium of the System Methylcyclohexane-Toluene, J. Chem. Eng. Data. 24 (1979) 103–105.
- [10] The NIST Bank, the National Institute of Standards and Technology, NIST. <http://trc.nist.gov/thermolit/main/home.html>.
- [11] H.C. Van Ness, S.M. Byer, R.E. Gibbs, Vapor-Liquid equilibrium: Part I. An appraisal of data reduction methods, AIChE J. 19 (1973) 238–244.

- [12] K. Kojima, H. Man Moon, K. Ochi, Thermodynamic consistency test of vapor-liquid equilibrium data. – Methanol - water, benzene-cyclohexane and ethyl methyl ketone - water , Fluid Phase Equilib. 56 (1990) 269–284.
- [13] H. Renon, and J.M. Prausnitz, Local compositions in thermodynamic excess functions for liquid mixtures. AIChE journal, 14(1968) 135-144.
- [14] D.S. Abrams, J.M. Prausnitz, Statistical thermodynamics of liquid mixtures: A new expression for the excess Gibbs energy of partly or completely miscible systems, AIChE J. 21 (1975) 116–128.
- [15] G.M. Wilson, Vapour-liquid equilibrium XI A new expression for the excess free energy of mixing. Journal of the American Chemical Society, 86(1964) 127–130.
- [16] N.A. Mali, S.S. Yadav, P.D. Ghuge, S.S. Joshi, Vapor-Liquid Equilibrium Data for Binary Mixtures of Dimethyl Carbonate with Methyl Acetate, Ethyl Acetate, n-Propyl Acetate, Isopropyl Acetate, n-Butyl Acetate, and Isoamyl Acetate at 93.13 kPa, J. Chem. Eng. Data. 62 (2017) 4356–4363.
- [17] P.D. Ghuge, N.A. Mali, and S.S. Joshi, Effect of CaCl_2 and ZnCl_2 salts on isobaric vapour-liquid equilibrium in separating the azeotropic mixture of ethanol+ water. Fluid Phase Equilibria 537 (2021) 113000.
- [18] J.M. Smith, H.C. Van Ness Introduction to chemical engineering thermodynamics, McGraw-Hill, New York. 1975

Chapter 6 Conclusions and Recommendations

6.1 Conclusions

Separating azeotropic mixtures can be a complex process that requires specialized distillation techniques. Different chemical manufacturing sectors often encounter minimum and maximum boiling azeotropes, which can vary in composition and amount. To address this challenge, we conducted a study to design energy-efficient distillation configurations for separating azeotropic mixtures. In our work, we developed innovative distillation configurations that could effectively separate difficult binary azeotropic systems and those that could not be separated using simple distillation methods.

Our focus was on developing advanced and novel distillation configurations that were both energy-efficient and effective in separating various binary systems, including minimum boiling azeotropic systems like THF + water, ethanol + water, and maximum boiling azeotropic systems like nitric acid + water. Tetrahydrofuran (THF) is an industrially useful organic solvent widely used in adhesives, polymer, paint and pharmaceutical industries. Ethanol can be used as a solvent, reactant or intermediate in producing various paints, perfumes, medicines and food products. Ethanol is a suitable feedstock for producing various renewable chemicals and products. Nowadays, anhydrous ethanol is used as a fuel additive. Concentrated nitric acid (HNO₃) is widely used in the nitration process as a nitrating agent, in the oxidation process as the oxidizing agent and various other agrochemical and explosive industries processes. Ammonium nitrate required in fertilizer industries is produced from concentrated nitric acid. We also explored systems like methylcyclohexane + toluene that are difficult to separate using simple distillation through VLE analysis.

Our research identified a range of distillation configurations that can improve separation efficiency while reducing energy consumption. By doing so, we hope to contribute to the development of more sustainable and efficient separation processes across a range of industries. To optimize the conceptual design of an advanced distillation system, it is essential to consider VLE data, a thermodynamic activity coefficient model, sensitivity analysis, and techno-economic optimization of design parameters. The VLE data helps determine optimal operating conditions, while the model accounts for non-ideal behavior. Sensitivity analysis identifies

critical parameters, and techno-economic optimization balances separation performance and equipment cost.

The economic feasibility of using extractive distillation and pressure swing distillation to separate an equimolar mixture of THF-water was compared. Four solvents, namely DMSO, 1, 2-propanediol (1, 2-PDO), glycerol, and ethylene glycol, were evaluated for the extractive distillation system. The results indicated that DMSO is the best solvent for extractive distillation, as it requires the least amount of TAC to achieve the necessary product purity. Heat integration was utilized to reduce the total annual cost of the system. For pressure swing distillation, the LPC pressure was fixed at 1 atm, and various operating pressures for HPC were analyzed. It was found that HPC with 10 atm pressure gave the minimum TAC. The findings suggest that extractive distillation, with or without heat integration, decrease TAC by 24.4% and 21.7%, respectively, and reduce operating costs by 34.96% and 31.70% compared to PSD without heat integration. TAC is 5.2% lower in extractive distillation with heat integration than PSD with partial heat integration. As a result, extractive distillation with DMSO as the solvent provides a more cost-effective method of separating an equimolar THF-water combination.

Thermodynamic modelling of binary and ternary systems of nitric acid HNO₃ / water / sulphuric acid vapour-liquid-equilibrium data was carried out using the eNRTL-RK model, with the Aspen Plus data regression system. The regressed parameters of the thermodynamic model were validated by comparing equilibrium diagrams with experimental literature data, and the model-predicted data showed good agreement with the experimental values. The eNRTL-RK model parameters obtained are appropriate for the simulation work, including nitric acid, water, and sulfuric acid. For dilute nitric acid dehydration with sulphuric acid as a solvent, a continuous distillation column sequence consisting of a preconcentrating column, extractive distillation column, and solvent recovery column was systematically designed and optimized. The best values were found by minimizing energy usage and total annual cost (TAC). Sulphuric acid is an appropriate solvent for the dehydration of nitric acid, resulting in a purity of up to 99.99 mass % at a solvent-to-feed ratio of one.

Experimental data was generated for the isobaric vapour-liquid equilibrium (VLE) at 94.6 kPa for binary ethanol + water and ternary systems of ethanol + water + calcium chloride,

ethanol + water + zinc chloride, and ethanol + water + lithium bromide. The mass fractions of salts were kept constant at 0.05, 0.1, and 0.15, respectively. The data was found to be thermodynamically consistent using the van Ness test. Comparison of the binary and ternary experimental data showed that the addition of salt changes the azeotropic point of the ethanol-water system. The azeotrope was eliminated when CaCl₂ and LiBr were added. CaCl₂ was found to be a better entrainer than ZnCl₂ in extractive distillation due to the modest change in the azeotropic point seen in ZnCl₂. A preliminary design showed that the distillate stream of the salt extractive distillation column contained more than 99.9 moles of ethanol. The electrolyte non-random two-liquid (eNRTL) model was used to correlate the VLE for the ternary system of water, ethanol, CaCl₂, ZnCl₂, and LiBr. The eNRTL model correlated well with experimental data.

The experimental vapour-liquid equilibrium data for binary systems such as methylcyclohexane + toluene, methylcyclohexane + anisole, toluene + anisole, methylcyclohexane + NEP, and toluene + NEP was generated at 92.0 kPa. The binary interaction parameters for the activity coefficient models, namely NRTL, UNIQUAC, and Wilson, were obtained by analyzing the experimental VLE data. The low RMSD and AAD values indicate that all three models can accurately predict the VLE behavior of all binary systems. To ensure the consistency of the laboratory VLE results, thermodynamic consistency tests such as infinite dilution and Van Ness tests were used. Based on the results, it can be inferred that NEP is a more effective extractive agent for separating methylcyclohexane and toluene systems compared to anisole. Hence, it is possible to separate methylcyclohexane and toluene systems using extractive distillation with entrainers such as anisole and NEP.

In our research, we explored energy-efficient distillation configurations for separating azeotropic mixtures, which can be quite challenging. We have identified distillation configurations that can improve separation efficiency while also reducing energy consumption. Our goal was to contribute to the development of more sustainable and efficient separation processes across industries. To optimize the conceptual design of an advanced distillation system, one must consider VLE data, a thermodynamic activity coefficient model, sensitivity analysis, and techno-economic optimization of design parameters. The reliability of a good distillation system mainly depends on the basic equilibrium data considered during its design,

thus, generation of VLE data is an inherent part of the advanced distillation design. This study is a testament to the power of scientific inquiry and its potential to solve complex problems in a practical and efficient way. Overall, our research findings can contribute significantly to the development of energy-efficient extractive distillation configurations. We hope that our work will be useful to researchers and practitioners across industries who are interested in improving the efficiency and sustainability of separation processes.

6.2 Recommendations for Future Work

Extractive distillation has undergone significant advancements over the years, and there are still immense opportunities for innovation, cost reduction, and energy efficiency. By exploring various process intensification concepts, we can identify new ways to optimize the extractive distillation process and reduce costs. To achieve this, it is essential to focus on research areas such as incorporating divided wall columns for extractive distillation systems and discovering new separating agents with high separation ability and low TAC. We can explore optimization based on TAC for ethanol-water separation, employing salt entrainers and identifying potential heat integration opportunities to minimize energy usage.

The experimental findings of this study indicate that the implementation of the discovered binary interaction parameter can significantly enhance the efficiency of the extractive distillation configuration for separating methylcyclohexane and toluene. Furthermore, utilizing binary interaction parameters has the potential to further optimize the extractive distillation configuration, offering a promising approach to improve the separation of these two chemical compounds. This approach could have significant implications for industrial processes that require efficient separation of these substances, making it a highly viable and effective solution.

Extractive distillation's performance is largely dependent on the choice of solvent and the correct optimization of the system's design parameters. Energy can be saved in the system by utilizing heat integration and advanced distillation configurations such as EDWC and VRC-assisted extractive distillation. However, more effort is required for practical implementation as most studies are limited to simulation analysis. Several advanced extractive distillation configurations need to be taken one step further towards pilot experimental analysis to establish proof-of-concept and enable their further adoption for commercial applications. It is, therefore, crucial to invest more effort and resources in experimental studies to help establish the practical viability of these innovative extractive distillation techniques.

Abstract

Name of the Student: Pravin Devram Ghuge

Registration No. : 20EE18J26015

Faculty of Study: Engineering Sciences

Year of Submission: 2023

AcSIR academic centre/CSIR Lab: CSIR-NCL

Name of the Supervisor: Dr. Nilesh A. Mali

Title of the thesis: Development of Energy Efficient Distillation Configurations for Separation of Binary Azeotropic systems

The conventional distillation proved challenging to produce the desired purity product due to the azeotropic mixture. Therefore, several advanced and novel distillation methods must be considered. This thesis demonstrates the conceptual design and optimization strategy of novel and energy-efficient advanced distillation configurations for separating various binary azeotropic systems. Beginning with crucial VLE data, a thermodynamic activity coefficient model, sensitivity analysis, and finally, techno-economic optimization of design parameters and heat integration. The conceptualization, optimization, and modelling of an industrial pressure swing and improved extractive distillation system creating an energy-saving design using heat integration was investigated and compared for separating the THF-water system. Four solvents have been evaluated for the extractive distillation system: DMSO, 1, 2-propanediol (1, 2-PDO), glycerol, and ethylene glycol. TAC in extractive distillation with heat integration is 5.2 % lower than in PSD with partial heat integration. As a result, extractive distillation using DMSO as a solvent is a less expensive technique. An extractive distillation configuration with sulphuric acid as a solvent is proposed for the dehydration of nitric acid. Thermodynamic modelling of binary and ternary systems of HNO₃/water/sulphuric acid using the eNRTL-RK model has been done, and it was validated using experimental data. Sulphuric acid, with a solvent-to-feed ratio of one, is an appropriate solvent for the dehydration of nitric acid, resulting in a purity of up to 99.99 mass %. The potential of salts (calcium chloride/zinc chloride and lithium bromide) as an entrainer for breaking the minimum boiling azeotrope of ethanol and water was analyzed by generating binary and ternary VLE data. The eNRTL model was used to correlate the experimental VLE data. With the addition of salts, the azeotropic point of the ethanol and water system can be eliminated, and calcium chloride could be a better choice. Methylcyclohexane and toluene are the low relative volatility components challenging to separate by simple distillation; thus, anisole and NEP were explored as separating agents for the extractive distillation of this mixture. The NRTL, UNIQUAC, and Wilson thermodynamic activity coefficient models could correlate with the experimental VLE behaviour. The Van Ness and the infinite dilution test confirmed the thermodynamic consistency.

List of Publications

List of Publications, Patents, Conference presentations (oral/poster), emanating from the thesis work

Publications related to thesis

1. **Ghuge, P.D.**, Mali, N.A. and Joshi, S.S., 2017. Comparative analysis of extractive and pressure swing distillation for separation of THF-water separation. *Computers & Chemical Engineering*, 103, pp.188-200.
2. **Ghuge, P.D.**, Mali, N.A. and Joshi, S.S., 2021. Effect of CaCl₂ and ZnCl₂ salts on isobaric vapor-liquid equilibrium in separation of the azeotropic mixture of ethanol+ water. *Fluid Phase Equilibria*, 537, p.113000.

Other Publications

3. Mali, N.A., Yadav, S.S., **Ghuge, P.D.** and Joshi, S.S., 2017. Vapor–Liquid Equilibrium Data for Binary Mixtures of Dimethyl Carbonate with Methyl Acetate, Ethyl Acetate, n-Propyl Acetate, Isopropyl Acetate, n-Butyl Acetate, and Isoamyl Acetate at 93.13 kPa. *Journal of Chemical & Engineering Data*, 62(12), pp.4356-4363.
4. **Ghuge, P.D.**, Mali, N.A. and Sirsam, R.S., 2018. Study of the effect of operating parameters on the extractive distillation of isopropyl alcohol–water mixture using dimethyl Sulphoxide as an entrainer. *Indian Chemical Engineer*, 60(2), pp.141-161.
5. **Ghuge, P.D.**, Mali, N.A. and Joshi, S.S., 2020. Extractive distillation configuration for nitric acid dehydration using sulfuric acid as a solvent. *Industrial & Engineering Chemistry Research*, 59(13), pp.6183-6193.

Conference Presentations (Oral/Poster)

Ghuge, P.D., Mali, N.A. Development of Energy Efficient Distillation Configuration for Separation of Binary Azeotropic System. National Science Day, CSIR-NCL, Pune.

Abstract

In this work, energy efficient extractive and pressure-swing distillation methods are analyzed in detail through steady state ASPEN Plus simulations to propose the most economic method for separation of equimolar mixture of THF-Water. Various solvents were evaluated and DMSO was identified as the most appropriate solvent, as it gave minimum Total Annual Cost (TAC) for desired purity. Configurations for extractive and pressure swing distillation with heat integration were also worked out. The optimum designs of extractive and pressure swing distillation with and without heat integration were compared. Results indicate that TAC of extractive distillation with heat integration is 5.2 % less than that of PSD with partial heat integration. Thermodynamic modeling of the vapor–liquid equilibrium of binary and ternary systems of nitric acid/water/sulfuric acid is carried out using the eNRTL-RK method. The model performance is validated by comparing the experimental data with the estimated data and is found to be in good agreement. A triple column extractive distillation configuration is designed, simulated, and optimized to concentrate dilute nitric acid using sulfuric acid as a solvent. The operating and structural parameters of the distillation configuration are optimized simultaneously with an objective of minimizing the energy consumption and the total annual cost (TAC) of the overall configuration

Key words: Extractive Distillation, Azeotrope, Pressure Swing Distillation, VLE



Comparative analysis of extractive and pressure swing distillation for separation of THF-water separation



Pravin D. Ghuge, Nilesh A. Mali*, Sunil S. Joshi

Chemical Engineering & Process Development Division, CSIR-National Chemical Laboratory, Dr. Homi Bhabha Road, Pune, Maharashtra, 411008, India

ARTICLE INFO

Article history:

Received 18 November 2016

Received in revised form 14 March 2017

Accepted 19 March 2017

Available online 23 March 2017

Keywords:

Azeotrope

Extractive distillation

Pressure swing distillation

THF-water

TAC

Optimization

ABSTRACT

In the present work, extractive and pressure-swing distillation methods are analyzed in detail through steady state ASPEN Plus simulations to propose the most economic method for separation of equimolar mixture of THF-Water. Various solvents were evaluated and DMSO was identified as the most appropriate solvent, as it gave minimum Total Annual Cost (TAC) for desired purity. In case of pressure swing distillation, various pressure ranges were explored to achieve minimum TAC. Configurations for extractive and pressure swing distillation with heat integration were also worked out. The optimum designs of extractive and pressure swing distillation with and without heat integration were compared on a common basis of feed conditions and purity constraints. Results indicate that TAC of extractive distillation with heat integration is 5.2% less than that of PSD with partial heat integration.

© 2017 Elsevier Ltd. All rights reserved.

1. Introduction

Tetrahydrofuran (THF) is an industrially useful organic solvent widely used in adhesives, polymer, paint and pharmaceutical industries. THF (boiling point 65.97 °C) forms a minimum boiling homogeneous azeotrope with water (boiling point 100 °C) at atmospheric pressure and 63.43 °C with azeotropic composition of 95.09 wt.% (82.87 mol%) of THF as shown in Fig. 1 (a) and (b). Thus, it is not possible to separate THF-water mixture by conventional distillation, Hence; various distillation techniques for azeotropic mixture separation such as pressure swing distillation (PSD), extractive distillation (ED) have to be considered. Each separation techniques may have its own pros and cons for separation of an azeotropic system. It may be possible to achieve the separation with desired purity by using one or more separation methods; however the most appropriate separation method should be selected based on operating cost and economics of the overall system.

Several authors have performed comparative study of pressure swing distillation and extractive distillation for various minimum and maximum boiling azeotropic systems. W. Luyben (2008a, 2013) studied the separation of minimum boiling acetone-methanol system and maximum boiling acetone-chloroform systems through steady state simulations. He found that extrac-

tive distillation was more suitable than pressure swing distillation in terms of both capital cost and energy consumption for both these cases. Similar studies were carried out for separation of equimolar di-*n*-propyl ether and *n*-propyl alcohol system (Lladosa et al., 2011), isopropyl alcohol and diisopropyl ether (Luo et al., 2014) and methanol and chloroform (Hosgor et al., 2014) by pressure swing distillation and extractive distillation. All these studies found pressure swing distillation more economical than extractive distillation in terms of total annual cost of complete system for respective azeotropic system. The various other reported studies (Wang et al., 2012; Yu et al., 2012; Wei et al., 2013) indicate that performance of extractive and pressure swing distillation, for separation of azeotropic system, varies from system to system. Hence, both are competitive with each other for the separation of azeotropic system for which azeotropic compositions are sensitive to pressure.

In this work, a comparative study of the extractive distillation and pressure swing distillation for THF-water separation is performed. To best of our knowledge, there is no literature data available on direct comparison of these two methods for THF-water separation. Extractive distillation system considered here comprised of extractive distillation column (EDC) and solvent recovery distillation column (SRDC). Pressure swing distillation system comprised of two column configuration operating at different pressures. For extractive distillation, four different solvents were evaluated to come up with the most optimum configuration, whereas for pressure swing distillation, six different pressure ranges were analyzed to arrive at the best pressure range. Config-

* Corresponding author.

E-mail address: na.mali@ncl.res.in (N.A. Mali).

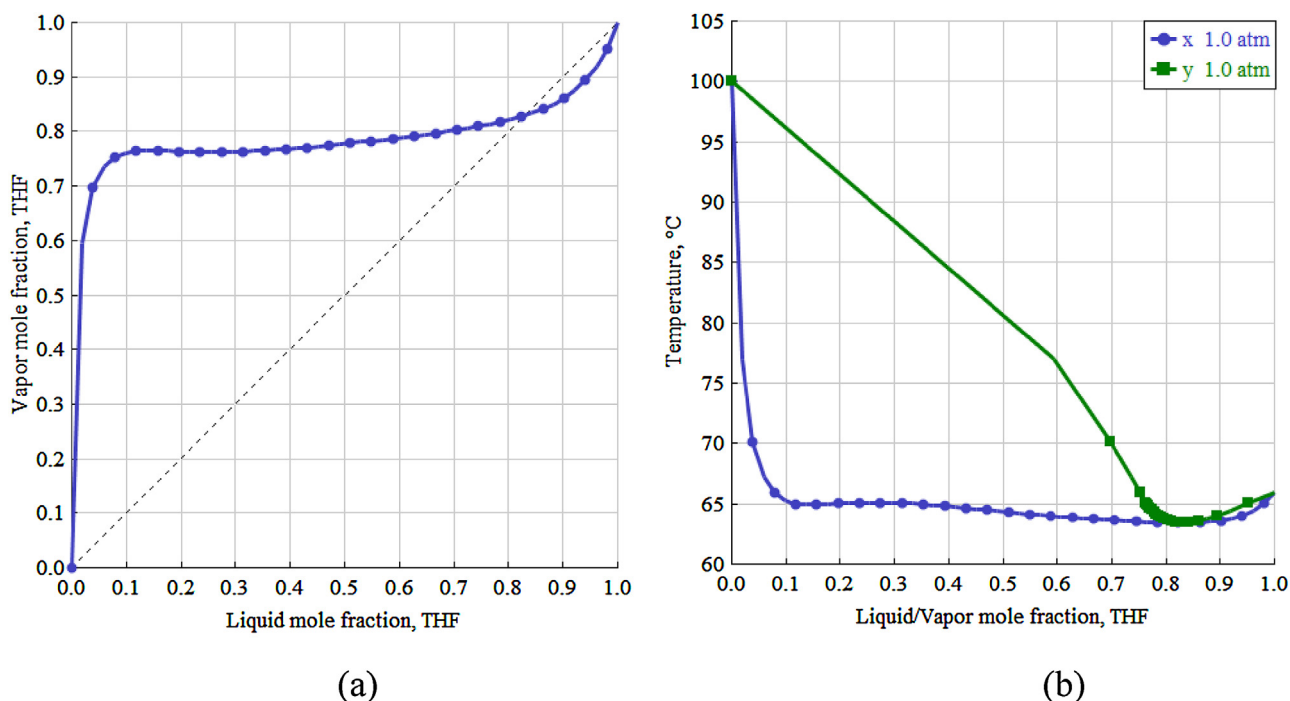


Fig. 1. (a) xy equilibrium diagram (b) Txy diagram for THF-water system at 1 atm pressure.

urations with partial and full heat integration were also analyzed for extractive and pressure swing distillation. For both the analysis, minimum Total Annual Cost (TAC) was taken as the decision making criterion.

2. THF-water separation using extractive distillation

In an extractive distillation system, the binary mixture is fed at one of the intermediate stage of the extractive distillation column (EDC); while the heavy or higher boiling solvent is added at few stages above the binary feed mixture stage. The addition of solvent doesn't introduce any additional azeotrope with the original mixture. Due to different feed locations of solvent and binary feed, extractive distillation column is divided into three subsections, as shown in Fig. 2, which are rectifying section, above the solvent feed stage; extractive section, in between the binary feed stage and solvent feed stage; and stripping section, below the binary feed stage. The presence of heavy solvent alters the relative volatility of the binary mixture and causes THF to move upward in the column and is recovered as a distillate in almost pure form, while water and heavy solvent are collected from the bottom of the EDC which is sent to the solvent recovery distillation column (SRDC) for further separation.

In SRDC, simple binary separation of water and heavy solvent is achieved based on the high relative volatility between them. Pure water is recovered as the distillate and the heavy solvent from the bottom of the column, which is then recycled back to the EDC. Usually, a cooler is placed in the recycled loop, between the two columns, to reduce the solvent feed temperature. A small amount of solvent is lost along with water stream, which is balanced by adding the pure solvent through solvent makeup stream.

Separation performance of an extractive distillation depends on the influence of the solvent on VLE of the binary mixture to be separated. Several authors proposed various solvents for the separation of THF-water mixture based on their simulation or experimental analysis. Xu and Wang (2006a,b) used the 1, 2-Propanediol as a solvent for the separation THF-water. Using rigorous simulation

in HYSYS simulator and experimental analysis of batch extractive distillation system they found that 1, 2-Propanediol was suitable solvent for this separation. Gomez and Gil (2009) simulated dehydration of THF through extractive distillation by taking 100 kmol/h of azeotropic feed as basis. Authors claimed purity of 99.95 mol% of THF can be achieved with glycerol as a solvent as compared to other two solvents considered 1, 2-propanediol and 1,4-butanediol. Fan et al. (2013), in their simulation work, used the ethylene glycol as an entrainer for the separation of 90 wt% THF and 10 wt% water with the feed rate of 3000 kg/h. They reported purity of 99.9 wt% THF from the distillate of the EDC.

Zhang et al. (2014) developed vapour liquid equilibrium (VLE) data for THF + Water + Solvent ternary system at atmospheric pressure with 1, 2-propanediol and DMSO as solvents. They found that DMSO is more capable solvent for the breaking of THF-water azeotrope than that of 1, 2-propanediol as the less amount of DMSO needed to achieve the separation. Deorukhkar et al. (2016) performed experiments on pilot distillation setup in batch, semi-batch and continuous modes with DMSO and 1, 2-propanediol as solvents. They proposed the DMSO as better solvent as compared to 1, 2-propanediol.

From the literature, it was found that for dehydration of THF, various solvents were reported based on simulations and experiments. But, it is difficult to conclude which one is the best for complete extractive distillation system including solvent recovery column, in terms of operating and capital cost, due to lack of common basis for the comparison. Hence, in this section, the most suitable solvent for separation of THF-water was identified by taking a basis of equimolar feed and target purity of 99.99 mol% for THF and water. Both capital and operating costs were estimated and presented in the form of TAC of the complete extractive distillation system with various reported solvents.

2.1. Basis of economical analysis

All economical calculations to find out TAC were performed according to the equations listed in Table 1, taken from Luyben and Chien (2011). Total annual cost (TAC) is the addition of total annual

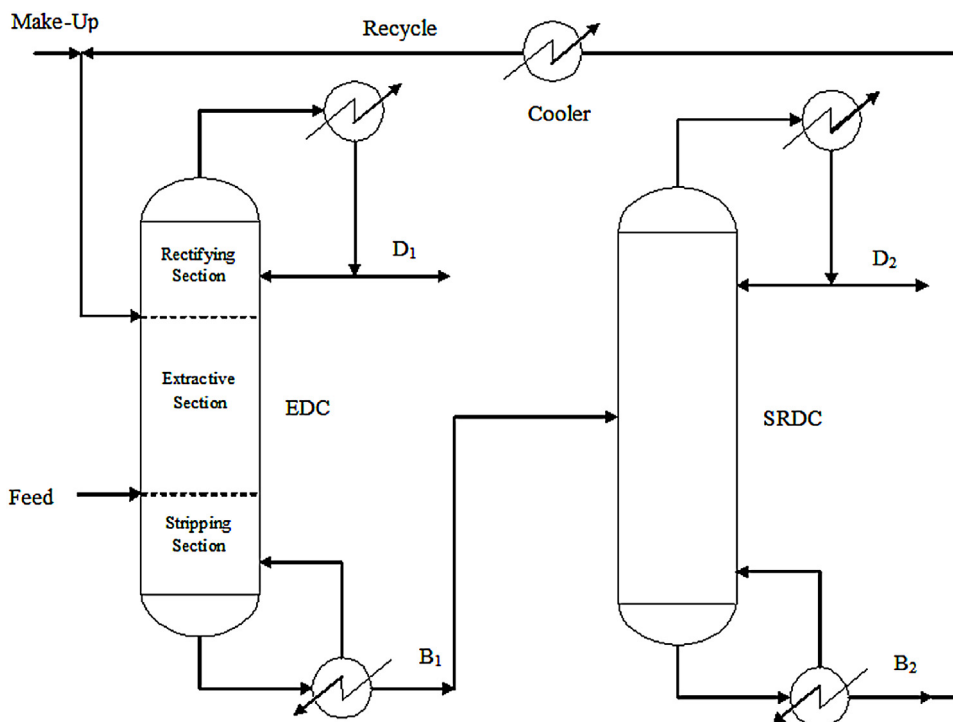


Fig. 2. Extractive Distillation System Flow Diagram.

Table 1
Basis of economics and equipment sizing.

Column Diameter (D): Aspen tray sizing
Height (H) of a distillation column,
$H = 1.2 \times 0.61 \times (N_s - 2)$ (D and H are in meters)
Column shell cost (\$) = $17640 \times (D)^{1.066} \times (H)^{0.802}$
Condenser:
Area (m ²), $A_c = \frac{Q_c}{U_c \times \Delta T_{lm}}$
Heat transfer coefficient (U_c) = 0.852 kW/m ² K
Capital cost (\$) = $7296 (A_c)^{0.65}$
Reboiler:
Area (m ²), $A_r = \frac{Q_r}{U_r \times \Delta T_{lm}}$
Heat transfer coefficient (U_r) = 0.568 kW/m ² K
Capital cost (\$) = $7296 (A_r)^{0.65}$
Cooler:
Area (m ²), $A_{cooler} = \frac{Q_{cooler}}{U_{cooler} \times \Delta T_{lm}}$
Heat transfer coefficient (U_{cooler}) = 0.852 kW/m ² K
Capital cost (\$) = $7296 (A_{cooler})^{0.65}$
Energy costs:
LP steam (433 K) = \$7.72 per GJ
MP steam (457 K) = \$8.22 per GJ
HP steam (537 K) = \$9.88 per GJ
TAC = $\frac{\text{Capital cost}}{\text{Payback period}} + \text{Energy cost}$
Payback period = 3 years

operating cost and total capital cost divided by payback period. In calculating the capital cost, only the cost of major equipments in distillation system like column shell, reboiler and condenser were considered and the cost of reflux drums, pump and valves were neglected as it would be very negligible as compared to cost of column and heat exchangers. The “Tray Sizing” functions with sieve tray in the Aspen plus simulator was used to determine the diameter of the columns. The height of column was assumed to be 20% more than that required height for the trays and a typical distance of 0.61 m between the trays was considered. As per ASPEN Plus distillation model (RADFRAC) notation, first stage is considered as a condenser while the last stage as a reboiler.

Table 2
Binary interaction parameter estimated by UNIFAC.

Component i Component j	THF Glycerol	THF 1, 2-Propanediol
A _{ij}	0	0
A _{ji}	0	0
B _{ij}	1298.88	819.92
B _{ji}	75.5122	-41.7627
C _{ij}	0.3	0.3

2.2. Simulation analysis of extractive distillation system

In this section, extractive distillation column and solvent recovery column were simulated simultaneously for separation of THF-water mixture with four solvents, DMSO, 1, 2-Propanediol (1, 2-PDO), Glycerol and Ethylene glycol to achieve required purity. This simulation results will form a basis for direct comparison among various solvents to find out the best one, in terms of minimum TAC. The equimolar feed composition of THF and water (50 mol% of THF and 50 mol% of water) with the flow rate of 100 kmol/h was taken as the basis for the simulation. The product purity specification of both the components was set to be at 99.99 mol% of THF and 99.99 mol% of water in the distillate of the EDC and SRDC, respectively.

The activity coefficient model NRTL was used to take into account the non-ideality of the liquid phase and ideal vapour phase behavior was assumed. The NRTL built-in binary interaction parameters available in the Aspen data bank were used for the simulation, while for the component pairs, THF-Glycerol and THF-1, 2-Propanediol, for which no ASPEN built-in interaction parameters were available, the parameters were estimated through UNIFAC group contribution method and are given in Table 2.

Simulation analysis of extractive distillation with DMSO as the solvent is discussed in detail here to elaborate the simulation approach. While deciding the operating pressure of the columns, it was ensured that cooling water can be used as an utility with outlet temperature of 305 K. Operating EDC at higher pressure would lead

Table 3
Comparison of designs of EDC at various operating pressures.

Parameters	EDC Operating Pressure						
	2 atm	1.5 atm	1 atm	0.9 atm	0.8 atm	0.7 atm	0.65 atm
N_T	21	21	21	21	21	21	21
D (m)	0.84	0.63	0.66	0.67	0.68	0.69	0.70
H (m)	13.90	13.90	13.90	13.90	13.90	13.90	13.90
RR	1.71	0.44	0.38	0.36	0.34	0.32	0.31
E/F	0.55	0.35	0.25	0.25	0.25	0.25	0.25
Q_R (kW)	1491.6	853.7	750.3	731.1	711.7	691.4	680.80
A_R (m ²)	85.88	58.83	30.28	27.56	25.02	22.61	21.44
Q_C (kW)	1071.5	581.9	573.4	568.1	563.7	559.8	558.07
A_C (m ²)	22.00	14.48	19.73	21.57	24.14	27.92	30.56
Total capital cost (10 ⁶ \$)	0.3079	0.2336	0.2107	0.2112	0.2133	0.2175	0.2209
Total operating cost (10 ⁶ \$/yr)	0.3531	0.1913	0.1681	0.1638	0.1595	0.1549	0.1525
TAC (10 ⁶ \$/yr)	0.4558	0.2691	0.2384	0.2342	0.2306	0.2274	0.2262

to increase in reboiler temperature and hence, the operating cost, as high pressure steam will be required as an utility in the reboiler. According to Luyben (2016), commonly used heuristics for distillation column pressure selection, does not always give an optimum column pressure for the separation under consideration. Hence, TAC of extractive distillation column at various operating pressures was estimated to find out a suitable EDC pressure with a constraint of having difference between cooling water return temperature and reflux drum temperature to be at least 20 K ($\Delta T_{lm} \geq 20$ K). The pressure was varied from 2 atm and was restricted to 0.65 atm as below 0.65 atm ΔT_{lm} goes below 20 K. The designs were obtained through detail sensitivity analysis of various operating parameters with fixed number of stages and the results are given in Table 3.

From the results in Table 3, it was observed that the TAC of the column increases significantly at higher operating pressures. For below atmospheric column pressures, capital cost increases as vacuum distillation operation demands bigger column diameter and larger condensers, but it decreases the operating cost as at reduced pressures relative volatility improves which leads to smaller reflux ratios and reboiler duties. In the present system, similar effect was observed for EDC at reduced pressures, but no significant reduction in TAC was observed. Also, an additional capital and operating cost for the vacuum system will further reduce the TAC advantage of reduced column pressure operation. Hence, in this case, it was decided to go ahead with atmospheric pressure for the EDC.

It was proposed to operate the solvent recovery column under vacuum to reduce the reboiler temperature and subsequently the required utility steam pressure. If the operating pressure is lower than 0.15 atm, condenser would need chilled water as a cooling utility, which consequently would increase the operating cost. Hence, SRDC was proposed to be operated at 0.15 atm since cooling water can be used as a cooling utility in the condenser of the column.

The various design variables in extractive distillation system which needs to be determined for optimum performance are as listed below.

- Solvent to feed ratio (E/F)
- Total number of stages of EDC (N_{T1}) and SRDC (N_{T2})
- Binary mixture feed stage (N_{FF}) for EDC
- Solvent feed stage location (N_{EF})
- Temperature of solvent feed (T_{EF})
- Molar reflux ratio of EDC (RR_1) and SRDC (RR_2)
- Feed stage location of SRDC (N_{F2}).

All these design variables were optimized to achieve the specified purity with minimum TAC. Sensitivity analysis was used to investigate the effect of all these parameters on product purities and heat duties of the columns. It is possible to achieve the desired purity with some minimum reflux ratio value, below which purity

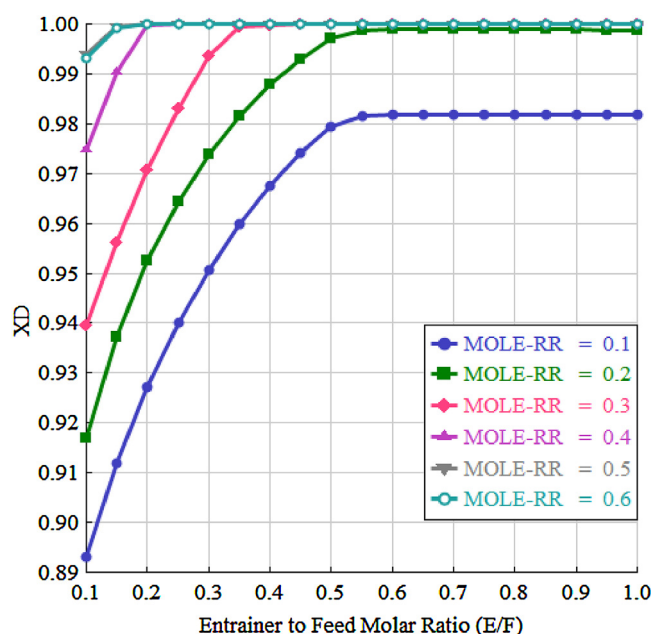


Fig. 3. Effect of E/F and reflux ratio on the distillate stream THF composition (X_D).

drops and above which purity does not improve significantly, but increases the reboiler duty unnecessarily. Thus, for a distillation column, there will be multiple values of molar reflux ratio for which desired purity can be achieved, but there will be a unique value of molar reflux ratio for which not only purity is matched, but also the reboiler duty is minimum. Hence, in the present analysis molar reflux ratio is considered as a design variable as for each combination of total stage number and feed stage locations, the molar reflux ratio value for which purity constraint is matched with minimum reboiler duty, was worked out. In present simulation analysis, the molar reflux ratio was estimated through Design Spec feature of ASPEN simulator for both the columns. The temperature of solvent feed (T_{EF}) was found to have significant effect on the distillate purity and the reboiler duty of EDC for different reflux ratios. From the sensitivity analysis results, the solvent feed temperature (T_{EF}) was fixed at 60 °C which is in good agreement with the suggestion of Knight and Doherty (1989) for solvent feed temperature.

For the EDC, the most important design variables are solvent to feed ratio (E/F) and molar reflux ratio (RR), as it directly affects the product purity and the energy consumption. The effect of solvent to feed molar ratio (E/F) and reflux ratio (RR_1) on the distillate THF mole composition (X_D) of EDC with $N_{T1} = 21$ can be seen from the sensitivity analysis results shown in Fig. 3. It was observed that, at higher reflux ratios (RR_1) and solvent to feed ratios (E/F), the mole

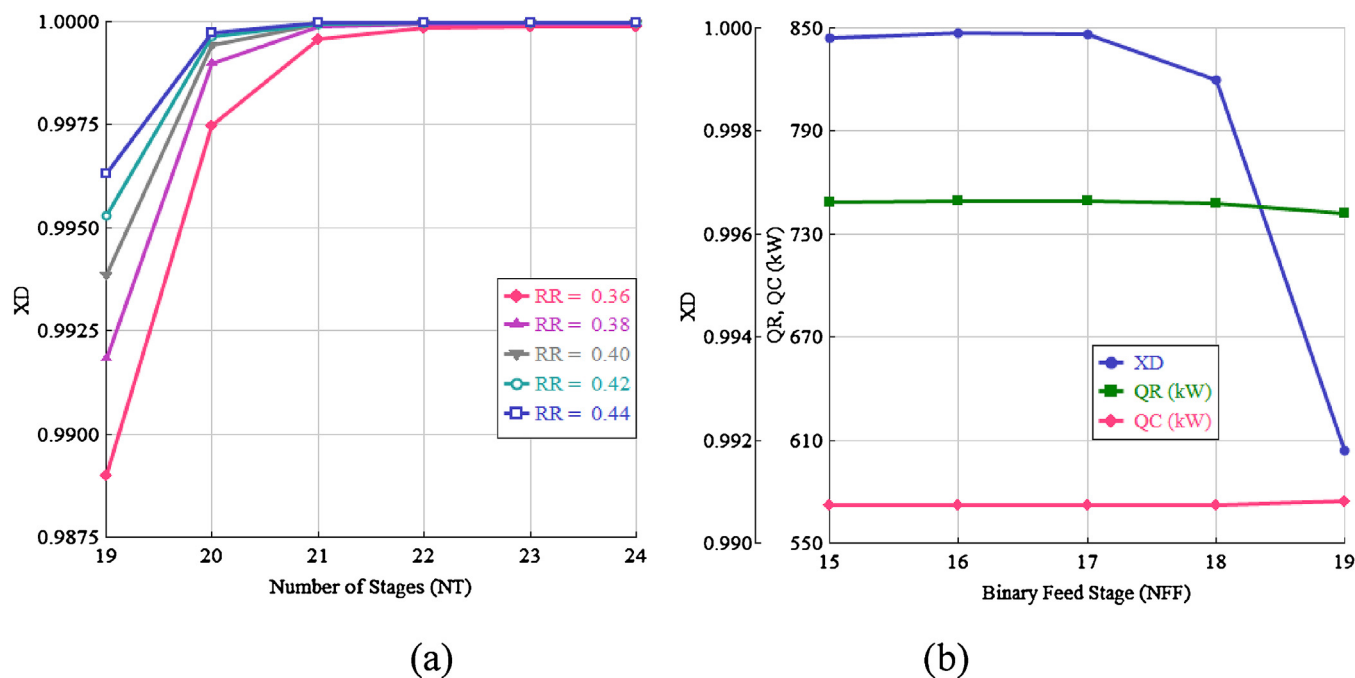


Fig. 4. (a) Effect of total number of stages (N_T) on the distillate purity (X_D). (b) Effect of binary feed stage (N_{FF}) on X_D , Q_R and Q_C for DMSO as a solvent.

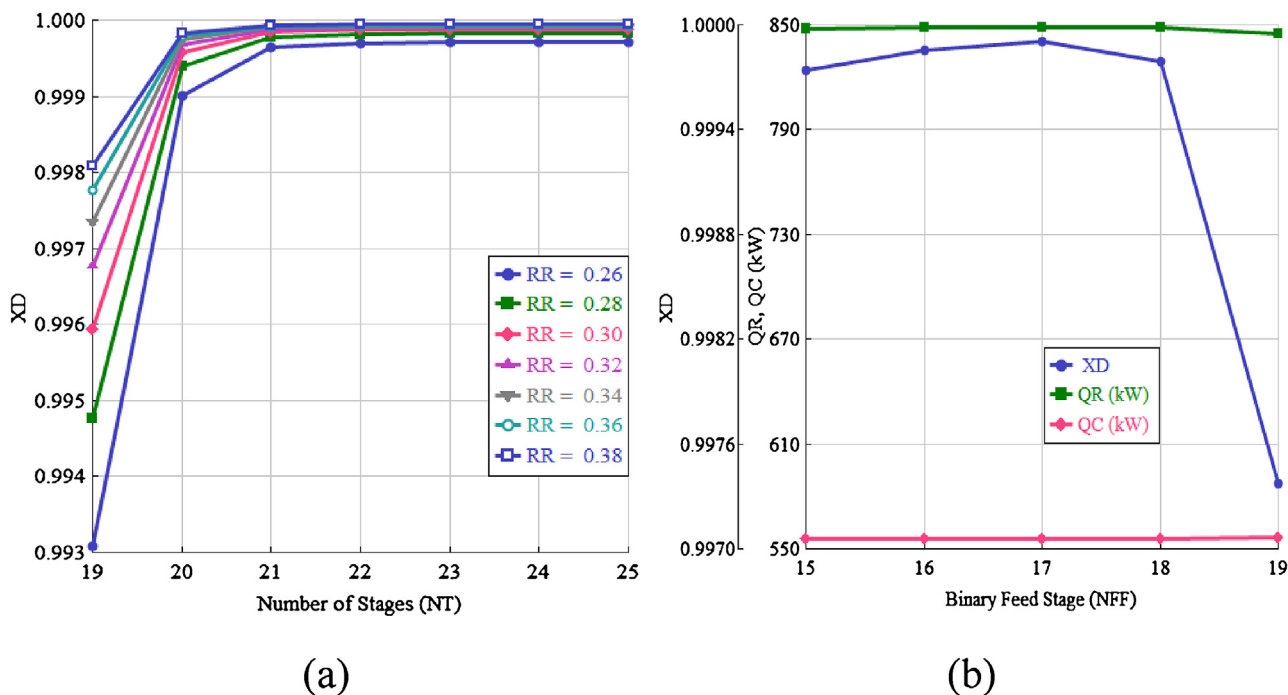


Fig. 5. (a) Effect of total number of stages (N_T) on the distillate purity (X_D). (b) Effect of binary feed stage (N_{FF}) on X_D , Q_R and Q_C for Ethylene Glycol as a solvent.

fractions of THF in the distillate are higher because, at higher values of solvent to feed ratio, the dilution of the solvent caused by the reflux is less which helps to increase the distillate purity. At fixed value of molar reflux ratio (say $RR_1 = 0.4$), solvent to feed molar ratio (E/F) of 0.25 or higher was required to achieve the desired purity of THF which is almost constant beyond this value as shown in Fig. 3. The reboiler duty (Q_R) increases significantly with increasing value of solvent to feed molar ratio (E/F). Thus, an optimal E/F value could be 0.25 because at this value desired purity of THF is achieved with minimum reboiler duty.

Addition of trays in the distillation column improves the separation capacity of the column, but it also increases the capital cost, so it is important to find out optimum number of stages in EDC and SRDC. Preliminary value of N_{T1} and N_{FF} was fixed by doing the sensitivity analysis of the various parameters to achieve the specified product purity with minimum energy consumption. The effect of varying total number of stages (N_T) on distillate purity (X_D) for each solvent case are as shown in Figs. 4–7(a). It was seen that, at $N_T = 21$, the desired product purity ($X_D = 0.9999$) is obtained and beyond this the composition of distillate does not change significantly with respect to the N_T for the DMSO, Ethylene glycol and

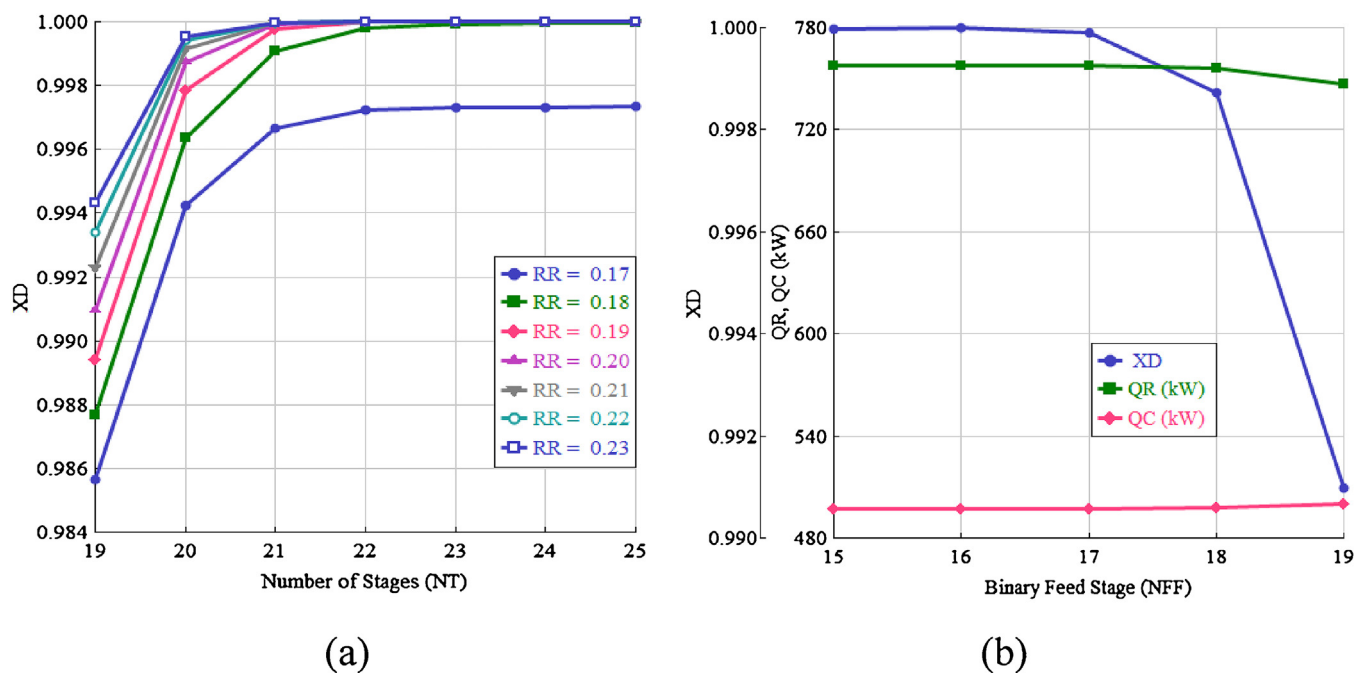


Fig. 6. (a) Effect of total number of stages (N_T) on the distillate purity (X_D). (b) Effect of binary feed stage (N_{FF}) on X_D , Q_R and Q_C for Glycerol as a solvent.

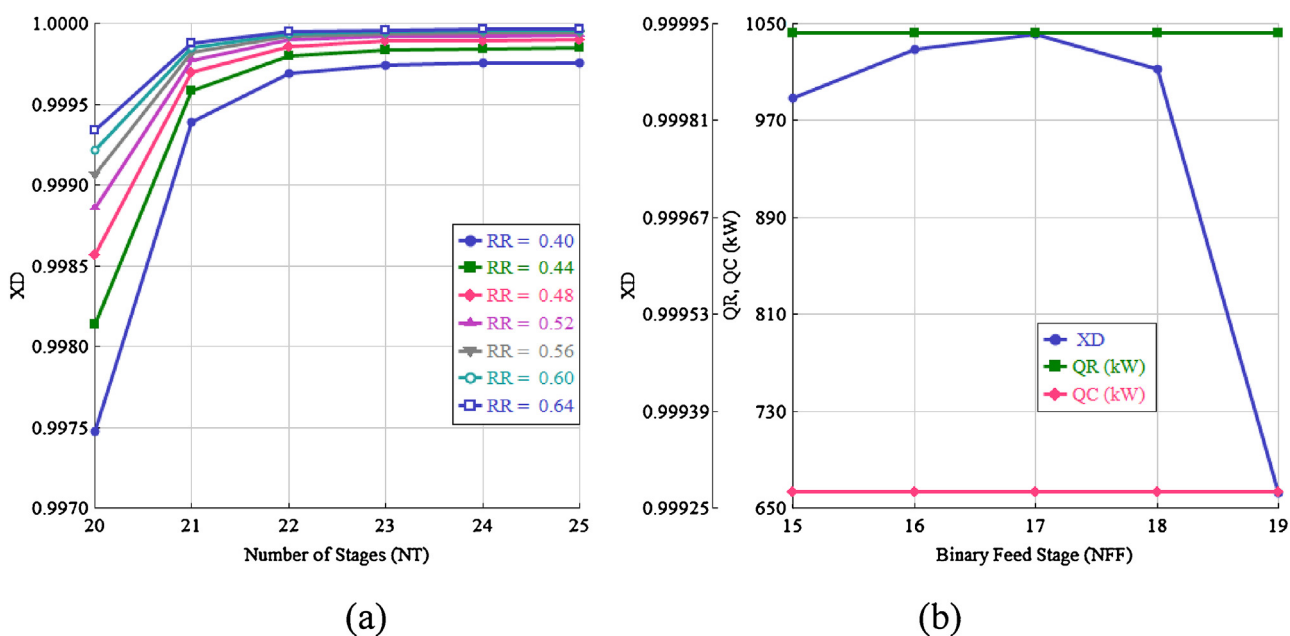


Fig. 7. (a) Effect of total number of stages (N_T) on the distillate purity (X_D). (b) Effect of binary feed stage (N_{FF}) on X_D , Q_R and Q_C for 1,2-Propanediol as a solvent.

Glycerol as solvents. In case of the 1,2-Propanediol as a solvent, similar effect was observed at $N_T = 22$.

Effect binary feed stage (N_{FF}) on X_D , Q_R and Q_C is shown in Figs. 4–7 (b) for each solvent case and it can be observed that, the desired product purity was achieved when binary mixture is fed at stage $N_{FF} = 17$ with minimum energy consumption. Table 4 shows the economic optimization results for EDC having DMSO as solvent. In similar manner optimum N_{T1} and N_{FF} values for each solvent case were obtained.

The solvent feed stage number (N_{EF}) was optimized to achieve the desired purity with minimum energy consumption. The effect of total number of stages (N_T) and solvent feed stage (N_{EF}) on the distillate composition (X_D) was plotted by using sensitivity analysis

of EDC and is as shown in Fig. 8. From this plot, it was observed that, at $N_{EF} = 5$, the maximum purity in the distillate was achieved with respect to the different N_T .

The details of economic optimization results for DMSO solvent are summarized in Table 4 and 5. First total number of stages of the EDC (N_{T1}) was varied to find out optimum stages by keeping the stages of the SRDC (N_{T2}) constant. In each case, the optimum binary mixture feed stage (N_{FF}), solvent feed stage (N_{EF}), Solvent to feed ratio and molar reflux ratio were obtained by minimizing the TAC of the system. From Table 4, it can be observed that, for simulation case 2, minimum TAC was obtained with 21 total number of stages and solvent flow rate of 25 kmol/hr ($E/F = 0.25$). For the SRDC, optimum stages were found by varying its stages and keeping number of

Table 4
Economic optimization results for EDC.

Parameter	Case 1	Case 2	Case 3	Case 4	Case 5
N_{T1}	19	21	23	25	27
N_{T2}	14	14	14	14	14
E/F (optimum)	0.25	0.25	0.25	0.2	0.2
N_{FF} (optimum)	16	17	19	21	23
N_{EF} (optimum)	5	5	5	5	5
D (m)	0.70	0.66	0.66	0.66	0.66
RR_1 (optimum)	0.56	0.38	0.38	0.40	0.40
Q_{R1} (kW)	821.4	750.5	746.8	744.9	744.6
Q_{C1} (kW)	644.5	573.7	570.0	581.5	581.2
Q_{cooler} (kW)	70	70	70	56	56
Total capital cost (10^6 \$)	0.4786	0.4729	0.4799	0.4849	0.4924
Total operating cost (10^6 \$)	0.3277	0.3118	0.3110	0.3104	0.3104
TAC (10^6 \$/yr)	0.4872	0.4695	0.4710	0.4721	0.4745

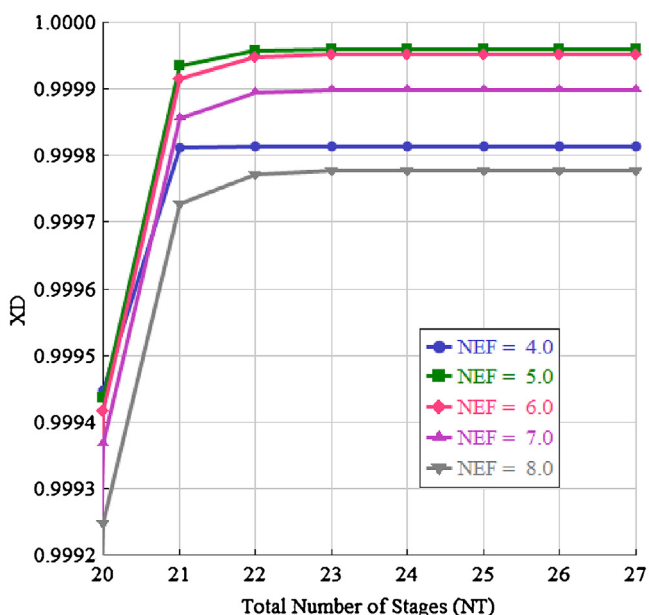


Fig. 8. Effect of solvent feed stage (N_{EF}) with respect to total number of stages (N_T) on the distillate composition (XD) for DMSO as solvent.

Table 5
Economic optimization results for SRDC.

Parameter	Case 6	Case 7	Case 8	Case 9
N_{T2}	12	14	16	18
N_{T1}	21	21	21	21
RR_2 (optimum)	0.13	0.1	0.08	0.08
E/F (optimum)	0.25	0.25	0.25	0.25
N_{F2} (optimum)	5	6	7	7
D_2 (m)	1.05	1.04	1.03	1.03
Q_{R2} (kW)	659.0	641.2	629.3	629.4
Q_{C2} (kW)	671.5	653.7	641.8	641.8
Total capital cost (10^6 \$)	0.4628	0.4729	0.4837	0.4969
Total operating cost (10^6 \$)	0.3161	0.3118	0.3092	0.3091
TAC (10^6 \$/yr)	0.4703	0.4695	0.4704	0.4748

stages in the EDC constant at optimum value 21 to obtain minimum TAC. It can be observed from Table 5, for the case 7, having total number of stages 14 with the feed stage location (N_{F2}) at 6 and molar reflux ratio of 0.1, gives the minimum TAC. The steady state design flowsheet with optimal operating conditions, reboiler and condenser duties, detail stream information and column diameter is given in Fig. 9 (a).

The complete simulation of extractive distillation systems with Ethylene glycol, Glycerol and 1, 2-Propanediol (1, 2-PDO) as a solvent, to achieve desired purity with minimum TAC, were performed

in a similar manner as explained above for the THF-water-DMSO system. Temperature profile of SRDC in each solvent case is shown in Fig. 10. The binary feed condition, operating pressures of both columns and required purity specifications of both product streams were kept same for the direct comparison purpose. The optimized operating conditions, reboiler and condenser duties, diameter of the columns and TAC of complete extractive distillation system for the respective solvent is summarized in Table 6. From these results, it can be observed that total operating cost and TAC required for the THF-water-DMSO system is less in comparison with all other solvent systems. So, it was concluded that DMSO is the best solvent among all considered solvents for the separation of equimolar THF-water mixture by extractive distillation, in terms of both energy consumption and TAC.

2.3. Heat integration for extractive distillation

Heat integration in the extractive distillation can be achieved by utilizing the heat from the bottom stream of the solvent recovery column in a heat exchanger to preheat the feed solution. Bottom stream of SRDC contains almost pure high boiling solvent which is recycled to the EDC. Preheating the feed solution will reduce the reboiler duty of EDC and hence, the TAC.

The total number of stages (N_T) and purity specifications of both the product stream were kept same as that for the system without heat integration. The other parameters were optimized in similar manner as in the previous case, to obtain the optimal design of the extractive distillation with heat integration. By utilizing the heat from the bottom stream in the SRDC, the temperature of feed increase up to 53.52 °C, which leads to reduction in the reboiler duty of extractive distillation column from 750.53 kW to 683.89 kW. The flowsheet with heat integration is shown in Fig. 9 (b). From Table 11, 3.44% reduction in TAC and 4.80% reduction in operating cost, is observed in extractive distillation with heat integration as compared to the design without heat integration.

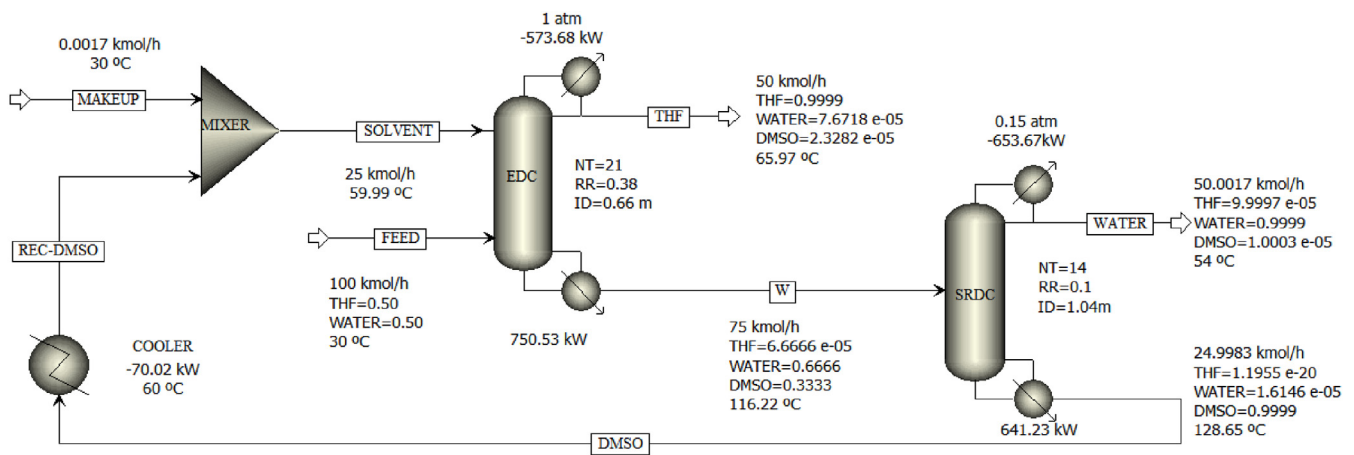
3. Pressure swing distillation (PSD)

In pressure swing distillation, two columns are operated at different pressures as shown in Fig. 11. For the minimum boiling azeotropic system, the fresh binary mixture feed is mixed with recycled distillate stream (D_2) from the second column operating at higher pressure (P_2), to form the mixed feed stream to the first column operating at lower pressure (P_1). The distillate streams (D_1), having compositions close to the azeotropic composition at pressure P_1 , is fed to the second column. Distillate stream of second column (D_2), containing nearly azeotropic composition at pressure P_2 , is recycled back to the low pressure column (LPC). The shift in azeotropic composition at different pressure will help to achieve the separation of the azeotropic binary mixtures. The pure products are withdrawn from the bottom streams B_1 and B_2 .

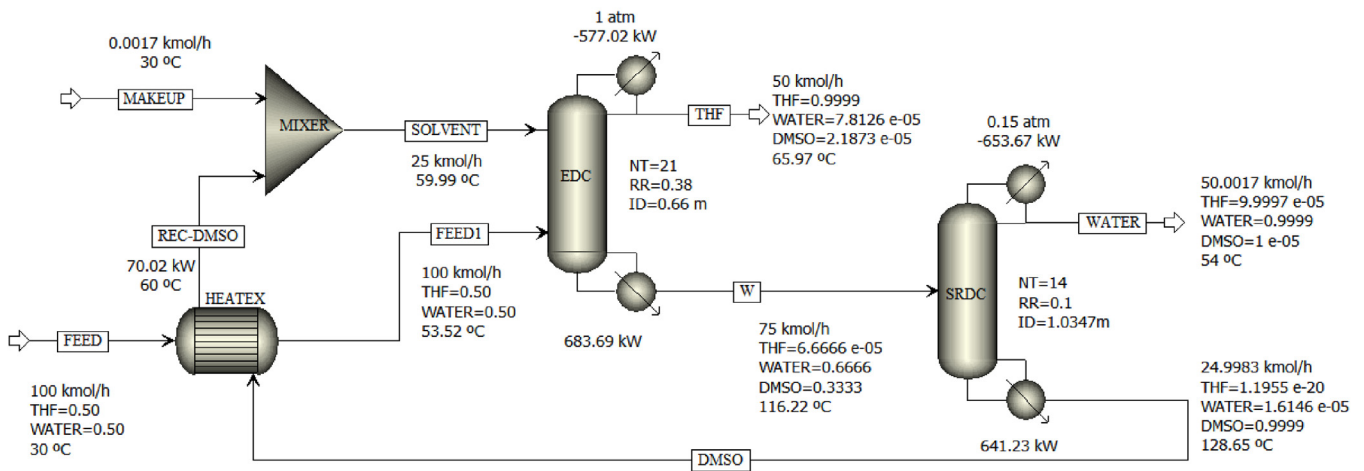
Abu-Eishah and Luyben (1985) in their simulation work explored the partial heat integration of PSD for THF-water system by taking the azeotropic feed composition and pressure $P_1 = 1$ atm and $P_2 = 7.8$ atm. Luyben (2008b) extended the work of Abu-Eishah and Luyben (1985) to fully heat integrated configuration which minimizes the energy consumption. In both the design cases, authors did not consider TAC of the overall pressure swing distillation system. There is no sufficient literature data on the optimum design of PSD design based on TAC. Hence, in this section, the complete optimized design of PSD for the separation of equimolar THF-water mixture is worked out.

Table 6
Optimized design parameters with TAC of THF–Water extractive distillation system for various solvents.

Parameter	DMSO		Ethylene Glycol		Glycerol		1,2-PDO	
	EDC	SRDC	EDC	SRDC	EDC	SRDC	EDC	SRDC
N_T	21	14	21	12	21	8	22	12
RR	0.38	0.1	0.34	0.08	0.20	0.05	0.60	0.11
E/F	0.25	–	0.5	–	0.25	–	0.6	–
N_{FF}	17	6	17	7	17	4	17	7
D (m)	0.66	1.04	0.65	0.91	0.61	0.96	0.73	0.97
H (m)	13.92	8.78	13.90	7.32	13.89	4.39	14.63	7.32
Q_R (kW)	750.5	641.2	846.2	628.9	757.3	719.4	1042.8	637.7
A_R (m ²)	30.29	36.18	37.54	26.90	29.45	44.41	47.90	45.00
Q_C (kW)	573.7	653.7	553.3	641.8	496.9	624.0	663.3	659.6
A_C (m ²)	19.73	34.64	19.04	34.00	17.10	33.06	22.82	34.95
Q_{cooler} (kW)	70.0		185.5		261.3		263.1	
A_{cooler} (m ²)	1.48		3.61		3.58		5.35	
Total capital cost (10 ⁶ \$)	0.4729		0.4481		0.4271		0.5210	
Total operating cost (10 ⁶ \$/yr)	0.3118		0.3385		0.3744		0.3765	
TAC (10 ⁶ \$/yr)	0.4695		0.4878		0.5167		0.5502	



(a) Configuration without heat integration



(b) Configuration with heat integration

Fig. 9. The optimal design flowsheet of extractive distillation system with DMSO as a solvent.

3.1. Simulation analysis of pressure swing distillation system

The steady state Aspen Plus simulator with RadFrac model and NRTL property package with built-in binary interaction parameter

was used for simulation of PSD system. The same feed conditions and product purity constraints were taken as a basis for the PSD analysis as that taken for the extractive distillation system in the

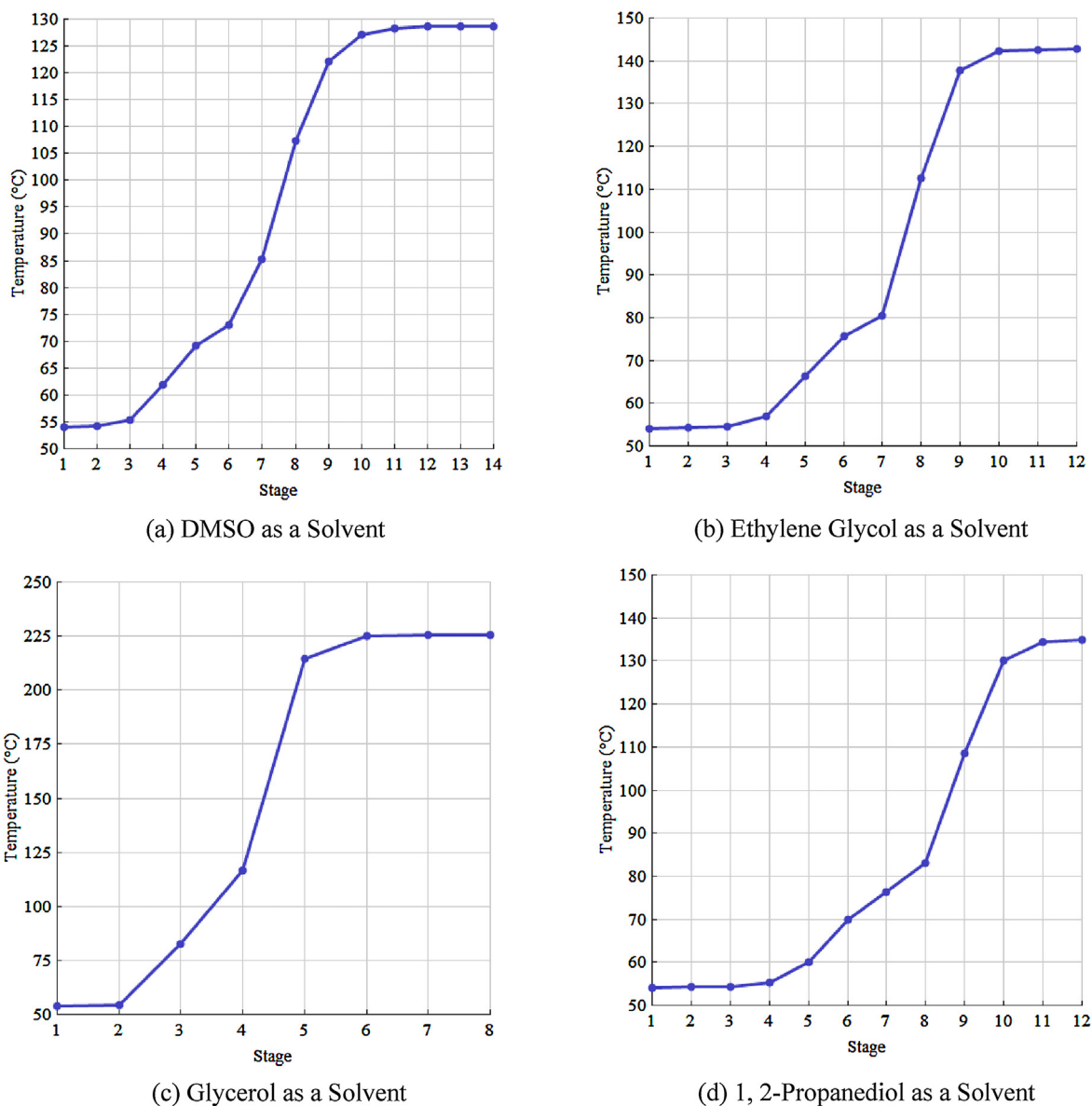


Fig. 10. SRDC Temperature profile.

previous section. The distillate composition of LPC is the azeotropic composition at low pressure while the distillate composition of HPC is the azeotropic composition at high pressure. Recycle flow rates were estimated by total material and component balance of the system.

3.2. Selection of pressure and N_T for columns

The effect of pressure on the azeotropic point and the boiling point of both the components are as given in Table 7. It can be observed that the azeotropic composition of THF-water system shifts significantly with a moderate change in pressure. Larger shifts in the azeotropic composition with pressure will reduce the recycle flow rate and hence, the reboiler duties of the columns. So, higher pressure will be preferred in HPC, but it would lead to high utility temperature requirement for the reboiler. The operating pressure of LPC was set at atmospheric pressure. Vacuum was not preferred for LPC as it would demand expensive chilled utility for the condenser operation. Atmospheric pressure operation allows LPC to

use cooling water with temperature of around 305 K to be used as utility in the condenser.

The pressure of the HPC was chosen by optimizing the flowsheet at two levels. In the first level, for the assumed HPC pressure, the number of stages was optimized such that TAC for the overall separation system obtained was the minimum. In the second level, TAC of the overall system for various operating pressure for the HPC were compared and the pressure with minimum TAC was taken as the optimum pressure for the HPC.

The economic optimization results for HPC operating at 5 atm, is summarized in Tables 8 and 9. First, the number of stages of LPC (N_{T1}) was varied from 12 to 15 while keeping the stages in the HPC (N_{T2}) same. Then the number of stages of HPC (N_{T2}) was varied from 14 to 17 while keeping N_{T1} same, to find out the minimum TAC. The Design Spec function was used to fix the optimum reflux ratio to achieve the specified purity of the product streams. Feed location of both the columns was obtained by sensitivity analysis result to minimize the heat duties of the columns. The results indicates that, LPC having $N_T = 13$ with feed stage at 10 and HPC

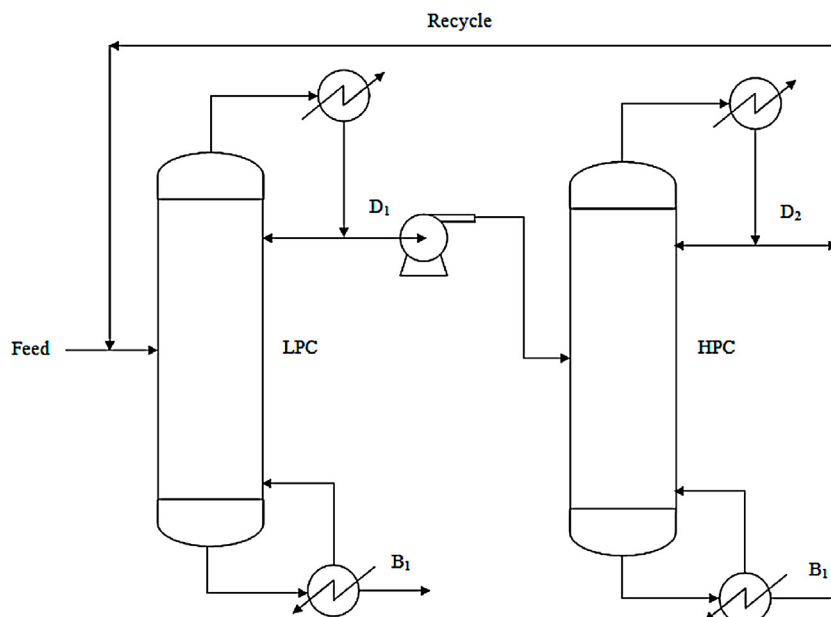


Fig. 11. Pressure Swing Distillation Flow Diagram.

Table 7
Effect of pressure change on Azeotropic composition for THF-water system.

Pressure (atm)	Boiling point of Water (°C)	Boiling point of THF (°C)	Boiling temperature of Azeotrope (°C)	Azeotropic Composition (mole fraction of THF)
0.1	46.06	8.9	8.74	0.9551
0.5	81.67	46.09	44.74	0.8732
0.8	93.88	59.26	57.17	0.8437
1	100.02	65.97	63.43	0.8287
2	120.69	89.03	84.54	0.7775
3	134.05	104.32	98.20	0.7442
4	144.16	116.11	108.54	0.7190
5	152.41	125.86	116.98	0.6986
6	159.43	134.25	124.14	0.6814
7	165.57	141.65	130.41	0.6666
8	171.05	148.31	135.99	0.6535
9	176.01	154.38	141.04	0.6418
10	180.55	159.97	145.67	0.6312
11	184.75	165.16	149.93	0.6215

Table 8
Economic Optimization Results for N_{T1} (LPC at 1 atm and HPC at 5 atm).

Parameters	Case 1	Case 2	Case 3	Case 4
N_{T1}	12	13	14	15
N_{T2}	16	16	16	16
N_{F1} (optimal)	9	10	11	12
RR_1 (optimal)	0.22	0.21	0.21	0.20
D_1 (m)	0.96	0.95	0.95	0.95
Q_{R1} (kW)	1411.3	1401.3	1394.0	1388.5
Q_{C1} (kW)	1437.8	1427.7	1420.5	1415.0
Total capital cost (10^6 \$)	0.4880	0.4934	0.4990	0.5047
Total operating cost (10^6 \$)	0.5800	0.5778	0.5761	0.5749
TAC (10^6 \$/yr)	0.7427	0.7423	0.7425	0.7431

Table 9
Economic Optimization Results for N_{T2} (LPC at 1 atm and HPC at 5 atm).

Parameters	Case 5	Case 6	Case 7	Case 8
N_{T1}	13	13	13	13
N_{T2}	14	15	16	17
N_{F2} (optimal)	6	6	7	8
RR_2 (optimal)	0.30	0.28	0.27	0.26
D_2 (m)	0.77	0.77	0.77	0.76
Q_{R2} (kW)	1199.2	1186.4	1177.4	1172.8
Q_{C2} (kW)	901.2	888.4	879.4	874.8
Total capital cost (10^6 \$)	0.4857	0.4892	0.4934	0.4973
Total operating cost (10^6 \$)	0.5827	0.5798	0.5778	0.5768
TAC (10^6 \$/yr)	0.7446	0.7429	0.7423	0.7425

having $N_T = 16$ with the feed stage at 7 gives minimum TAC for the complete pressure swing distillation system.

With fixed pressure of 1 atm and number of stages of 13 in LPC, the optimum pressure of HPC was fixed in such a way that the TAC of the overall system will be the minimum. HPC at various pressures was simulated, similar to that for 5 atm pressure and the results are summarized in Table 10 which includes heat duties, sizing, operating cost, capital cost and TAC of both the columns for various HPC pressures. The results show that, the minimum total operating cost

and TAC was obtained at HPC pressure 10 atm. Further increase in HPC pressure above 10 atm, would require expensive high pressure steam which will increase the operating cost and consequently, the TAC of the system. The optimal steady state design flowsheet of pressure swing distillation system with HPC at 10 atm pressure is as shown in Fig. 13 (a).

Table 10
Optimization results of PSD with various operating pressure of HPC.

	Case 1		Case 2		Case 3		Case 4		Case 5		Case 6	
	C ₁	C ₂	C ₁	C ₂	C ₁	C ₂	C ₁	C ₂	C ₁	C ₂	C ₁	C ₂
Pressure (atm)	1	3	1	5	1	8	1	9	1	10	1	11
N _T	13	16	13	16	13	16	13	16	13	16	13	16
N _F (optimal)	11	9	10	7	11	8	10	8	10	8	11	8
RR (optimal)	0.20	0.35	0.21	0.27	0.21	0.29	0.22	0.29	0.22	0.29	0.22	0.31
D (m)	1.12	1.04	0.95	0.77	0.86	0.66	0.85	0.64	0.83	0.63	0.82	0.63
H (m)	8.05	10.23	8.05	10.25	8.05	10.25	8.05	10.25	8.05	10.25	8.05	10.25
Q _R (kW)	1995.1	1887.5	1401.3	1177.4	1150.7	966.1	1108.1	934.5	1074.3	911.6	1047.8	899.6
A _R (m ²)	56.54	59.83	39.50	60.95	32.46	47.83	31.30	55.78	30.38	67.14	29.66	17.71
Q _C (kW)	2038.6	1621.6	1427.7	879.4	1171.1	619.0	1127.7	572.5	1093.3	535.5	1065.2	513.2
A _C (m ²)	75.77	28.69	53.07	12.12	43.53	6.98	41.91	6.15	40.63	5.52	39.59	5.12
Total capital cost (10 ⁶ \$)	0.6173		0.4934		0.4240		0.4242		0.4300		0.3599	
Total operating cost (10 ⁶ \$/yr)	0.8699		0.5778		0.4865		0.4695		0.4565		0.4907	
TAC (10 ⁶ \$/yr)	1.0757		0.7423		0.6279		0.6109		0.5999		0.6107	

Table 11
Economic analysis results for Extractive Distillation and Pressure Swing Distillation with and without heat integration.

Parameter	ED without heat integration		ED with heat integration		PSD without heat integration		PSD with partial heat integration		PSD with fully heat integration	
	C1	C2	C1	C2	C1	C2	C1	C2	C1	C2
NT	21	14	21	14	13	16	13	16	13	16
D (m)	0.66	1.03	0.66	1.03	0.83	0.63	0.83	0.63	0.81	0.79
H (m)	13.90	8.78	13.90	8.78	8.05	10.25	8.05	10.25	8.05	10.25
Q _R (kW)	750.53	641.23	683.69	641.23	1074.3	911.63	535.54	911.63	1025.5	1414.5
A _R (m ²)	30.29	36.18	27.59	36.18	30.38	67.14	15.14	67.14	28.99	104.14
Q _C (kW)	573.67	653.66	577.02	653.66	1093.3	535.54	1093.3	–	1057.2	–
A _C (m ²)	19.73	34.64	19.85	34.64	40.63	5.52	40.63	–	39.28	–
Q _{HE} (kW)	70.02		70.02		–		538.74		–	
A _{HE} (m ²)	1.48		1.67		–		15.23		–	
Capital cost (10 ⁶ \$)	0.2202	0.2527	0.2175	0.2527	0.2255	0.2045	0.2439	0.1823	0.2195	0.2382
Operating cost (10 ⁶ \$/yr)	0.1682	0.1437	0.1532	0.1437	0.2407	0.2158	0.1207	0.2158	–	0.3348
TAC (10 ⁶ \$/yr)	0.2416	0.2279	0.2257	0.2279	0.3159	0.2840	0.2020	0.2766	0.0732	0.4142
Total capital cost (10 ⁶ \$)	0.4729		0.4702		0.4300		0.4263		0.4577	
Total operating cost (10 ⁶ \$/yr)	0.3118		0.2969		0.4565		0.3365		0.3348	
TAC (10 ⁶ \$/yr)	0.4695		0.4536		0.5999		0.4786		0.4874	

3.3. Heat integration of pressure swing distillation

In pressure swing distillation, energy consumption can be further reduced by heat integration of both the columns. From Fig. 13 (a) for the PSD of THF/water mixture, it can be observed that condenser duty of HPC is 535.5 kW with top vapour temperature of 418.8 K and the reboiler duty of LPC is 1074.3 kW with bottom boiling liquid temperature of 370.7 K, which indicate that the heat integration is possible for this system as the temperature difference between top vapour of HPC and boiling liquid of LPC is almost 48.1 K, which is suitable for heat integration.

Design of heat integrated system can be done in two modes such as, partial heat integration and full heat integration. For designing both options of heat integration for PSD, the total number of stages and product purity of both the columns were kept same as that obtained for the PSD without heat integration in Section 3.2 and all other parameters were optimized accordingly.

3.3.1. Partial heat integration

In Partial heat integration system, condenser duty (Q_{C2}) of the HPC and reboiler duty (Q_{R1}) of the LPC are not equal. Therefore, to compensate the heat requirement of the LPC, an auxiliary reboiler (AR) is provided. In PSD configuration, given in Fig. 13 (a), the condenser duty of the HPC is not equal to the reboiler duty of LPC, hence the auxiliary reboiler of duty Q_{AR} = 538.74 kW will be required to meet the heat requirement of the LPC. The complete design flowsheet PSD with partial heat integration is given in Fig. 13 (b).

3.3.2. Full heat integration

In full heat integration, condenser duty (Q_{C2}) of HPC is set exactly equal to the reboiler duty (Q_{R1}) of the LPC and thus auxiliary reboiler is not required. The complete design flowsheet for PSD with full heat integration is given in Fig. 13 (c). To achieve this, Design Spec function in Aspen Plus was used to set both duties equal by varying

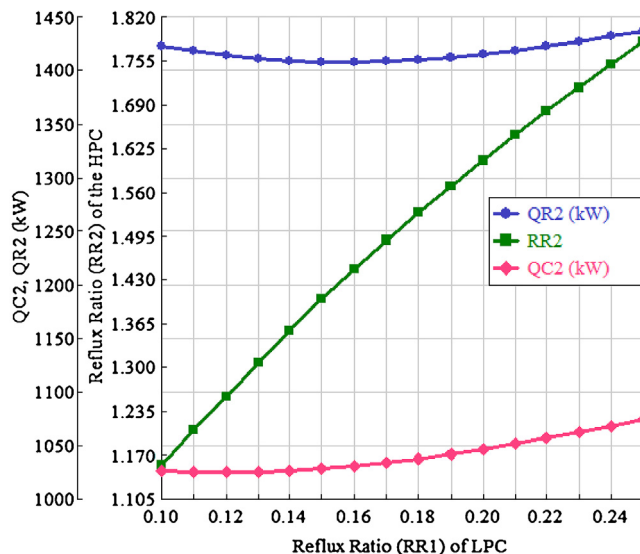
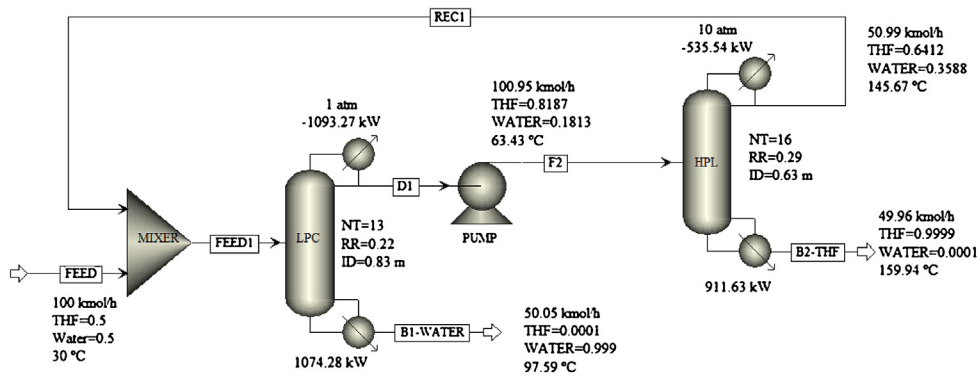
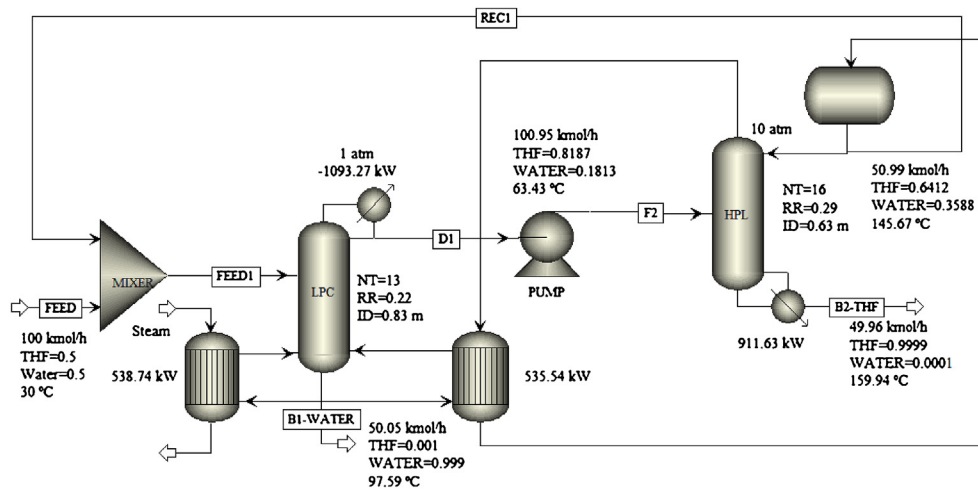


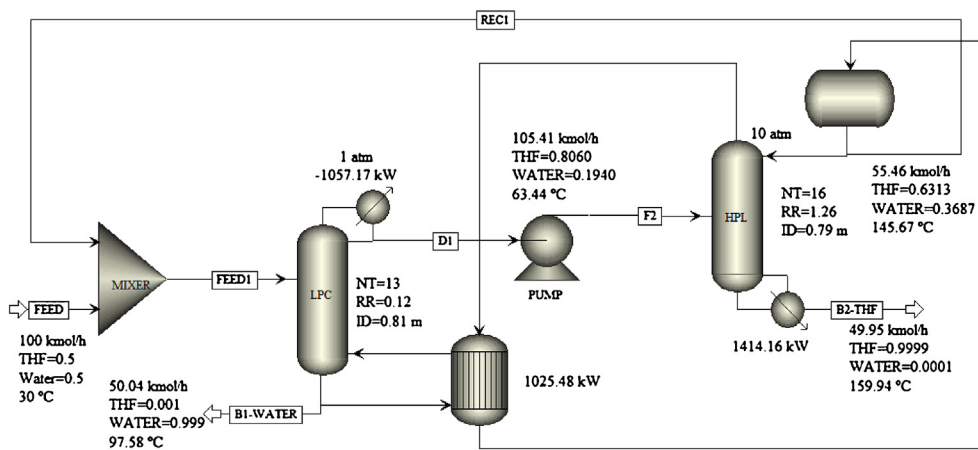
Fig. 12. Effect of reflux ratio (RR1) of LPC on the RR2, Q_{C2} and Q_{R2}.



(a) THF-water PSD without heat integration



(b) THF-water PSD with partial heat integration



(c) THF-water PSD with full heat integration

Fig. 13. The optimal steady state design flowsheets of Pressure Swing Distillation system.

the reflux ratio (RR_2) of the HPC. The reflux ratio (RR_1) of LPC was varied to minimize the energy consumption. Desired product purity was achieved by varying the bottom flow rate of the respective

columns. The effect of reflux ratio (RR_1) on the RR_2 , Q_{C2} and Q_{R2} is as shown in Fig. 12. It shows that optimum reflux ratio (RR_1) was 0.12 for which minimum condenser duty was $Q_{C2} = 1025.5$ kW and

corresponding reboiler duty and reflux ratio were $Q_{R2} = 1414.2$ kW and $RR_2 = 1.26$, respectively.

The cost analysis data and optimum design parameters for three alternatives are given in Table 11. The TAC of the partially heat integrated process is 0.4786 \$/yr, and full heat integrated process is 0.4874 \$/y. The results show that about 20.2% and 18.8% reduction in TAC was achieved by the PSD with partial and full heat integration, respectively as compared to the PSD without heat integration. For THF-Water PSD, the partial heat integration configuration appears to be more attractive over the PSD with full heat integration and without heat integration, in terms of TAC.

4. Comparison of extractive distillation and PSD for THF-Water separation

The most optimum designs of extractive distillation were compared with the most optimum design of PSD. The optimized design parameters with economical analysis of both, extractive distillation and pressure swing distillation, are given in Table 11. Reduction in TAC can be observed with heat integration in both designs. Results indicate that heat integration in extractive distillation leads to 3.4% reduction in TAC, which is mainly because of saving in operating cost. Partial and full heat integration in case of PSD results in 20.2% and 18.8% reduction in TAC, respectively as compared to basic configuration without heat integration. PSD configuration with partial heat integration is more economical as compared to fully heat integration because capital cost increases significantly in case of fully heat integrated system because of increased heat transfer area requirement for both column reboilers along with higher HPC diameter. Extractive distillation with heat integration requires 5.2% less TAC than that of PSD with partial heat integration.

5. Conclusion

In this paper, steady state simulation of extractive and pressure swing distillation for the separation of equimolar THF-water binary mixture was investigated in detail. Designs of extractive distillation system with various solvents were worked out and evaluated economically. DMSO was found to be the best solvent for extractive distillation of THF-water separation as it gave minimum TAC to achieve the desired purity of products. For Pressure swing distillation, LPC pressure was fixed at 1 atm and various operating pressures for HPC were analyzed. It was found that HPC with 10 atm pressure gave minimum TAC. Design of steady state extractive and pressure swing distillation with heat integration was also worked out.

As the basis, in terms of feed conditions and constraints in terms of product purity were same for the simulation analysis, the optimum configuration of extractive distillation with and without heat integration by using DMSO as the solvent was directly compared with the most optimum configuration of PSD with and without heat integration. Results indicate that extractive distillation with and without heat integration gives 24.4% and 21.7% reduction in

the TAC and 34.96% and 31.70% in the operating cost, respectively, over the PSD without heat integration. TAC of extractive distillation with heat integration is 5.2% less than that of PSD with partial heat integration. Hence, extractive distillation with DMSO as solvent appears to be better option economically for separation of equimolar THF-water mixture.

Acknowledgement

Authors are thankful to Council for Scientific and Industrial Research (CSIR), India for supporting the present work.

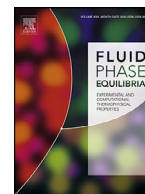
References

- Abu-Eishah, S.I., Luyben, W.L., 1985. Design and control of a two-column azeotropic distillation system. *Ind. Eng. Chem. Process Des. Dev.* 24, 132–140.
- Deorukhkar, O.A., Deogharkar, B.S., Mahajan, Y.S., 2016. Purification of tetrahydrofuran from its aqueous azeotrope by extractive distillation: pilot plant studies. *Chem. Eng. Proc.* 105, 79–91.
- Fan, Z., Zhang, X., Cai, W., Wang, F., 2013. Design and control of extraction distillation for dehydration of tetrahydrofuran. *Chem. Eng. Technol.* 36, 829–839.
- Gomez, P.A., Gil, I.D., 2009. Simulation of the tetrahydrofuran dehydration process by extractive distillation. *Latin Am. Appl. Res.* 39, 275–284.
- Hosgor, E., Kucuk, T., Oksal, I.N., Kaymak, D.B., 2014. Design and control of distillation processes for methanol-chloroform separation. *Comput. Chem. Eng.* 67, 166–177.
- Knight, J.R., Doherty, M.F., 1989. Optimal design and synthesis of homogeneous azeotropic distillation sequences. *Ind. Eng. Chem. Res.* 28, 564–572.
- Lladosa, E., Monton, J.B., Burguet, M., 2011. Separation of di-n-propyl ether and n-propylalcohol by extractive distillation and pressure-swing distillation: computer simulation and economic optimization. *Chem. Eng. Proc.* 50, 1266–1274.
- Luo, H., Liang, K., Li, W., Li, Y., Xia, M., Xu, C., 2014. Comparison of pressure-swing distillation and extractive distillation methods for isopropyl alcohol/diisopropyl ether separation. *Ind. Eng. Chem. Res.* 53, 15167–15182.
- Luyben, W.L., Chien, I.-L., 2011. Design and Control of Distillation Systems for Separating Azeotropes. John Wiley & Sons.
- Luyben, W.L., 2008a. Comparison of extractive distillation and pressure swing distillation for acetone-methanol separation. *Ind. Eng. Chem. Res.* 47, 2696–2707.
- Luyben, W.L., 2008b. Design and control of a fully heat-integrated pressure swing azeotropic distillation system. *Ind. Eng. Chem. Res.* 47, 2681–2695.
- Luyben, W.L., 2013. Comparison of extractive distillation and pressure swing distillation for acetone/chloroform separation. *Comput. Chem. Eng.* 50, 1–7.
- Luyben, W.L., 2016. Distillation column pressure selection. *Sep. Purif. Technol.* 168, 62–67.
- Wang, Q., Yu, B., Xu, C., 2012. Design and control of distillation system for methylal/methanol separation. Part 1: extractive distillation using DMF as an entrainer. *Ind. Eng. Chem. Res.* 51, 1281–1292.
- Wei, H.M., Wang, F., Zhang, J.L., Liao, B., Zhao, N., Xiao, F., Wei, W., Sun, Y.H., 2013. Design and control of dimethyl carbonate-methanol separation via pressure-swing distillation. *Ind. Eng. Chem. Res.* 52, 11463–11478.
- Xu, S., Wang, H., 2006a. A new entrainer for separation of tetrahydrofuran-water azeotropic mixture by extractive distillation. *Chem. Eng. Proc.* 45, 954–958.
- Xu, S., Wang, H., 2006b. Separation of tetrahydrofuran-water azeotropic mixture by batch extractive distillation process. *Chem. Eng. Res. Des.* 84, 478–482.
- Yu, B., Wang, Q., Xu, C., 2012. Design and control of distillation system for methylal/methanol separation. Part 2: Pressure swing distillation with full heat integration. *Ind. Eng. Chem. Res.* 51, 1293–1310.
- Zhang, Z., Huang, D., Lv, M., Jia, P., Sun, D., Li, W., 2014. Entrainer selection for separating tetrahydrofuran/water azeotropic mixture by extractive distillation. *Sep. Purif. Technol.* 122, 73–77.



Contents lists available at ScienceDirect

Fluid Phase Equilibria

journal homepage: www.elsevier.com/locate/fluid

Effect of CaCl_2 and ZnCl_2 salts on isobaric vapor-liquid equilibrium in separation of the azeotropic mixture of ethanol + water

Pravin D. Ghuge^{a,b}, Nilesh A. Mali^{a,b,*}, Sunil S. Joshi^{a,b}^a Chemical Engineering & Process Development Division, CSIR-National Chemical Laboratory, Dr. Homi Bhabha Road, Pune 411008, India^b Academy of Scientific and Innovative Research (AcSIR), Ghaziabad 201002, India

ARTICLE INFO

Article history:

Received 13 November 2020

Revised 23 February 2021

Accepted 25 February 2021

Available online 3 March 2021

Keywords:

Vapor-liquid equilibrium

Ethanol

Water

Azeotrope

Salts

eNRTL

ABSTRACT

Present work analyzes potential of calcium chloride (CaCl_2) and zinc chloride (ZnCl_2) salts as entrainer for breaking the minimum boiling azeotrope of ethanol and water. Isobaric vapor-liquid equilibrium (VLE) data for the binary systems of water + ethanol and ternary system of water + ethanol + calcium chloride, and water + ethanol + zinc chloride were measured at a constant pressure of 94.5 kPa. The effect of salts on the relative volatility of ethanol to water as well as on the vapor phase mole fractions of ethanol were also studied experimentally. From the experimental results, it is observed that with addition of salts, the azeotropic point of the ethanol and water system can be eliminated. Salting out effects in case of calcium chloride was more than that zinc chloride salt. The results obtained in this work showed that calcium chloride could be a better choice for separation of the water + ethanol azeotrope. Electrolyte nonrandom two-liquid (eNRTL) model was used to correlate the experimental VLE data. The model prediction with the regressed parameters was found in well agreement with the experimental data. The experimental data obtained in this work was found thermodynamically consistent using van Ness test.

© 2021 Elsevier B.V. All rights reserved.

1. Introduction

Ethanol has wide range of application in the chemical industry. It can be used as a solvent, reactant or intermediate in production of various paints, perfumes, medicines and food product [1]. Ethanol is used as a reasonable feed stock for producing various renewable chemicals and products. Nowadays, anhydrous ethanol is used as a fuel additive [2]. The production of anhydrous ethanol by conventional distillation technique is difficult due to the formation of minimum boiling azeotrope of ethanol-water mixture at atmospheric pressure. At azeotropic condition, liquid and vapor phase compositions are equal leading to relative volatility equal to one; hence, conventional distillation is not useful to purify the products beyond azeotropic compositions. Advanced distillation techniques [3] such as extractive distillation, azeotropic distillation and pressure-swing distillations are required to deal with azeotropic mixture separations.

Extractive distillation technique is the most preferable over the other distillation technique due to its lower energy requirement, flexibility in entrainer selection, simple operation and high purity product in case of dehydration of ethanol [4]. It is reported that

salts are effective entrainer in altering the vapor-liquid equilibrium behavior of the azeotropic mixture in such a way that the azeotrope formation can be completely eliminated. Mostly salts are having very low volatility, thus they are not vaporized in the extractive distillation process which results in high purity distillate product and low energy consumption [5]. Salts are preferred entrainer in extractive distillation due to its low cost and less toxicity. The lower entrainer to feed ratio leads to less amount of salt required to achieve the separation in the extractive distillation as compared to that with the organic solvent as entrainer [6]. Extractive distillation process using potassium acetate [5,7,8], calcium chloride [6,9–13], and magnesium chloride [14] as an entrainer was studied to obtain the anhydrous ethanol. Salts are added at the appropriate location in the top of the extractive distillation column, which alter the relative volatility in such a way that light component obtained as a distillate and salt with other component is obtained as bottom product [5]. Thus, salts have good potential to be considered as entrainer, instead of the conventional organic solvents, in the extractive distillation process.

The VLE data of binary azeotropic system with addition of the entrainer has great importance in design of the extractive distillation process. For extractive distillation with salts, information on change in the VLE behavior of the system due to presence of salts; specifically change in the vapor phase composition of the mixed solvent system is important. The experimental VLE data is help-

* Corresponding author.

E-mail address: na.mali@ncl.res.in (N.A. Mali).

List of symbols

x'_2	mole fractions of component i in the liquid phase on salt free basis
x_i	mole fractions of component i in the liquid phase
y_i	mole fractions of component i in the vapor phase
y_i^{exp}	experimental mole fraction of component i in vapor phase
y_i^{cal}	calculated mole fraction of component i in vapor phase
T	equilibrium temperature
T_i^{exp}	experimental temperature
T_i^{cal}	temperature calculated by ENRTL model
P	total pressure in the equilibrium system
P_i^s	saturated vapor pressure of pure component i at equilibrium temperature
u	standard uncertainties
z_3	mass fraction of salts in the liquid phase
Y_i	activity coefficient of component i
α_{21}	relative volatility of ethanol to water
ρ	density
n_D	refractive index

ful to understand if the given entrainer is capable to break the azeotrope or not while selection of the entrainer. Also, while designing of extractive distillation system, it is necessary to develop the thermodynamic model with appropriate parameters for simulation analysis. The accurate experimental VLE data is necessary for regressing the thermodynamic model parameters.

VLE data is reported in the literature for some salts having capability to break the azeotrope of ethanol water system which includes potassium acetate [15–18] strontium bromide [19,20], calcium nitrate [21], cobalt II chloride [22], and potassium and sodium iodide [23]. Isobaric VLE data for ethanol water system containing calcium chloride at constant mass concentration of 16.7 wt% was reported by Nishi [24] at atmospheric pressure, and with 0.974 mol/kg salt at 12.3 kPa pressure was reported by Meyer [25], VLE data at constant temperature of 298.15 K was reported by Mishima [26]. To the best of our knowledge, VLE data for varying concentration of calcium chloride at constant pressure was not yet reported in the literature. No literature is reported for ethanol + water + zinc chloride in the NIST literature data base.

The aim of present study is to investigate the effect various concentration of calcium chloride and zinc chloride salts on the azeotropic behavior of ethanol and water azeotropic system. In this work, isobaric vapor-liquid equilibrium data for binary system of ethanol + water, ternary system of ethanol + water + calcium chloride, ethanol + water + zinc chloride were determined at 94.5 kPa. The effects of varying concentration of salts on the phase equilibrium behavior of ethanol + water azeotropic system were discussed. Thermodynamic consistency of the obtained experimental VLE data was checked by van Ness test. The eNRTL model was used to correlate the experimental VLE data.

2. Experimental

2.1. Materials

Ethanol was supplied by Changshu Hongsheng Fine Chemical Co. Ltd. with mass fraction of 0.999. The mass fraction of ethanol was 0.999 and no impurities were detected by gas chromatography. Calcium chloride was supplied by Thermo Fisher Scientific India Pvt. Ltd. and zinc chloride was supplied by Loba Chemie Pvt. Ltd. The moisture content of salts was determined by Karl Fisher

titration and mass fraction of water was below 0.006. Ethanol and salts were used without further purification. The deionized water (conductivity less than $1.0 \mu\text{S cm}^{-1}$) was generated using ultra-pure water system provided by Siemens. Specifications of chemicals used in the experiments are listed in Table 1.

2.2. Experimental apparatus and procedure

The glass dynamic circulation VLE apparatus used to generate the vapor-liquid equilibrium data for binary as well as ternary system. The detail description of VLE apparatus and its working was reported earlier for generating the VLE data of various binary systems [27–29]. In the present work, ternary solution with constant salt concentration of 5, 10, 15 mass percentage and with varying concentration of ethanol were prepared gravimetrically using electronic weighing balance with an accuracy of $\pm 0.0001\text{g}$. The solution was stirred well, using magnetic stirrer, until all salts were completely dissolved. Approximately 330 ml solution was fed into the boiling chamber of VLE apparatus to find out its VLE data.

At the time of determination of this experimental data, the local atmospheric pressure was varying slightly between 95 to 96 kPa. Hence, we have used a vacuum pump provided by KNF, Germany (Model number SC920G) which ensures the constant pressure of 94.5 kPa with accuracy of ± 0.1 kPa throughout the experiment, which is slightly below the local atmospheric pressure. Once the equilibrium condition was reached, the temperature of equilibrium chamber was recorded using the hand held thermometer provided by Wika, India (Model CTH 7000) with an accuracy of ± 0.01 K and a very small quantity of sample was taken from sampling port to analyze the composition.

2.3. Analysis

The standard samples of ethanol-water binary mixtures covering whole composition range from pure ethanol to pure water were prepared gravimetrically and densities and refractive indices were measured at 298.15 K, given in Table S1 (Supplementary Information). The density meter provided by Rudolph Research Analytical, USA (Model number 2911 plus) was used to measure density with an accuracy of 0.0001. The refractometer from Atago, Japan (Model-RX-7000i) was used to measure the refractive index with an accuracy of ± 0.0001 and resolution of 0.00001. The calibration curves for density (ρ) and refractive index (n_D) verses mole fraction of ethanol are plotted, experimental data (Table S1) is also compared with literature data as shown in the Figs. S1 and S2 (Supplementary material), respectively, which shows the good agreements of the experimental data with literature data measured at 25 °C. The appropriate polynomial equation was fitted to the data and respective calibration equation was generated given in Table S2 (Supplementary Information). These equations were used to estimate the compositions of ethanol by measuring density or refractive index of the sample. It was observed that estimation of composition of ethanol at higher concentration using refractive index was quite difficult due lower difference in the refractive indices of the samples at higher concentration of ethanol. It was found that accuracy of the estimation using density measurement was more even at higher concentration of ethanol, hence, for binary system of ethanol and water density measurements was preferred to obtain the compositions.

In case of the ternary system of ethanol, water and salt, the vapor phase composition was analyzed using the density measurement, as salts are highly non-volatile, they do not appear in the vapor phase. The liquid phase composition was estimated by using material balance calculations across the complete VLE apparatus. The salt concentration in the liquid phase was assumed to be the

Table 1
Specification of the chemicals used in experiments.

Name	CAS No.	Source	Mass fraction purity	Analysis method
Ethanol	64-17-5	Changshu Hongsheng Fine Chemical Co., Ltd.	0.999	GC ^a
Calcium chloride	10043-52-4	Thermo Fisher Scientific India Pvt. Ltd	≥0.98	KF ^b
Zinc chloride	7646-85-7	Loba Chemie Pvt. Ltd.	≥0.98	KF ^b

^a GC = gas chromatography.

^b KF = Karl Fisher titration.

same as that of the initially introduced feed because all salt remain in liquid phase due to its very low volatility.

To validate the method for estimation of liquid phase composition using the material balance, experiments for ethanol + water without addition of salts were performed. In these experiments the liquid phase composition was estimated by a material balance calculation and was compared with the values obtained by density measurements. The absolute standard deviation between the compositions estimated using mass equations and the composition estimated using the density calibration curve, was found to be less than 0.005.

3. Results and discussion

3.1. Experimental data

To verify the reliability of the VLE still used in this work, the binary VLE data for water (1) + ethanol (2) system was generated at 94.5 kPa which is listed in the Table S3 (supplementary material). x_i and y_i are the mole fractions of component i in liquid and vapor phase, respectively. T is the equilibrium temperature. The experimental data obtained in this work is found in good agreement with the data estimated by the NRTL model using the Aspen Plus simulator with in-built binary interaction parameters. The experimental data is also in good agreement with the literature data, as shown in the Fig. S3 (Supplementary Information). The average absolute deviation of equilibrium temperature was 0.15 K and vapor composition was 0.0037 between experimental and estimated VLE data by NRTL model.

The isobaric VLE data for the ternary system of water (1) + ethanol (2) + calcium chloride (3) and water (1) + ethanol (2) + zinc chloride (3) were measured at 94.5 kPa. The data was generated for both salts for concentration of 0.05, 0.10, and 0.15, by mass, in each experimental run which are listed in Tables 2 and 3, respectively, where, x'_2 is the mole fractions of ethanol in the liquid phase on salt free basis, y_2 is the mole fraction of ethanol in vapor phase, z_3 is the mass fractions of salt in the liquid phase, x_1 and x_2 are the mole fractions (on salt basis) of water and ethanol, respectively. T is the equilibrium temperature.

3.2. Correlation of the VLE data

Vapor-liquid phase equilibrium for component i can be expressed with Eq. (1). [30]

$$y_i \Phi_i^y P = \gamma_i^s x_i \Phi_i^s P_i^s \exp \left[\frac{V_i (P - P_i^s)}{RT} \right] \quad (1)$$

where, liquid and vapor mole fractions of a more volatile component i represented by x_i and y_i , respectively. P is the system pressure and exponential term represents Poynting factor which is equal to one for low pressure system.

P_i^s , is the saturation vapor pressure of the pure component i at temperature T , which can be calculated by extended Antoine Eq. (2),

Table 2

Isobaric ternary vapor-liquid equilibrium data for temperature T , liquid phase mole fraction salt free basis x' , x_1 and x_2 are the mole fractions (on salt basis) of water and ethanol, respectively, liquid phase mass fraction of salt z , vapor phase mole fraction y for water (1) ethanol (2) + calcium chloride (3) at pressure of 94.5 kPa.^a

z_3 (%)	T/K	x'_2	x_1	x_2	y_2
About 5 %					
5.17	349.97	1.000	0.000	0.978	1.000
5.17	349.92	0.880	0.118	0.862	0.920
5.11	350.01	0.757	0.238	0.743	0.849
5.16	350.31	0.605	0.388	0.595	0.764
5.16	350.79	0.472	0.520	0.465	0.699
5.16	351.58	0.362	0.629	0.358	0.655
5.16	352.48	0.273	0.718	0.270	0.614
4.53	353.60	0.199	0.793	0.197	0.575
5.15	355.12	0.136	0.855	0.134	0.530
5.16	357.66	0.082	0.909	0.081	0.448
5.16	362.77	0.036	0.955	0.036	0.297
5.17	371.43	0.000	0.991	0.000	0.000
About 10 %					
10.32	350.46	1.000	0.000	0.954	1.000
10.32	350.21	0.879	0.116	0.842	0.939
10.33	350.27	0.775	0.216	0.745	0.885
10.31	350.55	0.604	0.382	0.583	0.802
10.31	350.85	0.471	0.513	0.456	0.740
10.30	351.30	0.362	0.620	0.352	0.694
10.29	351.90	0.273	0.708	0.266	0.655
10.29	352.97	0.198	0.783	0.193	0.612
10.29	354.41	0.135	0.846	0.132	0.560
10.29	357.09	0.081	0.900	0.079	0.484
10.33	362.71	0.036	0.945	0.035	0.320
10.32	372.04	0.000	0.982	0.000	0.000
About 15 %					
15.47	351.11	1.000	0.000	0.929	1.000
15.45	351.04	0.879	0.113	0.821	0.955
15.44	350.98	0.775	0.212	0.727	0.912
15.44	351.03	0.603	0.375	0.571	0.838
15.43	351.14	0.470	0.504	0.447	0.782
15.43	351.41	0.361	0.611	0.345	0.729
15.42	351.83	0.272	0.699	0.261	0.688
15.42	352.70	0.197	0.773	0.190	0.650
15.41	353.99	0.134	0.836	0.130	0.604
15.40	356.29	0.081	0.890	0.078	0.520
15.42	363.66	0.035	0.936	0.034	0.348
15.47	373.31	0.000	0.971	0.000	0.000

^a Standard uncertainty u are $u(x_i) = u(y_i) = 0.005$, $u(z_i) = 0.01\%$, $u(x'_2) = 0.005$, $u(T) = 0.01\text{K}$, $u(P) = 0.1\text{ kPa}$.

$$\ln(P_i^s/kPa) = C_{1i} + \frac{C_{2i}}{T + C_{3i}} + C_{4i}T + C_{5i}\ln T + C_{6i}T^{C_{7i}} \text{ for } C_{8i} \leq T \leq C_{9i} \quad (2)$$

where, C_{1i} to C_{9i} are the coefficients of pure components i , C_{8i} and C_{9i} represents the limits of temperature range, which were retrieved from the Aspen databank [31] and given in Table 4.

The Activity coefficient for a component i can be obtained by taking the partial derivative of the excess Gibbs free energy model with respect to n_i as given in Eq. (3), [30]

$$\ln \gamma_i = \left[\frac{\partial (nG^E/RT)}{\partial n_i} \right]_{T,P,n_j \neq i} \quad (3)$$

Table 3

Isobaric ternary vapor-liquid equilibrium data for temperature T, liquid phase mole fraction salt free basis x' , x_1 and x_2 are the mole fractions (on salt basis) of water and ethanol, respectively, liquid phase mass fraction salt z, vapor phase mole fraction y for water (1) ethanol (2) + zinc chloride (3) at pressure of 94.5 kPa.^a

z_3 (%)	T (K)	x'_2	x_1	x_2	y_2
About 5 %					
5.17	349.99	1.000	0.000	0.982	1.000
5.17	349.87	0.881	0.117	0.866	0.895
5.17	350.01	0.778	0.219	0.765	0.813
5.16	350.65	0.607	0.388	0.598	0.714
5.16	351.42	0.472	0.522	0.466	0.661
5.16	352.29	0.363	0.630	0.359	0.621
5.16	353.09	0.274	0.719	0.271	0.588
5.15	354.25	0.199	0.793	0.197	0.553
5.15	358.31	0.082	0.911	0.081	0.434
5.16	363.02	0.036	0.957	0.036	0.284
5.16	371.41	0.000	0.993	0.000	0.000
About 10 %					
10.31	350.41	1.000	0.000	0.963	1.000
10.31	350.13	0.881	0.115	0.850	0.903
10.32	350.27	0.777	0.216	0.752	0.823
10.33	350.71	0.606	0.382	0.589	0.724
10.31	351.40	0.472	0.515	0.459	0.667
10.30	352.14	0.363	0.622	0.354	0.631
10.29	353.23	0.274	0.711	0.268	0.595
10.28	354.35	0.199	0.785	0.195	0.558
10.28	355.86	0.136	0.849	0.133	0.515
10.28	358.42	0.082	0.903	0.080	0.437
10.29	363.54	0.036	0.949	0.035	0.286
10.31	371.50	0.000	0.985	0.000	0.000
About 15 %					
15.02	350.98	1.000	0.000	0.944	1.000
15.44	350.82	0.881	0.113	0.833	0.898
15.45	350.78	0.777	0.211	0.738	0.820
15.44	351.19	0.607	0.376	0.579	0.717
15.43	351.82	0.472	0.507	0.453	0.664
15.44	352.76	0.363	0.614	0.350	0.617
15.42	353.66	0.274	0.702	0.265	0.585
15.42	354.75	0.199	0.777	0.193	0.553
15.42	356.42	0.136	0.840	0.132	0.505
15.41	358.83	0.082	0.894	0.079	0.429
15.42	363.69	0.036	0.940	0.035	0.274
15.45	371.92	0.000	0.976	0.000	0.000

^a Standard uncertainty u are $u(x_i) = u(y_i) = 0.005$, $u(x'_2) = 0.005$, $u(z_i) = 0.01\%$, $u(T) = 0.01K$, $u(P) = 0.1$ kPa.

Table 4

Parameters of the extended Antoine Equation^a of pure components [31].

Parameters	C_1	C_2	C_3	C_4	C_5	C_6	C_7	C_8	C_9
Ethanol	66.3962	-7122.3	0	0	-7.1424	2.9×10^{-6}	2	159.0	514
Water	66.7412	-7258.2	0	0	-7.3037	4.2×10^{-6}	2	273.16	647.1

^a Where, P is in kPa and T is in K.

The liquid phase activity coefficient (γ_i) can be calculated using electrolyte non-random two liquid model (e-NRTL) proposed by Chen et al. [32] and Mock et al.[33] for mixed solvent electrolyte system which is based on the two fundamental assumptions such as like ion repulsion and local electro-neutrality. The Excess Gibbs free energy model leads to Eq. (4),

$$\ln \gamma_i^* = \ln \gamma_i^{*PDH} + \ln \gamma_i^{*Born} + \ln \gamma_i^{*lc} \quad (4)$$

In multicomponent electrolyte system the long range interaction contribution accounts with the Pitzer-Debye-Huckel (PDH) [34] formula, so the expression for activity coefficient is given by Eq. (5),

$$\ln \gamma_i^{*PDH} = - (1000/M_s)^{1/2} A_\phi \left[(2z_i^2/\rho) \ln(1 + \rho l_x^{1/2}) + (z_i^2 l_x^{1/2} - 2l_x^{3/2}) / (1 + \rho l_x^{1/2}) \right] \quad (5)$$

Table 5

Binary interaction parameter for the eNRTL model.

Component i	Component j	τ_{ij}	τ_{ij}	α_{ij}
Ethanol	Water	0.02	1.49	0.3
Water	CaCl ₂	12.23	-5.49	0.2
Ethanol	CaCl ₂	27.26	-13.88	0.05
Water	ZnCl ₂	10.30	-4.88	0.2
Ethanol	ZnCl ₂	114.13	-57.16	0.01

where, x_i is the mole fraction of a component i, M_s is the molecular weight of solvent, ρ is the closest approach parameter, A_ϕ is the Debye-Huckel parameter.

Expression derived for activity coefficient of from born equation [35] is given by Eq. (6),

$$\ln \gamma_i^{*Born} = (Q_e^2/2kT) [(1/\epsilon_s) - (1/\epsilon_w)] (z_i^2/r_i) 10^{-2} \quad (6)$$

where, ϵ_w is the dielectric constant of water, r_i is the Born radius, dielectric constants for each component used for thermodynamic modeling are given in the Supporting material, Table S4

The local interaction contribution excess Gibbs energy obtained with local composition NRTL equation. For electrolyte system containing molecular species (m) cation (c), and anion (a) can be expressed as follow by Eqs. (7)–(12).

$$\frac{G_m^{*E,lc}}{nRT} = \sum_m n_m \left(\frac{\sum_i X_i G_{im} \tau_{im}}{\sum_i X_i G_{im}} \right) + \sum_c z_c n_c \left(\frac{\sum_{i \neq c} X_i G_{ic} \tau_{ic}}{\sum_{i \neq c} X_i G_{ic}} \right) + \sum_a z_a n_a \left(\frac{\sum_{i \neq a} X_i G_{ia} \tau_{ia}}{\sum_{i \neq a} X_i G_{ia}} \right) \quad (7)$$

where,

$$X_i = C_i x_i = C_i \left(\frac{n_i}{n} \right), i = m, c, a \quad (8)$$

$$n = \sum_i n_i = \sum_m n_m + \sum_c n_c + \sum_a n_a \quad (9)$$

$$G_{ij} = \exp(\alpha_{ij} \tau_{ij}) \quad (10)$$

where, τ_{ij} and α_{ij} is are binary energy parameter and is the non-randomness factor respectively, represent the binary energy interaction parameter

For molecule- molecule τ_{ij} is,

$$\tau_{ij} = c_{ij} + \frac{d_{ij}}{T} \quad (11)$$

For molecule- electrolyte τ_{ij} is,

$$\tau_{ij} = c_{ij} + \frac{d_{ij}}{T} + e_{ij} \left[\frac{T_{ref} - T}{T} + \ln \left(\frac{T}{T_{ref}} \right) \right] \quad (12)$$

where, T_{ref} is the reference temperature, c_{ij} , d_{ij} , and e_{ij} are adjustable parameters obtained from regressing the VLE data in Aspen plus. Other physical properties of the components required such as, ideal gas heat capacity and heat of vaporization were obtained by retrieving the coefficients of respective equation from the Aspen plus [31], given the supporting materials, Tables S5 and S6, respectively.

The binary interaction parameters for electrolyte-NRTL model are determined using experimental vapor-liquid equilibrium data in the Aspen data regression system (DRS) is given in the Table 5. While performing the regression of the VLE data maximum likelihood principle was used as an objective function with Deming initialization method and Britt-Luecke algorithm. The root - mean - square deviation (RMSD) between the experimental and calculated values for the equilibrium temperature (T) and vapor phase

Table 6
The root-mean-square deviation (RMSD) for the equilibrium temperature (T) and vapor phase mole fraction (y_1) for the eNRTL model.

Salt	w ₃ (%)	RMSD y ₁	T/K
Calcium Chloride	5	0.010	0.23
	10	0.005	0.15
	15	0.006	0.34
Zinc Chloride	5	0.008	0.24
	10	0.008	0.25
	15	0.009	0.44

mole fraction of ethanol (y_2) are expressed as given by Eqs. (13) and (14),

$$\text{RMSD } (T_i) = \left(\sum_{i=1}^N (T_i^{\text{cal}} - T_i^{\text{exp}})^2 / N \right)^{0.5} \quad (13)$$

$$\text{RMSD } (y_i) = \left(\sum_{i=1}^N (y_i^{\text{cal}} - y_i^{\text{exp}})^2 / N \right)^{0.5} \quad (14)$$

The values for RMSD (y) and RMSD (T) are given in Table 6, which are less than 0.01 and 0.44 K respectively, According to the

calculated values of RMSD for equilibrium temperature and vapor phase mole fraction, the eNRTL model is suitable for the VLE analysis of the ternary system of water + ethanol + salts.

3.3. Thermodynamic consistency test

To confirm the quality of the VLE data measured, the thermodynamic consistency for all experimental results was checked by the van Ness test [36,37]. The van Ness test is expressed mathematically as Eq. (15),

$$\Delta y = \frac{1}{N} \sum_{i=1}^N \Delta y_i = \frac{1}{N} \sum_{i=1}^N 100 |y_i^{\text{cal}} - y_i^{\text{exp}}| \quad (15)$$

where, N is the number of experimental data, y_i^{exp} and y_i^{cal} is the mole fraction of component i in vapor phase obtained experimentally and calculated by eNRTL model respectively. According to this method, the measured VLE data are to be thermodynamically consistent, if Δy is less than one. The results obtained for van Ness test [36,37] for Δy are 0.854, 0.413 and 0.473 for system of water + ethanol + calcium chloride, 0.765, 0.672, 0.666 for the system of water + ethanol + zinc chloride at constant salt concentration of 0.05, 0.1 and 0.15 (mass fraction), respectively. As each values of Δy obtained for both the salt system are less than 1, is indicating that the experimental vapor-liquid equilibrium results obtained in this work are thermodynamic consistency.

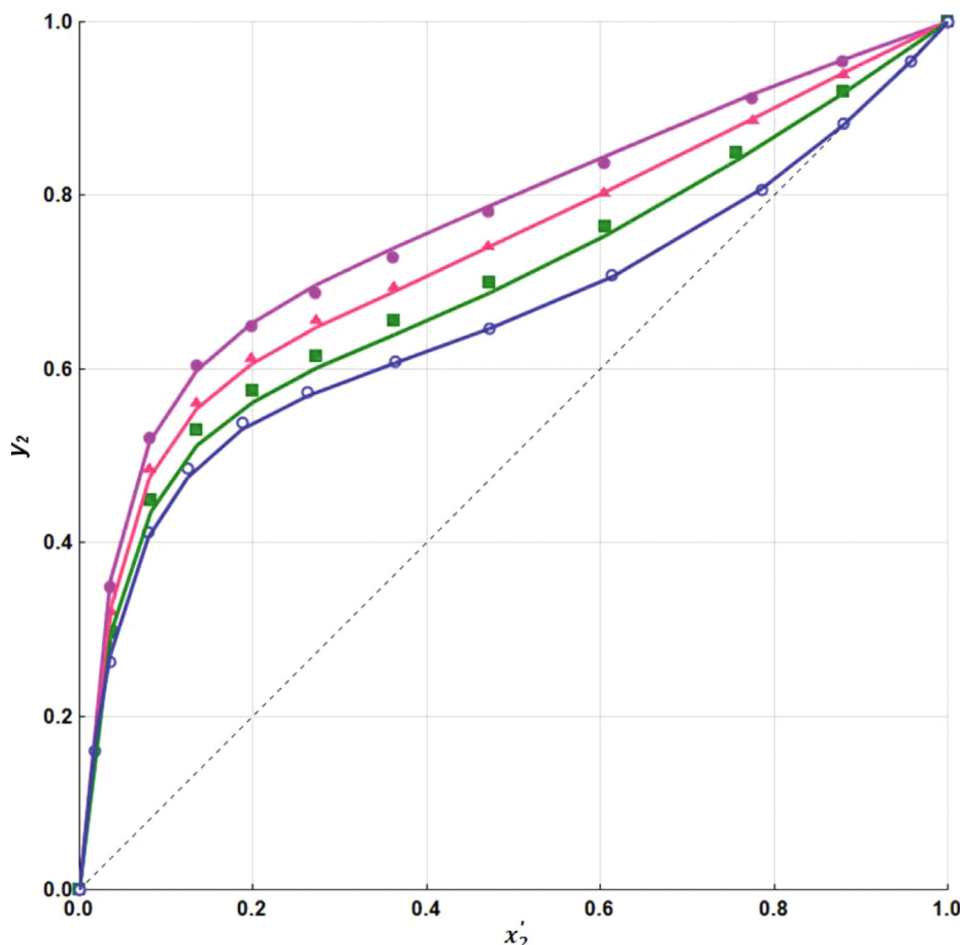


Fig. 1. Isobaric y-x' diagram for the system of water (1) ethanol (2) + calcium chloride (3) at 94.5 kPa; (o) salt free, (■) 5%, (▲) 10% and (●) 15 % w/w salt; solid line correlated by eNRTL model, x', liquid phase mole fraction (salt free basis); y, vapor phase mole fraction.

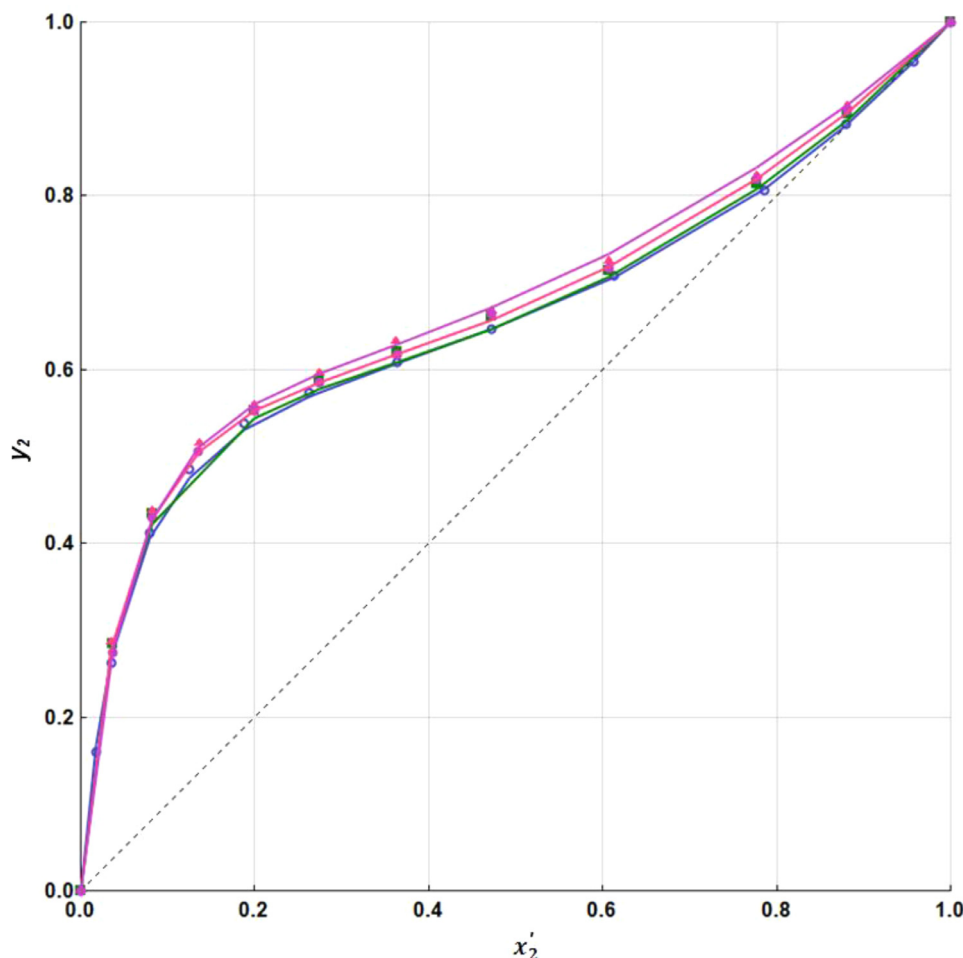


Fig. 2. Isobaric y - x' diagram for the system of water (1) ethanol (2) + zinc chloride (3) at 94.5 kPa; (○) salt free, (■) 5%, (▲) 10% and (●) 15 % w/w salt; solid line correlated by eNRTL model, x' , liquid phase mole fraction (salt free basis); y , vapor phase mole fraction.

3.4. Effect of salts on vapor-liquid equilibrium

To study the effect of salts on the vapor-liquid equilibrium of the ethanol and water azeotropic system, the isobaric y - x' and α - x diagrams for ternary systems of water + ethanol + calcium chloride and water + ethanol + zinc chloride are presented in Figs. 1–4, respectively. It can be seen from these figures that the equilibrium curve intersect the diagonal line at azeotropic point before addition of entrainer. As salt concentration increases, the interaction between salt and water becomes much stronger than the interaction between salt and ethanol. This is because water is highly polar solvent. Thus ethanol concentration shifts from azeotropic composition to pure ethanol. As shown in the Fig. 2 the concentration of ethanol in the vapor phase increases with addition of the calcium chloride salt which results in the upward shifting of the equilibrium curve with addition of calcium chloride. As the content of calcium chloride increases degree of curve shift increases. It means that calcium chloride exhibited the stronger salting out effect on ethanol; which leads to complete elimination of the azeotropic point. On the other hand zinc chloride exhibited very less salting out effect on ethanol, which results in very slight

shift in equilibrium curve; even at higher concentration of zinc chloride was observed.

The separation ability for both salts can also be expressed by the relative volatility. The effects of both the salts on relative volatility of ethanol to water are presented in the Figs. 3 and 4. Higher the relative volatility better is the separation of azeotrope. Both salts could eliminate the azeotrope formed by ethanol and water while calcium chloride showing better relative volatility values as compared to zinc chloride. Thus, calcium chloride can be a better entrainer choice than zinc chloride in the separation of ethanol and water azeotropic system.

For water+ ethanol+ salt ternary system equilibrium diagram are plotted for comparing the experimental data with literature data as shown in Fig. 5, the result shows that experimental data is in good agreement with the literature data. It is observed that from the Fig. 5, shift in equilibrium curve in case of CaCl_2 was more as compared to ZnCl_2 when both salts have same concentration of 15 %, So it can be conclude that CaCl_2 will act as good entrainer as compared to ZnCl_2 for separation of ethanol + water azeotropic mixture.

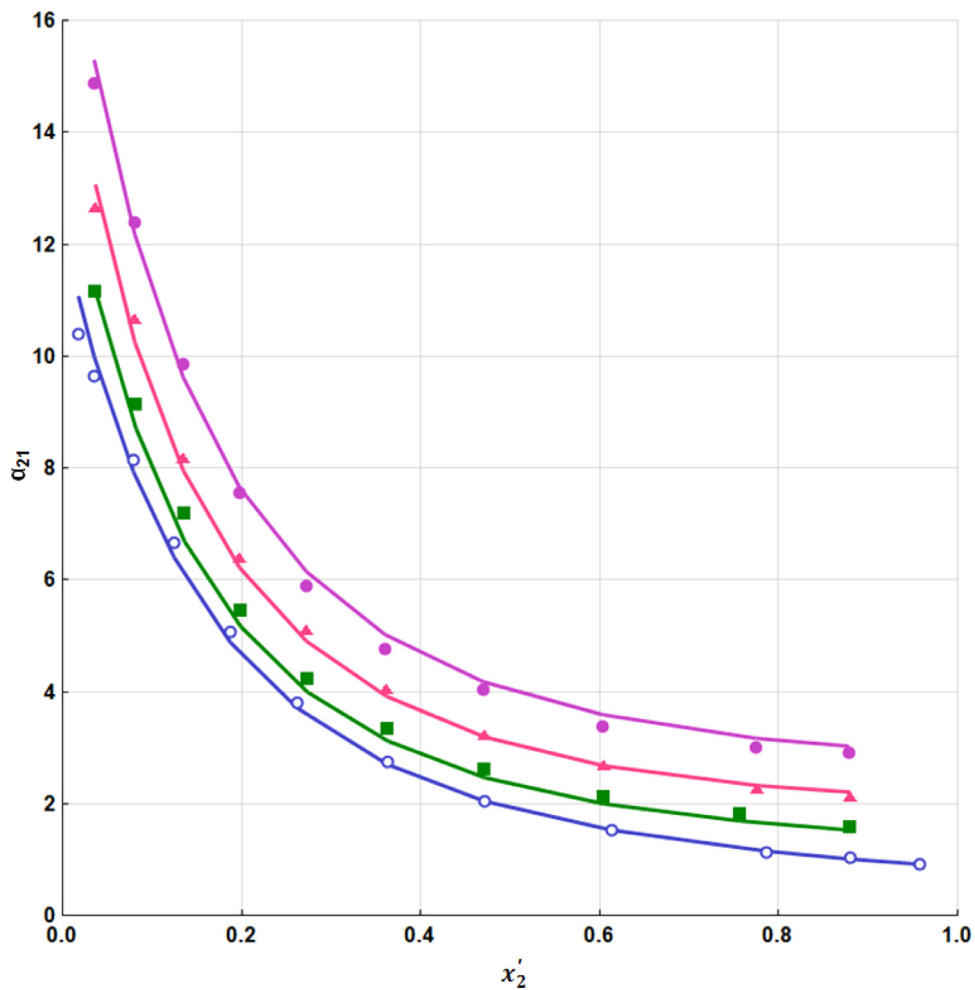


Fig. 3. Relative volatility (α_{21}) for the system of water (1) ethanol (2) + calcium chloride (3) at 94.5 kPa; (\circ) salt free, (\blacksquare) 5%, (\blacktriangle) 10% and (\bullet) 15 % w/w salt; solid line correlated by eNRTL model, x' , liquid phase mole fraction (salt free basis).

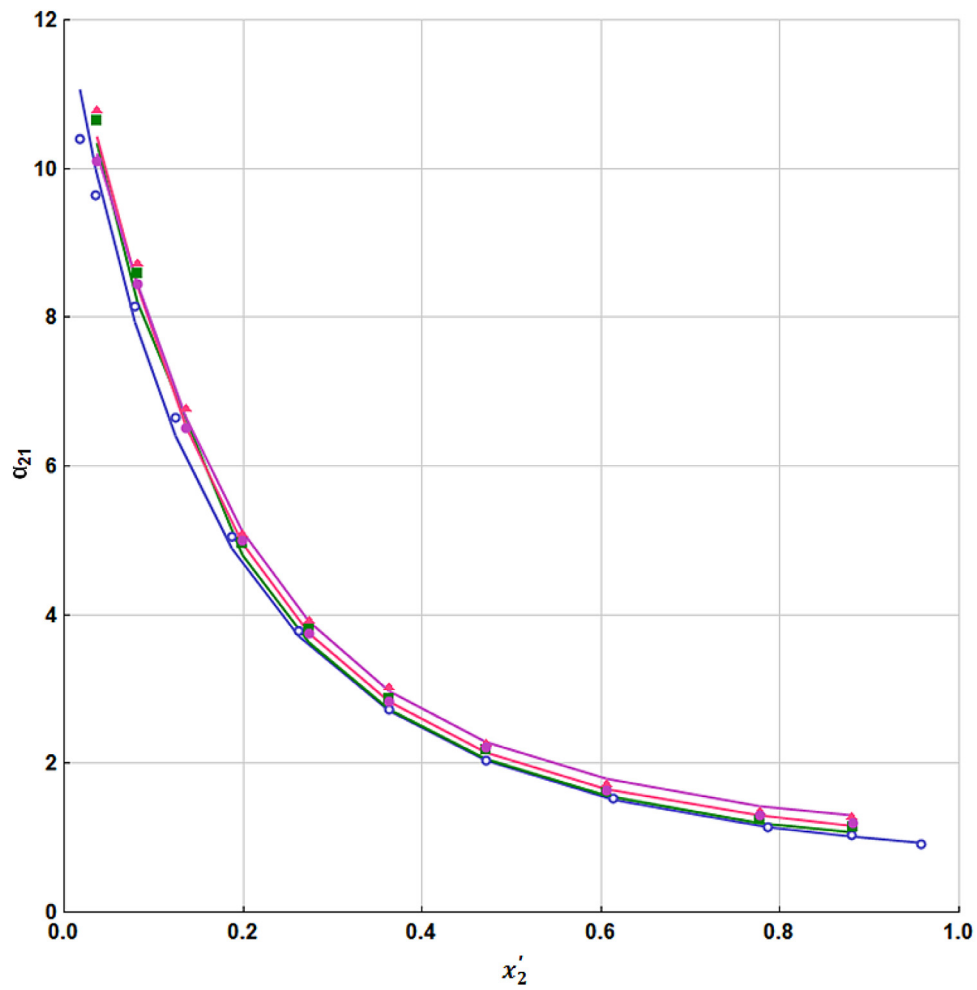


Fig. 4. Relative volatility (α_{21}) for the system of water (1) ethanol (2) + zinc chloride (3) at 94.5 kPa; (○) salt free, (■) 5%, (▲) 10% and (●) 15 % w/w salt; solid line correlated by eNRTL model, x' , liquid phase mole fraction (salt free basis).

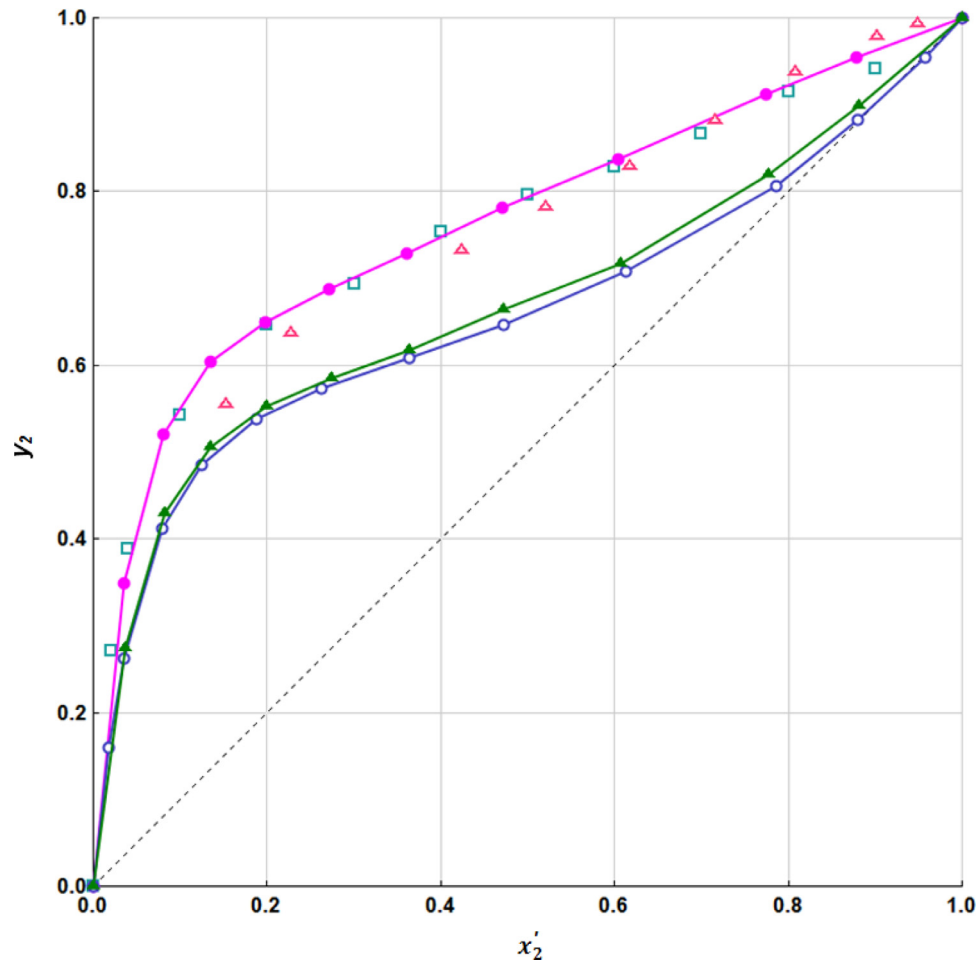


Fig. 5. Isobaric y-x' diagram for water (1) ethanol (2) + Salt (3) system, (○) salt free, (▲) 15% ZnCl₂, and (●) 15% CaCl₂ w/w salt (this study), (□) 16.7% CaCl₂ w/w salt [24], (Δ) 0.04 molar concentration of MgCl₂ [14] x', liquid phase mole fraction (salt free basis); y, vapor phase mole fraction.

4. Conclusions

The isobaric vapor-liquid equilibrium (VLE) data for binary ethanol + water and ternary system of ethanol + water + calcium chloride and ethanol + water + zinc chloride with constant mass fractions of salts of 0.05, 0.1 and 0.15, respectively, were determined at 94.5 kPa. The experimental data was found thermodynamically consistent using van Ness test. By comparing the experimental data of binary and ternary system showed that relative volatility of ethanol-water system improves with addition of salt. Addition of both salts eliminates the azeotrope completely. CaCl_2 salt improves relative volatility better than ZnCl_2 salt and hence, can be a better entrainer in the separation of ethanol and water using extractive distillation. Electrolyte nonrandom two-liquid (eNRTL) model was used to correlate the VLE for the ternary system of water + ethanol + $\text{CaCl}_2/\text{ZnCl}_2$ result showed that eNRTL model agreed well experimental data.

Declaration of Competing Interest

The authors declare that they have no known competing financial interests or personal relationships that could have appeared to influence the work reported in this paper.

CRediT authorship contribution statement

Pravin D. Ghuge: Writing – original draft, Software, Formal analysis, Investigation, Visualization. **Nilesh A. Mali:** Conceptualization, Methodology, Supervision, Writing – review & editing. **Sunil S. Joshi:** Resources, Funding acquisition.

Acknowledgment

Pravin Ghuge acknowledges the Council of Scientific and Industrial Research (CSIR) for Senior Research Fellowship (SRF) (31/11(1040)/2018-EMR-I). All authors are gratefully acknowledged the financial support from CSIR.

Supplementary materials

Supplementary material associated with this article can be found, in the online version, at doi:10.1016/j.fluid.2021.113000.

References

- [1] I.D. Gil, A.M. Uyazán, J.L. Aguilar, G. Rodríguez, L.A. Caicedo, Separation of ethanol and water by extractive distillation with salt and solvent as entrainer: process simulation, *Braz. J. Chem. Eng.* 25 (01) (2008) 207–215.
- [2] R.A. Dagle, A.D. Winkelman, K.K. Ramasamy, V.L. Dagle, R.S. Weber, Ethanol as a renewable building block for fuels and chemicals, *Ind. Eng. Chem. Res.* 59 (2020) 4843–4853.
- [3] Z. Lei, B. Chen, Z. Ding, *Special Distillation Processes*, Elsevier, Amsterdam, 2005.
- [4] Z. Lei, C. Li, B. Chen, Extractive distillation: a review, *Sep. Purif. Rev.* 32 (2) (2003) 121–213.
- [5] E.L. Ligeró, T.M.K. Ravagnani, Dehydration of ethanol with salt extractive distillation—a comparative analysis between processes with salt recovery, *Chem. Eng. Process.* 42 (2003) 543–552.
- [6] C.A.T. Cantero, G.L. Lopez, V.M. Alvarado, R.F.E. Jimenez, J.Y.R. Morales, E.M.S. Coronado, Control structures evaluation for a salt extractive distillation pilot plant: application to bio-ethanol dehydration, *Energies* 10 (2017) 1276.
- [7] R.A. Cook, W.F. Furter, Extractive distillation employing a dissolved salt as separating agent, *Can. J. Chem. Eng.* 46 (1968) 119–123.
- [8] D. Schmitt, A. Vogelpohl, Distillation of ethanol-water solutions in the presence of potassium acetate, *Sep. Sci. Technol.* 18 (6) (1983) 547–554.
- [9] D. Barba, V. Brandani, G. Di Giacomo, Hyperazeotropic ethanol salted-out by extractive distillation. Theoretical evaluation and experimental check, *Chem. Eng. Sci.* 40 (12) (1985) 2287–2292.
- [10] R.T.P. Pinto, M.R. Wolf-Maciel, L. Lintomen, Saline extractive distillation process for ethanol purification, *Comp. Chem. Eng.* 24 (2000) 1689–1694.
- [11] M. Llano-Restrepo, J. Aguilar-Arias, Modeling and simulation of saline extractive distillation columns for the production of absolute ethanol, *Comp. Chem. Eng.* 27 (2003) 527–549.
- [12] M.A. Hussain, J.L. Anthony, P.H. Pfromm, Reducing the energy demand of corn-based fuel ethanol through salt extractive distillation enabled by electro-dialysis, *AIChE J.* 58 (1) (2012) 163–172.
- [13] R.B. Soares, F.L.P. Pessoa, M.F. Mendes, Dehydration of ethanol with different salts in a packed distillation column, *Process. Saf. Environ. Prot.* 93 (2015) 147–153.
- [14] L. Zeng, Z. Li, A new process for fuel ethanol dehydration based on modeling the phase equilibria of the anhydrous MgCl_2 + ethanol + water system, *AIChE J.* 61 (2) (2015) 664–676.
- [15] D. Meranda, W.F. Furter, Vapor-liquid equilibrium data for system: ethanol-water saturated with potassium acetate, *Can. J. Chem. Eng.* 44 (1966) 298–300.
- [16] D. Meranda, W.F. Furter, Vapor-liquid equilibrium in alcohol-water systems containing dissolved acetate salts, *AIChE J.* 17 (1971) 38–42.
- [17] E. Vercher, R. Muñoz, A. Martínez-Andreu, Isobaric vapor-liquid equilibrium data for the ethanol-water-potassium acetate and ethanol-water-(potassium acetate/sodium acetate) systems, *J. Chem. Eng. Data* 36 (3) (1991) 274–277.
- [18] R.J. Zemp, A.Z. Francesconi, Salt effect on phase equilibria by a recirculating still, *J. Chem. Eng. Data* 37 (3) (1992) 313–316.
- [19] M.A. Galan, M.D. Labrador, J.R. Alvarez, Salt effect in liquid-vapor equilibrium: ethanol-water system saturated with strontium bromide, barium nitrate, and strontium nitrate, *J. Chem. Eng. Data* 25 (1980) 7–9.
- [20] E. Vercher, M.P. Peña, A. Martínez-Andreu, Isobaric vapor-liquid equilibrium data for the ethanol-water-strontium bromide system, *J. Chem. Eng. Data* 39 (2) (1994) 316–319.
- [21] H.M. Polka, J. Gmehling, Effect of calcium nitrate on the vapor-liquid equilibria of ethanol + water and 2-propanol + water, *J. Chem. Eng. Data* 39 (3) (1994) 621–624.
- [22] M.P. Peña, E. Vercher, A. Martínez-Andreu, Isobaric vapor-liquid equilibrium for ethanol+ water+ cobalt (II) chloride, *J. Chem. Eng. Data* 39 (4) (1994) 763–766.
- [23] D. Meranda, W.F. Furter, Vapor-liquid equilibrium in alcohol-water systems containing dissolved halide salts and salt mixtures, *AIChE J.* 18 (1) (1972) 111–116.
- [24] Y. Nishi, Vapor-liquid equilibrium relations for the system accompanied by hypothetical chemical reaction containing salt, *J. Chem. Eng. Jpn.* 8 (3) (1975) 187–191.
- [25] T. Meyer, H.M. Polka, J. Gmehling, Low-pressure isobaric vapor-liquid equilibria of ethanol/water mixtures containing electrolytes, *J. Chem. Eng. Data* 36 (3) (1991) 340–342.
- [26] K. Mishima, Y. Iwai, S. Yamaguchi, H. Isonaga, Y. Arai, M. Hongo, Correlation of vapor-liquid equilibria of ethanol-water-calcium chloride and methanol-ethanol-calcium chloride systems at 25 °C, *Mem. Fac. Eng. Kyushu Univ.* 46 (1986) 407–433.
- [27] N.A. Mali, S.S. Yadav, P.D. Ghuge, S.S. Joshi, Vapor-liquid equilibrium data for binary mixtures of dimethyl carbonate with methyl acetate, ethyl acetate, n-propyl acetate, isopropyl acetate, n-butyl acetate, and isoamyl acetate at 93.13 kPa, *J. Chem. Eng. Data* 62 (2017) 4356–4363.
- [28] B.R. Bhoi, N.A. Mali, S.S. Joshi, Experimental analysis of vapour-liquid phase equilibria for binary systems of diethyl carbonate with methyl, ethyl, isopropyl, n-butyl and isoamyl acetates at 95 kPa, *J. Chem. Thermodyn.* 150 (2020) 106189.
- [29] N.A. Mali, P.K. Mali, A.P. Patil, S.S. Joshi, Vapor-liquid equilibrium data for binary mixtures of acetic acid+anisole, acetone+anisole, and isopropanol+anisole at pressure 96.15 kPa, *J. Chem. Eng. Data* 62 (2017) 947–953.
- [30] J.M. Smith, H.C. Van Ness, *Introduction to Chemical Engineering Thermodynamics*, McGraw-Hill, New York, 1975.
- [31] Aspen Properties V8.4, Aspen Technology, Burlington, MA, 2013.
- [32] C.C. Chen, H.I. Britt, J.F. Boston, L.B. Evans, Local composition model for excess Gibbs energy of electrolyte systems, part I. Single solvent, single completely dissociated electrolyte systems, *AIChE J.* 28 (4) (1982) 588–596.
- [33] B. Mock, L.B. Evans, C.C. Chen, Thermodynamic representation of phase equilibria of mixed-solvent electrolyte systems, *AIChE J.* 32 (10) (1986) 1655–1664.
- [34] K.S. Pitzer, Electrolytes. From dilute solution to fused salts, *J. Am. Chem. Soc.* 102 (9) (1980) 2902–2906.
- [35] C.C. Chen, Y. Song, Generalized electrolyte-NRTL model for mixed-solvent electrolyte systems, *AIChE J.* 50 (8) (2004) 1928–1941.
- [36] L. Xu, D. Xu, P. Shi, K. Zhang, X. Ma, J. Gao, Y. Wang, Salts effect on isobaric vapor-liquid equilibrium for separation of the azeotropic mixture allyl alcohol + water, *Fluid Phase Equilib.* 457 (2018) 11–17.
- [37] H.C. Van Ness, S.M. Byer, R.E. Gibbs, Vapor-liquid equilibrium: part I. An appraisal of data reduction methods, *AIChE J.* 19 (2) (1973) 238–244.